INTEGRATED BIOSENSOR SYSTEMS: AUTOMATED MICROFLUIDIC PATHOGEN DETECTION PLATFORMS AND MICROCANTILEVER-BASED MONITORING OF BIOLOGICAL ACTIVITY

A Dissertation

Presented to the Faculty of the Graduate School

of Cornell University

In Partial Fulfillment of the Requirements for the Degree of

Doctor of Philosophy

by

Clarissa Shiao-Jia Lui

February 2010

INTEGRATED BIOSENSOR SYSTEMS: AUTOMATED MICROFLUIDIC PATHOGEN DETECTION PLATFORMS AND MICROCANTILEVER-BASED MONITORING OF BIOLOGICAL ACTIVITY

Clarissa Shiao-Jia Lui, Ph. D.

Cornell University 2010

Recent advances in micro- and nanofabrication technology have led to the development of a wide range of integrated biosensor platforms. Though multiple sensors and assays have been developed for the rapid and sensitive detection of cells, proteins, and other small molecules, few systems have successfully integrated sample preparation, sample handing, and detection components onto a single platform. This dissertation has aimed to tackle some of the challenges associated with developing innovative and portable biosensor platforms.

In this work, microfluidic modules for fluid handling using electrohydraulic pumps, magnetic bead-based sample preparation protocols, DNA extraction, purification, and real-time amplification detection were individually investigated and ultimately integrated into a single microfluidic chip platform. A LabView®-based instrument was designed to automate the platform, allowing the user to easily interface with the instrument and modify parameters via laptop-controlled software. Although technical challenges still remain for increasing cell capture efficiencies, detection sensitivities, and assay optimization, the platform presented here provides a solution for the portable field-deployable detection of foodborne pathogens with raw-sample-to-result capabilities.

In addition to an integrated microfluidic pathogen detection platform, we also developed a cantilever-based biosensing system for the monitoring of changes in biological activity of single cells. We fabricated an array of tipless gold-coated silicon nitride cantilevers with an exposed nitride pad at the tip for chemical functionalization to capture single cells. As part of these investigations, experiments were performed which successfully demonstrated the monitoring changes in the increased activity of bacterial flagella and detection of capture and subsequent immunogenic events in RBL mast cells. Our efforts in developing integrated biosensor systems not only demonstrates improvements in microfluidic devices and cantilever-based sensing technologies, but also provides exciting new avenues toward the development of innovative integrated biosensor systems.

BIOGRAPHICAL SKETCH

Clarissa Shiao-Jia Lui is the daughter of Chung Yao Lui and Elisa Lui and elder sister of Monica and Elaine. Born in Tulsa, Oklahoma on March 1, 1982, she spent the majority of her childhood in southern California, Taipei, Jakarta, and Texas. An early inclination towards science and math, along with an interest in creative writing, led her to pursue a degree in electrical engineering from the University of Texas at Austin. As an undergraduate, her summer activities ranged from internships at a civil engineering firm and a semiconductor company to undergraduate research on a temperature control system for portable microfluidic polymerase chain reaction devices with Dr. Shaochen Chen's.

Shortly after beginning her Ph. D. program in the Department of Biomedical Engineering, she joined Dr. Carl Batt's research group, where she worked on integrated microfluidic pathogen detection platforms and silicon nitride cantilever-based biosensing systems. In 2007-2008, Clarissa served as a Cornell NanoScale Facility fellow, working primarily to baseline photolithographic processes and create recipes for facility users. In 2008, she was awarded the CNF Nellie Yeh-Poh Lin Whetten Award. Besides research, she spends a healthy portion of her time volunteering to help generate interest in science and engineering among middle and high school kids through the CATALYST Academy, regional science fairs, and local elementary schools. She helped create and maintain Nanooze!, a web magazine about science and nanotechnology for kids. Clarissa also enjoys web design, travel, cooking, and crossword puzzles.

This work is dedicated to my loving parents, Chung and Elisa Lui for all their support, guidance, and encouragement, and to my beloved sisters, Monica and Elaine.

ACKNOWLEDGMENTS

Firstly, I would like to thank my mentor and advisor, Dr. Carl Batt for providing me with the freedom and support to pursue my scientific research interests, and for challenging me to always perform my best and expand my realm of knowledge and thinking, as well as encouraging me to stay involved with science outreach activities. I would also like to thank my committee members, Dr. Amit Lal and Dr. Thomas Sato, for their insight and for supporting my interdisciplinary research.

Many thanks to Nathaniel Cady and Magnus Bergkvist for their patience and supportive mentorship, and to Scott Stelick, Matthew Kennedy, and Ines Lopez-Calleja for working closely with me on the microfluidic pathogen detection platform. Special thanks to Andrew Melnychenko for all his help and to the undergraduate students who have worked with me over the years: Sushmitha Krishnan, Kunal Tiwari, Adepeju Adeniji, and Viktor Koltko. I would also like to acknowledge all the staff members in the CNF and NBTC for their patience and help. Many thanks to Dr. Shaochen Chen and Dr. Archie Holmes for kindling my interest in research during my undergraduate years, and for encouraging the pursuit of my doctorate degree.

I would like to thank all the previous and current members of the Batt Lab for making my Ph. D. experience an enjoyable and rewarding experience. Thanks to all my fellow graduate students in biomedical engineering for all the fun times. Special thanks to Diego Rey for having to share a lab aisle with me and to Abhishek Ramkumar for all the support and encouragement.

Finally, I would like to thank my parents, Chung and Elisa Lui, and my sisters, Monica and Elaine for all their love, patience, and enduring support.

TABLE OF CONTENTS

LIST OF FIGURES

CHAPTER 1

LITERATURE REVIEW: NUCLEIC ACID-BASED PATHOGEN DETECTION USING MICROFLUIDIC SYSTEMS

* Originally published as: Lui, C.; Cady, N. C.; Batt, C. A. Review: "Nucleic Acid-based Detection of Bacterial Pathogens Using Integrated Microfluidic Platform Systems", 2009. Sensors 9(5), 3713-3744. Open access article by MDPI.

1.0 Introduction

The advent of nucleic acid-based pathogen detection methods offers increased sensitivity and specificity over traditional microbiological techniques, driving the development of portable, integrated biosensors. The miniaturization and automation of integrated detection systems presents a significant advantage for rapid, portable field-based testing. In this review, we highlight current developments and directions in nucleic acid-based micro total analysis systems for the detection of bacterial pathogens. Recent progress in the miniaturization of microfluidic processing steps for cell capture, DNA extraction and purification, polymerase chain reaction, and product detection are detailed. Discussions include strategies and challenges for implementation of an integrated portable platform.

The rapid, reliable detection of pathogenic bacteria is imperative in many different industries, of which food and agriculture, healthcare, environmental monitoring, and bio-defense are the four main players [1]. With recent devastating outbreaks of *Salmonella* and *Escherichia coli* in the United States, the food industry is largely concerned with the detection of pathogenic bacteria in agricultural products and processed foods. The presence of pathogenic bacteria can cost the food industry and the consumer many millions of dollars every year due to food recalls, and is estimated to cause over 30,000 hospitalizations and over 1000 deaths each year in the United States [2]. In the healthcare sector, approximately 25% of physician visits are caused by infectious diseases, many due to pathogenic agents. The ongoing evolution of microbes due to changing ecological, environmental, and human demographical factors necessitates improvements in the readiness of healthy and emergency service providers to respond to threats through effective surveillance, treatment, and control

measures[3]. The development of a fast and sensitive platform for the detection of pathogens in human blood and waste samples is required in order to implement a quick and effective response to an outbreak. In the environmental monitoring arena, considerable attention is given to the evaluation of microbial cells in water and environment quality control, as well as for the study of microorganisms evolution and populations, for example in bio-waste composting substrates and their communities[4]. In the area of biodefense, biological agents are considered far more difficult to detect and defend against than chemical agents, and with bioterrorism now an issue of serious concern, the technology to counter a potential incident needs to be in place. To date, a multitude of reviews on micro total analysis systems for nucleic acid-based detection and microchip pathogen detection methods have been published[1, 2, 5-19], demonstrating great interest in the development of this field. A comprehensive literature survey was carried out for this section, and due to the immense amount of literature related to pathogenic detection, our study focuses primarily on rapid portable systems for the nucleic acid-based detection of bacterial pathogens.

1.1 Nucleic acid-based detection

Despite vast improvements in modern-day pathogen detection techniques, the tried and true culturing and plating method still remains the standard method of detection. This technique involves culturing and measuring the growth of individual viable microorganisms using either non-selective media, such as trypticase soy agar, or selective media specially formulated to detect a particular bacteria species. At lower detection levels, however, this method would require a lengthy pre-enrichment step to increase the numbers of viable target bacteria before detection could be conducted.

Detection is mainly through enumeration by ocular inspection, which leads to sources of uncertainty due to human variations in sampling and measurements[20]. Due to the low throughput, time consuming and labor intensive process of colony enumeration, this method exhibits low potential for integration and miniaturization into micro total analysis systems. Though several bacterial colony counters have been proposed to automate and standardize this process[21-23], culturing remains a time-consuming process and the required high-quality imaging equipment and software are expensive and cumbersome for integration into a portable system. The recent push for reliable, rapid detection techniques is prompting researchers to explore alternative methods, particularly for detection of bacteria with slower generation times such as the gastroenteritis-causing *Campylobacter* species, which require a minimum of 3-4 days for full-confirmation[24].

Nucleic acid-based methods in pathogen detection are promising in their rapid results, high specificity, and low detection limits of up to, in theory, a single cell. Developed in the mid-1980's, nucleic acid-based technology quickly achieved widespread use in the field of pathogen detection, with a particular focus in polymerase chain reaction (PCR) assays that were developed to detect virtually every clinically relevant bacterial pathogen[1]. In the past decades, our understanding of DNA has grown considerably, with currently 788 fully sequenced microbial genomes[25]. The versatility of nucleic acid-based methods allowed for the design of specific probe sequences, typically on the order of 10 to 30 base pairs in length, to target antibiotic resistance genes as well as for sub-typing of bacteria. DNA is an excellent vehicle for signal transduction due to its characteristic negative charge, and in addition to the typical optical and mechanical measurements, pathogen sensors are often designed to quantify hybridization events between analytes and probe DNA based upon electrical

measurements as well. Since these methods target nucleic acids, however, they do not indicate the viability of the target pathogen, so care must be exercised when performing these tests. On the other hand, there are situations where the detection of hibernating or non-viable pathogens is favorable, particularly when aiming to detect unculturable cells[26-28] or to quantify antibiotic effectiveness[29-31]. Nucleic acid-based techniques have a higher sensitivity, therefore requiring a higher level of quality control to prevent contamination, elevating the importance of effective sample preparation to a critical step for successful detection. Consideration of contamination, inhibitors in the specimen sample, and DNA degradation due to unfavorable conditions must be accounted for in the sensor design to help reduce the incidence of false positive or false negative results.

Modern advances in micro- and nanofabrication technology have led to the development of a wide range of nucleic-acid based biosensors that capitalize on the new capabilities of microfluidic technologies and micro total analysis systems in order to reduce reagent and power consumption, enhance analytical performance, and enable portability. These lab-on-a-chip devices incorporate multiple laboratory processes in a semi-automated and miniaturized format. Many of these technologies have been extensively studied[32], successfully commercialized, and are currently widely used in clinical and research laboratories. Nevertheless, portable biosensors systems for point-of-care diagnostics and on-site field testing are still in the infancy stage. Current portable systems tend to be costly and require additional resources as well as skilled operators, therefore rendering the technology unsuitable for point-of-care testing, especially in resource-poor regions such as Africa, Asia, and Latin America that would benefit the most from the development of these platforms[33, 34]. Performance of a biosensor platform in the third-world is challenged by the absence or scarcity of

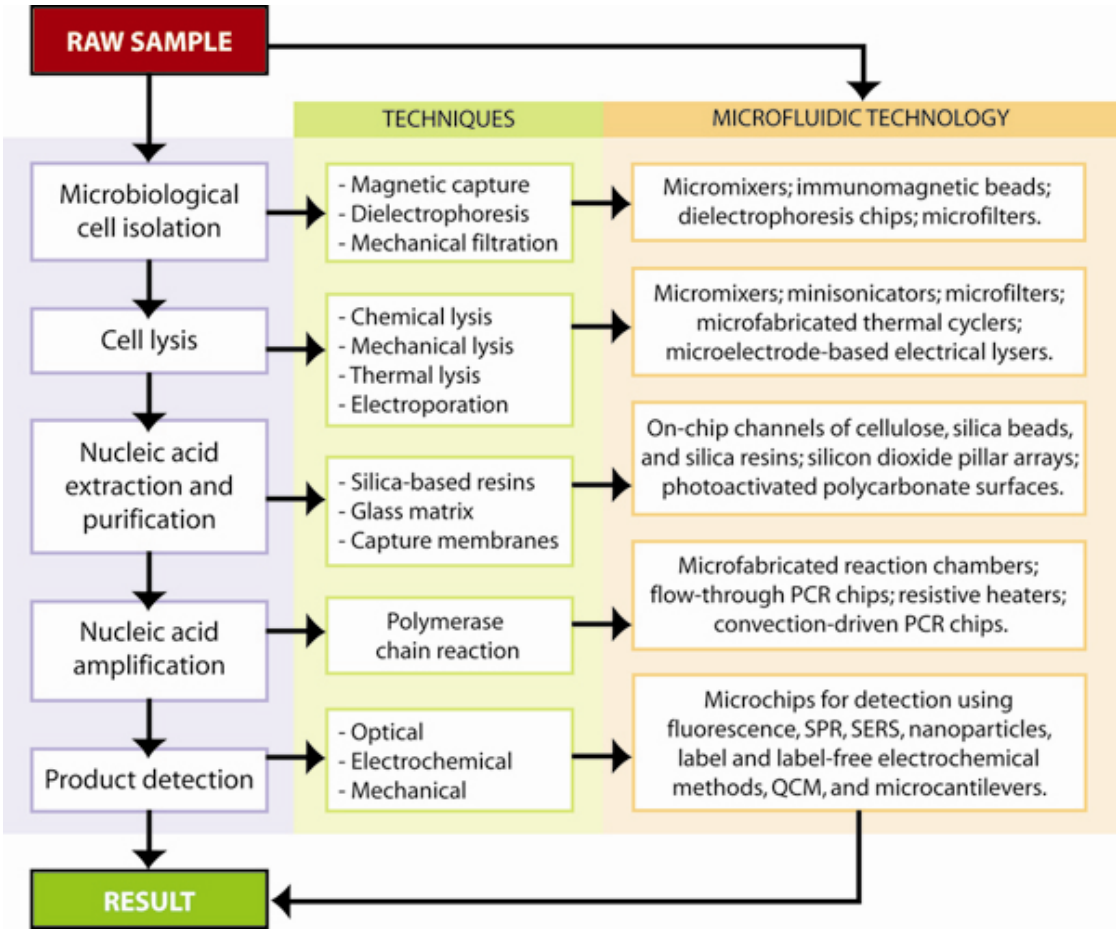

Figure 1-1. Diagrammatic representation of the processing flows in nucleic acid-based chip detection, the traditional techniques and translation into microfluidic technology.

trained workers, electricity, equipped laboratories, transportation, and refrigerated storage[34]. Specific areas that need to be addressed during further development include sample pre-treatment, long term storage of reagents, ease of use, and costs[35]. Point-of-care biosensor systems, particularly those utilizing disposable cartridges, must direct some attention towards the development of environmentally-friendly chemicals and materials[34]. Though multiple sensors and assays have been developed for lab-on-a-chip nucleic acid-based detection, few systems have successfully integrated all the necessary sample preparation, sample handling, and detection components into a single automated, portable platform with raw-sample-to-result capabilities. An overview of the translation of traditional microbiological techniques into microfluidic technology is represented in Figure 1-1.

1.2 Microfluidic nucleic-acid based pathogen detection systems

Proposed by Manz et al.[36] in the early 1990's, micro total analysis systems (μTAS) are integrated miniaturized platforms composed of multi-step sample preparation and detection systems on a single chip that has raw-sample-to-result capabilities – the quintessential "lab-on-a-chip" concept. μTAS systems have experienced rapid growth and development since the completion of the human genome project. The driving force for miniaturization has always been improvement in performance. At the microscale, faster, higher-throughput analysis using parallel systems can be achieved due to a combination of larger surface-to-volume ratios, reduced separation times, shorter diffusion paths, and more efficient reactions. This points not only to the potential for low costs associated with reduced reagent consumption, but also to the ability to analyze smaller samples that were previously insufficient in size. In terms of DNA detection, polymerase chain reaction (PCR) and various other sensing schemes

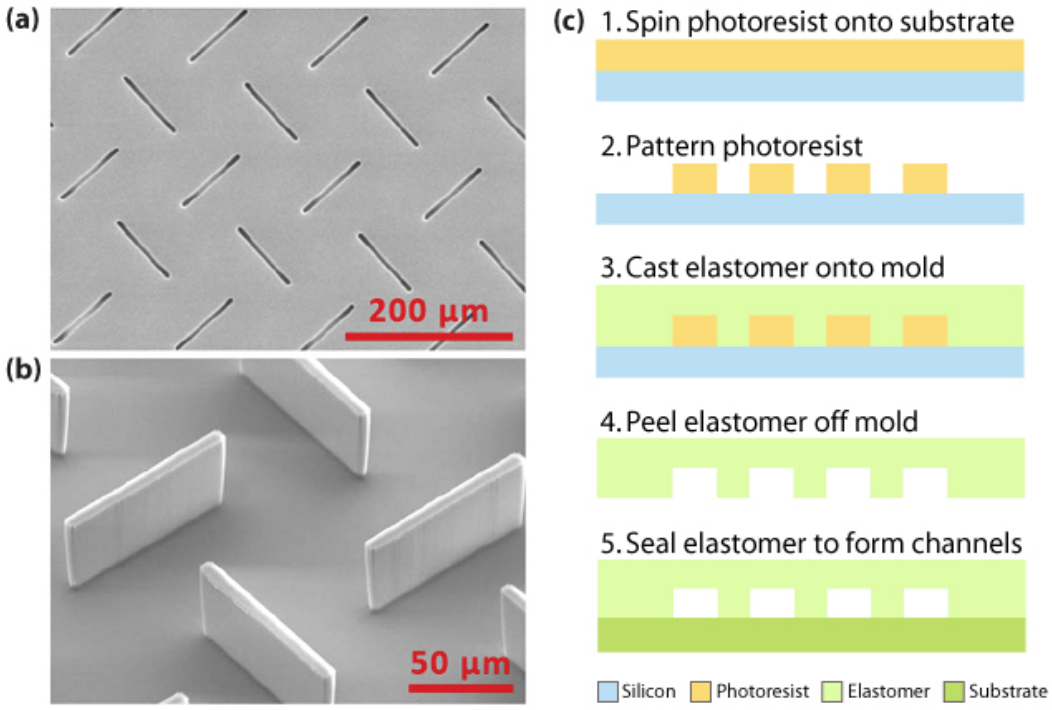

Figure 1-2. SEM micrograph of (a) PDMS mold for plastic casting and (b) the epoxy chip fabricated by casting (reprinted with permission[34], © 2007 Springer); (c) Schematic of the casting method showing an elastomer material poured over a molding template, peeled off, and sealed with an appropriate substrate, such as glass or silicon, to form microfluidic channels.

have been successfully carried using integrated microfluidic systems[32]. DNA sequencing and genotyping have been achieved through advances in microchannels technology and capillary array electrophoresis. Complete nucleic acid-based analysis involves complex processes, such as cell concentrating and capture, cell lysis, nucleic acid purification, amplification, and final detection.

Materials and fabrication for microfluidic sensors. The first generation of microfluidic devices built in the early 1990's were mainly fabricated in silicon and glass substrates by borrowing technology generated by the massive growth of the semiconductor industry, such as photolithography and etching techniques. Investigations into new unconventional substrate materials for biocompatible microfluidics, led to interest in ceramics, hydrogels, and even paper. To meet the demand for cheaper, more versatile alternatives, however, researchers began to explore the use of polymeric materials in microfluidic technology. Biocompatible polymeric materials can be easily selected for DNA-related analysis, since the magnitude of electroosmotic flow is significantly lower than that of glass and fused silica in similar pH environments, lessening the need for further coating treatments of the microchannel surfaces to prevent nonspecific adhesion[15]. However, different surface chemistries may need to be investigated in order to reduce unwanted polymer absorption of reagents and optimize the analysis system. One other drawback is the incompatibility of most polymers with a range of non-aqueous solvents commonly used in chemical production and drug discovery[19], although for most nucleic acid-based detection purposes this issue does not pose a problem.

There are two main methods to micromachine polymers. The cheaper, more commonly used method is replication, which involves methods such as hot embossing,

injection molding, and casting to transfer a pattern from a precision template or master to a polymer substrate. This master mold can be made from a variety of different materials: glass, silicon, metals, and more recently, high-aspect-ratio photoresists. Hot embossing is a simple procedure that involves heating the polymer to slightly above its glass transition temperature and applying it to a master under vacuum to form a polymer device with high structural integrity[37]. Though this process is quick and relatively inexpensive, it cannot be a fully automated process[38]. Injection molding is one of the most well-known technologies where heated polymer pellets are injected at high pressure into a mold to replicate features at rapid rates and high-volume production[39], as seen in Figure 1-2. Casting is by far the most widely used technique in the academic world. It is an easy, low-cost process of pouring a polymer material over a molding template and curing, after which the soft elastomer copy can simply be peeled off the mold and used[40]. Most commercial devices fabricated today are made from polymers such as polycarbonate (PC) and polymethylmethacrylate (PMMA), while polydimethylsiloxane (PDMS) is still widely used in research[19]. The more versatile, direct fabrication methods, such as laser ablation, optical lithography, and X-ray lithography, tend to be more suitable in a research setting due to customizability of each individual device. Laser ablation, a precise approach that can achieve submicron features, uses the energy of a pulsed laser to disrupt polymer bonds and remove polymer fragments from the ablated region to form a clean cut surface; however, the laser light may induce unwanted surface modifications on the polymer material[7, 41]. Optical lithography techniques of fabricating microfluidic channels include the patterning or layering of polymer and sacrificial material, where the sacrificial material is subsequently removed using appropriate solvents. Stereolithography is another optical technique where focused laser light is used to photocure a liquid polymer, but this process tends to be slow and tedious[7]. In order to push the

envelope on minimum feature sizes that can be realized in polymer devices, the use of X-ray lithography for patterning has also been investigated[42].

All microfluidic devices require a tight bond or seal of the channel or chamber to form an enclosed structure, and a variety of material-dependent techniques have been used to achieve reliable containment of the sample fluid. For PDMS-based microfluidic fabrication, O_2 plasma is commonly used to activate the PDMS surface to produce polar groups (Si-OH) and when two activated surfaces are brought in close proximity, an irreversible bond is formed capable of withstanding high pressures. Other bonding methods include lamination, thermal bonding, ultrasonic welding, and the use of adhesives.

On-chip fluid and reagent handling. Precise fluid control and flow stability in a microfluidic-based system is critical for successful DNA detection. As a sensitive detection system, the introduction and maneuvering of any fluids must be done with extreme care so as to prevent bubble formation within the channels or chambers. Though bubbles can be used as an actuation mechanism for various applications[43], the presence of undesired bubbles can adversely affect or block sample flow, causing detection failures, particularly in highly-sensitive optical detection schemes. Some research has been conducted in the implementation of bubble traps as a prevention scheme in microfluidic systems. There has been extensive research in microfluidic fluid-handling for the manipulation of on-chip fluids via pumps, valves, and mixers, discussed in the following.

Microfluidic Pumping: One of the earliest micropumps were developed by Jam Smits in the 1980s for the controlled delivery of insulin to maintain the blood sugar levels of

diabetics[44]. Since then, a variety of different pumping mechanisms have been explored for chemical and biological analysis applications, with attempts to make improvements in the areas of pressure generation, cost, power consumption, biocompatibility, and reliability. Some microfluidic applications where pumping serves a vitally important role include cellular capture and separations[45, 46], DNA purification[47], and flow-through PCR[48]. Microfluidic pumps currently employ a variety of different actuation mechanisms: thermopneumatics[49, 50], electrostatics[51-53], piezoelectrics[54-56], electromagnetics[57-59], and hydrogels[60, 61], among others. Some microfluidic pumps focus on controlled direction and delivery of micro- and nano-liter solutions over long periods of time, while others seek to achieve high pumping volumes at low power. Thermal and electrolytically-generated bubbles have been investigated for their utility in miniaturized pumps, microfluidic dosing experiments[62], and are favorable due to simple fabrication and ease of control. The disadvantage of thermal production of water vapor bubbles is the risk of denaturating biological molecules due to overheating[63]. In addition, the electrolytic production of bubbles has been shown to be far more energy efficient than thermal bubble generation[64]. Gravity, vacuums, wicking and capillary action have also been widely used to motivate fluids[17] and are generally favored in portable systems due to their low power consumption. Despite extensive research, however, there are still limited μTAS systems with on-board micropumps in existence, since most systems still rely on manual pipetting, syringe pumps, or induced electroosmotic flow for liquid transport.

Microfluidic Valving: In order to meet the complex plumbing requirements set forth by μTAS systems, particularly for high-throughput multiplexed systems where a

multitude of different samples and reagents need to be activated and inactivated with precise temporal control, microvalves have been investigated for a variety of applications. Typical valves at the macro-scale use hydraulic, pneumatic, manual, or solenoid activation[17], most of which can be easily rescaled to our microscale needs. Many of the actuation mechanisms and methods employed for microvalve construction draw upon the same principles used by microfluidic pumps[65-68], and therefore have similar associated advantages and disadvantages. Some actuation mechanisms heavily rely on the properties of the working fluid (i.e. electrokinetic manipulations), and can therefore be too specific in its application. For higher versatility, microfabricated mechanical valves are a robust alternative. Other valving mechanisms include temperature-control of paraffin[69], manipulation of the hydrophobicity properties of chemically modified elastomer for low pressure valving[70], electrochemical generation of microbubbles[71], and the usage of thermally-responsive polymer solutions[72]. The low power consumption need of a portable system tends to favor pneumatic or externally-coupled mechanical mechanisms. Some of the performance criteria to keep in mind when designing valves are size, dead volume, channel dimensions, actuation pressure, power consumption and scalability[66].

Microfluidic Mixing: The challenge of mixing of reagents and samples in a small volume can be difficult to overcome due to low Reynolds numbers, and diffusion and convection limitations at the microscale. A wide range of methods have been proposed to achieve efficient mixing of two or more fluid streams. At the macroscale, magnetic stirrers are the conventional solutions for homogenous mixing, and this idea has been adapted to the microscale using a miniaturized magnetic stir bar [73, 74]. Active mixing methods, such as those based on electro-hydrodynamic, magneto-

hydrodynamic, pressure perturbations, ultrasonic, centrifugal, and electrophoretic principles, often require moving parts and external power sources, which may reduce the feasibility of a portable system [17]. Mixing from oscillatory motion has been investigated with the use of piezoelectrics [55], gas bubbles [43, 75], and magnetic microspheres [76]. Passive mixers are typically designed to reduce diffusion lengths through increased surface area and the creative manipulation of fluids by the positioning of special microfabricated structures. Some notable passive mixers in literature include the kneading of fluids through the positioning of herringbone grooves on the channel surfaces [77], continuous-flow mixing capable of reaching 95% mixing completion in 15 milli-seconds, and innovative devices modified with Tesla structures [78] and J-shaped baffles [79]. Although passive mixers enjoy the advantages of low power consumption and the lack of wear and tear associated with mechanical parts, the complex channel topology needed to achieve efficient passive mixing can often be difficult to microfabricate. Appropriate micromixing technology should be chosen based on degree of mixing required, fluid volumes, power consumption, ease of fabrication, and feasibility.

Filtration and separation of bacterial cells. The current selection of nucleic acid-based biosensors with target detection of a highly specific DNA signature dictates the need for simple and effective methods of obtaining high-quality DNA. For the majority of biosensing applications, the starting samples consist of tissue, blood, environmental, or food samples [80] and need to undergo careful sample preparation for sensitive detection due to trace or low-abundance species. Although many of the assays based upon polymerase chain reaction (PCR) are fairly robust, a variety of contaminants can inhibit amplification and diminish the success of such analytical instruments. In order to circumvent this problem, target cells must first be extracted

and purified from a raw sample through a variety of cell separation and capture techniques. Cell concentrators increase the concentration of microorganisms through gentle means, so as to preserve specific activity or viability, and are important to help increase the sensitivity and strength of the final detection signal [81]. Also, raw samples taken from blood, soil, water, or food are often large in volume for microfluidic analysis, and this discrepancy in volumes makes concentration necessary due to time constraints and the need for rapid detection. The volume analyzed in a typical microscale pathogen detection device ranges from a couple picoliters to, at most, a few microliters. Cell separation is important for separating target cells from contaminants in the raw sample. The three main techniques for cell manipulation involve the use of magnetic, electrokinetic, and mechanical principles.

Magnetic manipulation techniques typically use magnetic particles that can selectively attach to cells of interest through the use of antibodies and other linking chemistries, and use magnetic field gradients to capture the bead-cell conjugates. Investigations into continuous flow separations [82, 83] and matrix-based manipulations [84] using magnetic capture have been promising. E. coli has been shown to be magnetically separated from PBS and whole blood on an integrated microfluidic device consisting of a chaotic mixer, incubation channel, and a capture channel [85]. The magnetic method is clean, versatile, and non-invasive, and with advances in magnetic bead materials and chemical modification techniques, the technique has the potential to become increasingly efficient and easily integrated into a portable system [18]. Cell manipulation using dielectrophoresis (DEP) takes advantage of the intrinsic dielectric properties of cells and their response to electric fields, and has been extensively studied on microscale devices [86]. A DEP chip fabricated from acrylic has been reported by Huang and colleageues to separate *B. cereus*, *E. coli*, and *L.*

monocytogenes from blood [87]. Using DEP microchip technology, live cells have been shown to be separated from dead cells through differences in cellular dielectric properties at differing states of viability [88]. In addition, single-cell trapping has been achieved using DEP in conjunction with laser-trapping forces [89]. Mechanical cell separations have been achieved using microfilters [90], microwells [91, 92], and surface-modified microchannels [93, 94]. Microbial cells have been concentrated using size-dependent filter-based microfluidic devices [90], which are typically rapid and highly efficient, though lacking in selectivity. For portable point-of-care devices, low cost and power consumption is necessary, without sacrificing on sensitivity, and magnetic bead-based separations have shown considerable promise in this area.

1.3 Pathogenic DNA extraction and purification

Upon cell capture and isolation from the raw sample, cell lysis is necessary to release the nucleic acids for further analysis. Among the various lysis methods, chemical lysis is most common. Chemical lysis can be easily incorporated into an integrated microfluidic design with methods such as on-chip mixing of captured cells with sodium dodecyl sulfate or guanidinium thiocyanate [95] and hydroxide electro-generation-induced cell poration and lysis [96] . Unlike mammalian cells, the efficient lysis of certain bacteria for DNA extraction can be more challenging. Gram-negative bacteria is commonly treated with alkaline buffers or guanadinium thiocyanate, whereas gram-positive bacteria is more difficult to lyse often requiring multistep methods, though heating in the presence of chelating resins, sometimes with beads, has been shown to be effective [97]. Heat-based techniques, such as freeze-thaw or freeze-boil methods[98] are also available, and pulsed laser irradiation of carboxyl-terminated magnetic beads [99] has been reported for on-chip pathogenic DNA

extraction. However, most thermal methods are seldom employed due to likelihood of denaturation due to high heat. Electrical pulsing methods have also been incorporated into microfluidic chips to electroporate cells [100]. Mechanical disruption methods, such as sonication, release cellular components into solution but often require more energy but have been demonstrated in microscale devices [101, 102]. High-frequency sonication uses piezoelectric materials to generate pressure waves that disrupt cell membranes, and though effective against hard-to-lyse cells, this method generates considerable amounts of unwanted heat and free radicals [97].

The traditional method of purifying DNA is performed via proteinase K digestion in the presence of detergents, phenol-chloroform extraction, and concentration by alcohol precipitation [97]. One of the most common modern techniques for DNA purification is through chemical lysis followed by capture using silica-based resins. DNA in chaotropic salt-containing buffers such as those containing guanidinium or sodium iodide salts, preferentially bind to silica surfaces, whereas other macromolecules such as proteins and lipids remain free in solution [103, 104]. These unwanted components are traditionally removed using centrifugation and alcohol washing steps using commercially-available kits. However, the fact that they are usually based upon particulate matrices presents challenges to integration onto μTAS devices. While incorporation of silica-based resins into a microfluidic device has been reported [104, 105], new innovative silica pillar arrays (see Figure 1-3) have also been investigated for microscale DNA purification [47] which circumvent the problems associated with filling channels with binding matrices after microfabrication.

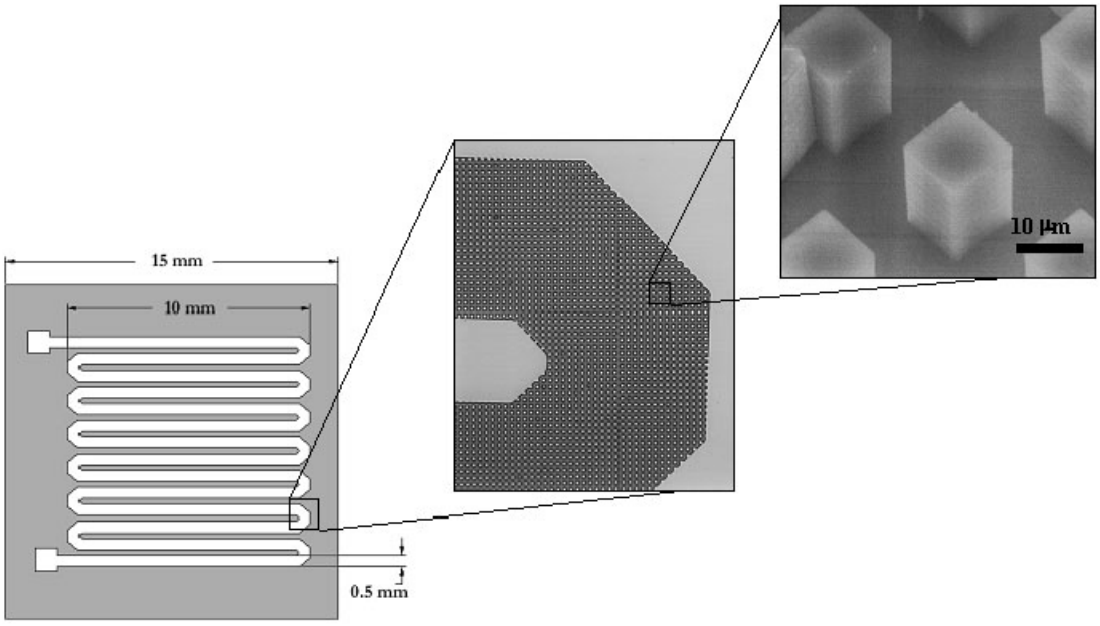

Figure 1-3. Schematic representation and SEM micrographs of channels containing microfabricated silica pillars used for microchip DNA purification (reprinted with permission [45], © 2003 Elsevier Science B.V.).

1.4 Pathogenic DNA detection

Polymerase chain reaction amplification and detection.

For smaller test samples, DNA amplification is often necessary to obtain a sufficiently strong DNA-detection signal. PCR is a three-step amplification process, depicted in Figure 1-4, first introduced in 1985 by Saiki et al. [106]. The principle of PCR is based on the isolation, amplification, and quantification of a short but unique DNA sequence present in the target bacteria's genetic material. For conventional PCR, forward and reverse primers are used to amplify the target sequence, and subsequent gel electrophoresis in conjunction with DNA-binding fluorescent dyes allows visualization of the result. Though this technique is significantly less time-consuming than the culturing and colony counting method, the typical laboratory PCR procedure time frame still ranges from 5 to 24 h, without taking enrichment times into account. Since bacterial nucleic-acid-based detection is mainly DNA-based, reverse-transcriptase PCR (RT-PCR) are less frequently used. On the other hand, real-time PCR typically employs an automated system and special fluorescent probes that track the amplification during the thermal cycling. Common probes used in these assays include the dual-labeled TaqMan® probes, hybridization Light-Cycler probes, intercalating SYBR Green® dye, Molecular Beacons, or Scorpions™. This technique offers a variety of advantages, including increased sensitivity, speed, broader dynamic range, and higher throughput. The major limitation of PCR points to the high cost of instrumentation and reagents, but the technology is highly amenable to miniaturization for applications in portable biosensing and point-of-care diagnostics.

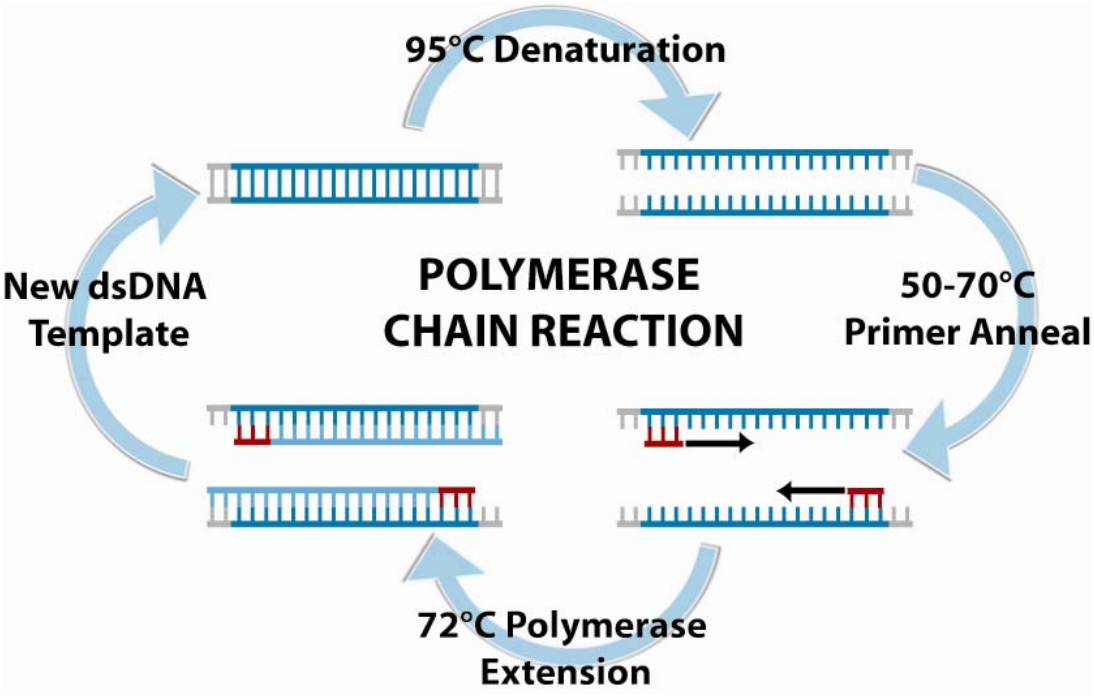

Figure 1-4. Polymerase chain reaction (PCR) is an amplification-based technique for DNA detection. The standard protocol involves raising the temperature of the reaction to 95°C to separate the DNA strands, lowering to the annealing temperature for the oligonucleotide primers to hybridize, and then raising to the optimal DNA polymerase temperature 72°C for primer extension. This process is repeated cyclically, creating many copies of the target sequence.

Since the introduction of the first PCR chip in 1995 by Northrup and colleagues [107], a multitude of PCR microfluidic technologies have facilitated a variety of improvements in microfluidic DNA amplification, such as smaller volumes, faster ramping rates, lower manufacturing costs, and higher integration. Successful chip-based DNA purification and PCR requires manufacturing of the detection microchips, as well as development of a platform to perform the necessary thermal cycling and DNA detection measurements. In order to amplify DNA with high specificity and high throughput, the cycling temperatures in PCR microfluidics must be precisely controlled to achieve desirable temperature kinetics for the denaturation, annealing, and extension steps. For single-chamber PCR thermal cycling, investigators have employed multiple techniques, including infrared light [108], thermoelectric heater-coolers [109], and resistive electrodes [110]. In addition to changing the temperature of the entire reaction chamber, other researchers have developed flow-through PCR devices, in which the sample is passed through different thermal regions on a serpentine or circular chip [48, 110, 111]. Convection-driven PCR microfluidics uses buoyancy forces to drive the sample fluid forward between the temperature zones [19], and has also been shown to be capable of rapid DNA amplification. For high-throughput analysis, multi-chamber PCR microfluidic devices have been constructed for parallel processing [112-114], though careful design is necessary to ensure temperature uniformity, reliability, and repeatability across the different chambers [19]. Methods of subsequent DNA detection are primarily grouped into optical, electrochemical, and mechanical techniques, as discussed in the following.

Optical methods in nucleic acid-based detection.

One of the primary methods of observing and quantifying DNA is through the use of optics. Traditional laboratory methods of quantification have utilized the specific

absorption of ultraviolet (UV) light at 260 nm by DNA. For most biosensing applications, techniques have mostly focused on the use of fluorescent dyes and, more recently, quantum dots. However, the past decade has shown an escalating surge of interest in techniques such as surface plasmon resonance (SPR), surface-enhanced Raman scattering (SERS) spectroscopy, interferometry, and colorimetry.

Fluorescence-based detection. Fluorescence is the optical technique most commonly employed due to its high level of sensitivity and low background noise. Fluorescent dyes can bind to DNA non-specifically through general interactions, or attach directly to specific locations on a DNA molecule, and the resulting signal can be easily detected with an appropriate imaging apparatus. The first label used in 1953 was fluorescein for the immunofluorescence of DNA, with rhodamine following not long after, both dyes utilizing isothiocyanate reactive groups to conjugate to the free amine groups on nucleic acids [115]. Ethydium bromide, one of the original non-specific DNA dyes, was first described for DNA quantification in 1967 [116], and is still commonly used for DNA visualization during gel electrophoresis. Since then, several sequence-independent dyes exhibiting high fluorescent signals when bound to DNA have been developed, including the YOYO and TOTO dyes [117], PicoGreen, and SYBR Green [118], among many others. The limitation of conventional fluorescent dyes lies in the background fluorescence, as well as the photobleaching and time degradation of fluorophores.

An interesting advancement in optical DNA detection was the development of fluorescent resonance energy transfer (FRET), which utilizes a distance-dependent phenomenon that occurs when a donor fluorophore and an acceptor chromophore (quencher) are in close proximity (typically 5-10 nm) and excitation energy is

transferred from the flourophore to the quencher, thus preventing fluorescence emission. Multiple detection techniques have been devised to harness this effect, including molecular beacons and 5' nuclease (Taqman®) real-time PCR detection. Molecular beacons are designed to preferentially base-pair with itself, forming a stem-loop structure that brings the flourophore and quencher into close proximity. A probe sequence in the loop region on the molecular beacon can hybridize with the target DNA, causing the step-loop structure to open, separating the fluorophore and quencher and resulting in fluorescence. Molecular beacons have been patterned and immobilized on solid supports due to their potential for label-free, real-time detection in the DNA array format. In the case of the Taqman® real-time PCR technique, the modified oligo-probe is degraded during the primer extension of PCR amplification, releasing the fluorophore and quencher into solution separately, as shown in Figure 1-5. Both methods are dependent on proper probe design to achieve sequence specificity to obtain a quantifiable fluorescent signal. Other types of probes used in DNA fluorescent detection include scorpions and light-up probes. Similar to molecular beacons, scorpions are linked to the primer but cannot be fully copied during PCR due to the presence of a blocking molecule, which allows it to be faster and more efficient than molecular beacons, while remaining sensitive enough to detect single-base mutations [119]. On the other hand, light-up probes are peptide nucleic acids tethered to a dye molecule that binds to the target DNA upon probe hybridization, and essentially "lights up" the fluorescence signal. These probes do not rely on the FRET process, and are capable of hybridizing more quickly and strongly than oligonucleotide probes [8].

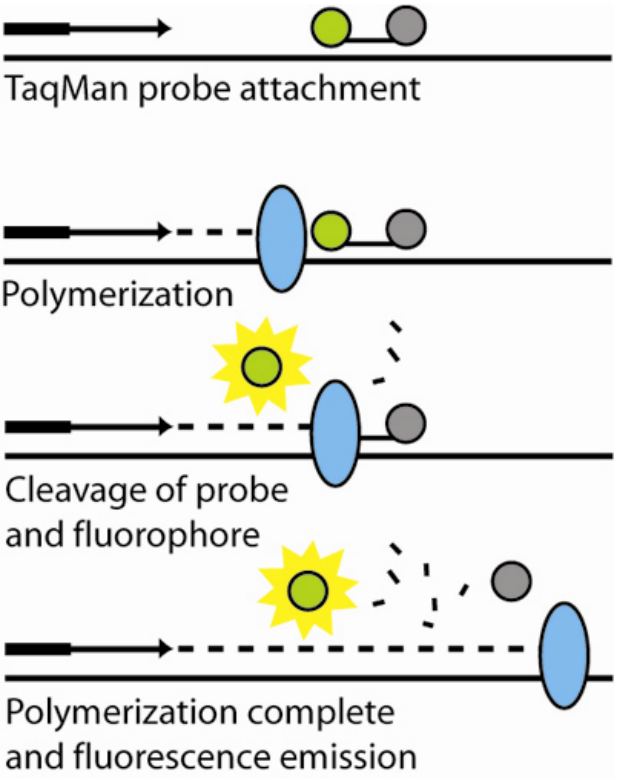

Figure 1-5. The TaqMan assay, also known as the 5' nuclease assay utilizes a third oligonucleotide labeled with a fluorophore (green) and quencher (gray), in which the fluorophore is quenched due to FRET conditions. During the reaction, the DNA polymerase (blue) degrades the probe, separating the fluorophore and quencher, allowing for fluorescence emission to occur.

In order to enhance the signal-to-background ratio of the fluorescent signal, a variety of different alternative techniques, such as quantum dots and fluorescence resonance energy transfer (FRET) have been explored. Quantum dots are advantageous in that they fluoresce throughout the visible and near infrared and can be excited with a single blue UV excitation source. In addition, they are resistant to photobleaching and have brighter, narrower emission bands so that theoretically, as many as 20 quantum dot reagents could be individually detected using narrow band-pass filters [115]. There have even been investigations in using quantum dots in conjunction with molecular beacons (see Figure 1-6). Multiple binding chemistries are readily available to for attachment of DNA molecules to quantum dots. Conversely, quantum dots are typically larger than conventional dyes, and have been suggested to negatively affect probe-target interactions and in some cases cause steric hindrance [120]. There exists a vast selection of chemistries and probes available for the fluorescent detection of non-specific and specific nucleic-acids, many of which are highly adaptable to miniaturization schemes for lab-on-a-chip applications. Modern-day fluorophores display excellent fluorescence, so there is little pressure for incremental improvement in this arena. However, with the continued push towards smaller instrumentation and sample sizes, chemical and photostability for robust sample preparation, shipping, storage, and manipulation becomes vitally important [115]. And though quantum dots are highly fluorescent and photostable, the problematic issue with size compatibility is still unresolved. The movement towards obtaining data from single-molecule fluorescent detection measurements signifies a need for a highly-fluorescent, photostable fluorophore capable of low-level multiplexed detection.

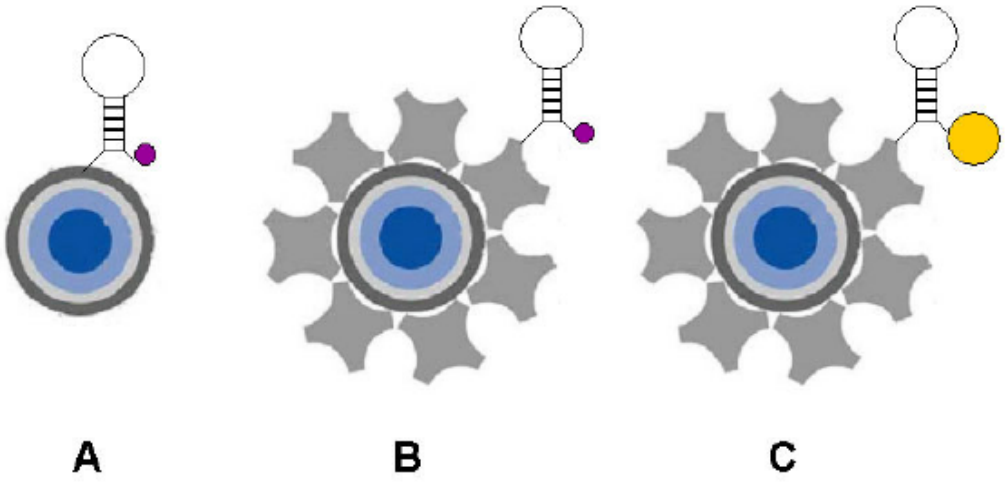

Figure 1-6. A representation of the three different quantum dot molecular beacon labeling strategies is shown. Carboxyl-modified quantum dots (blue core) were modified with amino-labeled molecular beacons (A) while streptavidin modified quantum dots (blue core dot with surrounding gray streptavidin molecules) were modified with biotin-labeled molecular beacons. Both dabcyl and Iowa Black FQ quenchers (small purple circles) were used, as well as 1.4nm Nanogold (gold colored circle), (reprinted with permission [119], © 2006 Elsevier Ltd.)

In the field of portable fluorescence detection, the design and integration of miniaturized excitation and emission sources for microchip devices has been challenging. Bubble formation becomes a major concern during PCR because they scatter light and can significantly reduce the sensitivity of an instrument relying on optical detection. Traditional excitation is done using bulky, bench-top sources, such as lasers and mercury lamps [104, 105, 121] and detection is typically accomplished with microscope-based CCD cameras, laser scanning microscopes, or other large instrumentation that severely inhibits portability [104, 105, 121] due to size and power consumption. In contrast to these larger systems, light-emitting diodes have been applied as low-power excitation sources, in conjunction with smaller footprint detectors such as photodiodes and miniaturized photomultiplier tubes [32, 103, 122, 123]. Miniaturized spectrometers have also been proposed, enabling detection of a continuous fluorescence spectrum, thus allowing multiplexed detection with the use of different labeling dyes. End-point detection conventionally involves an after-PCR fluorescence measurement, followed by processing steps of gel or capillary electrophoresis [124]. Real-time detection of PCR products has an advantage over end-point detection due to its potential for faster detection due to the ability to observe the yields in real-time rather than waiting for the entire PCR cycling process to complete, and also requires less complex machinery. From real-time PCR results, the initial DNA concentration can be extracted, offering more reliable results and could provide an important piece of data in analyzing the degree of pathogen contamination in raw samples.

Surface plasmon resonance. Surface plasmon resonance (SPR) is an optical technique the reports changes in the refractive index of a metal film that occurs during adsorption of target DNA molecules to that film. For most SPR-based biosensors,

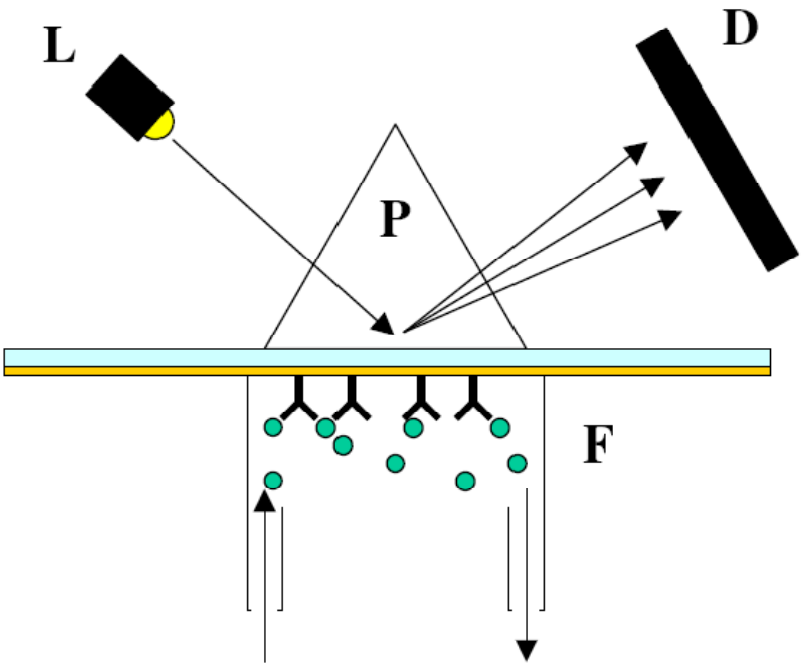

Figure 1-7. Surface plasmon resonance (SPR) is typically performed using an optical light source (L) coupled to a thin metal surface (S) through a prism (P). During experimentation, changes in the refractive index are measured by a detector (D). A flow cell (F) is commonly used to bring fluids into contact with the thin film, allowing for binding to other molecules on the film surface, (reprinted with permission [130]).

the metal film is composed of gold, and DNA probes are assembled on this gold surface such that the target binding event results in a change in measured refractive index [125-128]. The SPR system, illustrated in Figure 1-7, is particularly useful in determining binding and dissociation kinetics, and has even been shown to be sensitive enough to detect DNA mismatches [8]. By interfacing with imaging technology, SPR spectroscopy allows for studies of DNA assembly, hybridization, and protein-DNA interactions on bio-functionalized chips. Since SPR alone is often not sensitive enough to accurately monitor binding events of low molecular weight molecules and low packing density molecules, fluorescent tagging is often performed in conjunction with SPR in a technique called surface plasmon field-enhanced fluorescence spectroscopy (SPFS) [14]. Recent developments of multiplex SPR systems have been explored[129, 130], and though the use of SPR for DNA detection is not as widely reported as alternative methods, the high sensitivity of this technique makes it a viable and useful option of nucleic acid-based sensing on microchips.

Raman detection. Raman spectroscopy allows for measurement of a "chemical fingerprint" for analyte identification by studying the vibrational, rotational and other low-frequency modes in a system. Typically, laser-based monochromatic light excitation is used to excite in the visible wavelength range [16]. Surface-enhanced raman scattering (SERS) techniques have been applied by a number of investigators for sequence specific DNA detection [131, 132]. Multiplexed SERS detection was demonstrated by Docherty and colleagues using three dye-labeled oligonucleotides on microchips [133], though complex computational analysis is still needed for improved peak shapes. A major advantage of Raman methods lies in the fact that water is virtually Raman transparent, and therefore adsorption by water molecules does not pose a problem during detection. The technology is easily miniaturized, and a variety

of surface and resonance enhancement techniques can be utilized to improve sensitivity [16].

Electrochemical methods in nucleic acid-based detection.

Many of the electrochemical methods for DNA detection are comparable to fluorescence techniques in their simplicity, high sensitivity, low cost, and compatibility with microfabrication technology. An added advantage of electrochemical methods is their potential for portability, whereas fluorescence methods typically employ bulkier instrumentation. A variety of different electrochemical techniques are used to detect DNA hybridization, some with labels such as electroactive hybridization indicators, enzymes, or nanoparticles. A general strategy for electrochemical DNA detection is shown in Figure 1-8. The wealth of immobilization chemistries available for patterning probe sequences on a variety of electrode substrates allows for detection to be accomplished using inexpensive electrochemical analyzers. On the other hand, a variety of different label-free electrochemical nucleic acid sensors have also been reported [134], such as capacitance-based sensing of changes in the biolayer dielectric [135]. The three main detection signals that are measured during electrochemical detection are: current, potential, or impedance.

Labeling techniques. Electroactive hybridization indicators, such as cationic metal complexes or organic compounds that recognize the DNA helix structure intercalate selectively into double-stranded DNA, are extremely common [8, 136] for electrochemical detection. Despite its popularity, this technique does not have the specificity to detect mutations in DNA sequences [8]. Enzymatic labels are attached to target or probe nucleic acids directly for highly specific detection: when enzyme-

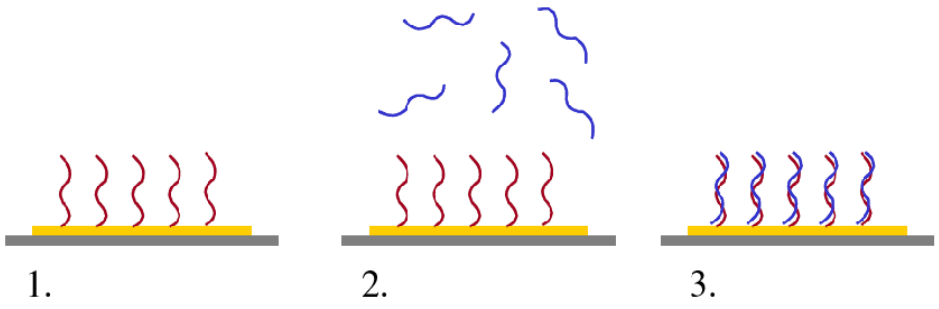

Figure 1-8. A general strategy for electrochemical DNA detection begins with immobilization of a ssDNA capture probe on an electrode surface: (1) After probe immobilization, baseline electrical measurements are taken and then target DNA is added; (2) Target DNA is allowed to hybridize with the capture DNA; (3) Another set of electrical measurements are made to detect the electrode changes caused by DNA hybridization. Detection can often be further enhanced by modifying the DNA with electroactive compounds or metallic nanoparticles, i.e., indirect detection [130].

labeled DNA reacts or hybridizes with immobilized probes or single-stranded DNA, the rise of amperometric current has been shown to be proportional to the number of hybridization strands. Labeling with soybean peroxidase (SBP), a thermostable enzyme, has been demonstrated to provide measurements in real time without any need for a washing step. The three-component sandwich assay is a variation on the enzyme approach where a label is designed to a probe-target complex that eliminates the need to directly modify the target strand with the label, and paves the way for reliable multiple-target detection. Colloidal gold nanoparticles have also been incorporated into the sandwich assay format for significant signal enhancement [137, 138], pushing the detection limit of PCR amplicons to as low as 0.8 femtomoles of DNA. Willner and colleagues have added a second dimension to the nanoparticle approach by developing quantum dot CdS particle-labeling of DNA to provide photoelectrochemical detection of hybridization events. Operation of the sensing scheme involves exposure of the aggregate to visible blue light to trigger a current between the CdS nanoparticle aggregate and the gold electrode [35]. Other electrochemical sensing approaches have involved materials such as magnetite [139] and carbon nanotubes [140].

Amperometric detection. One of the most common electrochemical detection methods, amperometric detection senses the oxidation or reduction of an electrochemically active analyte at the electrode interface, which is typically constructed out of platinum, gold, and carbon. The operation of this sensor relies on the linear relationship between analyte concentration and measured current. In cases where direct electron exchange cannot occur between the electrode and the biomolecules, special mediators called redox mediators are required to reversibly exchange electrons between the sensor and enzyme [141]. One demonstration of an

amperometric-based flow-through immunofiltration assay has detected between 100 – 600 cells per ml of *E. coli* within 30 minutes [142]. Though the amperometric method is capable of detecting cells directly using antigen-antibody biorecognition elements, investigations of nucleic acid-based amperometric detection of microbial contamination in food and water have also been reported [143].

Potentiometric detection. Potentiometric methods yield a logarithmic concentration response, enabling the detection of extremely small concentration changes with continuous measurement capabilities, but are the least implemented in biosensors, possibly due to lower selectivity and higher limits of detection in certain environmental samples. Modified ion-selective field effect transistors (ISFETs), devices consisting of a p-type silicon substrate with two n-doped regions separated by a short distance (gate) and covered by an insulator layer, have been shown to use the semiconductor field effect to detect biological recognition events [144]. However, incompatibility of materials with immobilization techniques, complicated fabrication and packaging, along with device instability impose severe limitations on this technology [11].

Conductimetric and Impedimetric Detection. Electrochemical impedance spectroscopy (EIS) is a powerful technique that applies a small amplitude sinusoidal excitation signal to a given system and measures the response in either current, voltage, capacitance, resistance, or some other signal form [11]. First applied to the detection of bacteria biomass in foods over ten years ago by measuring electrical impedance changes due to bacterial growth, the method is now widely accepted and applied [1]. More recently, disposable conductimetric biosensors with a detection limit of 83 CFU per ml have been reported that use polyclonal antibodies against E. coli

[145]. The advantage of EIS lies in its label-free detection, however, it has a limiting factor of poor sensitivity as compared to other traditional methods[1] and careful circuit design must be done to ensure reliability [146]. To combat this low sensitivity, high density microelectrode arrays [147], sandwich assays [148], and nanowires [149] have been implemented for pathogen detection.

Mechanical methods in nucleic acid-based detection

Fluorescence, amplification and electrochemical-based techniques all exploit various intrinsic properties of DNA to create a measurable signal. One of the most basic properties of DNA is mass. Like any molecule, DNA possesses a certain mass that can be measured directly using frequency-based detection methods. The laws of physics dictates that solid rigid objects have inherent resonant frequencies that can be shifted by attaching an additional mass and from this frequency shift, one can mathematically extract the associated change in mass.

Quartz crystal microbalance. The quartz crystal microbalance (QCM) is an instrument that utilizes a piezoelectric quartz crystal that can be vibrated at high frequencies with an electrical current to perform frequency-based measurement of DNA mass. The QCM can easily be converted to a DNA sensor by immobilizing probe DNA on the surface of the quartz crystal, and subsequent hybridization to target DNA will cause a change in resonant frequency. DNA hybridization events have been detected using QCM, with enough selectivity to discriminate between complimentary and non-complimentary target DNA, proving the capability of distinguishing between variant DNA sequences [150, 151]. QCM-based system have also been used as end-point measurements for PCR-based detection systems via immobilization of the capture probe on the quartz crystal [152]. In some instances, target DNA have been

modified with secondary compounds, such as gold nanoparticles, for the increased mass and associated increased measurement sensitivity. Using 50 nm diameter gold particles, the sensitivity of a system couldbe increased to between 10^{-15} and 10^{-16} M of DNA [153]. One major limitation with QCM is the difficulty of incorporating multiplexed detection of multiple samples, although there have been a few isolated reports [85]. Another major issue is the need for dry conditions, meaning that after hybridization, the QCM must be dried for accurate measurements, due to the significant vibrational damping imposed by liquid medium. For most systems, liquid phase analysis is critical and the advantages of performing measurements in a liquid environment are obvious.

Cantilever-based detection. Cantilever-based detection systems replaces the QCM with a miniature cantilever, typically fabricated from silicon or some other crystalline material, though there have been reports of polymer-based cantilevers. The cantilevers are oscillated, usually through piezoelectric means [154, 155]. Conventional detection is performed by monitoring the deflection of laser light off the surface of the cantilever tip. Measurements of resonant frequency shifts due to hybridization of target DNA with immobilized single-stranded capture DNA has been achieved using these systems, and has proven to possess sufficient sensitivity to detect single-base mismatches, as well as differentiation between complementary and non-complementary sequences [156]. The presence of laser and signal detection instrumentation, however, poses a challenge in miniaturization.

1.5 Integrated pathogen detection systems

Integration of all the microfabricated components needed to perform DNA detection to achieve portable, automated raw-sample-to-result functionality is no easy task. Several groups have already begun to address this challenge, with the incorporation of micropumps, microvalves, micromixers, heaters, detectors, and other analytical components. Significant progress has been demonstrated in various types of platforms including but not limited to, capillary driven test strips, centrifugal microfluidic devices, droplet-based microfluidic platforms, and large-scale system integration platforms. Though true μTAS systems are primarily still in the laboratory development stage, partially integrated μTAS devices have been developed for commercial applications. Of the different types of μTAS systems, PCR microfluidics is among the most prevalent and has been integrated with on-chip sample preparation and capillary electrophoresis.

The functional integration of PCR and capillary electrophoresis on a single microchip was successfully integrated by Koh et al. for the detection and identification of two model bacteria, Escherichia coli O157 and Salmonella typhimurium [157]. Similar systems were fabricated in a variety of different materials, namely PMMA, polycarbonate, and PDMS [15]. More recently, DNA purification and real-time PCR were successfully integrated for the single-chip detection of Listeria monocytogenes by Cady et al. on a portable instrument shown in Figure 1-9(a) with on-board pumping, valving, thermal cycling, and detection functionalities. In this work, DNA purification was performed by running lysed cell samples through a channel arrayed with 10 μm silicon oxide pillars and PCR was conducted in a serpentine amplification

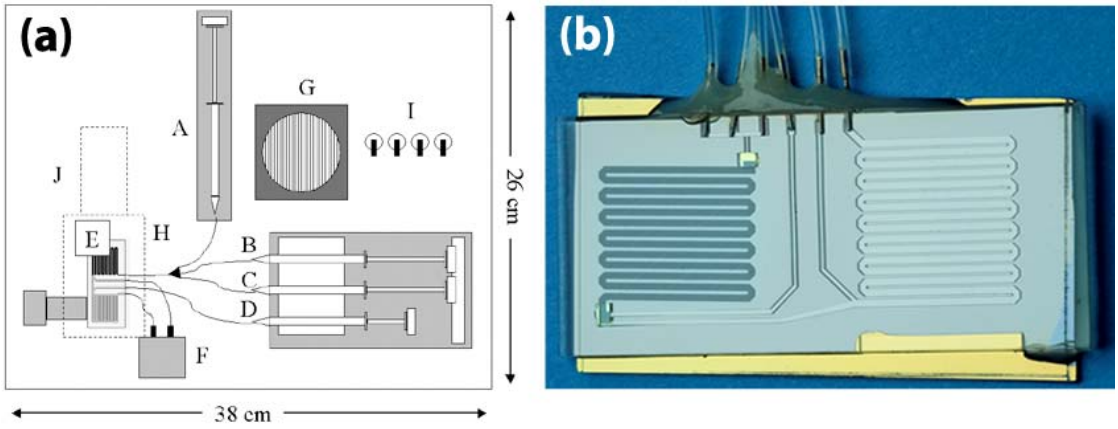

Figure 1-9. (a) A schematic of the assembled bacterial detection system is shown. The system includes integrated syringe pumps (A-D), Moog micro valve (F), cooling fan (G), LED-based fluorescence excitation / detection system (H – dotted outline) with PMT detector (J), power toggle switches (I). The microfluidic purification/detection chip (E) is inserted into the unit directly above the thermoelectric heater cooler. The syringes are connected to the chip via TygonTM tubing (black lines) and contain the sample lysate (A), ethanol wash buffer (B), dH2O (C), and PCR master mix (D). The Moog micro valve (F) is also connected to the chip via tubing and controls pressurization and fluid flow through the chip outputs. The entire unit measures 36cm x 28cm x 15cm. Reprinted with permission[32], © 2003 Elsevier Science B.V.; (b) Photographic image of the microfluidic purification/detection chip (E) .

channel using an external thermal cycler, and real-time detection was performed with LED-excitation of TaqMan and measurements using a miniaturized PMT [32, 47]. Automated sample preparation PDMS chips have also been developed to isolate nucleic acids from small numbers of bacterial cells with all cell isolation, cell lysis, DNA and mRNA purification and recovery processes carried out on a single standalone nanoliter-volume chip [158, 159]. A fully-integrated chip for immunomagnetic bead-based sample preparation, PCR, and DNA microarray detection has been developed for the detection of Eschericia coli K12 from rabbit blood samples [160]. Other fully-integrated DNA-based assays that have been shown to be capable of multiple pathogen detection make use of individual electrode surfaces immobilized with capture probes [161, 162]. In one particular system, signal amplification is achieved via tagging of the target DNA with gold nanoparticles and detection is based on measuring the amount of subsequent electrocatalytic deposition of silver metal onto the nanoparticles [162]. Other integration formats include the innovative compact disk device, also known as LabCD [163], a commercial product which utilizes centrifugal forces for pumping of fluids through reservoirs, valves, mixing chambers, and heating chambers. The control of flow rates through the device is tuned via different disk spin speeds, and is capable of achieving sample preparation, DNA purification, and PCR amplification.

In the laboratory setting, fully integrated systems exist for DNA analysis of complex biological samples employing the concept of raw-sample-to-result. One such system employs thermally-actuated paraffin-based microvalves and electrochemical and thermopneumatic pumps to achieve sample preparation (magnetic bead-based cell capture, cell pre-concentration and purification, and cell lysis), PCR, DNA hybridization and electrochemical detection on a single device. It has been

demonstrated to show detection of pathogenic bacteria from milliliters of whole blood samples. An integrated portable genetic analysis system for pathogen detection has been prototyped by Mathies et al. using rapid PCR amplification followed by capillary electrophoretic separation of labeled analyte and fluorescent detection, and has been demonstrated directly on *E. coli* and *Staphylococcus aureus* cells[164]. In the push for detection in smaller sample volumes, fully integrated nanoliter-volume systems have also been developed in recent years [165]. The commercially-available Cepheid GeneXpert®(GX) system employs single-use microfluidic cartridges to integrate sample preparation, amplification, and detection. Utilized by the U.S. Postal Service for the detection of anthrax spores, the GX system has been shown to be both user-friendly and effective [166, 167]. Other commercial μTAS systems for DNA analysis have also been developed by numerous microfluidic companies in a variety of formats and functionalities, including ACLARA BioSciences, Fluidigm Corporation, Affymetrix, Agilent Technologies, Alderon Biosciences, Roche Molecular Diagnostics, and Motorola Inc [15, 168].

1.6 Impact and Future Directions

The development of a fast, sensitive, multiplexed, and easy to operate pathogen sensing systems will have global impacts on healthcare, agriculture, environmental monitoring, and bio-defense. Different strategies have been used in both research and commercial settings to develop nucleic acid-based sensors and lab-on-a-chip systems. With the need for portable, disposable DNA chips to replace traditional, expensive, and bulky instrumentation, applications for DNA-sensing devices are being rapidly driven towards rapid pathogen detection, DNA sequencing, and drug discovery. Miniaturization and reliability are the main challenges to widespread distribution of

portable nucleic acid-based sensors with raw-sample-to-result functionality. One major bottleneck limiting the portability of nucleic acid-based microfluidic system lies in the difficulty of integrating sample preparation. In order to realize these handheld diagnostic systems, on-chip processing of raw samples and mastery of automated microfluidic control must be achieved. Enabling technologies discussed in this review will have a significant impact on the future development of handheld (point of care) nucleic acid-based detection systems. As mentioned in this review, dielectrophoretic (DEP) sample preparation, filtration-based separation, and immunomagnetic separation are all viable options for enriching target microorganisms from samples. Although DEP offers several advantages over other methods, such as its ability to distinguish between live and dead cells, this technology is more difficult to integrate into miniaturized systems. This is primarily due to complex electronic control architectures, and the incompatibility of this technique with heterogeneous sample matrices. At this time, filtration-based sample preparation, followed by immunomagnetic separation, is the most compatible purification technology with point of care systems. Passive methods, such as those offered by capillary forces, gravity, or creative topography are generally preferred due to lower power consumption, but battery-powered or hand-powered options can also provide a practical approach [34].

Following sample preparation, nucleic acid extraction/purification and nucleic acid detection must be addressed for the development of viable point of care detection systems. Multiple research groups have demonstrated that a microfluidic solid phase extraction approach towards nucleic extraction and purification is most compatible with miniaturized devices. The use of solid phase resins or microfabricated structures provides compatibility with microfluidic architectures and reduces the total volume of

purified nucleic acid for subsequent detection. Detection technologies must also be optimized for point of care systems. As described, fluorescence-based detection methods, such as fluorogenic real-time PCR provide extremely high sensitivity. The complexity of the detection optics may limit the applicability towards miniaturized devices, but multiple research groups, including ours, have demonstrated optical detection in portable, low-power platforms. Competing methods, such as electrical detection may not provide the needed sensitivity for nucleic acid-based detection, but could offer less complex detection components. Of the currently used electrical techniques, impedance-based methods provide the highest sensitivity with the most information-rich output, and should be further investigated. Mechanical detection methods often require complex optical or electrical analysis (such as cantilever-based techniques), which make them no better suited to point of care applications than optical methods. From this standpoint, future point of care detection systems will mostly likely be based upon a microfluidic platform using solid phase extraction, PCR amplification, and a fluorescence-based optical readout. Concurrent development of high sensitivity electrical detection methods, such as transistor-based detection, may yield effective detection elements for far-term analytical systems.

To further decrease processing time and detection limits, further investigations into technologies with even higher specificity and sensitivity are needed. Nanotechnology will play a vital role in the development of new techniques for nucleic acid detection. The implementation μTAS systems will allow for easy standardization of methods necessary for the reliability and repeatability of results. However, the need for disposability imposes a limit on the size and cost of portable sensors, hence increasing the complexity of the technology may become too uneconomical for production. Much of the current published work, however, is promising, utilizing passive microfluidic

components that are easily integrated into disposable devices. And, efforts to push towards non- or minimally instrumented diagnostic devices are in place [17].

REFERENCES

[1] Lazcka, O.; Del Campo, F.J.; Muñoz, F.X. Pathogen detection: A perspective of traditional methods and biosensors. *Biosens. Bioelectron.* **2006**, *22*, 1205-1217.

[2] Leonard, P.; Hearty, S.; Brennan, J.; Dunne, L.; Quinn, J.; Chakraborty, T.; O'Kennedy, R. Advances in biosensors for detection of pathogens in food and water. *Enzyme Microb. Technol.* **2003**, *32*, 3-13.

[3] Belgrader, P.; Benett, W.; Hadley, D.; Long, G.; Raymond Mariella, J.; Milanovich, F.; Nasarabadi, S.; Nelson, W.; Richards, J.; Stratton, P. Rapid pathogen detection using a microchip PCR array instrument. *Clin. Chem.* **1998**, *44*, 2191-2194.

[4] Chroni, C.; Kyriacou, A.; Georgaki, I.; Manios, T.; Kotsou, M.; Lasaridi, K. Microbial characterization during composting of biowaste. *Waste Manag.* **2009**, *29*, 1520-1525.

[5] Arora, K.; Chand, S.; Malhotra, B.D. Recent developments in bio-molecular electronics techniques for food pathogens. *Anal. Chim. Acta* **2006**, *568*, 259-274.

[6] Auroux, P.-A.; Koc, Y.; deMello, A.; Manz, A.; Day, P.J.R. Miniaturized nucleic acid analysis. *Lab Chip* **2004**, *4*, 534-546.

[7] Becker, H.; Gartner, C. Polymer microfabrication methods for microfluidic analytical applications. *Electrophoresis* **2000**, *21*, 12-26.

[8] Campàs, M.; Katakis, I. DNA biochip arraying, detection, and amplification strategies. *Trends. Analyt. Chem.* **2004**, *23*, 49-62.

[9] Haeberle, S.; Zengerle, R. Microfluidic platforms for lab-on-a-chip applications. *Lab Chip* **2007**, *7*, 1094-1110.

[10] Mothershed, E.A.; Whitney, A.M. Nucleic acid-based methods for the detection of bacterial pathogens: Present and future considerations for the clinical laboratory. *Clin. Chim. Acta* **2006**, *363*, 206-220.

[11] Palchetti, I.; Mascini, M. Electroanalytical biosensors and their potential for food pathogen and toxin detection. *Anal. Bioanal. Chem.* **2008**, *391*, 455-471.

[12] Ricci, F.; Volpe, G.; Micheli, L.; Palleschi, G. A review on novel developments and applications of immunosensors in food analysis. *Anal. Chim. Acta* **2007**, *605*, 111-129.

[13] Sapsford, K.E.; Bradburne, C.; Delehanty, J.B.; Medintz, I.L. Sensors for detecting biological agents. *Materials Today* **2008**, *11*, 38-49.

[14] Sassolas, A.; Leco-Bouvier, B.D.; Blum, L.J. DNA Biosensors and Microarrays. *Chem. Rev.* **2008**, *108*, 109-139.

[15] Sun, Y.; Kwok, Y.C. Polymeric microfluidic system for DNA analysis. *Anal. Chim. Acta* **2006**, *556*, 80-96.

[16] Viskari, P.J.; Landers, J.P. Unconventional detection methods for microfluidic devices. *Electrophoresis* **2006**, *27*, 1797-1810.

[17] Weigl, B.; Domingo, G.; LaBarre, P.; Gerlach, J. Towards non- and minimally instrumented, microfluidics-based diagnostic devices. *Lab Chip* **2008**, *8*, 1999-2014.

[18] Yi, C.; Li, C.-W.; Ji, S.; Yang, M. Microfluidics technology for manipulation and analysis of biological cells. *Anal. Chim. Acta* **2006**, *560*, 1-23.

[19] Zhang, C.; Xu, J.; Ma, W.; Zheng, W. PCR microfluidic devices for DNA amplification. *Biotechnol. Adv.* **2006**, *24*, 243-284.

[20] Jarvis, B.; Hedges, A.J.; Corry, J.E.L. Assessment of measurement uncertainty for quantitative methods of analysis: Comparative assessment of the precision (uncertainty) of bacterial colony counts. *Int. J. Food Microbiol.* **2007**, *116*, 44-51.

[21] Zhang, C.; Chen, W.-B.; Liu, W.-L.; Chen, C.-B. An Automated Bacterial Colony Counting System. In IEEE International Conference on Sensor Networks, Ubiquitous, and Trustworthy Computing, Taichung, Taiwan, 2008, pp. 233-240.

[22] Lamprecht, M.R.; Sabatini, D.M.; Carpenter, A.E. Cell Profiler™: free, versatile software for automated biological image analysis. *BioTechniques* **2007**, *42*, 71-75.

[23] Wang, X.; Yamaguchi, N.; Someya, T.; Nasu, M. Rapid and automated enumeration of viable bacteria in compost using a micro-colony auto counting system. *J. Microb. Methods* **2007**, *71*, 1-6.

[24] Yamazaki, W.; Taguchi, M.; Kawai, T.; Kawatsu, K.; Sakata, J.; Inoue, K.; Misawa, N. Comparison of Loop-Mediated Isothermal Amplification Assay and Conventional Culture Methods for Detection of *Campylobacter jejuni* and *Campylobacter coli* in Naturally Contaminated Chicken Meat Samples. *Appl. Environ. Microbiol.* **2009**, *75*, 1597-1603.

[25] Maglott, D.; Ostell, J.; Priott, K.D.; Tatusova, T. Entrez Gene: gene-centered information at NCBI. *Nucleic Acids Res.* **2005**, *33*, D54-D58.

[26] Winfield, M.D.; Groisman, E.A. Role of Nonhost Environments in the Lifestyles of *Salmonella* and *Escherichia coli*. *Appl. Environ. Microbiol.* **2003**, *69*, 3689-3694.

[27] Rahman, I.; Shahamat, M.; Chowdhury, M.A.; Colwell, R.R. Potential virulence of viable but nonculturable *Shigella dysenteriae* type 1. *Appl. Environ. Microbiol.* **1996**, *62*, 115-120.

[28] Effendi, I.; Austin, B. Dormant/unculturable cells of the fish pathogen *Aeromonas salmonicida*. *Microb. Ecol.* **1995**, *30*, 183-192.

[29] Rovery, C.; Greub, G.; Lepidi, H.; Casalta, J.-P. PCR Detection of Bacteria on Cardiac Valves of Patients with Treated Bacterial Endocarditis. *J. Clin. Microb.* **2005**, *43*, 163-167.

[30] Bartosch, S.; Fite, A.; Macfarlane, G.T.; McMurdo, M.E.T. Characterization of Bacterial Communities in Feces from Healthy Elderly Volunteers and Hospitalized Elderly Patients by Using Real-Time PCR and Effects of Antibiotic Tratement on the Fecal Microbiota. *Appl. Environ. Microbiol.* **2004**, *70*, 3575-3581.

[31] Rosamond, J.; Allsop, A. Harnessing the Power of the Genome in the Search for New Antibiotics. *Science* **2000**, *287*, 1973-1976.

[32] Cady, N.C.; Stelick, S.; Kunnavakkam, M.V.; Batt, C.A. Real-time PCR detection of *Listeria monocytogenes* using an integrated microfluidics platform. *Sens. Actuators. B Chem.* **2005**, *107*, 332-341.

[33] Dineva, M.A.; Mahilum-Tapay, L.; Lee, H. Sample preparation: a challenge in the development of point-of-care nucleic acid-based assays for resource-limited settings. *Analyst* **2007**, *132*, 1193-1199.

[34] Chin, C.D.; Linder, V.; Sia, S.K. Lab-on-a-chip devices for global health: Past studies and future opportunities. *Lab Chip* **2007**, *7*, 41-57.

[35] Linder, V. Microfluidics at the crossroad with point-of-care diagnostics. *Analyst* **2007**, *132*, 1186-1192.

[36] Manz, A.; Graber, N.; Wildmer, H.M. Miniaturized total chemical analysis systems: a novel concept for chemical sensing. *Sens. Actuators. B Chem.* **1990**, *1*, 240-248.

[37] Qi, S.; Liu, X.; Ford, S.; Barrows, J.; Thomas, G.; Kelly, K.; McCandless, A.; Lian, K.; Goettert, J.; Soper, S.A. Microfluidic devices fabricated in poly(methyl methacrylate) using hot-embossing with integrated sampling capillary and fiber optics for fluorescence detection. *Lab Chip* **2002**, *2*, 88-95.

[38] Narasimhan, J.; Paputsky, I. Polymer embossing tools for rapid prototyping of plastic microfluidic devices. *J. Micromech. Microeng.* **2004**, *14*, 96-103.

[39] Mair, D.A.; Geiger, E.; Pisano, A.P.; Frechet, J.M.J.; Svec, F. Injection molded microfluidic chips featuring integrated interconnects. *Lab Chip* **2006**, *6*, 1346-1354.

[40] Xia, Y.; Whitesides, G.M. Soft Lithography. *Angew. Chem.* **1998**, *37*, 550-575.

[41] Duncan, A.C.; Weisbuch, F.; Rouais, F.; Lazare, S.; Baquey, C. Laser microfabricated model surfaces for controlled cell growth. *Biosens. Bioelectron.* **2002**, *17*, 413-426.

[42] Mappes, T.; Achenbach, S.; Mohr, J. X-ray lithography for devices with high aspect ratio polymer submicron structures. *Microelec. Eng.* **2007**, *84*, 1235-1239.

[43] Garstecki, P.; Fuerstman, M.J.; Fischbach, M.A.; Sia, S.K.; Whitesides, G.M. Mixing with bubbles: a practical technology for use with portable microfluidic devices. *Lab Chip* **2006**, *6*, 207-212.

[44] Laser, D.J.; Santiago, J.G. A review of micropumps. *J. Micromech. Microeng.* **2004**, *14*, R35-R64.

[45] Kruger, J.; Singh, K.; O'Neill, A.; Jackson, C.; Morrison, A.; O'Brien, P. Development of a microfluidic device for fluorescence activated cell sorting. *J. Micromech. Microeng.* **2002**, *12*, 486-494.

[46] Cabrera, C.R.; Yager, P. Continuous concentration of bacteria in a microfluidic flow cell using electrokinetic techniques. *Electrophoresis* **2000**, *22*, 355-362.

[47] Cady, N.C.; Stelick, S.; Batt, C.A. Nucleic acid purification using microfabricated silicon structures. *Biosens. Bioelectron.* **2003**, *19*, 59-66.

[48] Li, S.; Fozdar, D.; Ali, M.F.; Li, H.; Shao, D.; Vykoukal, D.M.; Vykoukal, J.; Floriano, P.N.; Olsen, M.; McDevitt, J.T.; Gascoyne, P.R.C.; Chen, S. A Continuous-Flow Polymerase Chain Reaction Microchip With Regional Velocity Control. *J. Microelectromech. Syst.* **2006**, *15*, 223-236.

[49] Roxhed, N.; Rydholm, S.; Samuel, B.; Van der Wijngaart, W.; Griss, P.; Stemme, G. A compact, low-cost microliter-range liquid dispenser based on expandable microspheres. *J. Micromech. Microeng.* **2006**, *16*.

[50] Cooney, C.G.; Towe, B.C. A thermopneumatic dispensing micropump. *Sens. Actuators. A Phys.* **2004**, *116*, 519-524.

[51] Zeng, S.; chen, C.-H.; James C. Mikkelsen, J.; Santiago, J.G. Fabrication and characterization of electroosmotic micropumps. *Sens. Actuators. B Chem.* **2001**, *79*, 107-114.

[52] Machauf, A.; Nemirovsky, Y.; Dinnar, U. A membrane micropump electrostatically actuated across the working fluid. *J. Micromech. Microeng.* **2005**, *15*, 2309-2316.

[53] Sounart, T.L.; Michalske, T.A.; Zavadil, K.R. Frequency-dependent electrostatic acutation in microfluidic MEMS. *J. Microelectromech. Syst.* **2005**, *14*, 125-133.

[54] Kock, M.; Harris, N.; Evans, A.G.R.; White, N.M.; Brunnschweiler, A. A novel micromachined pump based on thick-film piezoelectric actuation. *Sens. Actuators. A Phys.* **1998**, *70*, 98-103.

[55] Yang, Z.; Matsumoto, S.; Goto, H.; Matsumoto, M.; Maeda, R. Ultrasonic micromixer for microfluidic systems. *Sens. Actuators. A Phys.* **2001**, *93*, 266-272.

[56] Graf, N.J.; Bowser, M.T. A soft-polymer piezoelectric bimorph cantilever-actuated persitaltic micropump. *Lab Chip* **2008**, *8*, 1664-1670.

[57] Lemoff, A.V.; Lee, A.P. An AC magnetohydrodynamic micropump. *Sens. Actuators. B Chem.* **2000**, *63*, 178-185.

[58] Rinderknecht, D.; Hickerson, A.I. A valveless micro impedance pump driven by electromagnetic actuation. *J. Micromech. Microeng.* **2005**, *15*, 861-866.

[59] Yamamata, C.; Lotto, C.; Al-Assaf, E.; Gijs, M.A.M. A PMMA valveless micropump using electromagnetic actuation. *Microfluid. Nanofluidics* **2005**, *1*, 197-207.

[60] Harmon, M.E.; Tang, M.; Frank, C.W. A microfluidic actuator based on thermoresponsive hydrogels. *Polymer* **2003**, *44*, 4547-4556.

[61] Bassetti, M.J.; Chatterjee, A.N.; Aluru, N.R.; Beebe, D.J. Development and modeling of electrically triggered hydrogels for microfluidic applications. *J. Microelectromech. Syst.* **2005**, *14*, 1198-1207.

[62] Bohm, S.; Timmer, B.; Olthuis, W.; Bergveld, P. A closed-loop controlled electrochemically actuated micro-dosing system. *J. Micromech. Microeng.* **2000**, *10*, 498-504.

[63] Metref, L.; Herrera, F.; Berdat, D.; Gijs, M.A.M. Contactless Electrochemical Actuator for Microfluidic Dosing. *J. Microelectromech. Syst.* **2007**, *16*, 885-892.

[64] Squires, T.M.; Quake, S.R. Microfluidics: Fluid physics at the nanoliter scale. *Rev. Mod. Phys.* **2005**, *77*.

[65] Yu, Q.; Bauer, J.M.; Moore, J.S.; Beebe, D.J. Responsive biomimetic hydrogel valve for microfluidics. *Appl. Phys. Lett.* **2001**, *78*, 2589-2591.

[66] Studer, V.; Hang, G.; Pandolfi, A.; Ortiz, M.; Anderson, W.F.; Quake, S.R. Scaling properties of a low-actuation pressure microfluidic valve. *J. Appl. Phys.* **2004**, *95*, 393-398.

[67] Selvaganapathy, P.; Carlen, E.T.; Mastangelo, C.H. Electrothermally actuated inline microfluidic valve. *Sens. Actuators. A Phys.* **2003**, *104*, 275-282.

[68] Grover, W.H.; Skelley, A.M.; Liu, C.N.; Lagally, E.T.; Mathies, R.A. Monolithic membrane valves and diaphram pumps for practical large-scale integration into glass microfluidic devices. *Sens. Actuators. B Chem.* **2003**, *89*, 315-323.

[69] Liu, R.H.; Bonanno, J.; Yang, J.; Lenigk, R.; Grodzinski, P. Single-use, thermally actuated paraffin valves for microfluidic applications. *Sens. Actuators. B Chem.* **2004**, *98*, 328-336.

[70] Feng, Y.; Zhou, Z.; Ye, X.; Xiong, J. Passive valves based on hydrophobic microfluidics. *Sens. Actuators. A Phys.* **2003**, *108*, 138-143.

[71] Hua, S.Z.; Sachs, F.; Yang, D.X.; Chopra, H.D. Microfluidic Actuation Using Electrochemically Generated Bubbles. *Anal. Chem.* **2002**, *74*, 6392-6396.

[72] Stoeber, B.; Yang, Z.; Liepmann, D.; Muller, S.J. Flow control in microdevices using thermally responsive triblock copolymers. *J. Microelectromech. Syst.* **2005**, *14*, 207-213.

[73] Lu, L.-H.; Ryu, K.S.; Liu, C. A magnetic microstirrer and array for microfluidic mixing. *J. Microelectromech. Syst.* **2002**, *11*, 462-469.

[74] Ryu, K.S.; Shaikh, K.; Goluch, E.; Fan, Z.; Liu, C. Micro magnetic stir-bar mixer integrated with parylene microfluidic channels. *Lab Chip* **2004**, *4*, 604-613.

[75] Tsai, J.-H.; Lin, L. Active microfluidic mixer and gas bubble filter driven by thermal bubble micropump. *Sens. Actuators. A Phys.* **2002**, *97-98*, 665-671.

[76] Suzuki, H.; Ho, C.-M.; Kasagi, N. A Chaotic Mixer for Magnetic Bead-Based Micro Cell Sorter. *J. Microelectromech. Syst.* **2004**, *13*, 779-790.

[77] Stroock, A.D.; Dertinger, S.K.W.; Ajdari, A.; Mezic, I.; Stone, H.A.; Whitesides, G.M. Chaotic Mixer for Microchannels. *Science* **2002**, *295*, 647-651.

[78] Hong, C.-C.; Choi, J.-W.; Ahn, C.H. A novel in-plane passive microfluidic mixer with modified Tesla structures. *Lab Chip* **2004**, *4*, 109-113.

[79] Lin, Y.-C.; Chung, Y.-C.; Wu, C.-Y. Mixing enhancement of the passive microfluidic mixer with J-shaped baffles in the tee channel. *Biomed. Microdevices* **2007**, *9*, 215-221.

[80] Jacobson, S.C.; McKnight, T.E.; Ramsey, J.M. Microfluidic devices for electrokinetically driven parallel and serial mixing. *Anal. Chem.* **1999**, *71*, 4455-4459.

[81] Song, S.; Singh, A.K. On-chip sample preconcentration for integrated microfluidic analysis. *Anal. Bioanal. Chem.* **2005**, *38*, 41-43.

[82] Han, K.-H.; Frazier, A.B. Continuous magnetophoretic separation of blood cells in microdevice format. *J. Appl. Phys.* **2004**, *96*, 5797.

[83] Inglis, D.W.; Riehn, R.; Austin, R.H.; Sturm, J.C. Continuous microfluidic immunomagnetic cell separation. *Appl. Phys. Lett.* **2004**, *85*, 5093.

[84] Lee, H.; Purdon, A.M.; Westervelt, R.M. Manipulation of biological cells using a microelectromagnet matrix. *Appl. Phys. Lett.* **2004**, *85*, 1063.

[85] Grodzinski, P.; Yang, J.; Liu, R.H.; Ward, M.D. A Modular Microfluidic System for Cell Pre-concentration and Genetic Sample Preparation. *Biomed. Microdevices* **2003**, *5*, 303-310.

[86] Cui, L.; Zhang, T.; Morgan, H. Optical particle detection integrated in a dielectrophoretic lab-on-a-chip. *J. Micromech. Microeng.* **2002**, *12*, 7-12.

[87] Huang, Y.; Rubinsky, B. Flow-through micro-electroporation chip for high efficiency single-cell genetic manipulation. *Sens. Actuators. A Phys.* **2003**, *104*, 205-212.

[88] Li, H.; Bashir, R. On the Design and Optimization of Micro-Fluidic Dielectrophoretic Devices: A Dynamic Simulation Study. *Biomed. Microdevices* **2004**, *6*, 289-295.

[89] Cui, L.; Holmes, D.; Morgan, H. The dielectrophoretic levitation and separation of latex beads in microchips. *Electrophoresis* **2001**, *22*, 3893-3901.

[90] Zhu, L.; Zhang, Q.; Feng, H.; Ang, S.; Chau, F.S.; Liu, W.-T. Filter-based microfluidic device as a platform for immunofluorescent assay of microbial cells. *Lab Chip* **2004**, *4*, 337-341.

[91] Khademhosseini, A.; Yeh, J.; Jon, S.; Eng, G.; Suh, K.Y.; Burdick, J.A.; Langer, R. Molded polyethylene glycol microstructures for capturing cells within microfluidic channels. *Lab Chip* **2004**, *4*, 425-430.

[92] Tani, H.; Maehana, K.; Kamidate, T. Chip-based bioassay using bacterial sensor strians immobilized in three-dimensional microfluidic network. *Anal. Chem.* **2004**, *76*, 6693-6697.

[93] Chang, W.C.; Lee, L.P.; Liepmann, D. Biomimetic technique for adhesion-based collection and separation of cels in a microfluidic channel. *Lab Chip* **2005**, *5*, 64-73.

[94] Chen, T.; Small, D.A.; McDermott, M.K.; Bentley, W.E.; Payne, G.F. Enzymatic Methods for *in situ* Cell Entrapment and Cell Release. *Biomacromolecules* **2003**, *4*, 1558-1563.

[95] Irimia, D.; Tompkins, R.G.; Toner, M. Single-cell chemical lysis in picoliter-scale closed volumes using a microfabricated device. *Anal. Chem.* **2004**, *76*, 6137-6143.

[96] Carlo, D.D.; Ionescu-Zanetta, C.; Zhang, Y.; Hung, P.; Lee, L.P. On-chip cell lysis by local hydroxide generation. *Lab Chip* **2005**, *5*, 171-178.

[97] Huang, Y.; Maher, E.L.; Bell, J.L.; Madou, M. MEMS-based sample preparation for molecular diagnostics. *Anal. Bioanal. Chem.* **2002**, *372*, 49-65.

[98] Griffiths, L.J.; Anyim, M.; Doffman, S.R.; Wilks, M.; Millar, M.R.; Agrawal, S.G. Comparison of DNA extraction methods for *Aspergillus fumigatus* using real-time PCR. *J. Med. Microb.* **2006**, *55*, 1187-1191.

[99] Lee, J.-G.; Cheong, K.H.; Huh, N.; Kim, S.; Choi, J.-W.; Ko, C. Microchip-based one step DNA extraction and real-time PCR in one chamber for rapid pathogen identification. *Lab Chip* **2006**, *6*, 886-895.

[100] Lu, H.; Schmitdt, M.A.; Jensen, K.F. A microfluidic electroporation device for cell lysis. *Lab Chip* **2005**, *5*, 23-29.

[101] Wang, H.-Y.; Bhunia, A.K.; Lu, C. A microfluidic flow-through device for high throughput electrical lysis of bacterial cells based on continuous dc voltage. *Biosens. Bioelectron.* **2006**, *22*, 582-588.

[102] Fox, M.B.; Esveld, D.C.; Valero, A.; Luttge, R.; Mastwijk, H.C.; Bartels, P.V.; Van den Berg, A.; Boom, R.M. Electroporation of cells in microfluidic devices: a review. *Anal. Bioanal. Chem.* **2006**, *385*, 474-485.

[103] Higgins, J.A.; Nasarabadi, S.; Karns, J.S.; Shelton, D.R.; Cooper, M.; Gbakima, A.; Koopman, R.P. A handheld real time thermal cycler for bacterial pathogen detection. *Biosens. Bioelectron.* **2003**, *18*, 1115-1123.

[104] Koh, C.G.; Tan, W.; Zhao, M.Q.; Ricco, A.J.; Fan, Z.H. Integrating polymerase chain reaction, valving, and electrophoresis in a plastic device for bacterial detection. *Anal. Chem.* **2003**, *75*, 4591-4598.

[105] Liu, J.; Enzelberger, M.; Quake, S. A nanoliter rotary device for polymerase chain reaction. *Electrophoresis* **2002**, *23*, 1531-1536.

[106] Saiki, R.K.; Scharf, S.; Faloona, F.; Mullis, K.B.; Horn, G.T.; Erlich, H.A.; Arnheim, N. Enzymatic amplification of betaglobin genomic sequences and restruction site analysis for diagnosis of sickle cell anemia. *Science* **1985**, *230*, 1350-1354.

[107] Northrup, M.A.; Ching, M.T.; White, R.M.; Watson, R.T. DNA amplification in a microfabricated reaction chamber. In, Yokohama, Japan, Year, pp. 924-926.

[108] Giordano, B.C.; Ferrance, J.; Swedberg, S.; Huhmer, A.F.R.; Landers, J.P. Polymerase chain reaction in polymeric microchips: DNA amplification in less than 240 seconds. *Anal. Biochem.* **2001**, *291*, 124-132.

[109] Lin, Y.-C.; Huang, M.-Y.; Young, K.-C.; Chang, T.-T.; Wu, C.-Y. A rapid micro-polymerase chain reaction system for hepatitis C virus amplification. *Sens. Actuators. B Chem.* **2000**, *71*, 2-8.

[110] Schneegass, I.; Kohler, J.M. Flow-through polymerase chain reactions in chip thermocyclers. *Mol. Biotechnol.* **2001**, *82*, 101-121.

[111] Sun, K.; Yamaguchi, A.; Ishida, Y.; Matsuo, S.; Misawa, H. A heater-integrated transparent microchannel chip for continuous-flow PCR. *Sens. Actuators. B Chem.* **2002**, *84*, 283-289.

[112] Ottesen, E.A.; Hong, J.W.; Quake, S.R.; Leadbetter, J.R. Microfluidic Digital PCR Enables Multigene Analysis of Inidividual Environmental Bacteria. *Science* **2006**, *314*, 1464-1467.

[113] Marcus, J.S.; Anderson, W.F.; Quake, S.R. Parallel Picoliter RT-PCR Assays Using Microfluidics. *Anal. Chem.* **2006**, *78*, 956-958.

[114] Lagally, E.T.; Emrich, C.A.; Mathies, R.A. Fully integrated PCR-capillary electrophoresis microsystem for DNA analysis. *Lab Chip* **2001**, *1*, 102-107.

[115] Waggoner, A. Fluorescent labels for proteomics and genomics. *Curr. Opin. Chem. Biol.* **2006**, *10*, 62-66.

[116] LePecq, J.B.; Paoletti, C. A fluorescent complex between ethidium bromide and nucleic acids. Physical-chemical characterization. *J. Mol. Biol.* **1967**, *27*, 87-106.

[117] Rye, H.S.; Dabora, J.M.; Quesada, M.A.; Mathies, R.A.; Glazer, A.N. Fluorometrix assay using dimeric dyes for double and single stranded DNA and RNA with picogram sensitivity. *Anal. Biochem.* **1993**, *208*, 144-150.

[118] Rengarajan, K.; Cristol, S.M.; Mehta, M.; Nickerson, J.M. Quantifying DNA concentrations using fluorometry: a comparison of fluorophores *Mol. Vis.* **2002**, *8*, 416-421.

[119] Mackay, J.; Landt, O. Real-Time PCR Fluorescent Chemistries. In *Protocols for Nucleic Acid Analysis by Nonradioactive Probes*, 2nd Edition Ed.; Hilario, E., Mackay, J., Ed.^Eds.; Humana Press, 2007; 353 353, pp. 237-261,

[120] Taylor, J.R.; Fang, M.M.; Nie, S. Probing specific sequences on single DNA moleucles with bioconjugated fluorescent nanoparticles. *Anal. Chem.* **2000**, *72*, 1979-1986.

[121] Hong, J.W.; Fujui, T.; Seki, M.; Yamamoto, T.; Endo, I. Integration of gene amplification and capillary gel electrophoresis on a polydimethylsiloxane-glass hybrid microchip. *Electrophoresis* **2001**, *22*, 328-333.

[122] Dasgupta, P.K.; Eom, I.; Morris, K.J.; Li, J. Light emitting diode-based detectors absorbance, fluorescence, and spectroelectrochemical measurements in a planar flow-through cell. *Anal. Chim. Acta* **2003**, *500*, 337-364.

[123] Belgrader, P.; Young, S.; Yuan, B.; Primeau, M.; Christel, L.A.; Pourahmadi, F.; Northrup, M.A. A Battery-Powered Notebook Thermal Cycler for Rapid Multiplex Real-Time PCR Analysis. *Anal. Chem.* **2001**, *73*, 286-289.

[124] Paegel, B.M.; Blazej, R.G.; Mathies, R.A. Microfluidic devices for DNA sequencing: sample preparation and electrophoretic analysis. *Curr. Opin. Chem. Biol.* **2003**, *14*, 42-50.

[125] Brockman, J.M.; Frutos, A.G.; Corn, R.M. A multistep chemical modification procedure to create DNA arrays on gold surfaces for the study of protein-DNA interactions with surface plasmon resonance imaging. *J. Am. Chem. Soc.* **1999**, *121*, 8044-8051.

[126] Geudon, P.; Livache, T.; Martin, F.; Lesbre, F.; Roget, A.; Bidan, G.; Levy, Y. Characterization and optimization of a real-time, parallel, label-free, polypyrrole-based DNA sensor by surface plasmon resonance imaging. *Appl. Chem.* **2000**, *72*, 6003-6009.

[127] Lehr, H.P.; Reimann, M.; Brandenburg, A.; Sulz, G.; Klapproth, H. Real-time detection of nucleic acid interactions by total internal reflection fluorescence. *Anal. Chem.* **2003**, *75*, 2414-2420.

[128] McDonnell, J.M. Surface plasmon resonance: towards an understanding of the mechanisms of biological molecular recognition. *Curr. Opin. Chem. Biol.* **2001**, *5*, 572-577.

[129] Lesuffleur, A.; Im, H.; Lindquist, N.C.; Lim, K.S.; Oh, S.-H. Laser-illuminated nanohole arrays for multiplex plasmonic microarray sensing. *Opt. Express* **2008**, *16*, 219-224.

[130] Usui-Aoki, K.; Shimada, K.; Nagano, M.; Kawai, M.; Koga, H. A novel approach to protein expression profiling using antibody microarrays combined with surface plasmon resonance technology. *Proteomics* **2005**, *5*, 2396-2401.

[131] Cao, Y.C.; Jin, R.; Mirkin, C.A. Nanoparticles with Raman Spectroscopic Fingerprints for DNA and RNA Detection. *Science* **2002**, *297*, 1536-1540.

[132] Fabris, L.; Dante, M.; Braun, G.; lee, S.J.; Reich, N.O.; Moskovits, M.; Nguyen, T.-Q.; Bazan, G.C. A Heterogeneous PNA-based SERS method for DNA detection. *J. Am. Chem. Soc.* **2007**, *129*, 6086-6087.

[133] Docherty, F.T.; Monaghan, P.B.; Keir, R.; Graham, D. The first SERRS multiplexing from labelled oligonucleotides in a microfluidics lab-on-a-chip. *Chem. Commun.* **2004**, 118-119.

[134] Erdemm, A.; Pividori, M.I.; Lermo, A.; Bonanni, A.; Del Valle, M.; Alegret, S. Genomagnetic assay based on label-free electrochemical detection using magneto-composite electrodes. *Sens. Actuators. B Chem.* **2005**, *114*, 591-598.

[135] Berney, H.; West, J.; Haefele, E.; Alderman, J.; Lane, W.; Collins, J.K. A DNA diagnostic biosensor: development, characterisation and performance. *Sens. Actuators. B Chem.* **2000**, *68*, 100-108.

[136] Wang, J.; Rivas, G.; Cai, X. Screen-printed electrochemcial hybridization biosensor for the detection of DNA sequences from the *Escherichia coli* pathogen. *Electroanalysis* **2005**, *9*, 395-398.

[137] Pingarron, J.M.; Yanez-Sedeno, P.; Gonzalez-Cortes, A. Gold nanoparticle-based electrochemical biosensors. *Electrochim. Acta* **2008**, *53*, 5848-5866.

[138] Guo, S.; Wang, E. Synthesis and electrochemical applications of gold nanoparticles. *Anal. Chim. Acta* **2007**, *598*, 181-192.

[139] Castaneda, M.T.; Merkoci, A.; Pumera, M.; Alegret, S. Electrochemical genosensors for biomedical applications based on gold nanoparticles. *Biosens. Bioelectron.* **2006**, *22*, 1961-1967.

[140] Cheng, G.; Zhao, J.; Tu, Y.; He, P.; Fang, Y. A sensitive DNA electrochemical biosensor based on magnetite with a glassy carbon electrode modified by multi-walled carbon nanotubes in polypyrrole. *Anal. Chim. Acta* **2005**, *533*, 11-16.

[141] Eggins, B.R. *Chemical Sensors and Biosensors*, Ed.; John Wiley & Sons Ltd., 2002.

[142] Abdel-Hamid, I.; Ivnitski, D.; Atanasov, P.; Wilkins, E. Flow-through immunofiltration assay system for rapid detection of *E. coli* O157:H7. *Biosens. Bioelectron.* **1999**, *14*, 309-316.

[143] Baeumner, A.J.; Cohen, R.N.; Miksic, V.; Min, J. RNA biosensor for the rapid detection of viable *Escherichia coli* in drinking water. *Biosens. Bioelectron.* **2002**, *18*, 405-413.

[144] Bergveld, P. Thirty years of ISFETOLOGY: What happened in the past 30 years and what may happen in the next 30 years. *Sens. Actuators. B Chem.* **2003**, *88*, 1-20.

[145] Alocilja, E.C.; Radke, S.M. Market analysis of biosensors for food safety. *Biosens. Bioelectron.* **2003**, *18*, 841-846.

[146] Barssoukov, E.; Macdonald, J.R. *Impedance Spectroscopy Theory, Experiment and Applications*, Ed.; John Wiley & Sons Ltd.: Hoboken, New Jersey, 2005.

[147] Radke, S.M.; Alocilja, E.C. A high density microelectrode array biosensor for detection of *E. coli* O157:H7. *Biosens. Bioelectron.* **2005**, *20*, 1662-1667.

[148] Muhammad-Tahir, Z.; Alocilja, E.C. A conductometric biosensor for biosecurity. *Biosens. Bioelectron.* **2003**, *18*, 813-819.

[149] Pal, S.; Alocilja, E.C.; Downes, F.P. Nanowire labeled direct-charge transfer biosensor for detection *Bacillus* species. *Biosens. Bioelectron.* **2007**, *22*, 2329-2336.

[150] Gheorghe, M.; Guiseppi-Elie, A. Electrical frequency dependent characterization of DNA hybridization. *Biosens. Bioelectron.* **2003**, *19*, 95-102.

[151] Hang, T.C.; Guiseppi-Elie, A. Frequency dependent and surface characterization of DNA immobilization and hybridization. *Biosens. Bioelectron.* **2004**, *19*, 1537-1548.

[152] Tombelli, S.; Mascini, M.; Sacco, M.; Turner, A.P. A DNA piezoelectric biosensor assay coupled with a PCR for bacterial toxicity determination in environmental samples. *Anal. Chim. Acta* **2000**, *418*, 1-9.

[153] Liu, T.; Tang, J.; Jiang, L. Sensitivity enhancement of DNA sensors by nanogold surface modification. *Biochem. Biophys. Res. Commun.* **2002**, *295*, 14-16.

[154] Fritz, J.; Baller, M.K.; Lang, H.P.; Rothuizen, H.; Vettiger, P.; Meyer, E.; Guntherodt, H.; Gerber, C.; Gimzewski, J.K. Translating biomolecular recognition into nanomechanics. *Science* **2000**, *288*, 316-318.

[155] Liu, F.; Zhang, Y.; Ou-Yang, Z. Flexoelectric origin of nanomechanic deflection in DNA-microcantilever system. *Biosens. Bioelectron.* **2003**, *18*, 655-660.

[156] Hansen, K.M.; Ji, F.; Wi, G.; Datar, R.; Cote, R.; Majumdar, A.; Thundat, T. Cantilever-based optical deflection assay for discrimination of DNA single-nucleotide mismatches. *Anal. Chem.* **2001**, *73*, 1567-1571.

[157] Koh, C.G.; Tan, W.; Zhao, M.-q.; Ricco, A.J.; Fan, Z.H. Integrating polymerase chain reaction, valving, and electrophoresis in a plastic device for bacterial detection. *Anal. Chem.* **2003**, *75*, 4591-4598.

[158] Hong, J.W.; Studer, V.; Hang, G.; Anderson, W.F.; Quake, S.R. A nanoliter-scale nucleic acid processor with parallel architecture. *Nat. Biotechnol.* **2004**, *22*, 435-439.

[159] Taylor, M.T.; Belgrader, P.; Joshi, R.; Kintz, G.A.; Northrup, M.A. Fully automated sample preparation for pathogen detection performed in a microfluidic cassette. In, Kluwer, Boston, USA, Year, p. 670.

[160] Liu, R.H.; Yang, J.; Lenigk, R.; Bonanno, J.; Grodzinski, P. Self-contained, fully integrated biochip for sample preparation, polymerase chain reaction amplification, and DNA microarray detection. *Anal. Chem.* **2004**, *76*, 1824-1831.

[161] Yeung, S.S.W.; Lee, T.M.H.; Hsing, I.-M. Electrochemistry-Based Real-Time PCR on a Microchip. *Anal. Chem.* **2008**, *80*, 363-368.

[162] Yeung, S.-W.; Lee, T.M.-H.; Cai, H.; Hsing, I.-M. A DNA biochip for on-the-spot multiplexed pathogen identification. *Nucleic Acids Res.* **2006**, *34*, e118.

[163] Eckersten, A.; Orlefors, A.E.; Ellstrom, C.; Erickson, K.; Lofman, E.; Eriksson, A.; Eriksson, S.; Jorsback, A. High-throughput SNP scoring in a disposable microfabricated CD device. In, Kluwer, Enschede, Netherlands, Year, p. 521.

[164] Lagally, E.T.; Scherer, J.R.; Blazej, R.G.; Toriello, N.M.; Diep, B.A.; Ramchandani, M.; Sensabaugh, G.F.; Riley, L.W.; Mathies, R.A. Integrated portable genetic analysis microsystem for pathogen/infectious disease detection. *Anal. Chem.* **2004**, *76*, 3162-3170.

[165] Blazej, R.G.; Kumaresan, P.; Mathies, R.A. Microfabricated bioprocessor for integrated nanoliter-scale Sanger DNA sequencing. *Proc. Natl. Acad. Sci. U.S.A.* **2006**, *103*, 7240-7245.

[166] Holland, C.A.; Kiechle, F.L. Point-of-care molecular diagnostic systems - past, present, and future. *Curr. Opin. Microbiol.* **2005**, *8*, 504-509.

[167] Ulrich, M.P.; Christensen, D.R.; Coyne, S.R.; Craw, P.D.; Henchal, E.A.; Sakai, S.H.; Swenson, D.; Tholath, J.; Tsai, J.; Weir, A.F.; Norwood, D.A. Evaluation of the Cepheid GeneXpert® system for detecting Bacillus anthracis. *J. Appl. Microbiol.* **2006**, *100*, 1011-1016.

[168] Lee, T.M.-H.; Hsing, I.-M. DNA-based bioanalytical microsystems for handheld devices applications. *Anal. Chim. Acta* **2006**, *556*, 26-37.

CHAPTER 2

MICRO AND NANOCANTILEVER-BASED SENSORS FOR SINGLE CELL AND SINGLE-MOLECULE BIOAPPLICATIONS

2.0 Introduction

The development of the field of micromechanical and microelectromechanical (MEMS) systems has enabled the exploration of new mechanical transduction modes, spawning an innovative family of chemical and biological sensors. Prior to the late 1980's, the primary modes of transduction used in sensors fell under the categories of thermal, mass, electrochemical, and optical [1]. The widespread use of atomic force microscopy (AFM) and the development and significant improvements to microfabricated AFM probes signifies an important trend in technological approaches to MEMS sensors. In recent years, however, we have seen advances in sensor technology in response to the demand for faster, user-friendly, inexpensive and highly sensitive methods for recognition of biological and chemical molecules. The field chemical and biological detection and monitoring is progressing at a rapid rate, driving the limits of detection down to the level of a single cell or single molecule, and spurring on the development of innovative MEMS sensors for widespread applications in basic research, healthcare, medical diagnostics, environmental screening, drug screening, and military applications, among others.

Modeled after the microfabricated probes commonly used in atomic force microscopy (AFM), cantilever-based sensors constitute a promising area for microbiosensor and nanobiosensor development. The attraction and potential of microcantilevers lies in their ability to transduce a number of different phenomena, such as changes in mass, temperature, and surface stress into quantifiable changes in bending and shifts in resonant frequency. The high sensitivity of this technique allows for high resolution and label-free detection and analysis of cellular and molecular measurements. In addition, the ease of integration of this technology into a multiplexed automated

system lends to its appeal by allowing for parallelization and scalability. To date, a multitude of reviews on cantilever-based biosensor systems for a multitude of applications have been published [1, 3-8], demonstrating great interest in the development of this field. A comprehensive literature survey was carried out for this present paper, and due to the immense amount of literature related to this topic, our study focuses primarily on micro and nanocantilever-based sensors for single-cell and single-molecule applications. In this review, we highlight current developments and directions in cantilever-based sensors. A variety of different cantilever designs, fabrication protocols, detection schemes and applications will be detailed. Discussions will also include strategies and challenges for future implementation into an integrated platform.

2.1 Cantilever fabrication and transduction mechanisms

Microcantilevers are typically fashioned from silicon, silicon nitride or silicon oxide materials, which are commercially available in the form of AFM probes with a variety of different shapes and dimensions. Arrays of 10 to thousands of microcantilevers can be batch fabricated on a single wafer, which shows great promise for parallel, fast, and real-time monitoring of thousands of targets without labeling. By taking advantage of the well-established thin film processing technologies of the semiconductor industry, cantilever fabrication can be performed with low cost, high yield, and excellent reproducibility. When these cantilevers are fabricated in the nanoscale, the expected limits of detection fall into the femtomole to attomole range, with the possibility of single-molecule detection in real time [7]. The standard fabrication process generally involves thin-film deposition, photolithographic patterning and etching, and surface and bulk micromachining. Typically, a sacrificial layer is deposited onto a pre-

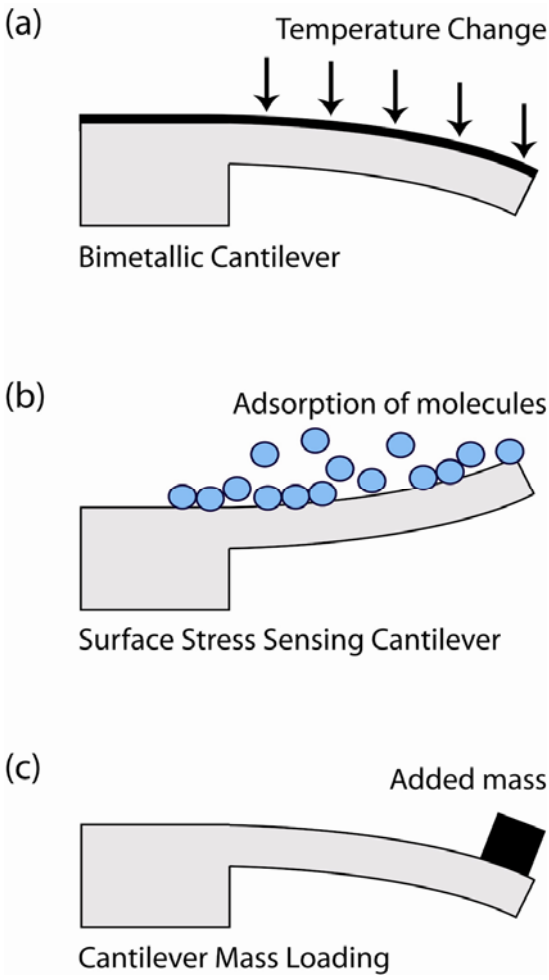

Figure 2-1. Schematic drawings of cantilever transduction principles: (a) a bimetallic temperature and heat sensing cantilever in which the two layers react differently to changes in temperature, causing bending of the cantilever (b) surface stress sensing cantilever upon the adsorption of molecules, whereupon surface stress caused by the interactions between the molecules bends the cantilever (c) detection of additional mass loading of the cantilever by an added mass at the free tip.

patterned substrate before the deposition and patterning of the stress-free structural layer. The structural layer must be uniform and stress-free in order to ensure identical cantilevers across the wafer and to avoid initial cantilever deformation. The details of cantilever design and fabrication are largely defined by the choice of sensor operation, readout method, and specific applications.

Microcantilevers can be visualized as miniaturized diving boards, with a clamped end and a free end. When a force is applied to the free end of the cantilever, the mechanical behavior can be described using Hooke's law:

$$F = -k_{spring}\Delta z \ ,$$

where the deflection Δz is directly proportional to the applied force F, and the cantilever spring constant k_{spring} determines the flexibility and sensitivity of a cantilever. Assuming a rectangular cantilever beam, the spring constant can be defined by its dimension and material constants:

$$k_{spring} = \frac{Ewt^3}{4tL^3}$$

where E is the Young's modulus of the cantilever, w is the cantilever width, t is the thickness, and L is the length. Lower spring constants typically lead to the higher measurement sensitivity, particularly when operating in the static mode, but are noise-limited by the thermal motion of the cantilever [9]. Cantilevers made of softer materials are often more desirable for static deflection mechanisms. Investigation into using polymers, such as SU-8, as cantilever material has been shown to be successful and almost equally inexpensive, fast, and reliable, though there are challenges

associated with achieving stable immobilization of biomolecules onto polymer surfaces [7].

As shown in Figure 2-1, there are three main mechanisms that a microcantilever can use to transduce a recognition event into micromechanical motion: (1) the bimetal or heat mode where bending motion of the cantilever caused by a change in temperature, (2) surface stress or static mode where changes on the surface of an asymmetrical cantilever creates a mechanical stress leading to an expansion or contraction of one side of the cantilever, and (3) the dynamic or resonance mode where a frequency shift or change in force constant occurs due to additional mass loading or viscosity changes [5]. For biosensing applications, the first two mechanisms typically more commonly employed due to compatibility. Some other transduction mechanisms that have been investigated using microcantilevers include depositing magnetic material or trapping magnetic beads on the cantilever surface for subsequent manipulation and detection with an electromagnet [10-12].

In the dynamic or resonance mode of cantilever operation, the resonance frequency of an oscillating cantilever can be expressed as:

$$f = \frac{1}{2\pi}\sqrt{\frac{k}{m^*}}$$

where k is the spring constant and m^* is the effective mass of the cantilever. When mass loading with a force of F applied at the end of the cantilever causes an end deflection of *h*, the fundamental resonant frequency can be written as:

$$f = \frac{t}{2\pi(0.98)L^3}\sqrt{\frac{E}{\rho}}$$

where ρ is the density of the cantilever material and t and L are the thickness and length, respectively. The changes in the mass and in the spring constant cause a shift in the resonance frequency, which can therefore be written as follows [13]:

$$df(m^*, K) = \left(\frac{\partial f}{\partial m^*}\right) dm^* + \left(\frac{\partial f}{\partial K}\right) dK = \frac{f}{2}\left(\frac{dK}{K} - \frac{dm^*}{m^*}\right)$$

However, resonance frequency shifts cannot always be isolated to mass changes. Occasionally, changes in the spring constant are caused by changes in differential surface stress due to unsolicited molecular adsorption. In order to minimize these unwanted effects, cantilevers can be designed with localized adsorption areas at the free end of the cantilever [14]. On the other hand, there are cases where the changes in surface stress upon biomolecular adsorption are investigated by measuring the resonant frequency shifts. When the cantilever sensor is operation in a liquid environment, however, the resonance peak and the quality factor Q both shift toward lower values due to damping, which considerably reduces the resolution of mass change measurements. The challenges associated with operating cantilever-based sensors in liquids have been vigorously tackled by many research groups, and a variety of methods have been proposed and demonstrated to enhance the Q factors [15-17].

The surface stress or static mode of cantilever operation can be described using a modification of Stoney's formula in which the radius of curvature of a bent cantilever can be expressed as the following equation:

$$\frac{1}{R} = \frac{6(1-v)}{Et^2}\Delta\sigma$$

where R is the cantilever's radius of curvature, v is Poisson's ratio, and Δσ is the differential surface stress between the top and bottom surfaces of the microcantilever. With knowledge of the radius of curvature R, the tip displacement of the cantilever can be calculated by:

$$\Delta z = \frac{3L^2(1-v)}{Et^2}\Delta\boldsymbol{\sigma}$$

where *L* is the length of the cantilever. Cantilever deflections due to analyte-binding are caused by a combination of bulk, surface, and intersurface interactions. Studies have shown cantilever response increases of two orders of magnitude when immobilization of receptor molecules are done on nanostructured surfaces instead of smooth gold. Furthermore, analyte-permeable polymer coatings have also been used to scale up the response of the cantilever and increase sensor sensitivity [1]. Different methods for chemical and biological functionalization of cantilever sensors are discussed in the next section.

Obtaining the frequency response of a cantilever in the absence of fluid is a routine and simple measurement. However, when the viscous effects of fluids are introduced, the dampening effect lowers the resonance frequency, decreases the quality factor, and the theoretical models become more complex. A derivation based upon the inviscid fluid model allows us to estimate the approximate resonant frequency of the cantilever when immersed in viscous fluids, as follows:

$$\frac{f_{fluid}}{f_{vacuum}} = \left(1 + \frac{\pi \rho_f b}{4\rho L}\right)^{-1/2}$$

Where f_{fluid} and f_{vacuum} are the resonant frequencies in vacuum and fluid, respectively, ρ is the density of the beam, b and L are the width and thickness of the cantilever, and ρ_f is the density of the fluid [17].

2.2 Detection schemes

The operation of any cantilever-based sensor requires real-time measurements of cantilever deflections with nanometer accuracy, which can be obtained by monitoring the changes in directly-related parameters, such as cantilever tip position, spatial orientation, radius of curvature, and intrinsic stress. Detection of the read-out signals from the biosensor may be electrical, optical, or some other signal that can be converted into a measurable electrical signal. In order to ensure the best possible performance, the inherent advantages and disadvantages of the different readout techniques should be analyzed and tailored for the application.

Optical Readout Schemes. Optical detection of cantilever deflection is one of the most well-studied, efficient, and sensitive methods currently available. The technique has been widely adopted in modern AFM instruments. Typically a focused laser diode beam is focused onto the free end of a cantilever at a predetermined angle, and the subsequent reflection is monitored using a high-resolution split photodiode or position-sensitive detector, as illustrated in Figure 2-2(a). When the cantilever bends, the reflected light hitting the detector shifts position in a way that is proportional to the cantilever deflection. The method is simple and reliable and has been used in the vast

majority of work on cantilever sensors. However, the major drawback of this technique is the increase in light-scattering effects as the dimensions of the cantilever decrease. If the liquid or gaseous medium in the cantilever environment is not does not have the appropriate optical properties or turbidity, the signal level degrades due to interference. The cantilever must be sufficiently reflective in order to obtain a strong, clean signal. Another limitation of optical detection is the bandwidth of photo-detectors, which usually ranges on the order of several hundred kilohertz and is incompatible with smaller and stuffer cantilevers operating in resonance mode. Beyond these limitations, optical beam techniques are also more challenging to miniaturize and make manufacture due to size limitations of the laser and alignment challenges. Many novel optical approaches have been investigated, including using a simple spot photo-detector to monitor intensity fluctuations, which can be enhanced in combination with a knife-edge obstacle [18]. More accurate high-bandwidth optical measurements have been carried out using interferometric schemes which involve placing a cleaved end of an optical fiber very close to the cantilever surface and measuring the interference base upon the reflection back into the fiber. Most notably, Rugar et al. used this technique to measure subnanometer deflections designed for ultra-sensitive force measurements in an attempt to permit single-spin magnetic resonance microscopy [19]. Though very sensitive and highly scalable, interferometry remains limited by the wavelength of laser light and is therefore only compatible for very small deflections.

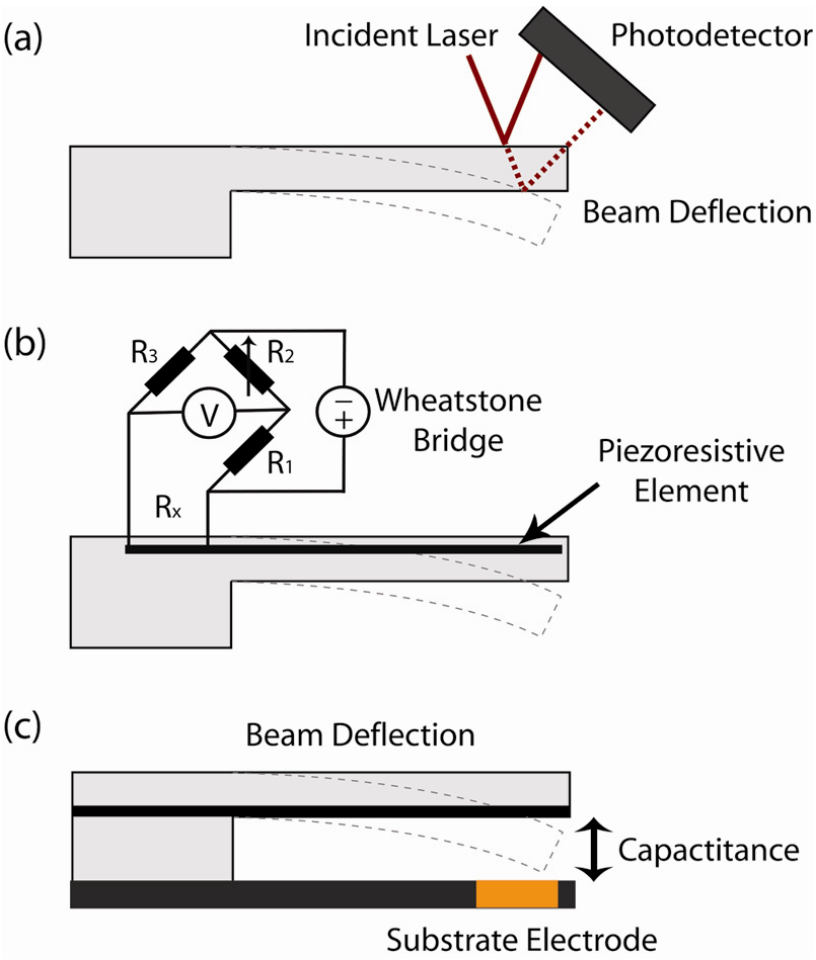

Figure 2-2. Schematic drawings of cantilever readout schemes: (a) the optical detection scheme shows the typical AFM setup where an incident laser beam is reflected off the back of the cantilever into a photodetector mount, and changes in the bending of the cantilever is reflected in changes in beam position (b) the typical piezoresistive detection scheme measures the electrical signals from the patterned piezoresistive material along the length of the cantilever using a standard Wheatstone bridge configuration (c) the capacitive detection scheme usually has the cantilever acting as one electrode, and the substrate beneath the cantilever acting as another electrode, with the changes in capacitance between the two indicating a change in the position of the cantilever due to bending.

Piezoresistive Readout Schemes. When a piezoresistive material is placed under stress, an associated change in the electrical conductivity can be observed. When implemented onto a cantilever, this effect can be used to monitor the stress and bending of the cantilever sensor. Typically, a single-crystal silicon cantilever is fabricated with appropriately-shaped doped regions, with a dc-biased Wheatstone bridge used to read out the resistivity [20-25], as illustrated in Figure 2-2(b). Doped polysilicon cantilevers exhibiting excellent piezoresistivity, as well as polymer SU-8 cantilevers with integrated gold resistors , have also been investigated [26, 27]. As the readout system becomes integrated with the cantilever sensor, this technique requires no optical components and can operate in non-opaque liquids. The compatibility with CMOS fabrication, along with the removal of the alignment system commonly used in optical setups, allows for ease of miniaturization and portability. On the other hand, the deflection resolution for the piezoresistive readout system is on the order of one nanometer, whereas optical readouts can achieve deflection resolutions of one Angstrom.

Though the initial prototypes of piezoresistive cantilevers were fraught with short circuit problems caused by faradaic currents, the development of passivated resistors allowed for compatibility with electrolyte solutions [3]. Another major disadvantage of the piezoresistive technique is that a current needs to be passed through the cantilever, often resulting in additional dissipation of heat and associated thermal drifts, leading to parasitic cantilever deflection and piezoresistance changes [1, 28]. Methods have been proposed to compensate for this drift by using a reference cantilever [8], and in some cases, the ability to control the heat dissipation may be useful as a tool for breaking ligand-receptor bonds to regenerate the cantilever sensing layer [29] and for monitoring polymerase chain reactions (PCR) [30].

Capacitive Readout Schemes. Capacitance-based cantilever readouts are based on the principle that if the distance between two parallel plates is changed, the capacitance between the two plates changes as well. With a conductive layer on the cantilever acting as one plate, and a conductive substrate surface acting as the other plate as shown in Figure 2-2(c), highly sensitive measurements can be made to provide absolute displacements. However, larger-scale displacements are more difficult to monitor. Furthermore, the technique is incompatible with electrolyte solutions due to the faradaic currents between the capacitor plates, and therefore of very limited used in biosensor applications [3].

2.3 Cantilever Actuation

For sensing the frequency changes of cantilever sensors, it is often necessary to drive the cantilever at a controlled frequency. In the absence of any external actuation, the cantilever is subject only to thermal noise $k_B T$, which at room temperature is very low, therefore requiring longer measurement times. In commercially available AFM systems, the external force is driven by a piezoelectric motor mounted near the cantilever, and the entire measurement platform is mechanically excited. In liquid environments, this method is hindered by the standing waves acoustically generated in the medium. To circumvent this, direct and controlled driving of the cantilever can be achieved by depositing a piezoresistive layer, similar to that of the piezoresistive readout scheme, and applying the appropriate electrical signals [31-33]. Some other methods for actuating cantilever sensors include the use of magnetic materials, where a thin magnetic layer is evaporated onto the cantilever and controlled by applying an external magnetic field [34]. Alternatively, a conductive pathway can be patterned and the cantilever can be driven with an ac current and the application of a constant

external field [35]. Other investigated techniques for cantilever actuation rely upon the electrostatics or heat [8].

2.4 Cantilever surface functionalization

The basic principle of a biosensor involves "detector molecules" that attached or immobilized onto a solid surface in such a way that a specific signal can be obtained from the sensor when the target molecules or cells selectively react with the surface biomolecules. In order the ensure uniformity and long-term stability of a bioreceptor molecule on the cantilever, chemical functionalization is typically first applied to the bare surface. Ideally, a closed monolayer of chemistry would allow for a receptor to covalently anchor to the surface at high density but with enough spatial movement to allow for interaction with the target biomolecules [36]. The biological surface functionalization of materials has been extensively studied over the years for applications in basic research, biosensing [37-40], medical implants [41], tissue engineering [42-45], and biomimetics [46, 47], each with varying degrees of maturity. Though biosensor immobilization has been largely focused for DNA-based diagnostics, a number of new targets have emerged on the scene, including but not limited to cells, proteins, peptides and other such biologically "down-stream" components in cell expression and cell-cell communications processes [36]. Many of the surface functionalization and molecular recognition techniques for cantilever-based sensors have been adopted from advances in other biosensor devices, such as quartz crustal microbalance (QCM), surface acoustic wave devices (SAW), chemical field effect transistors (chemFET), and surface enhanced Raman spectroscopy (SERS) sensors [6].

Strong polarization forces at metal surfaces and strong ionic or covalent interactions on many inorganic metal oxides and semiconductor materials may cause denaturation and loss of specificity of the biomolecules receptors, and therefore incompatible when left bare and untreated. The usual solution for this is to deposit a layer of special spacer or linker molecules on the sensor substrate [36]. For this reason, cantilevers are often fabricated with noble metal film coating on one or both surfaces. Sputtered or evaporated gold films can be precisely controlled in thickness and distribution, and are commonly used to help anchor successive molecular layers. One easy method to deposit a uniform layer of linker molecules is to utilize the self-assembling properties of special molecules, such as alkane chain molecules with thiol (-SH) groups for assembly on gold substrates and silanes (-SiOX) on silicon substrates. Self-assembled monolayers spontaneously form uniform, densely packed, robust monolayers with tunable chain lengths and chemical properties, and are therefore highly suitable candidates to link the receptor molecules to the substrate [48]. Methods to attach thiols with different chemistries on each side of cantilever have also been proposed to increase specificity and enhance the biosensor signal [3]. Another technique used to create desired functional groups on a substrate surface is to graft polymers via plasma-treatment and subsequent spin-coating [49, 50]. Langmuir-Blodgett (LB) deposition has also been used to generate ordered organic multilayer formation using amphiphilic molecules without the need for reactive surface sites [51, 52].

The characterization of the deposited biomolecule layers is also crucial to the cantilever functionalization process. In particular, the activity of receptors needs to be quantified in order to determine the efficiency of the biosensor. A number of different methods can be used to verify the receptor linking chemistries, including fluorescent microscopy to determine spatial distribution, atomic force microscopy to view the

morphology, and enzyme linked immunosorbent assays (ELISA) to monitor the amount of active antibodies on the substrate surface [3].

2.5 Cantilever-based biosensing

Nucleic Acids. Direct immobilization of DNA probes via self-assembly of thiol-labeled oligonucleotides is one of the most common, easy-to-use methods for gold-coated microcantilevers, which are easy to fabricate and available commercially. The sulfur linkage between the thiol and the gold causes a measurable change in surface stress during DNA probe immobilization. Subsequent hybridization with target DNA can be enhanced by optimizing the buffer concentrations and maximization of reactive probe sites can be achieved by creating mixed layers with molecules like mercaptohexanol (MCH) [7]. In 2000, Fritz *et al.* first reported on the sensitive and specific monitoring of oligonucleotide hybridization using functionalized cantilevers with the ability to detect a single base pair mismatch [2]. The hybridization assay used for this work is shown schematically in Figure 2-3. Thundat *et al.* reported the discrimination of a single-nucleotide polymorphism without the need of a reference cantilever. Hansen et al. further evaluated this technology and found that the direction of cantilever bending was dependent upon the number and location of mismatch sites along the strand pairs [53]. Various parameters have been studied, including the effects of ionic strength upon the hybridization [54] and the impact of singles strand extensions on cantilever deflection [55]. Empirical models were developed to predict the deflections upon hybridization, which asserted that hydration forces, density of surface coverage, and degree of disorder on the cantilever surface were main contributors to the deflections [56]. Other novel techniques have been integrated, such as the use of gold nanoparticles functionalized with DNA probes to detect single base

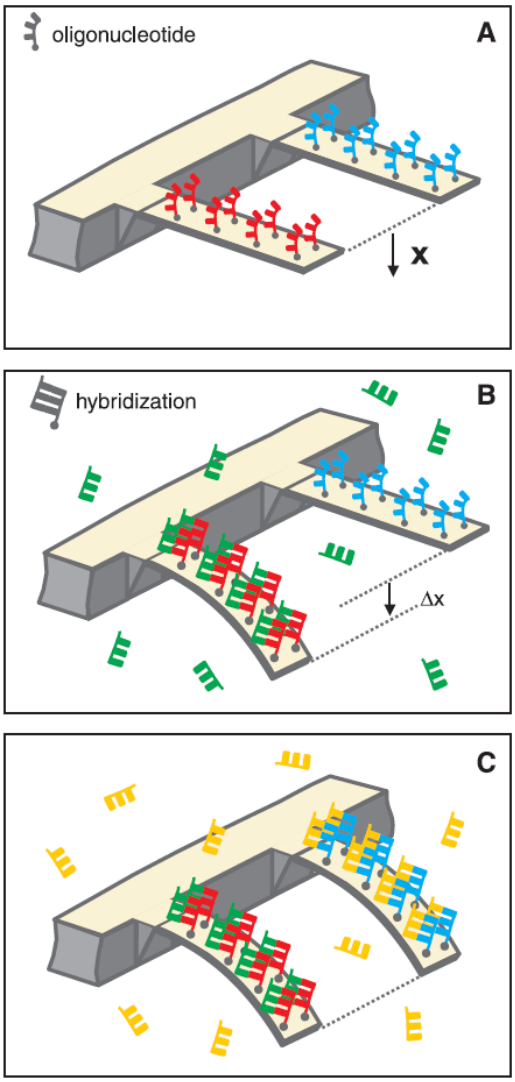

Figure 2-3. Schematic illustration of a cantilever-based hybridization assay. Each cantilever is functionalized on one side with a different oligonucleotide (red or blue). In A, the differential signal is set to zero as a baseline measurement. In B, upon injection of the first complementary DNA strand (green), hybridization occurs on the cantilever with the matching sequence (red), increasing the differential signal. In C, injection of the second complementary DNA oligo (yellow) causes the cantilever functionalized with the second oligo (blue) to bend. Reprinted with permission [2]. Copyright 2000 American Association for the Advancement of Science.

pair mismatch via resonance [57]. Recent efforts in this arena have focused on improving sensor performance by optimizing piezoresisitve cantilevers in order to shrink the device footprint and promote sensor portability [4].

Proteins. Numerous studies have reported the use of antibodies as receptors for detecting proteins. Surface stress changes caused by ultralow concentrations (0.2 ng/ml) of prostate specific antigen (PSA), a prostate cancer detection marker, were also detected using a single cantilever sensor, and showed particular clinical relevance due to the fact that the background buffered solutions used in t he experiments contained physiological levels (1 mg/ml) of both human serum albumin and human plasminogen [58]. Wee et al. have reported the detection of cardiac disease markers, PSA and C-reactive proteins (CRP), with self-sensing piezoresistive cantilevers [59]. The sensing of high-affinity but reversible biotin-streptavidin interactions were also successfully conducted using silicon nitride cantilever transducers functionalized with biotin and deflection responses in 100 nM streptavidin reached 50 nm in magnitude within 10 minutes of exposure [3]. Moulin et al. fabricated gold-coated silicon nitride cantilevers modified with heparin to differentiate between low density lipoproteins (LDL) and their oxidized form (oxLDL) by bending in opposite directions upon exposure to 120 μg/ml of LDL and 10 μg/ml of oxLDL, respectively [60]. The first demonstration of chiral discrimination using microcantilevers was shown by Dutta *et al*.. Instead of using smooth cantilevers, nanostructured cantilevers with gold surfaces were capable of exhibiting up to several microns of tip deflection upon adsorption of protein A and biotin-labeled albumin, and additional micrometer scale deflections were observed upon interaction with immunoglobulin G and avidin [61]. Alvarez and colleagues reported the use of cantilevers functionalized with a BSA-conjugated synthetic hapten to detect the presence of the pesticide

dichlorodiphenyltrichloroethane (DDT) [62]. Knowles et al. have reported the detection of protein aggregation and amyloid growth associated with Alzheimer's and Parkinson's diseases through surface stress measurements using microfabricated cantilever array systems [63]. The detection of interactions between vimentin antibodies and antigens using cantilever-based biosensors shows promise in early osteosarcoma detection, and similar sensors for cancer marker diagnosis paves the road for future platforms that could revolutionize the healthcare and life science industry [7]. The leading advantage of cantilever-based biosensors, in contrast to conventional enzyme-linked immunoassays for antigen-antibody reactions, arises from its ability to perform label-free single-reaction detections without additional reagents.

Cells. In 2001 Ilic *et al.* first reported the detection of mass changes due to the presence of a single *E. coli* cell at the tip of a cantilever in air, and the findings were later confirmed by Zhang and Ji [64, 65]. In an extension of Ilic and colleagues work, composite self-excited PZT-glass cantilevers were shown to detect down to 700 *E. coli* O157:H1 cells/ml in fluid by Campbell and Mutharasan [66]. The detection of single bacterial cells, attached specifically via appropriate biological receptors at the free end of a single cantilever, has been performed both in air and in liquid by numerous groups. The cantilever-based detection of food pathogens such as *Salmonella enterica* by Weeks *et al* [67]., *Vaccinia* virus by Gunter *et al.* [68], and fungal spores from *Aspergillus niger* by Nugaeva *et al*. [69] have also been reported. Real-time detection of whole *B. subtilis* spores in liquids by Dhayal *et al.* demonstrated the utility of peptide-functionalized silicon cantilever arrays, and antibody-coated cantilevers with high selectivity have been shown to distinguish target spores from complicated spore mixtures [70]. The response of oscillating cantilevers to bacteria adsorption was recently characterized by Ramos and colleagues to correlate the frequency response to

a variety of different parameters, including site of immobilization, stiffness of bacterial cells, and added mass [71]. The interrogation of living cells grown directly on a cantilever surface to external chemical stimuli has also been proposed and investigated by a number of groups. Gfeller *et al.* showed the monitoring of active bacterial growth by coating oscillating cantilevers with a thin nutritive layer of agarose and measuring the subsequent resonant shift caused by a mass increase of growing bacteria [72]. Mass sensing of mammalian HeLa cells in fluids have also been conducted on "living cantilever arrays" for single-cell activity studies [73]. Collectively, these reports show promise for the use of cantilever-based biosensors in medical diagnostics, food supply monitoring, environmental monitoring, and other bio-detection applications.

2.6 Cantilever-based biosensor systems

Integration of cantilever-based biosensing systems with electronic readout methods and microfluidic techniques to achieve portable and automated testing faces many challenges. Many research groups have already developed cantilever systems that incorporate numerous elements and components. The development of multiplexed cantilever-based biosensor systems offers a new set of challenges, one of which being the difficulty of immobilizing different bio-receptors in each cantilever of an array. Manalis et al. have pursued a novel approach by integrating microfluidic channels within the cantilevers so as to enhance the sensitivity and push the limits of detection for fluidborne analytes [15].

Commercial platforms devoted primarily to the specific functionalization of individual cantilevers have been developed by different companies, including the Autodrop

(Microdrop), the CantiSpot (Cantion), the NanoDrop, and the Cantisens FU-401 (Concentris) [74, 75]. Furthermore, there are several commercial cantilever biosensor platforms that integrate cantilever arrays currently available. Most notably, the development of the artificial nose for gas-based sensing of molecules using a cantilever-based system has been widely publicized [76]. Concentris offers silicon cantilever arrays for static and dynamic measurements [74]. The Cantion nanomechanical cantilever arrays come with an integrated electrical read-out instrument that controls the fluidic system, allowing the user to functionalize each cantilever individually [75]. The VeriScan 3000 System from Protiveris is diesnged to measure up to 64 microcantilever sensors in real-time to detect molecular interactions between proteins, antibodies, antigens, or DNA. The instrument combines patented laser technologies, advanced electronics, microfluidics, a proprietary biochip, and advanced software capabilities [77]. More recently, Kalinex Inc. commercialized a biochemo-opto-mechanical microcantilever array chip with 1000 microcantilevers/chip that can test 100-200 different compounds [78]. In order to gain an edge against competing commercial sensing technologies such as quartz crystal microbalance, surface plasmon resonance, and surface acoustic wave, cantilever biosensor platforms need to provide sturdier, faster, cheaper analysis with higher sensitivities and reliability.

2.7 Conclusion and future directions

In summary, the recent development of microcantilever-based sensors for the sensitive small-scale transduction of label-free biomolecules detection is gaining momentum and popularity in the field of sensing technologies. The biological interactions on the cantilever surface can be directly translated into mechanical bending or changes in

resonant frequency, which can be detected with a variety of different techniques, each with its own advantages and drawbacks. A wide range of applications can be tackled with this approach, such as the detection of cells, specific proteins, DNA sequences, and other small biomolecules. The ability to integrate of this technology into a multiplexed automated and portable system shows promise for widespread use across several industries where rapid and sensitive biodetection is critical.

In order to compete with other sensing technologies, cantilever-based sensing has several fronts that require further investigation and improvement. First and foremost, the enhancement of cantilever response in order to improve the speed and sensitivity is necessary. The incorporation of cantilevers into microfluidic devices allows for a dramatic reduction in the sample volumes, as well as a shortening of the temporal response, which would allow greater sensitivity in real-time. Alternatively, the Manalis group has shown significantly-enhanced sensitivity with low limits of detection using specially designed cantilevers that have microfluidic channels integrated directly into the individual cantilevers, thus eliminating the dampening effect and laser-scattering effects normally encountered by a cantilever immersed in fluid. The microfluidic channels are pre-coated with receptor molecules in order to achieve the selectivity in detection. Various cantilever dimensions and shapes can be further investigated to optimize for stress, mass, or temperature sensitivities.

Bio-receptor surface functionalization would require an increased effort in development to acheive greater selectivity. Novel packaging techniques to extend the shelf-life of existing coatings would also need investigation. In addition, incorporation of nanostructuring and application of novel nanoparticle-based techniques on the cantilever surface could lead to even lower limits of detection and require more

studies. Through innovations in cantilever design, development of novel methods for bio-receptor functionalization, and integration of different readout methods into a single system, the present shortcomings in microcantilever technology can be overcome in order to realize portable high-throughput screening of biomolecules across industries involved in basic research, healthcare, medical diagnostics, environmental screening, drug screening, and military applications.

REFERENCES

[1] Lavrik, N.V.; Sepaniak, M.J.; Datskos, P.G. Cantilever transducers as a platform for chemical and biological sensors. *Rev. Sci. Instrum.* **2004**, *75*, 2229-2253.

[2] Fritz, J.; Baller, M.K.; Lang, H.P.; Rothuizen, H.; Vettiger, P.; Meyer, E.; Guntherodt, H.; Gerber, C.; Gimzewski, J.K. Translating biomolecular recognition into nanomechanics. *Science* **2000**, *288*, 316-318.

[3] Raiteri, R.; Grattarola, M.; Butt, H.-J.; Skládal, P. Micromechanical cantilever-based biosensors. *Sens. Actuators. B Chem.* **2001**, *79*, 115-126.

[4] Goeders, K.M.; Colton, J.S.; Bottomley, L.A. Microcantilevers: Sensing Chemical Interactions via Mechanical Motion. *Chem. Rev.* **2008**, *108*, 522-542.

[5] Fritz, J. Cantilever biosensors. *Analyst* **2008**, *133*, 855-863.

[6] Hansen, K.M.; Thundat, T. Microcantilever biosensors. *Methods* **2005**, *37*, 57-64.

[7] Carrascosa, L.G.; Moreno, M.; Alvarez, M.; Lechuga, L.M. Nanomechanical biosensors: a new sensing tool. *Trends. Analyt. Chem.* **2006**, *25*, 196-206.

[8] Ziegler, C. Cantilever-based biosensors. *Anal. Bioanal. Chem.* **2004**, *379*, 946-959.

[9] Kim, T.S.; Yoon, D.S.; Lee, J.H. Nanomechanical Cantilever Devices for Biological Sensors. In *Micromanufacturing and Nanotechnology*, Ed.; Mahalik, N.P., Ed.^Eds.; Springer, 2006, pp. 299-322,

[10] Gao, P.; Yao, S.; Li, E.; Li, S. Design and analysis of label free immunosensor based on microcantilever array and magnetic bead for bio-detection. In Bioinformatics and Biomedical Engineering 2007, The 1st International Conference on, 2007, pp. 1053-1056.

[11] Icoz, K.; Iverson, B.D.; Savran, C. Noise analysis and sensitivity enhancement in immunomagnetic nanomechanical biosensors. *Appl. Phys. Lett.* **2008**, *93*.

[12] Lee, S.H.; Jung, K.S. Magnetic Manipulation of a Microcantilever for a New Concept in Atomic Force Microscopy. *IEEE Transactions on Magnetics* **2007**, *43*, 2737-2739.

[13] Brath, F.G.; Humphery, J.A.C. *Sensors and sensing in biology and engineering*, Ed.; Springer: New York, 2002; p.^pp. 337-345.

[14] Lui, C.; Bergkvist, M.; Batt, C.A.; Sato, T. Quantification of flagellar response of single-cell E. coli to chemotactic agents using microfabricated silicon nitride cantilevers. In Sensors, 2008 IEEE, Lecce, Italy, 2008, pp. 1464-1467.

[15] Burg, T.P.; Godin, M.; Knudsen, S.M.; Shen, W.; Carlson, G.; Foster, J.S.; Babcock, K.; Manalis, S.R. Weighing of biomolecules, single cells and single nanoparticles in fluid. *Nature* **2007**, *446*, 1066-1069.

[16] Maali, A.; Hurth, C.; Boisgard, R. Hydrodynamics of oscillating atomic force microscopy cantilevers in viscous fluids. *J. Appl. Phys.* **2005**, *97*.

[17] Sader, J.E. Frequency response of cantilever beams immersed in viscous fluids with applications to the atomic force microscope. *J. Appl. Phys.* **1998**, *84*, 64-76.

[18] Carr, D.W.; Evoy, S.; Sekaric, L.; Craighead, H.G.; Parpia, J.M. Measurement of mechanical resonance and losses in nanometer scale silicon wires. *Appl. Phys. Lett.* **1999**, *75*.

[19] Rugar, D.; Yannoni, C.S.; Sidles, J.A. Mechanical detection of magnetic resonance. *Nature* **1992**, *360*, 563-566.

[20] Chui, B.W.; Stone, T.D.; Kenny, T.W.; Mamin, H.J.; Terris, B.D.; Rugar, D. Low-stiffness silicon cantilevers for thermal writing and piezoresistive readback with the atomic force microscope. *Appl. Phys. Lett.* **1996**, *69*, 2767-2769.

[21] Tortonese, M.; Barrett, R.C.; Quate, C.F. Atomic resolution with an atomic force microscope using piezoresistive detection. *Appl. Phys. Lett.* **1993**, *62*, 834-836.

[22] Linnemann, R.; Gotszalk, T.; Hadjiiski, L.; Rangelow, I.W. Characterization of a cantilever withi an integrated deflection sensor. *Thin Solid Films* **1995**, *264*, 159-164.

[23] Hansen, O.; Boisen, A. Noise in piezoresistive atomic force microscopy. *Nanotechnology* **1999**, *10*, 51-60.

[24] Thaysen, J.; Boisen, A.; Hansen, O.; Bouwstra, S. Atomic force microscopy probe with piezoresistive read-out and highly symmetrical Wheatstone bridge arrangement. *Sens. Actuators. A Phys.* **2000**, *83*.

[25] Minne, S.C.; Manalis, S.R.; Quate, C.F. Parallel atomic force microscopy using cantilevers with integrated piezoresistive sensors and integrated piezoelectric actuators. *Appl. Phys. Lett.* **1995**, *67*, 3918-3920.

[26] Nordstrom, M.; Keller, S.; Lillemose, M.; Johansson, A.; Dohn, S.; Haefliger, D.; Blagoi, G.; Havsteen-Jakobsen, M.; Boisen, A. SU-8 Cantilevers for Bio/chemical Sensing; Fabrication, Characterisation and Development of Novel Read-out Methods. *Sensors* **2008**, *8*, 1595-1612.

[27] Thaysen, J.; Yalcinkaya, A.D.; Vettiger, P.; Menon, A. Polymer-based stress sensor with integrated readout. *J. Phys. D: Appl. Phys.* **2002**, *35*, 2698-2703.

[28] Shekhawat, G.; Tark, S.-H.; Dravid, V.P. MOSFET-Embedded Microcantilevers for Measuring Deflection in Biomolecular Sensors. *Science* **2006**, *311*, 1592-1595.

[29] Raiteri, R.; Grattarola, M.; Berger, R. Micromechanics senses biomolecules. *Materials Today* **2002**, *5*, 22-29.

[30] Marie, R.; Thaysen, J.; Christensen, C.B.V.; Boisen, A. A cantilever-based sensor for thermal cycling in buffer solution. *Microelec. Eng.* **2003**, *67-68*, 893-898.

[31] Miyahara, Y.; Deschler, M.; Fujii, T.; Watanabe, S.; Bleuler, H. Non-contact atomic force microscope with a PZT cantilever used for deflection sensing, direct oscillation and feedback actuation. *Appl. Surf. Sci.* **2002**, *188*, 450-455.

[32] Lee, S.S.; White, R.M. Self-excited piezoelectric cantilever oscillators. *Sens. Actuators. A Phys.* **1996**, *52*, 41-45.

[33] Manalis, S.R.; Minne, S.C.; Atalar, A.; Quate, C.F. Interdigital cantilevers for atomic force microscopy. *Appl. Phys. Lett.* **1996**, *69*, 3944.

[34] Lantz, M.A.; O'Shea, S.J.; Welland, M.E. Force microscopy imaging in liquids using ac techniques. *Appl. Phys. Lett.* **1994**, *65*, 409.

[35] Buguin, A.; Roure, O.D.; Silberzan, P. Active atomic force microscopy cantilevers for imaging in liquids. *Appl. Phys. Lett.* **2001**, *78*, 2982.

[36] Kasemo, B. Biological surface science. *Surface Science* **2002**, *500*, 656-677.

[37] Suarez, G.; Ismail, A.; Jackson, R.J.; Chang, S.C.; Harris, A.J.; Burdess, J.S.; Hedley, J.; McNeil, C.J. Direct Adsoprtion of Chemically Modified Biomolecules Onto Gold: A Rapid Method for Biological Functionalization of MEMS. In, Year, pp. 113-118.

[38] Goddard, J.M.; Hotchkiss, J.H. Polymer surface modification for the attachment of bioactive compounds. *Progress in Polymer Sci.* **2006**, *32*, 698-725.

[39] Hoa, X.D.; Kirk, A.G.; Tabrizian, M. Towards integrated and sensitive surface plasmon resonance biosensors: A review of recent progress. *Biosens. Bioelectron.* **2007**, *23*, 151-160.

[40] Huang, X.-J.; Choi, Y.-K. Chemical sensors based on nanostructured materials. *Sens. Actuators. B Chem.* **2006**, *122*, 659-671.

[41] Hildebrand, H.F.; Blanchemain, N.; Mayer, G.; Chai, F.; Lefebvre, M.; Boschin, F. Surface coatings for biological activation and functionalization of medical devices. *Surface and Coatings Technology* **2005**, *200*, 6318-6324.

[42] Rezwan, K.; Chen, Q.Z.; Blaker, J.J.; Boccaccini, A.R. Biodegradable and bioactive porous polymer/inorganic composite scaffolds for bone tissue engineering. *Biomaterials* **2006**, *27*, 3413-3431.

[43] Chan, G.; Mooney, D.J. New materials for tissue engineering: towards greater control over the biological response. *Trends in Biotechnology* **2008**, *26*, 382-392.

[44] Falconnet, D.; Csucs, G.; Grandin, H.M.; Textor, M. Surface engineering approaches to micropattern surfaces for cell-based assays. *Biomaterials* **2006**, *27*, 3044-3063.

[45] Meyers, S.R.; Khoo, X.; Huang, X.; Walsh, E.B.; Grinstaff, M.W.; Kenan, D.J. The development of peptide-based interfacial biomaterials for generating biological functionality on the surface of bioinert materials. *Biomaterials* **2009**, *30*, 277-286.

[46] Tamerler, C.; Sarikaya, M. Molecular biomimetics: nanotechnology and bionanotechnology using genetically engineered peptides. *Phil. Trans. R. Soc. A* **2009**, *367*, 1705-1726.

[47] Koch, K.; Bhushan, B.; Barthlott, W. Multifunctional surface structures of plants: An inspiration for biomimetics. *Progress in Mat. Sci.* **2008**, *54*, 137-178.

[48] Berger, R.; Delamarche, E.; Lang, H.P.; Gerber, C.; Gimzewski, J.K.; Meyers, E.; Guntherodt, H.-J. Surface stress in the Self-Assembly of Alkanethiols on Gold. *Science* **1997**, *276*, 2021-2024.

[49] Ratner, B.D. Characterization of graft polymers for biomedical applications. *J. Biomed. Mat. Res.* **1980**, *14*, 665-687.

[50] Krishnamoorthy, S.; Hinderling, C.; Heinzelmann, H. Nanoscale patterning with block copolymers. *Materials Today* **2002**, *9*, 40-47.

[51] Ai, H.; Jones, S.A.; Lvov, Y.M. Biomedical applications of electrostatic layer-by-layer nano-assembly of polymers, enzymes, and nanoparticles. *Cell Biochem. Biophys.* **2003**, *39*, 23-43.

[52] Petty, M.C. *Langmuir-Blodgett Films: An Introduction*, Ed.; Cambridge University Press: Cambridge, 1996.

[53] Hansen, K.M.; Ji, H.-F.; Wu, G.; Datar, R.; Cote, R.; Majumdar, A.; Thundat, T. Cantilever-Based Optical Deflection Assay for Discrimination of DNA Single-Nucleotide Mismatches. *Anal. Chem.* **2001**, *73*, 1567-1571.

[54] Wu, G.; Ji, H.; Hansen, K.; Thundat, T.; Datar, R.; Cote, R.; Hagan, M.F.; Chakraborty, A.K.; Majumdar, A. Origin of nanomechanical cantilever motion generated from biomolecular interactions. *Proc. Natl. Acad. Sci. U.S.A.* **2001**, *98*, 1560-1564.

[55] McKendry, R.; Zhang, J.; Arntz, Y.; Strunz, T.; Hegner, M.; Lang, H.P.; Baller, M.K.; Certa, U.; Meyer, E.; Guntherodt, H.-J.; Gerber, C. Multiple label-free biodetection and quantitative DNA-binding assays on a nanomechanical cantilever array. *Proc. Natl. Acad. Sci. U.S.A.* **2002**, *99*, 9783-9788.

[56] Hagan, M.F.; Majumdar, A.; Chakraborty, A.K. Hybridization dynamics of surface immobilized DNA. *J. Chem. Phys.* **2004**, *120*, 4958.

[57] Su, M.; Li, S.; Dravid, V.P. Microcantilever resonance-based DNA detection with nanoparticle probes. *Appl. Phys. Lett.* **2003**, *82*, 3562.

[58] Wu, G.; Datar, R.H.; Hansen, K.M.; Thundat, T.; Cote, R.J.; Majumdar, A. Bioassay of prostate-specific antigen (PSA) using microcantilevers. *Nature Biotechnology* **2001**, *19*, 856-860.

[59] Wee, K.W.; Kang, G.Y.; Park, J.; Kang, J.Y.; Yoon, D.S.; Park, J.H.; Kim, T.S. Novel electrical detection of label-free disease marker proteins using piezoresistive self-sensing micro-cantilevers. *Biosens. Bioelectron.* **2004**, *20*, 1932-1938.

[60] Moulin, A.M.; O'Shea, S.J.; Welland, M.E. Microcantilever-based biosensors. *Ultramicroscopy* **2000**, *82*, 23-31.

[61] Dutta, P.; Tipple, C.A.; Lavrik, N.V.; Datskos, P.G.; Hofstetter, H.; Hofstetter, O.; Sepaniak, M.J. Enantioselective Sensors Based on Antibody-Mediated Nanomechanics. *Anal. Chem.* **2003**, *75*, 2342-2348.

[62] Alvarez, M.; Calle, A.; Tamayo, J.; Lechuga, L.M.; Abad, A.; Montoya, A. Development of nanomechanical biosensors for detection of the pesticide DDT. *Biosens. Bioelectron.* **2003**, *18*, 649-653.

[63] Knowles, T.P.J.; Shu, W.; Huber, F.; Lang, H.P.; Gerber, C.; Dobson, C.M.; Welland, M.E. Label-free detection of amyloid growth with microcantilever sensors. *Nanotechnology* **2008**, *19*.

[64] Ilic, B.; Czaplewski, D.; Zalalutdinov, M.; Craighead, H.G.; Neuzil, P.; Campagnolo, C.; Batt, C. Single cell detection with micromechanical oscillators. *J. Vac. Sci. Technol. B* **2001**, *19*, 2825-2828.

[65] Zhang, J.; Ji, H.-F. An Anti E. Coli O157:H7 Antibody-immobilized Microcantilever for the Detection of Escherichia coli (E. coli). *Analytical Sci.* **2004**, *20*, 585.

[66] Campbell, G.A.; Mutharasan, R. Detection of pathogen Escherichia coli O157:H7 using self-excited PZT-glass microcantilevers. *Biosens. Bioelectron.* **2005**, *21*, 462-473.

[67] Weeks, B.L.; Camarero, J.; Noy, A.; Miller, A.E.; Yoreo, J.J.D.; Stanker, L. A microcantilever-based pathogen detector. *Scanning* **2006**, *25*, 297-299.

[68] Gunter, R.L.; Delinger, W.G.; Manygoats, K.; Kooser, A.; Porter, T.L. Viral detection using an embedded piezoresistive microcantilever sensor. *Sens. Actuators. A Phys.* **2003**, *107*, 219-224.

[69] Nugaeva, N.; Gfeller, K.Y.; Backmann, N.; Lang, H.P.; Duggelin, M.; Hegner, M. Micromechanical cantilever array sensors for selective fungal immobilization and fast growth detection. *Biosens. Bioelectron.* **2005**, *21*, 849-856.

[70] Dhayal, B.; Henne, W.A.; Doorneweerd, D.D.; Reifenberger, R.G.; Low, P.S. Detection of Bacillus subtilis Spores Using Peptide-Functionalized Cantilever Arrays. *J. Am. Chem. Soc.* **2006**, *128*, 3716-3721.

[71] Ramos, D.; Tamayo, J.; Mertens, J.; Calleja, M. Origin of the response of nanomechanical resonators to bacteria adsorption. *J. Appl. Phys.* **2006**, *100*.

[72] Gfeller, K.Y.; Nugaeva, N.; Hegner, M. Micromechanical oscillators as rapid biosensor for the detection of active growth of Escherichia coli. *Biosens. Bioelectron.* **2004**, *21*, 528-533.

[73] Park, K.; Jang, J.; Irimia, D.; Sturgis, J.; Lee, J.; Robinson, J.P.; Toner, M.; Bashir, R. 'Living cantilever arrays' for characterization of mass of single live cells in fluids. *Lab Chip* **2008**, *8*, 1034-1041.

[74] Concentris. www.concentris.ch.

[75] Cantion. www.cantion.com.

[76] Lang, H.P.; Baller, M.K.; Berger, R.; Gerber, C.; Gimzewski, J.K.; Battiston, F.M.; Fornaro, P.; Ramseyer, J.P.; Meyer, E.; Guntherodt, H.J. An artificial nose based on a micromechanical cantilever array. *Anal. Chim. Acta* **1999**, *393*, 59-65.

[77] Protiveris. www.protiveris.com.

[78] Kalinex. www.kalinex.com.

CHAPTER 3

MICROFLUIDIC SAMPLE PREPARATION MODULES

3.0 Introduction

Miniaturized microfluidic modules are an easy and effectively solution for low-cost diagnostic devices and high-throughput analysis systems. Precise fluid control and flow stability in a microfluidic-based system is critical for the implementation of successful biodetection strategies. Most biosensing applications require the starting samples consist of tissue, blood, environmental, or food samples [1] and therefore must undergo careful sample preparation for sensitive detection due to trace or low-abundance species. In this chapter, we will outline our polymeric microfabrication methods and present our microfluidic solutions to the challenges of microscale fluid handling and sample preparation.

3.1 Polymeric Microfabrication Methods

Polymers are high molecular weight macromolecular substrates that are classified in three main groups according to their thermophysical behavior: thermoplastic, elastomer, and thermoset. Thermoplastics are polymers that soften and flow upon heating to allow for the material to be molded into specific shapes, and some common ones include polyethylene (PE), polypropylene (PP), nylon, polymethyl methacrylate (PMMA), and polycarbonate (PC). Elastomeric polymers, on the other hand, are weakly cross-linked polymers that are flexible and can be stretched by applying an external force. Common elastomers include polydimethylsiloxane (PDMS) and epoxy. Lastly, thermosets are heavily cross-linked polymers that are generally rigid and brittle materials that provide greater thermal stability. Unsaturated polyesters, vinyl esters, and urethane are among some of the materials that fall under this last group of polymers [2].

Different fabrication protocols with different constraints and advantages have been investigated over the years, however, the polydimethylsiloxane (PDMS) molding technique using standard SU-8 technology has emerged as the prevalent technique for creating microfluidic chambers and channels. Though alternative techniques such as injection molding are preferred for mass manufacturing and cost efficiency, PDMS molding is the widely accepted rapid prototyping technology in research environments due to its simplicity and quick turnaround time [3]. As one of the most actively developed polymers for microfluidics, the casting of PDMS against a suitable mold can achieve sub-0.1-μm fidelity. PDMS is optically clear, allowing for optical detection through the material from 240 to 1100 nm. It is also inert, non-toxic, and non-flammable, therefore lending itself favorably to the construction of biological and medical devices [4].

PDMS belongs to a group of polymeric organosilicon compounds commonly referred to as silicones, and is typically supplied in two components, a base monomer and a curing agent. The chemical formula for PDMS is $(H_3C)_3SiO[Si(CH_3)_2O]_nSi(CH_3)_3$ where n is the number of repeating monomer $[SiO(CH_3)_2]$ units. Controlling the number of repeat units of this polymer chain and degree of cross-linking allows for the user to manipulate PDMS into different rheological forms, such as fluids, emulsions, lubricants, resins, elastomers, and rubbers [5]. Silicon hydride groups present in the curing agent react with vinyl groups present in the base monomers to form a cross-linked elastomeric solid. A variety of different mixing ratios have been investigated by various research groups, but the 10:1 base: curing agent volume ratio remains the gold standard. The commercially available version, such as the Sylgard 184 from Dow Corning) is provided as a kit. The mixture of PDMS pre-polymer conforms to the

shape of the master and undergoes a period of curing. At temperatures above 60°C, curing of the PDMS can occur within an hour. At room temperature, however, it can take over 12 hours for the PDMS to harden. The low surface energy and elasticity of PDMS allows for easy release from the master mold with minimal damage or wear. Beyond its usefulness in microfluidic device fabrication, PDMS has also found applications ranging from contact lenses to bathroom caulking to shampoos [5]. The main purpose of this section is to detail the casting method process flow for the creation of PDMS devices used in our nucleic acid-based pathogen detection microfluidic systems.

3.1.1 Microfabrication of the SU-8 Mold

SU-8 (MicroChem, Newton, MA) is a commonly used negative photoresist in creating microfluidic molds. Due to the versatility and high optical transmission above 360 nm of the photoresist, structures of various heights with near vertical sidewalls can be easily constructed. The schematic in Figure 3-1 illustrates the SU-8 mold fabrication and PDMS casting method process flows.

Photomask Design & Production. Computer-aided design (CAD) software called L-Edit (v.12.1) was used to create the pattern for the microfluidic molds. Typically, 5-inch chrome-coated quartz masks are employed as the pattern-transfer medium, however, the option exists to use several high-resolution printed transparencies stacked, adhered together with pea-sized dabs of petroleum jelly at intervals around the transparency perimeter, microscope-aligned, and fixed with scotch tape. In the former method, the pattern transfer is optically transferred from the CAD file to the mask using a laser-interferometer metered pattern generater (GCA/MANN 3600F). The latter method is significantly cheaper, but ends up sacrificing in terms of

resolution and alignment precision and therefore only suitable for feature sizes larger than 50 μm. In our experience, the ink on a single printed transparency was not opaque enough (resulting in graininess of the unexposed regions of photoresist), and a minimum of three to four transparencies were needed for successful pattern transfer. For the fabrication of the photomasks for our microfluidic devices, we ultimately opted to use quartz masks to maintain the resolution.

Substrate Preparation. Substrate wafers (typically 4-inch silicon wafers) need to be properly cleaned of contaminants, such as dust particles or chemical contaminants, to avoid problems such as surface unevenness, blocked patterns, or unexpected changes in the chemical properties of the photoresist. Though it is common practice that new wafers do not require additional cleaning, it is often advisable to clean the wafers regardless. Though the preparation of ultraclean silicon surfaces by cleaning and surface conditioning for the manufacture of integrated circuits (IC) has evolved immensely over the years, wet chemical processes are still the simplest and most widely used method. For fabricating microfluidic molds, the main concern in substrate preparation is to ensure a clean enough surface for the successful adherence of the photoresist to the substrate. A variety of different cleaning methods exist that we have used to prepare substrates for microfluidic molds, and are listed as follows:

(1) Piranha clean: Piranha solution is highly reactive, comprising of 3:1 volume ratios of 98 weight % of sulfuric acid and 30 weight % of hydrogen peroxide, which makes this process dangerous to handle. This process is effective in the removal of gross organic materials from silicon wafers, such as hardened photoresist polymer patterns and other visible contaminants of organic nature. Many cleanroom facilities have since installed automated Piranha-based wafer cleaning tools that help in isolating the

process from the user as well as reducing the amount of solution being used during the process. This automated process cleans the surface with Piranha solution, rinses thoroughly with deionized water, and spin-dries the wafer.

(2) RCA clean: The "RCA Standard Clean" process consists of two consecutively applied heated solutions. The first solution consists of a mixture of NH_4OH (ammonium hydroxide), H_2O_2 (hydrogen peroxide) and deionized water. The second solution comprises of a mixture of HCl (hydrochloric acid), H_2O_2 (hydrogen peroxide) and deionized water. The solutions are both heated to approximately 75°C, and the standard cleaning time of 10 minutes is each followed by a quench and overflow rinse in running deionized water. The wafers are then spun dry and immediately transferred to a pre-cleaned enclosure for storage before further processing. The RCA is clean is necessary for most MOS processes, but may be excessive processing for microfluidic applications.

(3) Photoresist hot strip bath: A two-bath system comprising of heated mixtures (70°C) of solvents were used to strip positive photoresist off of wafers to allow for wafer reusability. The solvents in the strip bath are composed of N-methyl-2-pyrrolidine (NMP) and tetramethylammonium hydroxide (TMAH), which are both highly effective in stripping photoresist. The two-bath system is used such that the first bath removes the bulk of the photoresist, and the second bath strips away any remaining traces of photoresist. The strip bath is followed by a quench and overflow rinse in running deionized water and a heated spin-dry step.

(4) Acetone/IPA clean: Prior to wafer priming and/or photoresist spinning, the wafer is centered on the spinner chuck and spun at 3000 rpm. Upon reaching the target spin

speed, a spray bottle is used to target a stream of acetone at the wafer center for 10 seconds to remove any existing contaminants or dust particles. Without removing the acetone stream, a second spray bottle full of isopropyl alcohol (IPA) is targeted at the same spot for an additional 5 seconds. Finally, the acetone stream is removed, and the IPA is continued for additional 5 seconds before allowing the wafer to spin dry.

(5) Reactive Oxygen Etching: The Gasonics Aura 1000 is an automated high-volume photoresist asher that utilizes a microwave source to create a stream of reactive oxygen for dry stripping of photoresist. The temperature of the wafer is raised by application of a heat lamp during this process, which expedites the stripping process. This process can be used to remove up to 4μm of organic photoresist, but for thicker layers, attempts to use this process may result in burning of the photoresist and rendering the wafer unsalvageable.

In order to ensure the adhesion of the photoresist to the wafer surface, a dehydration bake can be performed to remove the presence of water or water vapor. Adhesion can be further promoted via an adhesion promoter or wafer priming steps. The application of Omnicoat^{TM} (MicroChem, Newton, MA) primer is commonly used to improve photoresist adhesion to the silicon substrate. In our samples, 5ml of Omnicoat^{TM} was deposited onto the substrate, spun at 3000 rpm and baked at 200°C for 1 minute. This primer also allows for easy stripping of difficult to remove photoresist from the surface by immersion in Nano^{TM} Remover PG (MicroChem, Newton, MA), an NMP-based solvent stripping solution.

Photoresist Patterning. The prepared substrate is placed on top of the spin chuck in the photoresist spinner, and carefully centered for optimal uniformity in the

photoresist coating. Approximately 5 ml of the SU-8 of choice is placed in the center of the wafer. For a 200 um layer, the wafer is spun at 3000 rpm for 30 seconds with a ramp-up of 1000 rev/min^2. For a 200 um coating, the coated substrate is placed on a 65C hot plate for 20 minutes, and then transferred to a 95C hot plate for 60 minutes. The mask is loaded onto the pattern transfer tool (EV620), brought into close proximity to the photoresist-coated substrate for alignment, and then pressure-sealed to the substrate. The lamp shutter is opened for a set amount of time (in our case 60 seconds) for exposure. After exposure, the wafer is placed on a 65C hot plate for 10 minutes, and then transferred to a 95C hot plate for 30 minutes. The wafer is placed inside a beaker filled with SU-8 developer for 15-20 minutes and agitated constantly (using tweezers). The finished wafer is rinsed with fresh SU-8 developer, IPA, and deionized water before drying under a nitrogen or air gun. For thick SU-8 structures greater than 250 μm, it is advisable to cycle through the spin and pre-bake steps several times to achieve the desired height. Typically, 30 second rest times are interleaved with the longer exposure time necessary to harden the SU-8 without causing the photoresist to permanently adhere to the optical mask. The finished SU-8 mold is then affixed to the bottom of a petri dish using silicon sealant and stored for future use.

3.1.2 Microfluidic Device Assembly

Microfluidic structures are constructed by casting polydimethylsiloxane (PDMS) (Sylgard 184, Dow Corning, Midland, MI) onto an SU-8 negative photoresist mold. In a small plastic weightboat, PDMS pre-polymer is mixed vigorously with a curing agent at 10:1 mass ratio using a standard wooden tongue depressor. The mixture is

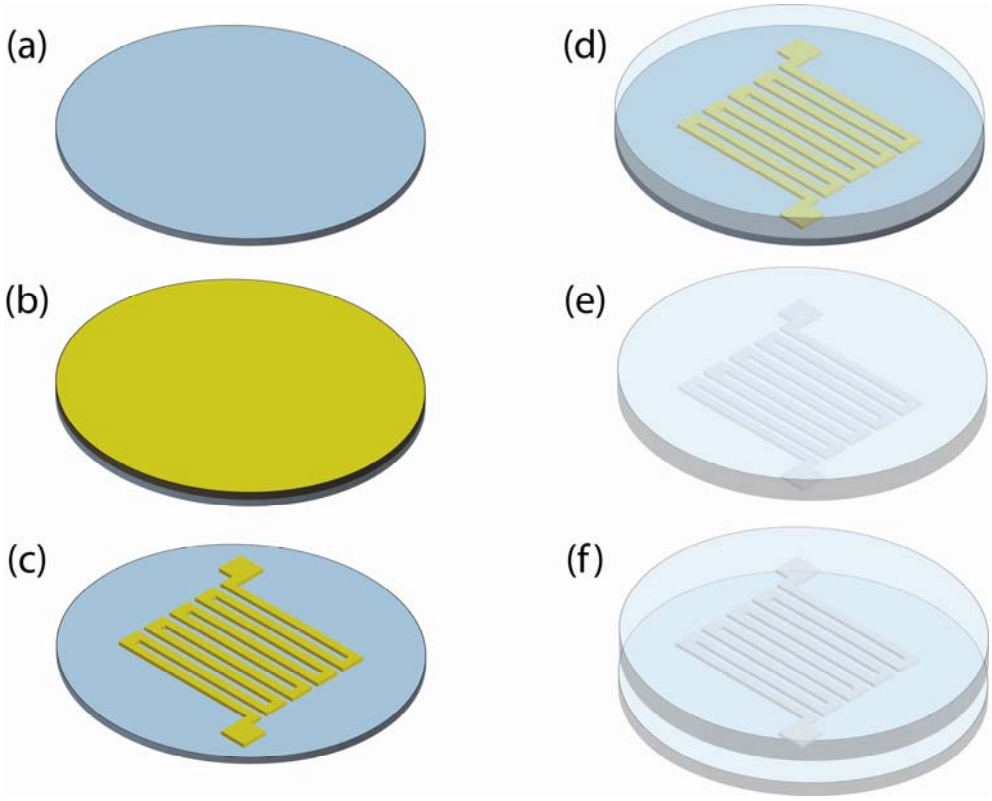

Figure 3-1. Schematic drawings of the SU-8 mold fabrication and PDMS casting method process flows. (a) The process begins with a clean bare silicon wafer; (b) SU-8 photoresist is spun onto the wafer; (c) the desired pattern is exposed and developed; (d) the wafer is placed inside a plastic dish and PDMS is poured and cured; (e) the cured PDMS pattern is removed from the mold, and (f) the PDMS layer is aligned and bonded a substrate layer.

then placed inside a vacuum chamber and degassed for 5-10 minutes till the air bubbles have disappeared. The mixture is then poured into the Si/SU-8 mold. Small residual air bubbles may occur at this point that usually removed during the 60 minute curing step at 60°C and do not typically pose a problem unless the bubble appears at a crucial location on the mold. After cooling, the PDMS can be carefully cut out with a sharp scalpel and peeled off the mold, yielding a transparent polymer containing a pattern of channels and chambers.

One of the major advantages of PDMS is that it can seal to itself or to other surfaces, reversibly or irreversibly without distortion of the microchannels. In our case, forming an irreversible seal involves applying oxygen plasma for 30 seconds to treat the PDMS cutout and a substrate (depending on application, it can be glass, silicon, or another piece of PDMS). This treatment generates silanol groups (Si-OH) on the surface of the PDMS by the oxidation of methyl groups, allowing the surface oxidized PDMS to seal to When the cutout and the substrate are aligned and pressed together within 1 minute of removal from the plasma chamber, a tight seal will be created. This PDMS assembly needs to be baked at 60°C for at least 30 minutes to ensure the integrity and longevity of the seal.

3.1.3 PDMS Membranes

PDMS membranes are fabricated by spinning a thin layer of PDMS onto a circular transparency cutout. Prior to spinning, the transparencies are cleaned with DI water and dried with nitrogen to ensure the removal of unwanted dust particles that could result in holes or defects in the membranes. PDMS pre-polymer and curing agent must be well-mixed, requiring at least 10 min. of vigorous manual mixing and 30 min. of degassing in order to prevent pockets of uncured pre-polymer that form holes and

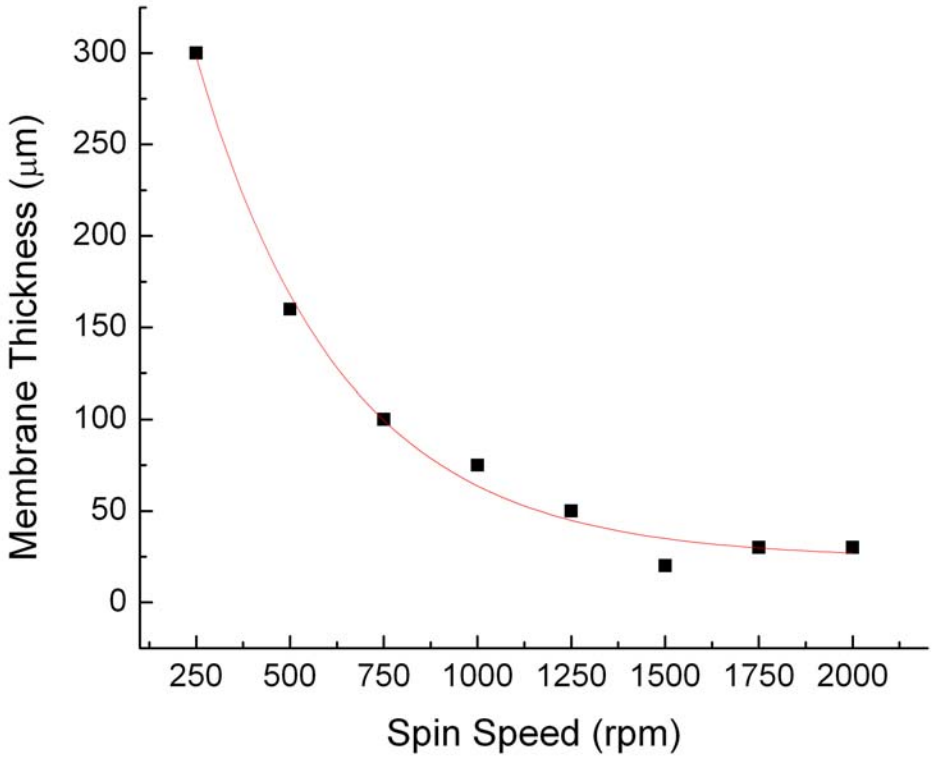

Figure 3-2. PDMS membranes were prepared by spin-coating onto a transparency, baking until hardened, and then subsequent plasma-treating and bonding to a glass surface. Pieces of the PDMS membrane were removed from the glass substrate, and the edge was measured with a profilometer to determine membrane thicknesses at different spin speeds.

weak spots in the membrane. Spinning at 1000 rpm for 30 seconds with a 500 rpm/min. ramp yields a PDMS membrane that is approximately 60 um thick, but will also hold up to the pressures generated within the microfluidic device without tearing. The membranes are baked in a covered container at 60°C for at least 30 minutes. The bonding of the PDMS membranes are performed using the same protocol as described in the previous section.

PDMS spun at different speeds yield membranes of different thicknesses with a limitation of around 25μm under normal 10:1 pre-polymer-to-curing agent ratios and spinning conditions, as graphed in Figure 3-2. By changing the mixing ratio to 5:1, the membranes formed showed more rigidity and were more difficult to remove from the transparency. The 20:1 mixing ratio yielded more elastic membranes, as demonstrated previously by several groups [6, 7]. In order to measure the thickness, PDMS membranes were prepared by spin-coating onto a transparency, baking until hardened, and then subsequent plasma-treating and bonding to a glass surface. Pieces of the PDMS membrane were carefully removed with tweezers from the glass substrate, and the edge height was measured with a profilometer to determine membrane thicknesses at different spin speeds. We observed that with our current mixing ratio and spinning setup, the thinnest membrane we were able to achieve was approximately 30 μm. Although for our purposes, the thicker membranes have proved to be more durable in sustaining higher pressures. There have been reports of novel methods to make ultra-thin PDMS membrane devices of 70 nm thicknesses by diluting the PDMS with hexane and spinning on Teflon-coated silicon wafers [8].

3.1.4 PDMS Passivation

The high surface-to-volume ratio in microfluidic channel designs increases the possibility of enzymes, cells, and proteins non-specifically adhering to the hydrophobic surface of the PDMS channel walls, this reducing the efficiency of the device. In order to reduce non-specific surface adsorption, many groups have investigated a variety of surface modification procedures, some involving highly complex chemical reactions. In our experiments, we sought to investigate simpler flow-through solutions that only require a single incubation. The use of bovine serum albumin (BSA) at relatively high concentrations (2 mg/ml) is a well-documented process for passivation of PDMS devices, and can be achieved by flowing the solution through the device and incubating at room temperature for a short period of time (10-15 min.). An alternative process proposed by Boxshall *et al.* involved the adsorption of 1% Pluronic® 127, a poly(ethylene oxide)-based (PEO) co-copolymer containing poly(propylene oxide) (PPO) and demonstrated approximately 50% reduction in protein adsorption and almost 90% reduction in cell adhesion [9]. This process, however, required a 24 hour incubation period at room temperature, which increased the likelihood of air bubble development within the chambers.

The experiment involved incubating the device with the different passivation agents for the appropriate time period, introducing and trapping conjugated beads and target salmonella cells within a serpentine microfluidic chamber, and flowing guanadinium thiocyanate (GuSCN) lysis buffer over the trapped beads. 200µl of the subsequent lysate was collected and analyzed with real-time PCR to determine initial DNA

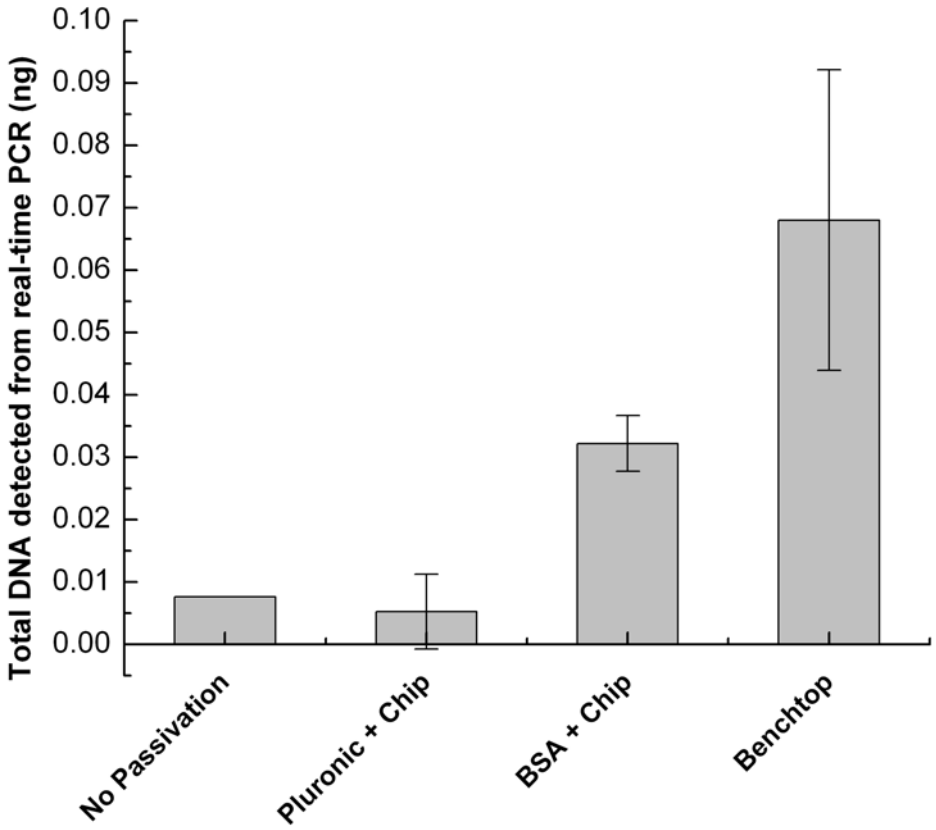

Figure 3-3. Comparison of the differences in DNA yields from magnetic bead-based cell capture and lysis when pre-treated with different surface passivation molecules. 1.5E+7 cells were incubated with 40 µL of anti-salmonella magnetic beads for 10 minutes and introduced into the microfluidic device and captured with an external permanent magnet. Lysis was subsequently performed by flowing through 200 µl of lysis buffer and 200 µl of collected lysate was analyzed with real-time PCR. Pre-treating with 2% BSA showed a 4-fold improvement in DNA yield when compared to the chip with no pre-treating. The pre-treatment with Pluronic performed less than admirably, likely due to the tendency for increased bubble formation.

concentrations. As shown in Figure 3-3, the short incubation with BSA proved to be the most effective in improving the yield of DNA from cell lysate, and became the standard protocol in all our subsequent microfluidic pathogen detection experiments. A single experiment using 1% Tween, another PEO-derived surfactant was also attempted, but unsuccessful due to the excessive formation of bubbles within the microfluidic chambers.

3.2 Microfluidic Module: Electro-Hydraulic Pumps

Low-power electrolysis-based microfluidic pumps utilizing the hydraulic press principle, integrated with microfluidic channels in polydimethylsiloxane (PDMS) substrates, are presented. The electro-hydraulic pumps (EHPs), consisting of electrolytic, hydraulic and fluidic chambers, were investigated using two types of electrodes: stainless steel for larger volumes and annealed gold electrodes for smaller-scale devices. Using a hydraulic chamber and a thin flexible PDMS membrane, this novel prototype successfully separates the reagent fluid from the electrolytic fluid, which is particularly important for biological and chemical applications. The stainless steel electrode EHPs, manufactured with 6 mm- to 75 mm chamber diameters and 1:1 to 1:3 chamber volume ratios, produced flow rates of 1.25 to 30 μl/min at 3 to 7 VDC, with compatibility with various tested fluids (deionized water, PBS, and ethanol), and could sustain pressures up to 150 kPa. The gold electrode EHPs were manufactured with 3mm diameters and 1:1 chamber volume ratios, and produced flow rates of 1.24 to 7.00 μl/min at 2.5 to 10 VAC, with a higher maximum sustained pressure of 343 kPa, suggesting greater device robustness using methods compatible with microfabrication. The hydraulic advantage of the device can be easily tuned by changing the volume ratios of the chambers; and since the reservoirs would be pre-

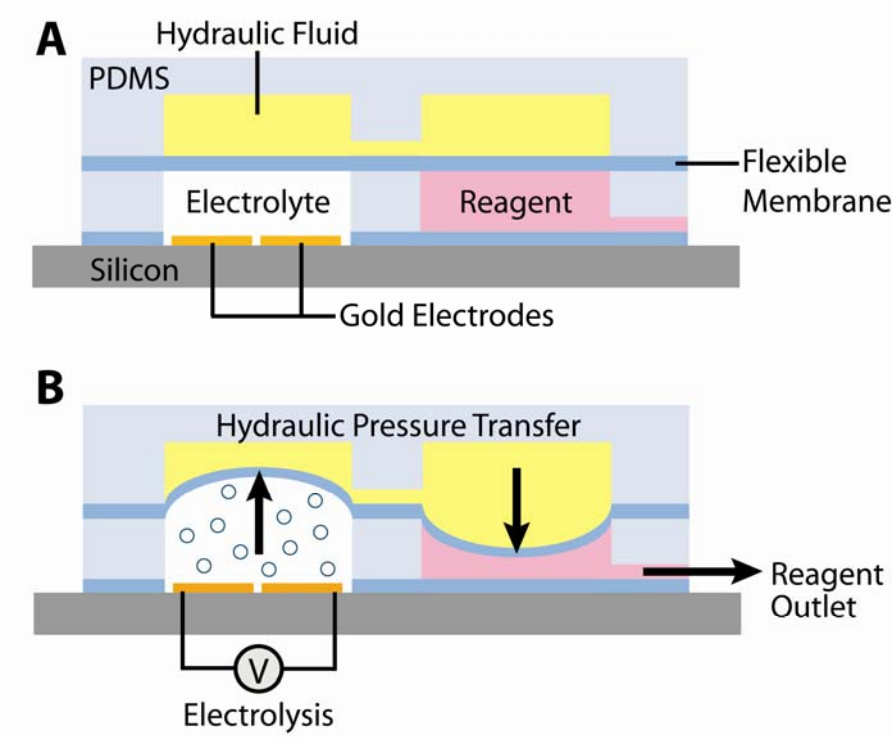

Figure 3-4. The Electro-hydraulic Pump. Overall schematic of the electro-hydraulic pump shows the mechanism of activation. Pumping fluid (electrolyte) is subjected to an electrical current, causing bubble formation through electrolysis. Pressure is transferred through a flexible membrane to a hydraulic fluid chamber, which then forces fluid out of the reagent reservoir.

filled with sample and sealed prior to testing, external fluid coupling is not required. The proposed technology is low-cost, low-power and disposable, with a high level of reproducibility, allowing for ease of fabrication and integration into existing microfluidic lab-on-a-chip and analysis systems.

3.2.1 Background on Microfluidic Pumps

Precise low-power control of biological fluid flow at the microscale is crucial for the successful development of lab-on-a-chip and portable polymerase chain reaction (PCR) systems [10]. In the past decade, extensive research in microfluidic device technology [11-13] has paved new paths for micro total analysis systems (μTAS) and other multi-functional detection platforms [13-17] with applications in genomic sequencing [18-21], drug discovery [22-24], single-cell analysis [25-30], and diagnostics [10, 31-33]. Since traditional syringe pumps have a low potential for integration [34], considerable interest has been shown in developing small-scale microfluidic pumps to replace the macro-scale mechanical pumps [35-38].

Microfluidic pumps currently employ a variety of different actuation mechanisms: thermopneumatics [39, 40], electrostatics [41-43], piezoelectrics [44-46], electromagnetic [47-49], and hydrogels [50, 51], among others. Some microfluidic pumps focus on controlled delivery of micro- and nanoliter solutions over long periods of time, while others seek to achieve high pumping volumes at low power. Thermal and electrolytically-generated bubbles have been investigated for their utility in miniaturized pumps, microfluidic dosing experiments [52], and are favorable due to simple fabrication and ease of control. The disadvantage of thermal production of H_2O vapor bubbles is the risk of denaturation of biological molecules due to overheating

[53]. In addition, the electrolytic production of bubbles has been shown to be far more energy efficient than thermal bubble generation [12].

In this article, we illustrate a new approach for fabricating a low-power microfluidic electro-hydraulic pump (EHP), based on the generation of electrolytic bubbles inside a microfluidic chamber [54-59]. The novelty of this device lies in using the existing electrolytic technology in conjunction with a hydraulic chamber, in order to actuate the reagent chamber. The new pump design efficiently isolates the actuation mechanism from the reagent chamber as to prevent contamination between the different fluids, which is of particular importance for biological and chemical applications [53]. In addition, the hydraulic advantage of the device can be easily tuned by changing the volume ratio of the electrolytic chamber and the reagent chamber. Operation of the EHP would not require external fluid coupling, since the reservoirs would be pre-filled with sample and sealed prior to testing. The pump demonstrates ease of fabrication and operation, low power consumption, customizability, and has great potential for effortless integration into existing microfluidic systems.

3.2.2 Theory of Operation

The basic microfluidic EHP design consists of two pumping chambers that separate contain pumping fluid (electrolyte) and liquid reagents, and is shown in the schematic in Figure 3-4. Electrodes are placed in the electrolyte chamber (EC) and gas bubbles are produced via electrolysis when a voltage is applied. The increased pressure within the EC chamber due to the generation of gas bubbles is transferred to the fluid in the hydraulic chamber (HC) via a thin flexible membrane. The HC is split into two effective chambers, one that responds to the EC and that actuates the reagent chamber

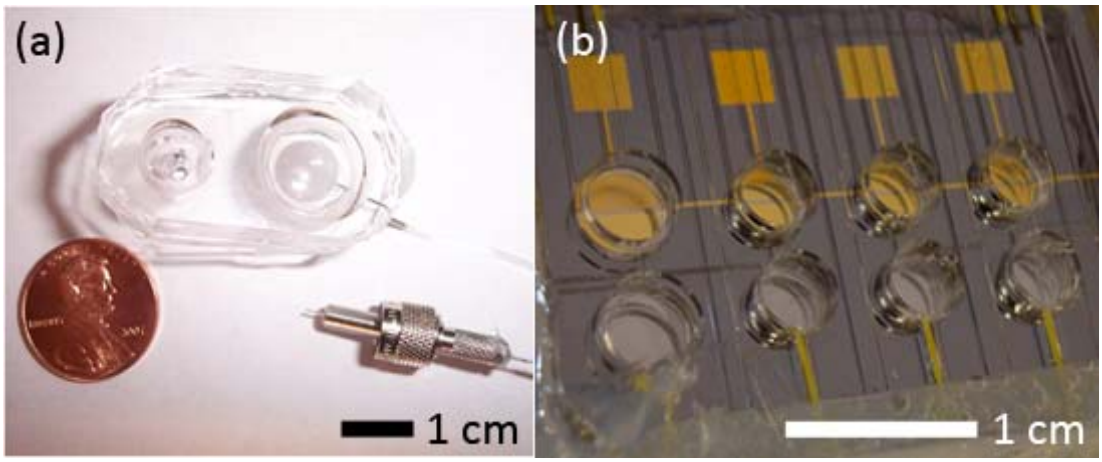

Figure 3-5. Completed prototype EHP pump. (a) 1 mL stainless steel model with a 5:4 hydraulic advantage, shown with a microfluidic connector (b) Device containing four gold electrode EHP modules with 15 μL reagent reservoirs

(RC). The pressure applied to the hydraulic fluid from the EC is translated to the RC, forcing the reagent to move through an outlet. Small amounts of electrical energy can be used to pump fluids in a controlled manner. Unlike previous pump designs [54-59], this design separates the reagent fluid from the electrolyte, and also demonstrates the utility of having a hydraulic advantage.

Pascal's law of fluid dynamics states that a change in pressure applied to an enclosed fluid is transmitted undiminished to every point of the fluid and the walls of the container vessel, and has been demonstrated in applications such as the hydraulic press. The microfluidic EHP system incorporates this hydraulic press principle into the pump design. When a force F_1 is applied to a chamber area of A_1, a resulting pressure P is transmitted to the second chamber of area A_2 as a force of F_2. The pressure is constant in both chambers, as illustrated in Equation (1). Therefore, the force F_2 is larger than F_1 by the multiplying factor A_2/A_1.

$$P = \frac{F_1}{A_1} = \frac{F_2}{A_2} \quad (1)$$

Assuming no losses in the system, the total input work and the total output work of the HC should be equal, as in Equation (2). From this, we can extract that the ratio of the diameter of the RC over the diameter of the EC is directly proportional to the pressure output and that for a larger A_1/A_2, we can obtain higher output pressures for the same volume of displaced reagent.

$$W = F_1 D_1 = F_2 D_2 \quad (2)$$

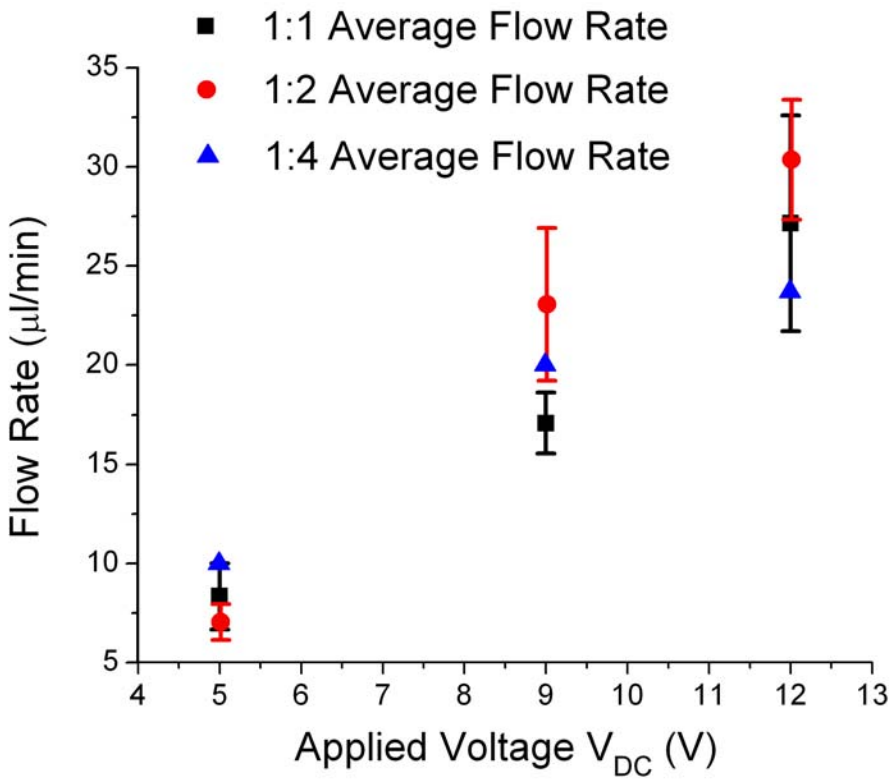

Figure 3-6. Conservation of Flow Rate. The effect of chamber area ratio (EC:RC) on pump output flow rate is investigated for DI water at different applied DC voltages. This shows that for different area ratios, the effective flow rate is constant, at a given applied voltage for electrolysis.

The hydraulic advantage of this pump design dictates that the volume of reagent fluid pumped is limited by the size of the EC. The flow rate of the pumps is controlled by the amount of voltage applied to the electrolytic chamber. Therefore, the chamber design is important and has to be tailored for specific applications. Since actuation of the pump does not require larger external devices, the pumps as well as the associated electronics can be scaled dramatically. This innovative design can provide higher output pressures than traditional pumps, and the sizes of the electrolyte and reagent chambers can be modified to provide a hydraulic advantage.

3.2.3 Materials & Methods

The EHP fluidic structures are constructed by casting polydimethylsiloxane (Sylgard 184, Dow Corning, Midland, MI) onto an SU-8 negative photoresist mold. For the investigation of larger-scale stainless steel EHPs, the SU-8 molds are modified with hemispherical lenses to control chamber volumes. PDMS pre-polymer is mixed with a curing agent at a 10:1 mass ratio and degassed in a vacuum chamber before pouring into the SU-8 mold. To fabricate the flexible membrane, PDMS is spun onto a thin plastic transparency at spin speed of 1000 rpm. The individual PDMS components are baked at 60°C for 60 minutes until hardened. The EHP is assembled with the top hydraulic fluid chambers and the bottom electrolyte and reagent chambers separate by a thin flexible PDMS membrane.

Stainless Steel Electrode EHPs. Stainless steel pins (Swan Secure Products, Inc, Baltimore, MD) were secured with epoxy adhesive in the polystyrene base of the electrolyte pump chambers. These electrodes showed no signs of degradation over a five week period and the completed system could withstand 150 KPa of pressure without leaking. To optimize the microfluidic EHP design, we developed a method to

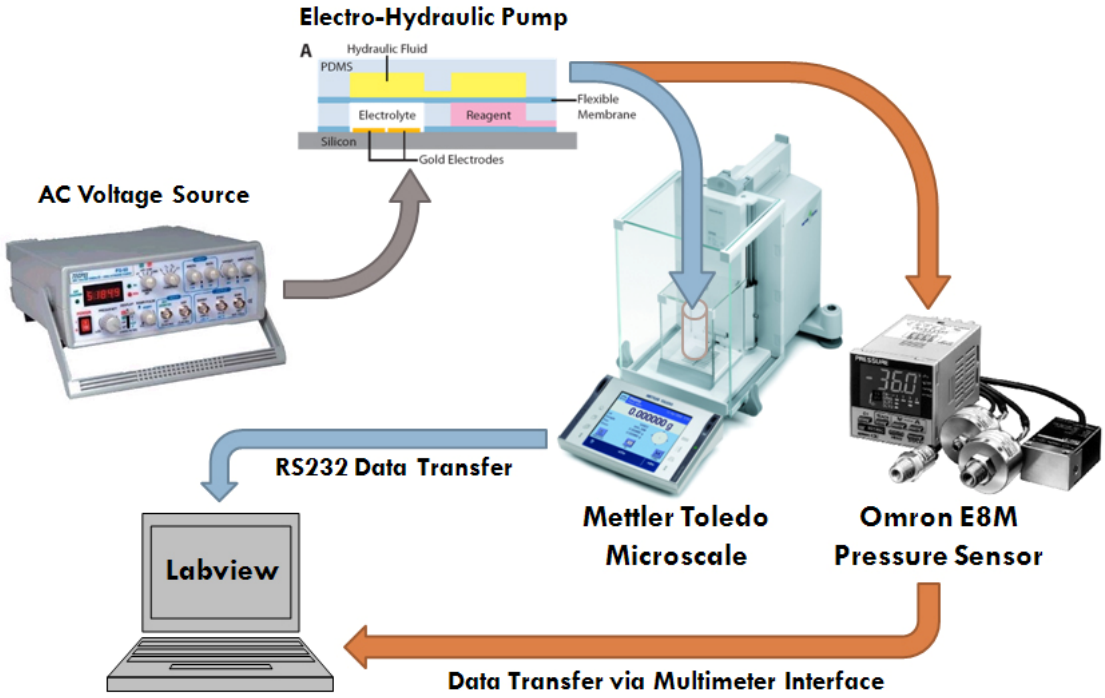

Figure 3-7. EHP Testing Setup. The testing of gold electrode EHPs involved measuring using a high-sensitivity microbalance in conjunction with National Instruments Labview® software to capture the flow rates in real time. The pressure testing was conducted in a similar fashion, by connecting a pressure sensor to the pump outlet and monitoring with Labview®.

fill the EHP chambers and to develop novel microfluidic connections between EHPs and microfluidic components. Microfluidic connectors involving modified SMA fiber optic connectors were designed. One end of the connector was a SMA fiber optic connector threaded with 0.25 mm 27-gauge stainless steel tubing, while the corresponding end incorporated 0.62 mm Tygon tubing. Small gauge tubing (Tygon, PEEK, etc.) was then attached with pressure-tight fittings. The SMA mating adapter kept these two pieces of tubing aligned, and when tightened, formed a watertight seal between the two connectors. The connection was reusable and could be used repeatedly without compromising its watertight seal. Figure 3-5(a) shows a completed stainless steel electrode EHP prototype and a section of the microfluidic connector.

Gold Electrode EHPs. In In order to further miniaturize the system for ease of fabrication and integration with existing microfluidic platforms, 250 nm-thick gold electrodes were e-beam evaporated onto a bare silicon wafer with a 500nm thermal oxide layer, and annealed at 400°C for 120 minutes. The annealing step prevents the rapid peeling of gold during electrolysis and helps prolongs the life of the device. The PDMS chamber assembly is plasma treated, aligned to the gold electrodes, and bonded to the wafer surface. Small gauge tubing (PEEK) was inserted into the inlets and outlets, and secured using silicone sealant, shown in Figure 3-5(b). After filling of the chambers and re-sealing, copper wires were attached to the electrode pads using conductive silver epoxy.

3.2.4 Experimental Setup & Protocol

The microfluidic EHP pumps and control system underwent exhaustive testing to determine flow rates and reliability with different applied pumping parameters. The electrolyte used in the electrolyte chamber was TRIS-acetate, EDTA. Flow rate

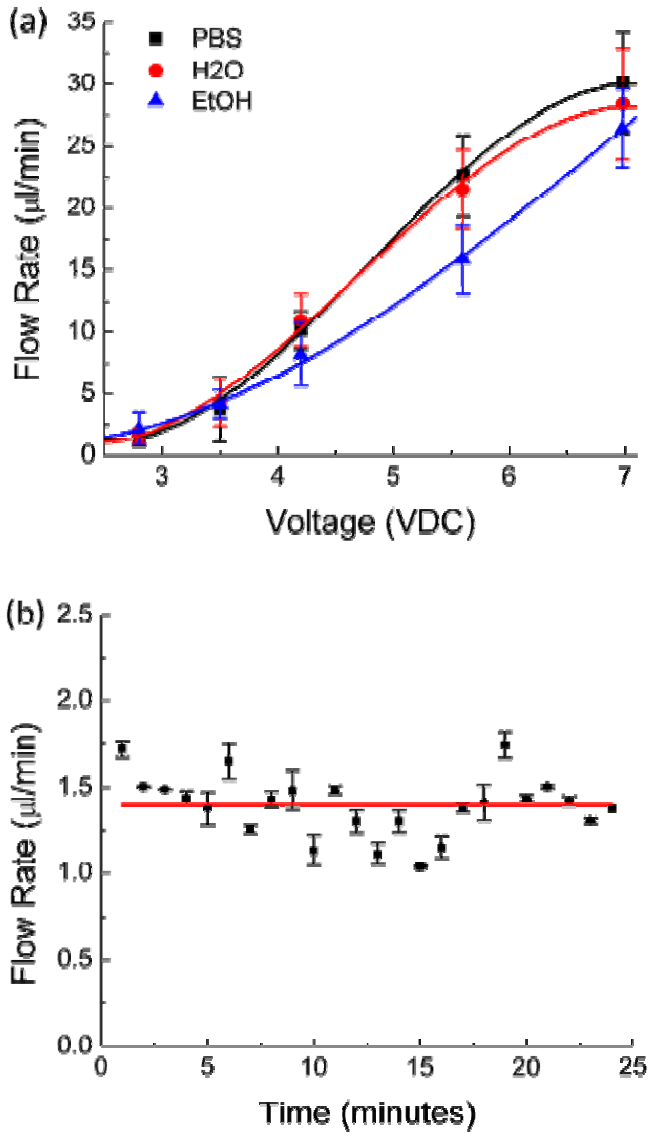

Figure 3-8. Stainless Steel Electrode EHP Testing. The testing of stainless steel electrode EHPs involved measuring (a) the effect of voltage on the flow rate of various solvents (deionized water, PBS, ethanol); (b) the flow rate of a device powered at 7.0 VDC over an operation time of 3 hours was monitored to determine long term flow rate variation.

analysis was conducted to determine the minimum and maximum rates, as well as the steady state rates of sustained pumping.

For the stainless steel EHP devices, calibration curves of flow rate vs. applied voltage were created using a variety of different reagents, including buffers and solvents. Variation in the flow rates with respect to the size of the respective electrolyte and reagent chambers was examined. The diameter of the chambers was varied from 6 mm- to 75 mm and the chamber volume ratios varied from 1:1 to 1:3. In this manner we could systematically examine the effect of reservoir size and hydraulic advantage on the pumping rates and pressure.

Due to the smaller volumes and shorter operation times of the gold electrode EHP devices, the flow rates of 3 mm-diameter devices were measured using a high-sensitivity microbalance in conjunction with National Instruments Labview® software to capture the flow rates in real time. The pressure testing was conducted in a similar fashion, by connecting a pressure sensor to the pump outlet and monitoring with Labview®. A schematic of the laboratory setup is shown in Figure 3-7.

3.2.5 Results and Discussion

Stainless Steel Electrodes. Figure 3-8(a) shows the proportional dependence of fluid flow rate on the applied DC voltage for a pump with 12mm diameter chambers using PBS, Ethanol and DI water as reagents. The chambers were filled with 0.93 mL of fluid and voltages applied to induce the electrolytic process. The flow rate was measured volumetrically over time. The average maximum flow rate was 16 μL/min for sustained flow powered at 7 VDC (Figure 3-8(b)). The chambers are hemispherical, creating a dome-shaped chamber. Bubbles formed in the electrolyte

chamber uniformly rose to the peak of this dome and the flexible membrane could be stretched to make contact with the entire hydraulic chamber surface. This reduced all of the dead volume in the chambers and resulted in more consistent pumping profiles. During testing, EHP outputs were attached to a pressure sensor during fluid pumping at 10.6V (approx. 30µl/min) and maximum pressure was measured upon device failure (fluid leakage). The maximum pressure of 150 KPa was obtained with 20 mm diameter electrolytic chambers and 25mm reagent chambers (a hydraulic ratio of 1.6:1). This pressure exceeds the requirements for pumping through lab-on-a-chip systems.

Since the hydraulic fluid can be assumed to be incompressible, the pressure generated by electrolysis is transferred to the reagent chamber without any loss. Also, the pressure generated is independent of the reagent chamber allowing for flexibility for the pump to be suited for different applications. Figure 3-6 shows the invariability of the output flow rate at different DC voltages, with increasing EC:RC area ratios. The volume flow rates for different area ratios at a given DC voltage fall within the error bars on the graph, indicating no significant variation.

A flow rate standard deviation in +/-0.5 µL/min was observed over time. Notably, pumping at lower flow rates (1-5 µL/min) resulted in more stable flow rate profiles when compared to higher flow rates, which can be attributed to more uniform bubble production within the electrolyte chamber. This fluctuation is in part due to the irregular bubble formation and lack of feedback control. Long-term testing demonstrated that EHPs could be operated for 30 min per day for up to 5 weeks (using large volume reagent reservoirs). Although these tests showed that pumps continued to be operational for extended periods of time, it was noted that the electrolysis

chamber lost pressure between subsequent tests. Therefore, re-pressurization was required during each test, resulting in a short (1-2 min) delay before fluid was expelled from the pump. This further demonstrates the need for a feedback control system to monitor fluid expulsion and resulting flow rate.

Gold Electrodes. In order to minimize power consumption, the flow rates were measured volumetrically for varying applied AC voltages, as shown in Figure 3-9(a). The maximum flow rates for the gold electrode EHP devices were 7.00µl/min, 4.03µl/min, 2.43µl/min, and 1.24µl/min for the applied AC voltages of 10V, 7.5V, 5.0V, and 2.5V, respectively (shown in Figure 3-9(b)). Due to smaller volumes, the pumps only required 5 minutes of operation to deliver the reagent chamber fluid. The maximum flow rates are achieved within the first two minutes of operation. Unlike its stainless steel counterpart, the annealed gold electrodes allowed us to double the electrode lifetime (from approx. 10 minutes to 20 minutes), and switching from DC to AC operation reduced power consumption and further extended the lifetime to 40 minutes. The current through the device was measured for the different voltages, and a sample current is shown in Figure 3-10(a). Bubble coalescence events caused variations in the current measurement (shown as spikes indicated by red arrows). The steady state current relationship to applied voltage is shown in Figure 3-10(b).

Due to the smaller scales of the gold electrode EHP, the maximum pressure exerted during operation of the pumps at 10 VAC is 65 KPa. The EHP outputs were attached to a pressure sensor and monitored real-time via Labview® in order to measure the maximum pressure the device is able to sustain before leakage failure was determined

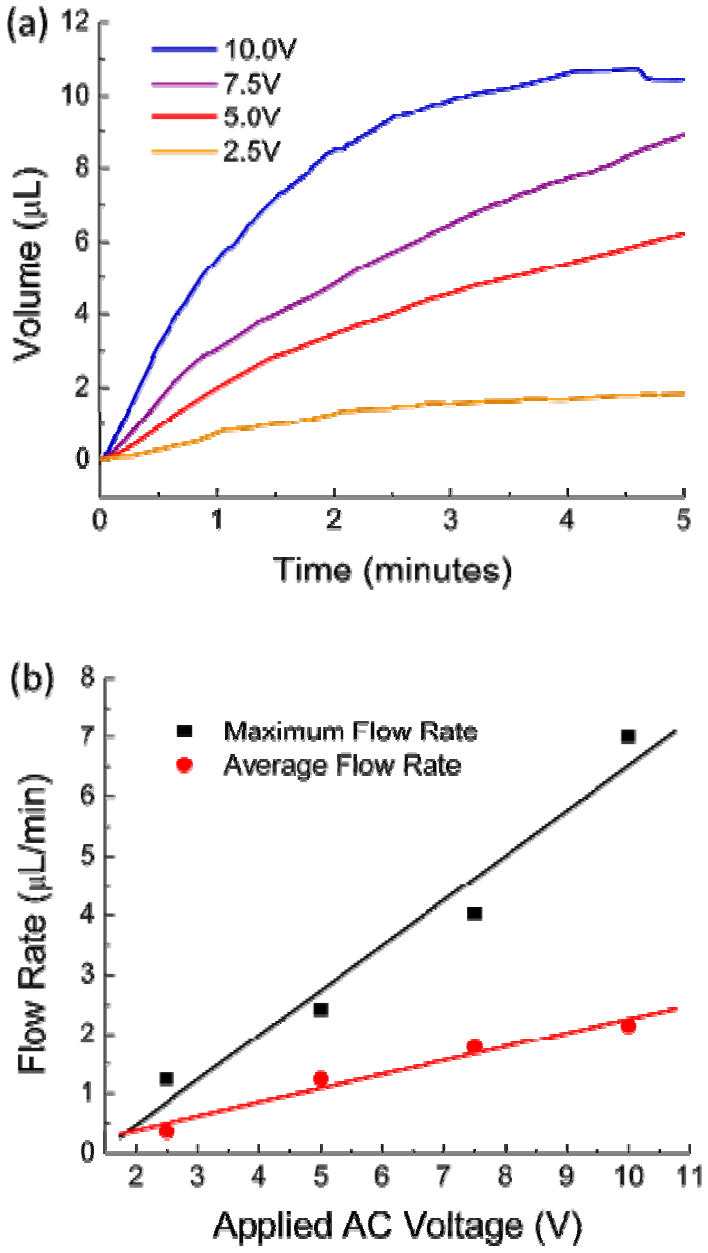

Figure 3-9. Gold Electrode EHP Flow Rate Testing. The flow rate testing on gold electrode EHPs involved measuring (a) the fluid volume expelled from the device at each applied AC voltage (b) the effect of varying voltage on the flow rate

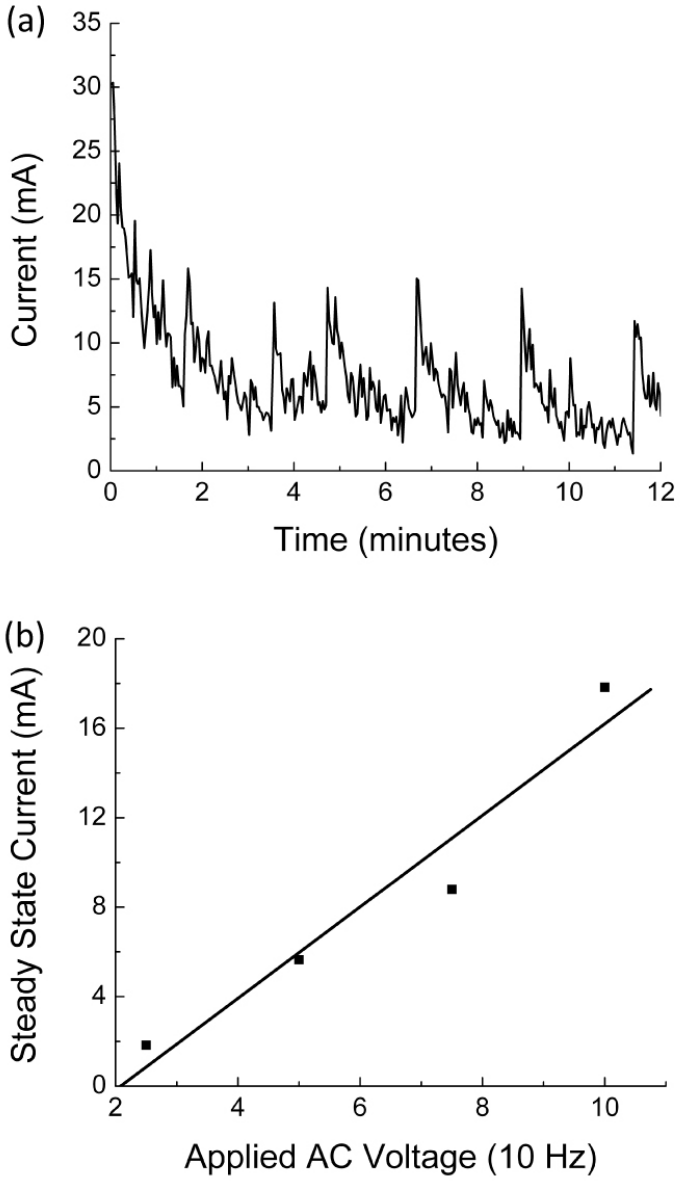

Figure 3-10. Gold Electrode EHP Current Testing. The current testing involved measuring (a) the raw sample current of a device powered at 5 VAC (10 Hz) over 12 minutes, with current spikes (red arrows) correlating with bubble coalescence events (b) the steady state current achieved at each applied AC voltage (10 Hz).

(as shown in Figure 3-11). This measured pressure (343 KPa) exceeds the maximum pressure obtained from the larger stainless steel EHPs, suggesting that a stronger seal at the device inputs, outputs and electrodes can be formed using microfabricated techniques.

Apart from the miniaturization advantage and the low power consumption, precise pumping rates with low variability are important for many microfluidic devices and it is clear that opportunities exist to establish a feed back control to regulate the voltage applied to the system. Therefore, future designs will focus on the design and integration of a feedback control system to measure the flow rate and use this information for operational feedback.

3.2.6 Section Summary

In summary, we have demonstrated that EHPs can provide the necessary fluid flow rates and pressures for microfluidic analytical systems. The proposed technology is low-cost and disposable with a high level of reproducibility. The polymer-based fabrication methods are compatible with standard microfabrication technologies, making it possible to directly integrate these pumps with lab-on-a-chip systems. The work resulted in an improved EHP design that could deliver a wide range of flow rates (1.25µl/min to 30µl/min) and was compatible with aqueous buffers and organic solvents (water, PBS, and ethanol). We note that improvements could be made to increase longevity of gold electrodes with improved designs and materials, as well as investigations into pulsed device operation. In addition, feedback control could be implemented to improve the flow rate variance in sustained long-term pumping.

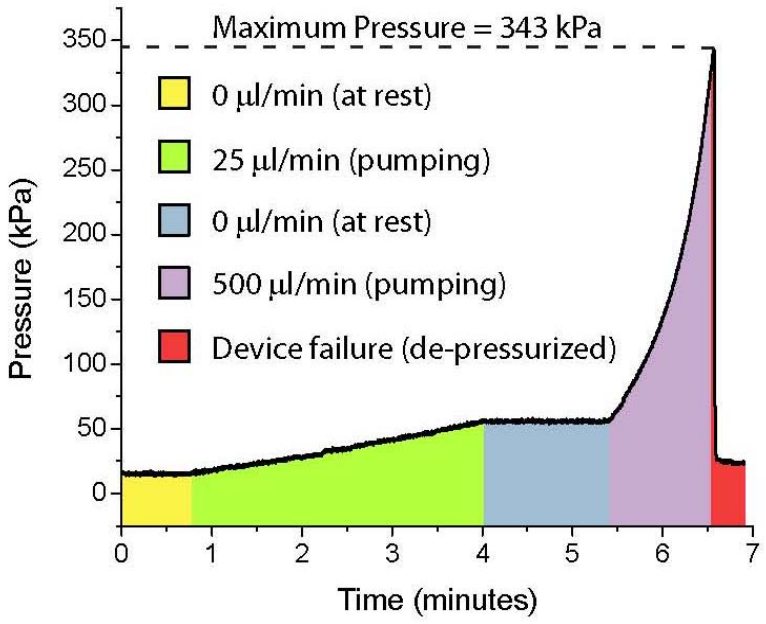

Figure 3-11. Gold Electrode EHP Pressure Testing. The maximum pressure testing involved pressurizing with an external pump and monitoring using a pressure sensor hooked to the pump outlet, to the point of device failure at 343 kPa.

Pumps were fabricated entirely from polymeric materials (polystyrene and PDMS), suggesting the feasibility of low-cost, high throughput manufacturing. In addition, an electronic module was developed to deliver precise pumping voltages under software control. Fluid flow rates were proportional to the applied voltage, making it possible to roughly predict control pumping parameters. While the stainless steel electrodes were effective, the integration of the gold electrodes represented a challenge in developing a more integrated manufacturing approach to the system. The deposition of the electrodes by processes compatible with standard silicon processing allows us to move forward with a more integrated, scalable manufacturing process. Our approach holds great potential for the miniaturization of pressure-driven microfluidic applications in which fluid must be delivered quickly and efficiently.

3.3 Microfluidic Module: Magnetic Bead-Based Sample Preparation

The emergence of novel microfluidic and MEMS technologies in recent years is driving the study of fluid flow control at the microscale. The demand for integrated lab on a chip systems with increased speed, efficiency, and ease of use has grown considerably, of which the selective sorting of cells and biomolecules is of considerable interest. Many efforts have been put into transforming conventional biological laboratory processes into miniaturized microfluidic systems in order to minimize time and reagent costs. Magnetic beads play a vital role in many biomedical applications, particular in separations. The basic magnetic bead-based separation system consists of two main components: (1) the microscale beads used as a solid phase carrier to selectively bind to the target of interest and (2) a magnetic field source [60]. The application of an external magnetic field allows fast and selective separation

of target samples suspended in fluids using a noninvasive biocompatible manipulation process.

3.3.1 Introduction to Magnetic Bead-based Separations

Microscale magnetic beads are commercially available with a variety of different surface functionalizations and commonly used for laboratory scale biochemical assays and separations. The breads typically range from 10 nm to 10 μm and are typically composed of a mixture of polymer and iron oxide particles, Fe_2O_3 and Fe_3O_4 suspended in an aqueous mixture. These beads are typically synthesized in a three-step process, which involves: (1) preparation of porous uniform polymer microspheres, (2) filling of the pores with iron salt solutions to allow precipitation of magnetite nanoparticles within the pores upon chemical reaction initiation, and (3) deposition of a polymer to fill and close the mores of the microspheres. The matrices of the magnetic particles are commonly composed of agarose, cellulose, silica, silane, porous glass, mica, or polystyrene. Magnetic beads have been reported for use in the detection of immunological reactions, DNA hybridization, blood cell separations, and cellular therapy, among others. Several groups, notably Pankhurst et al., Pamme *et al.*, and Gijs have reviewed the handling and varying applications of magnetic nanoparticles in microfluidic systems [61-63].

Permanent magnets, particularly high-strength rare earth magnets, are the easiest methods of generating a strong magnetic field to capture magnetic beads within a solution. Electromagnets, on the other hand, have the ability of modulate the strength of the magnetic field by varying the current flow through the device. A variety of different schemes have been investigated, including the quadrupole magnet configuration, loosely-packed magnetizable matrices or columns, and micro-coils

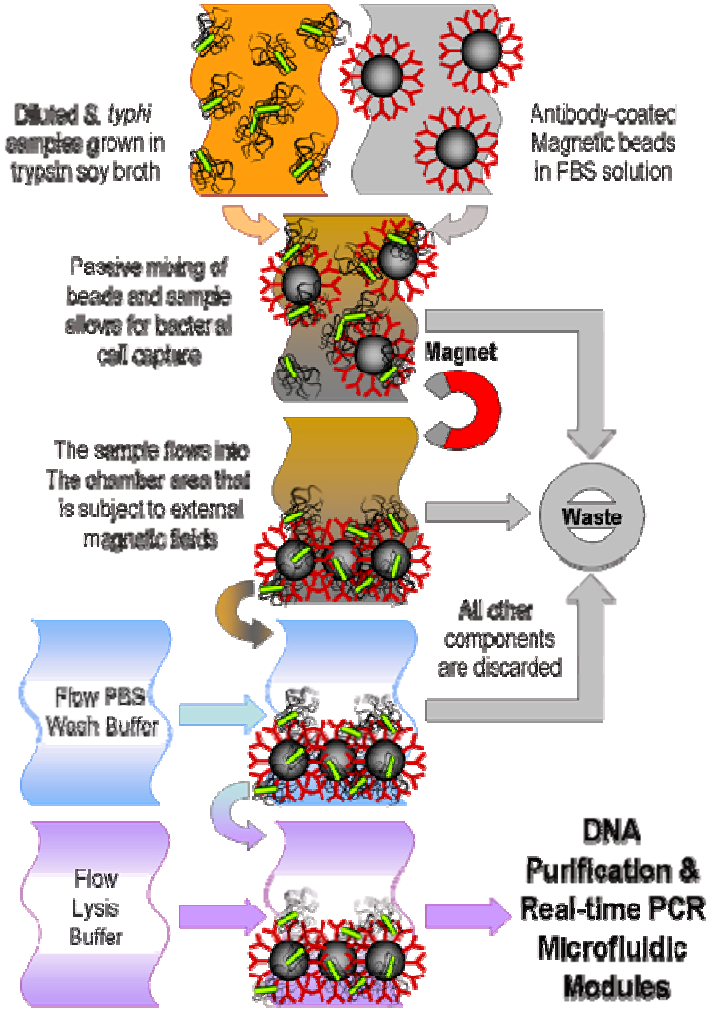

Figure 3-12. The process flow for microfluidic immunomagnetic cell isolation, buffer wash, and subsequent chemical lysis of *Salmonella typhi* using antibody-coated paramagnetic beads and external magnetic field capture.

localized high magnetic field gradients [60, 61, 64, 65]. For beads greater than 2 μm in diameter, a centimeter-sized rare earth permanent magnet is capable of immobilizing the beads in a flow setup. With smaller beads, some form of magnetic gradient intensifier is necessary, and a number of schemes have been proposed [66-72], though many face limited success in sorting or manipulating cells [73-75].

Magnetic bead-based cell separation is particularly useful in selecting specific populations of cells from a raw sample through differentiation of the chemicals of the cell surfaces. One of the first demonstrations of magnetic separation was achieved by Melville *et al.* in 1975, where red blood cells were separated by whole blood based upon native magnetic susceptibility [76]. Separation by selective attachment of magnetic beads was demonstrated by Molday *et al.* in 1977 [77], and recently achieved on microfluidic devices as an inexpensive method for isolating rare cells [78-81]. A number of companies offer magnetic particles and separation kits optically adjusted for the application of choice, each pushing for improved binding properties and better separation [82-87]. A typical magnetic bead-based cell separation process flow is shown in Figure 3-12.

Rapid homogeneous mixing is vital for many lab-on-a-chip systems, particularly when using bead-based sample preparation schemes. To prevent the beads from settling due to the effects of gravity, a number of different micromixing schemes have been proposed in recent years [88-93]. Since turbulence is difficult to attain at the microscale, microfluidic mixing has been largely dominated by diffusion, which tends to be slow and inefficient. Chamber micromixing is of particular interest for many biological applications, and a number of different designs have been investigated. The principle of bubble-induced acoustic microstreaming has been previously

(a)

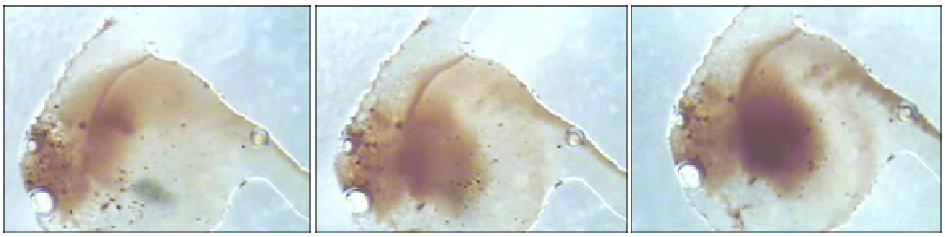

(b)

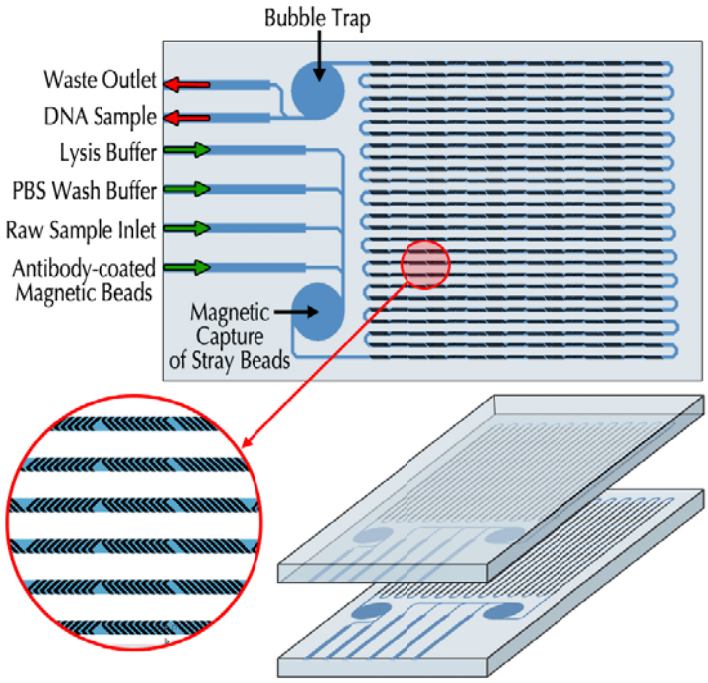

Figure 3-13. (a) Photographs of magnetic beads within a microfluidic chamber placed atop a 6-node rotating magnet configuration (b) The herringbone grooves inside the serpentine channels have been shown to enhance the mixing of two different solutions, and in this design, the groove design is molded into two slabs of PDMS with appropriate inlets and outlets which are then bonded together into a single device. An external permanent fridge magnet (~200 Gauss) is manually placed beneath the device for magnetic bead capture, and bubble trap chambers strategically placed to capture stray bubbles.

demonstrated using a multi-bubble induced chamber mixer, and demonstrates excellent mixing and immunomagnetic cell capture of target pathogens from a heterogeneous biological solution [94, 95]. We propose a microfluidic device based upon this bubble-induced mixing principle that enables separation of target cells tagged with antibody-coated magnetic microbeads. In this design, tagged cells are introduced into a chamber and an external magnetic field is applied to immobilize the cells. The subsequent chemical lysis of the captured cells is improved through the application of a piezoelectric membrane to actuate the beads and enhance mixing.

3.3.2 Device Microfabrication

Our device designs have undergone several iterations and improvements. Our initial design incorporated an 8mm diameter microfluidic chamber with 6-prong permanent magnets beneath the chamber that rotated at 50 revolutions/min in order to mix the magnetic beads, as shown in Figure 3-13(a). This first design proved to be bulky in size and less efficient due to magnetic beads adsorbing to the bottom of the chamber. In order to move away from a design with too many mechanical moving parts, our second mixer design involved fabricating herringbone grooves within a serpentine channel in a modification off the original design by Strook *et al* [96], and were used in some of our initial magnetic bead-based experiments (see Figure 3-13(b)). Our current design shown in Figure 3-14 is an active mixer and incorporates two main elements: (a) an array of four PDMS-based bubble traps used for the enhancement of piezoelectric actuation of the microbeads and (b) a circular chamber resting atop an electromagnet used to capture and retain magnetic beads. The bubble trap layer is formed from PDMS with designated areas for manual punch-out using a 1mm-diameter stainless steel corer. The chamber layer consists of an 8mm-diameter

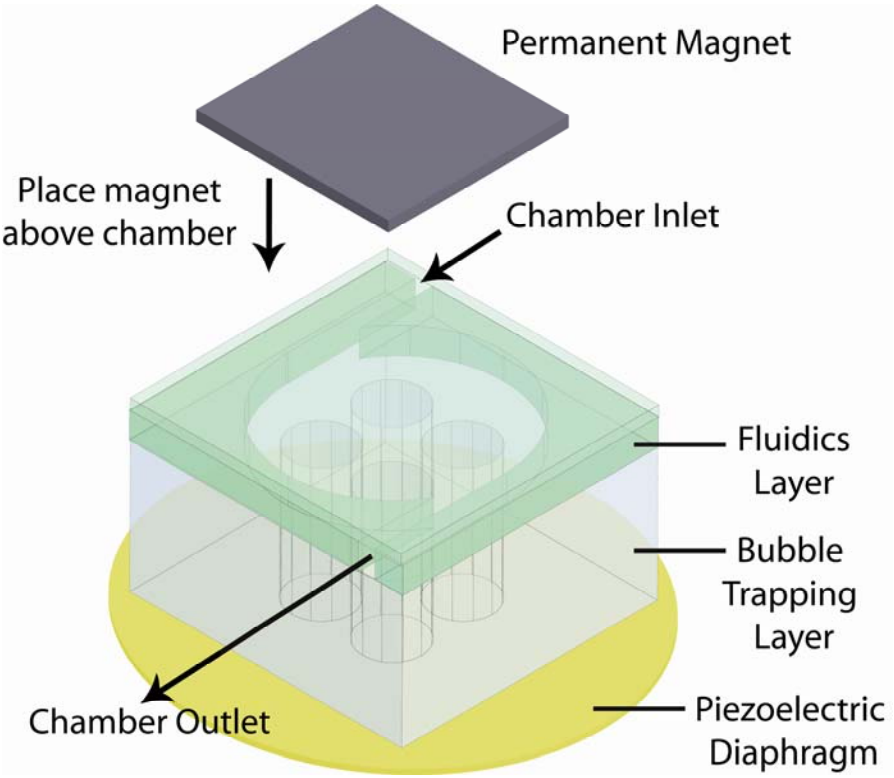

Figure 3-14. Schematic of the current mixer design which includes incorporates an array of four PDMS-based bubble traps used for the enhancement of piezoelectric actuation of the microbeads and a circular chamber resting atop an electromagnet used to capture and retain magnetic beads.

250μm-height chamber with 100μm-width inlet and outlet channels formed within a PDMS slab. PDMS membranes of 100μm thickness flank the top and bottom of the device assembly such that the distance between the magnet, piezoelectric diaphragm and the microfluidic mixer device is minimized.

The mixer fluidic structures are constructed by casting polydimethylsiloxane (Sylgard 184, Dow Corning, Midland, MI) onto an SU-8 negative photoresist mold, as described in previous sections. PDMS pre-polymer is mixed with a curing agent at a 10:1 mass ratio and degassed in a vacuum chamber before pouring into the SU-8 mold. PDMS membranes are formed by spinning onto a thin plastic transparency atspin speed of 1000 rpm. The individual PDMS components are baked at 60°C for 60 minutes until hardened, then plasma-treated, assembled and aligned with the bottom fluid chambers and the top bubble traps flanked with flexible PDMS membranes. The entire assembly is placed atop a silicon wafer. To improve the transfer of energy to the device, the piezoelectric diaphragm is attached to the bubble trap side of the device using a quick-hardening epoxy. The electromagnet is placed beneath the wafer, directly underneath the chamber area. Small-gauge PEEK tubing is threaded into plastic tubing and inserted into the inlets and outlets, and secured using silicone sealant.

3.3.3 Microbiological Protocols and Regaents

Salmonella typhi was obtained from frozen cell stock and grown in a trypsin soy broth (TSB, BD, Franklin Lakes, NJ) agar plate culture for 24 hours. A single bacterial colony was removed from the plate culture and grown in 5 mL of liquid TSB media at 37°C and gentle agitation for 12 hours. The final culture concentration was estimated

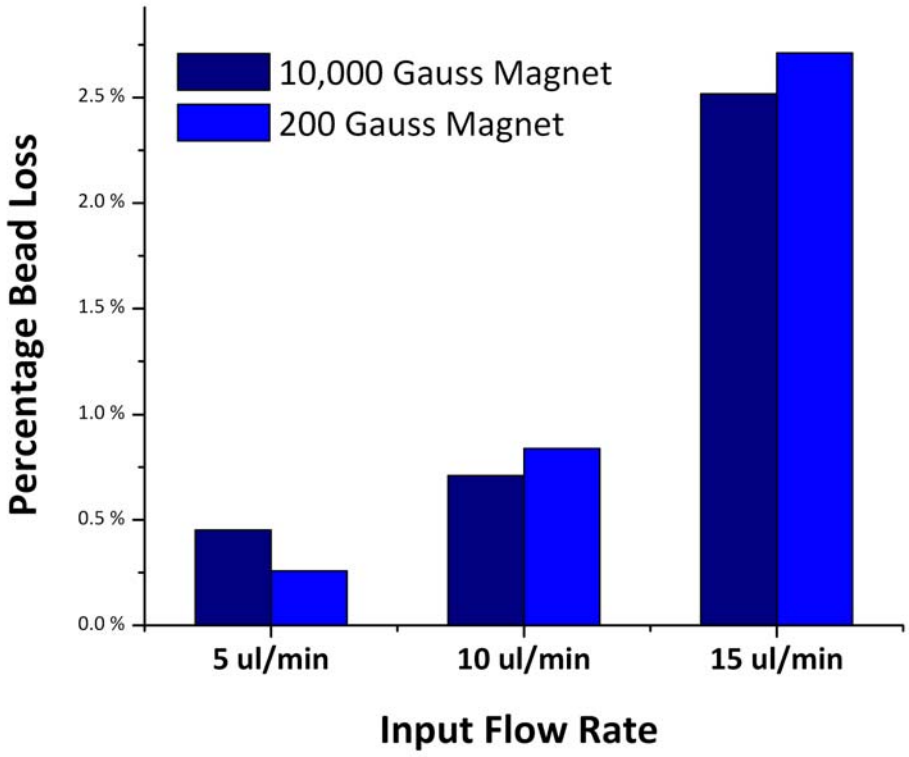

Figure 3-15. Percentage bead loss is comparable at different microfluidic flow rates of 5, 10, and 15 μl/min for two permanent magnets of different pull forces (10,000 Gauss and 200 Gauss), though for the stronger magnet, aggregation and adsorption of the beads on the PDMS sidewall surface was shown to occur, making re-suspension of the beads more challenging.

to be 5 x 10^9 cells/ml, as determined by serial dilution and standard plate counting methods on TSB agar plates. 2 mg/ml of bovine serum albumin (BSA) was flown through the PDMS device for surface passivation prior to experimentation. The cell lysis buffer used was composed of 5M guanidinium isothiocyanate (GuSCN), 1% Triton X100, and 0.1M acetate buffer, at a pH of 6.4 (Sigma).

3.3.4 Experimental Setup

The initial bead concentrations were determined using a hemocytometer. 40 µl Dynal anti-Salmonella beads incubated with various dilutions of cells in phosphate buffered saline (10^9, 10^8, 10^7, 10^6, 10^5, 10^4, 10^3, 10^2 cells/ml) for 10 minutes on a shaker was pumped through the device using a Harvard Apparatus (Holliston, MA) syringe micropump at a constant flow rate of 5µl/min. For the herringbone passive mixers, cell lysis was performed by flowing through 200 µl of lysis buffer in parallel with the bead-cell conjugates. A low pull force permanent magnet was used to capture the beads within the chamber. For the bubble-actuated piezoelectric mixing design, the cell-bead solution is introduced into the chamber first, captured with a permanent magnet, and lysis is subsequently performed by flowing through 200 µl of lysis buffer, removing the permanent magnet, and incubating within the microfluidic chamber with piezoelectric actuation for 10 minutes at room temperature. A control experiment was conducted using the piezoelectric mixing design by fabricating mixing chambers without the bubble traps. All benchmark benchtop separations were conducted using in Eppendorf tubes using a magnetic bead capture system from Dynal. For both mixer designs, the output lysates from the mixer device were collected in 200µl fractions and purified using a standard Qiagen DNeasy purification kit and protocol. The real-time PCR amplification of nucleic acid targets was carried out on an ABI Prism 7000 real-time thermocycler (Applied Biosystems, Foster City, CA) using standard protocols,

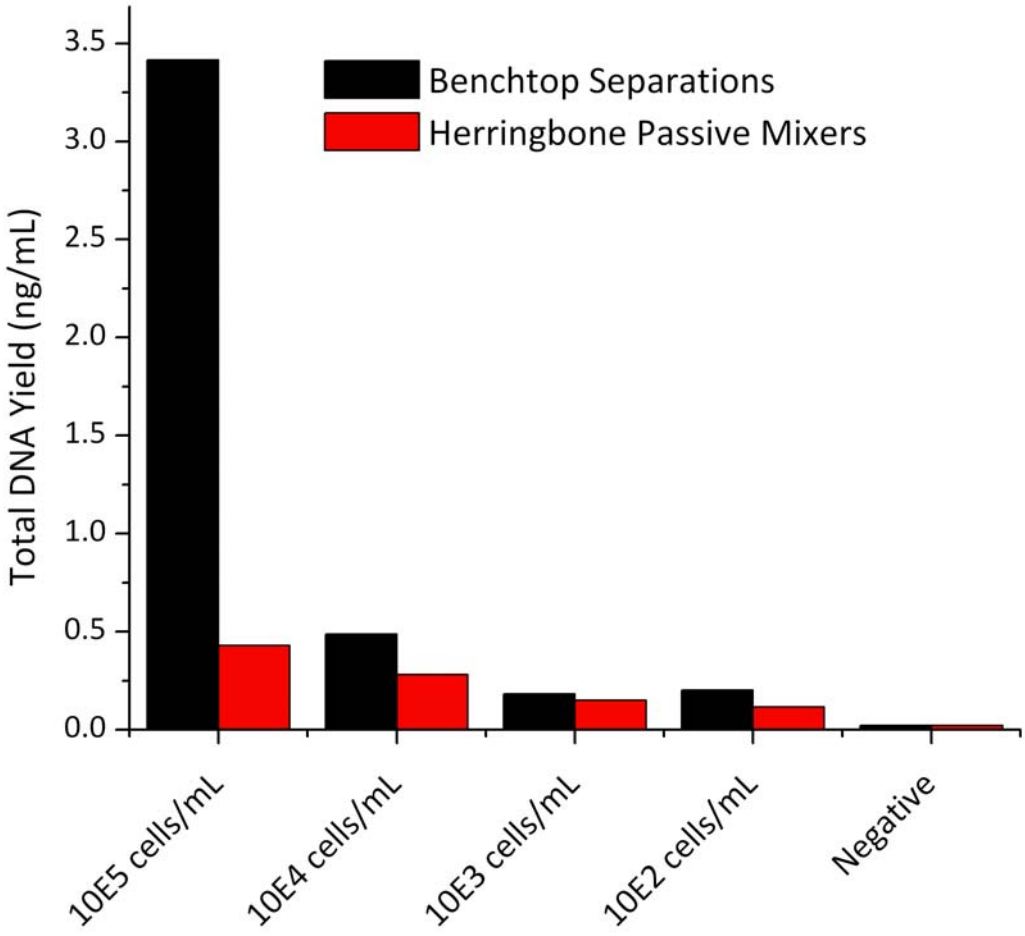

Figure 3-16. Total DNA yield for the herringbone passive mixer at different concentrations of cells conjugated with magnetic beads captured using a single permanent magnet of pull force 200 Gauss. The captured cells were mixed with lysis buffer and subsequently purified and analyzed with real-time PCR. The DNA yield for the higher cell concentrations is shown to be poor compared to the benchtop separation method, but improves at lower cell concentrations.

and the following reagents: TaqMan MasterMix, forward and reverse primers, TaqMan probe, and nuclease-free water.

One of the main concerns with fluorescence-based detection, as is the case with our system, is noise or interference arising from escaped beads drifting into the real-time PCR chamber. Hence, the percentage bead retention was a major focus in our studies. Bead counts were performed to study the retention of beads within the chamber at different flow rates and cell culture concentrations. Two types of magnets were used in our experiments to investigate the differences arising from the use of a strong magnetic field (10,000 Gauss) versus weak magnetic field (200 Gauss). The thickness and type of material in between the magnet and the chamber filled with magnetic beads was also an important factor. In our devices, we performed preliminary investigations into the differences between applying the magnet through a glass slide and through a PDMS membrane, and ultimately chose to continue with the membrane-based device for improved capture and ease of fabrication and integration. For our purposes, the primary measure of the efficiency of the magnetic bead-based microfluidic capture and lysis module lay in the amount of DNA yield of the output collection, as estimated by subsequent real-time PCR.

3.3.5 Results & Discussion

In our experiments, it was observed that a magnet with a higher pull force resulted in aggregation of the beads, as well as adsorption of the beads to the PDMS side wall surface closest to the magnet. A magnet with lower pull force provided efficient attraction with far less aggregation in comparison, allowing for a more even distribution of beads in the chamber and for easier re-suspension. For this reason, the lower pull force magnet would be best suited for most mixing applications. For the

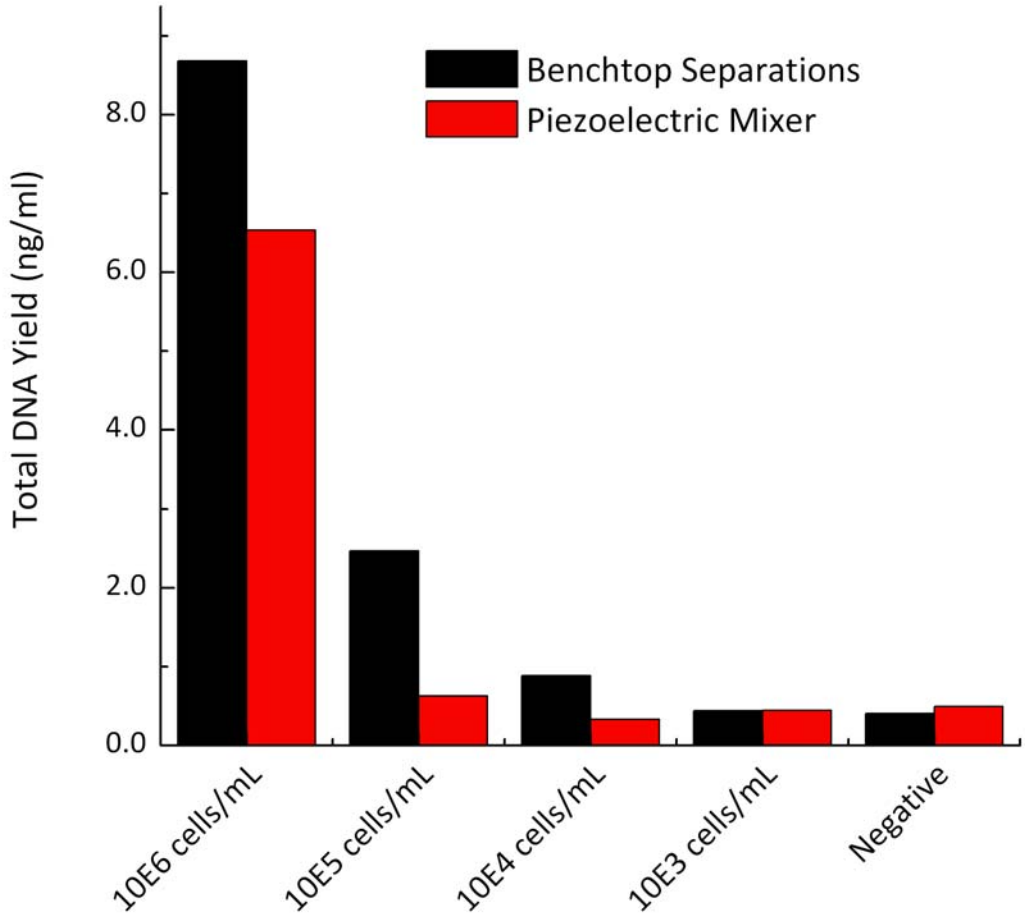

Figure 3-17. Total DNA yield for the piezoelectric chamber mixer without bubble traps at different concentrations of cells conjugated with magnetic beads captured using a single permanent magnet of pull force 200 Gauss. The captured cells were mixed with lysis buffer and subsequently purified and analyzed with real-time PCR. The DNA yield for the higher cell concentrations is shown to be almost 75% compared to the benchtop separation method, but degrades at lower cell concentrations.

bulk of our experiments, we used permanent magnets that required manual placement. For further integration into an automated system, however, the use of electromagnets were explored and discussed in further detail in Chapter 4.

The concentration of the initial bead solution was not supplied by the manufacturer was determined by using a hemocytometer, and determined to be $1.20 \times 10^6 \pm 0.175 \times 10^6$ beads/ml. The bead solution was introduced into the passive herringbone microfluidic mixer device, and beads are magnetically captured within the channels. The waste liquid at the output of the device was analyzed with a hemocytometer to determine the percentage of bead loss. The results are shown in Figure 3-12. For both types of magnets, the percentage of bead loss is comparable for the flow rates of 5, 10, and 15 μl/min. However, the rare earth magnet outperforms the lower pull force magnet at higher flow rates.

In our experiments, we are particularly interested in the amount of DNA we can extract from a given starting sample. Total DNA yield for the herringbone passive mixer at different cell culture concentrations using a single permanent magnet of pull force 200 Gauss is shown in Figure 3-16. The capture for the higher cell concentrations is shown to be poor compared to the benchtop separation method, but improves at lower cell concentrations. Overall, this method showed a lot of bead aggregation and bead adsorption to the PDMS sidewalls, and therefore resuspension and subsequent mixing efforts were less successful.

The piezoelectrically-actuated mixing chamber without the bubble-actuation trap showed up to 75% capture when compared to the benchtop separation methods at the higher cell concentrations, but the percent capture quickly degraded with decreasing

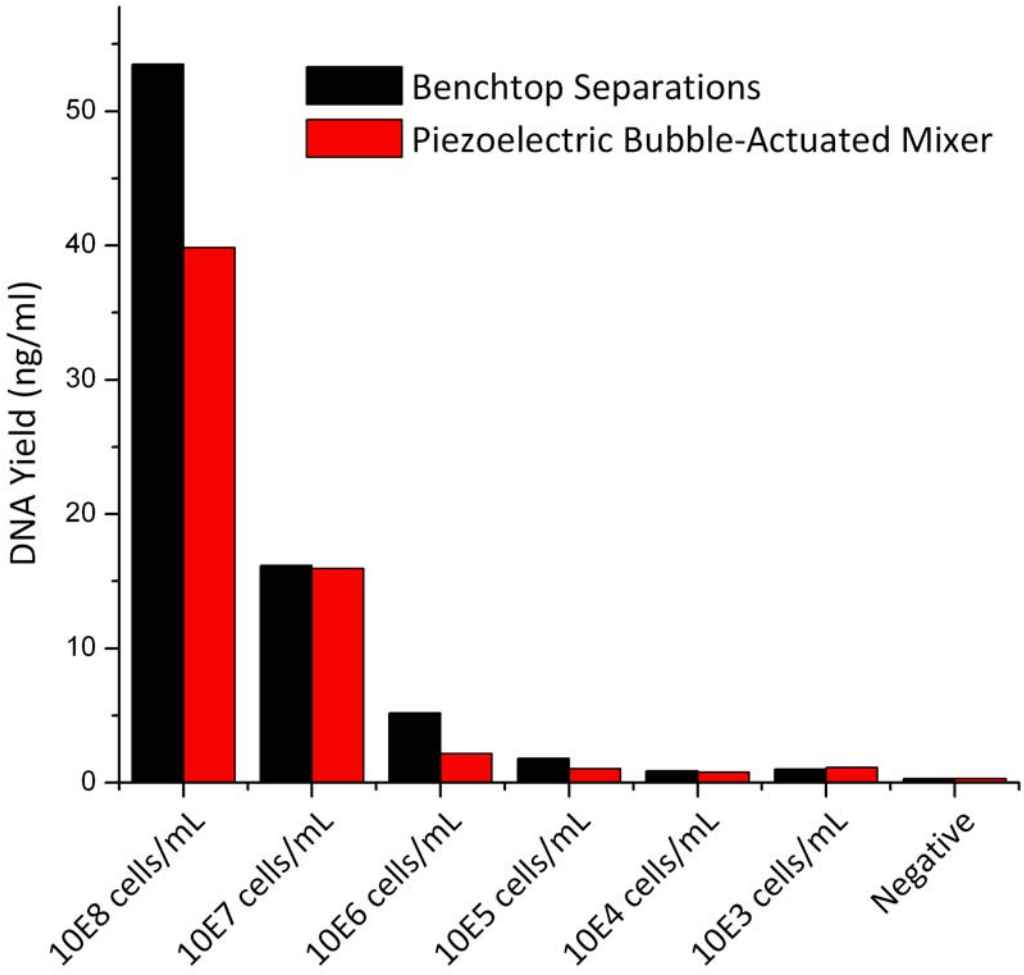

Figure 3-18. Total DNA yield for the piezoelectric bubble-actuated mixer designed with bubble traps. Different concentrations of cells conjugated with magnetic beads were introduced through the device using a single permanent magnet of pull force 200 Gauss. The captured cells were mixed with lysis buffer and subsequently purified and analyzed with real-time PCR. The DNA yield for the higher cell concentrations is shown to be almost comparable to the benchtop separation method, but unlike the previous designs, maintains a favorable DNA yield percentage at lower cell concentrations.

concentrations (See Figure 3-17). In contrast, the device with bubble traps for bubble-actuated piezoelectric mixing showed much improved percent capture at the lower cell concentrations (See Figure 3-18), which is promising for cell isolation in scenarios with low initial cell counts. This final device design also showed the greatest ability for bead re-suspension and mixing following the capture step and was less fraught with bead adsorption problems. .

3.3.6 Section Summary

In summary, we have demonstrated that magnetic bead-based sample preparation can be successfully implemented at the microfluidic scale in conjunction with a bubble-based piezoelectric actuation scheme. The proposed technology is low-cost and disposable with a high level of reproducibility. In addition, the polymer-based fabrication methods are compatible with standard microfabrication technologies, making it possible to directly integrate these pumps with lab-on-a-chip systems. The work resulted in an improved sample preparation design that could successfully perform mixing activities with magnetic beads without the threat of bead aggregation or bead adsorption onto the PDMS side walls. This design also showed an improvement over previous designs in terms of DNA yield, which is one of our primary concerns for this sample preparation step. We note that improvements such as the use of an electromagnet could be made to further automate this sample preparation step, and address this in the following chapter. This approach holds great potential for the miniaturization of the sample preparation step in which separation, mixing, and cell lysis must be performed quickly with lower reagent volumes but without sacrificing on efficiency.

REFERENCES

[1] Jacobson, S.C.; McKnight, T.E.; Ramsey, J.M. Microfluidic devices for electrokinetically driven parallel and serial mixing. *Anal. Chem.* **1999**, *71*, 4455-4459.

[2] Sun, Y.; Kwok, Y.C. Polymeric microfluidic system for DNA analysis. *Anal. Chim. Acta* **2006**, *556*, 80-96.

[3] Zaouk, R.; Park, B.Y.; Madou, M.J. Fabrication of Polydimethylsiloxane Microfluidics Using SU-8 Molds. In *Microfluidic Techniques Reviews and Protocols*, Ed.; Minteer, S.D., Ed.^Eds.; Humana Press, 2006; 321 321, pp. 17-21,

[4] McDonald, J.C.; Whitesides, G.M. Poly(dimethylsiloxane) as a Material for Fabricating Microfluidic Devices. *Acc. Chem. Res.* **2002**, *35*, 491-499.

[5] Noori, A.; Upadhayaya, S.; Selvanganapathy, P.R. Materials and Microfabrication Processes for Microfluidic Devices. In *Microfluidics for Biological Applications*, Ed.; Tian, W.-C., Finehout, E., Ed.^Eds.; Springer, 2008, pp. 35-92,

[6] Huang, R.; Lele, S.P.; Anand, L., "Non-linear mechanical behavior of the elastomer polydimethylsiloxane (PDMS) used in the manufacture of microfluidic devices," 2005.

[7] Liu, M.; Sun, J.; Sun, Y.; Bock, C.; Chen, Q. Thickness-dependent mechanical properties of polydimethylsiloxane membranes. *J. Micromech. Microeng.* **2009**, *19*, 1-4.

[8] Thangawng, A.L.; Ruoff, R.S.; Swartz, M.A.; Glucksberg, M.R. An ultra-thin PDMS membrane as a bio/micro-nano interface: fabrication and characterization. *Biomed. Microdevices* **2007**, *9*, 587-595.

[9] Boxshall, K.; Wu, M.-H.; Cui, Z.; Cui, Z.; Watts, J.F.; Baker, M.A. Simple surface treatments to modify protein adsoption and cell attachment properties within a poly(dimethylsiloxane) micro-bioreactor. *Surface and Interface Analysis* **2005**, *38*, 198-201.

[10] Cady, N.C.; Stelick, S.; Kunnavakkam, M.V.; Batt, C.A. Real-time PCR detection of Listeria monocytogenes using an integrated microfluidics platform *Sens. Actuators. B Chem.* **2005**, *107*.

[11] Beebe, D.J.; Mensing, G.A.; Walker, G.M. Physics and Applications of Microfluidics in Biology. *Ann. Rev. Biomed. Eng.* **2002**, *4*, 261-286.

[12] Squires, T.M.; Quake, S.R. Microfluidics: Fluid physics at the nanoliter scale. *Rev. Mod. Phys.* **2005**, *77*.

[13] Haeberle, S.; Zengerle, R. Microfluidic platforms for lab-on-a-chip applications. *Lab Chip* **2007**, *7*, 1094-1110.

[14] Reyes, D.R.; Iossifidis, D.; Auroux, P.A.; Manz, A. Micro Total Analysis Systems. 1. Introduction, Theory and Technology. *Analytical Chemistry* **2002**, *74*, 2623-2636.

[15] Auroux, P.A.; Iossifidis, D.; Reyes, D.R.; Manz, A. Micro Total Analysis Systems. 2. Analytical Standard Operations and Applications. *Anal. Chem.* **2002**, *74*, 2637-2652.

[16] Erickson, D.; Li, D. Integrated microfluidic devices. *Anal. Chim. Acta* **2004**, *507*, 11-26.

[17] Dittrich, P.S.; Tachikawa, K.; Manz, A. Micro total analysis systems. Latest advancements and trends. *Anal. Chem.* **2006**, *78*, 3887-3908.

[18] Blazej, R.G.; Kumaresan, P.; Mathies, R.A. Microfabricated bioprocessor for integrated nanoliter-scale Sanger DNA sequencing. *Proc. Natl. Acad. Sci. U.S.A.* **2006**, *103*, 7240-7245.

[19] Fredlake, C.P.; Hert, D.G.; Mardis, E.R.; Barron, A.E. What is the future of electrophoresis in large-scale genomic sequencing? *Electrophoresis* **2006**, *26*, 3689-3702.

[20] Chen, L.; Manz, A.; Day, P.J.R. Ultrasensitive PCR and Real-Time Detection from Human Genomic Samples Using a Bidirectional Flow Microreactor. *Anal. Biochem.* **2008**, *372*, 128-130.

[21] Dewald, A.H.; Poe, B.L.; Landers, J.P. Electrophoretic microfluidic devices for mutation detection in clinical diagnostics. *Expert Opinion on Medical Diagnostics* **2008**, *2*, 963-977.

[22] Kang, L.; Chung, B.G.; Langer, R.; Khademhosseini, A. Microfluidics for drug discovery and development: From target selection to product lifecycle management *Drug Discovery Today* **2007**, *13*, 1-13.

[23] Pihl, J.; Karlsson, M.; Chiu, D.T. Microfluidic technologies in drug discovery. *Drug Discovery Today* **2005**, *10*, 1377-1383.

[24] El-Ali, J.; Sorger, P.K.; Jensen, K.F. Cells on chips. *Nature* **2006**, *442*, 403-411.

[25] Andersson, H.; Berg, A.v.d. Microtechnologies and nanotechnologies for single-cell analysis. *Curr. Opin. Biotech.* **2004**, *15*, 44-49.

[26] Gao, J.; Yin, X.F.; Fang, Z.L. Integration of single cell injection, cell lysis, separation and detection of intracellular constituents on a microfluidic chip. *Lab Chip* **2004**, *4*, 47-52.

[27] Borland, L.M.; Kottegoda, S.; Phillips, K.S.; Allbritton, N.L. Chemical Analysis of Single Cells. *Ann. Rev. Anal. Chem.* **2008**, *1*, 165-190.

[28] Sato, K.; Mawatari, K.; Kitamori, T. Microchip-based cell analysis and clinical diagnosis system. *Lab Chip* **2008**, *8*, 1992-1998.

[29] Toriello, N.M.; Douglas, E.S.; Thaitrong, N.; Hsiao, S.C.; Francis, M.B.; Bertozzi, C.R.; Mathies, R.A. Integrated microfluidic bioprocessor for single-cell gene expression analysis. *Proc. Natl. Acad. Sci. U.S.A.* **2008**, *105*, 201373-201378.

[30] Cohen, D.; Dickerson, J.A.; Whitmore, C.D.; Turner, E.H.; Palcic, M.M.; Hindsgaul, O.; Dovichi, N.J. Chemical Cytometry: Fluorescence-Based Single-Cell Analysis. *Ann. Rev. Anal. Chem.* **2008**, *1*, 165-190.

[31] Belgrader, P.; Benett, W.; Hadley, D.; Long, G.; Raymond Mariella, J.; Milanovich, F.; Nasarabadi, S.; Nelson, W.; Richards, J.; Stratton, P. Rapid pathogen detection using a microchip PCR array instrument. *Clin. Chem.* **1998**, *44*, 2191-2194.

[32] Zaytseva, N.V.; Goral, V.N.; Montagna, R.A.; Baeumner, A.J. Development of a microfluidic biosensor module for pathogen detection. *Lab Chip* **2005**, *5*, 805-811.

[33] Lee, T.M.-H.; Hsing, I.-M. DNA-based bioanalytical microsystems for handheld devices applications. *Anal. Chim. Acta* **2006**, *556*, 26-37.

[34] Zhang, C.; Xu, J.; Ma, W.; Zheng, W. PCR microfluidic devices for DNA amplification. *Biotechnol. Adv.* **2006**, *24*, 243-284.

[35] Grover, W.H.; Skelley, A.M.; Liu, C.N.; Lagally, E.T.; Mathies, R.A. Monolithic membrane valves and diaphram pumps for practical large-scale integration into glass microfluidic devices. *Sens. Actuators. B Chem.* **2003**, *89*, 315-323.

[36] Laser, D.J.; Santiago, J.G. A review of micropumps. *J. Micromech. Microeng.* **2004**, *14*, R35-R64.

[37] Woias, P. Micropumps—past, progress and future prospects. *Sens. Actuators. B Chem.* **2005**, *105*, 28-38.

[38] Iverson, B.D.; Garimella, S.V. Recent advances in microscale pumping technologies: a review and evaluation. *Microfluid. Nanofluidics* **2008**, *5*, 145-174.

[39] Cooney, C.G.; Towe, B.C. A thermopneumatic dispensing micropump. *Sens. Actuators. A Phys.* **2004**, *116*, 519-524.

[40] Roxhed, N.; Rydholm, S.; Samuel, B.; Van der Wijngaart, W.; Griss, P.; Stemme, G. A compact, low-cost microliter-range liquid dispenser based on expandable microspheres. *J. Micromech. Microeng.* **2006**, *16*.

[41] Zeng, S.; chen, C.-H.; James C. Mikkelsen, J.; Santiago, J.G. Fabrication and characterization of electroosmotic micropumps. *Sens. Actuators. B Chem.* **2001**, *79*, 107-114.

[42] Machauf, A.; Nemirovsky, Y.; Dinnar, U. A membrane micropump electrostatically actuated across the working fluid. *J. Micromech. Microeng.* **2005**, *15*, 2309-2316.

[43] Sounart, T.L.; Michalske, T.A.; Zavadil, K.R. Frequency-dependent electrostatic acutation in microfluidic MEMS. *J. Microelectromech. Syst.* **2005**, *14*, 125-133.

[44] Kock, M.; Harris, N.; Evans, A.G.R.; White, N.M.; Brunnschweiler, A. A novel micromachined pump based on thick-film piezoelectric actuation. *Sens. Actuators. A Phys.* **1998**, *70*, 98-103.

[45] Yang, Z.; Matsumoto, S.; Goto, H.; Matsumoto, M.; Maeda, R. Ultrasonic micromixer for microfluidic systems. *Sens. Actuators. A Phys.* **2001**, *93*, 266-272.

[46] Graf, N.J.; Bowser, M.T. A soft-polymer piezoelectric bimorph cantilever-actuated persitaltic micropump. *Lab Chip* **2008**, *8*, 1664-1670.

[47] Lemoff, A.V.; Lee, A.P. An AC magnetohydrodynamic micropump. *Sens. Actuators. B Chem.* **2000**, *63*, 178-185.

[48] Rinderknecht, D.; Hickerson, A.I. A valveless micro impedance pump driven by electromagnetic actuation. *J. Micromech. Microeng.* **2005**, *15*, 861-866.

[49] Yamamata, C.; Lotto, C.; Al-Assaf, E.; Gijs, M.A.M. A PMMA valveless micropump using electromagnetic actuation. *Microfluid. Nanofluidics* **2005**, *1*, 197-207.

[50] Bassetti, M.J.; Chatterjee, A.N.; Aluru, N.R.; Beebe, D.J. Development and modeling of electrically triggered hydrogels for microfluidic applications. *J. Microelectromech. Syst.* **2005**, *14*, 1198-1207.

[51] Harmon, M.E.; Tang, M.; Frank, C.W. A microfluidic actuator based on thermoresponsive hydrogels. *Polymer* **2003**, *44*, 4547-4556.

[52] Bohm, S.; Timmer, B.; Olthuis, W.; Bergveld, P. A closed-loop controlled electrochemically actuated micro-dosing system. *J. Micromech. Microeng.* **2000**, *10*, 498-504.

[53] Metref, L.; Herrera, F.; Berdat, D.; Gijs, M.A.M. Contactless Electrochemical Actuator for Microfluidic Dosing. *J. Microelectromech. Syst.* **2007**, *16*, 885-892.

[54] Neagu, C.R.; Gardeniers, J.G.E.; Elwenspoek, M.; Kelly, J.J. An electrochemical microactuator: principle and first results. *J. Microelectromech. Syst.* **1996**, *5*, 2-9.

[55] Hua, S.Z.; Sachs, F.; Yang, D.X.; Chopra, H.D. Microfluidic Actuation Using Electrochemically Generated Bubbles. *Anal. Chem.* **2002**, *74*, 6392-6396.

[56] Munyan, J.W.; Fuentes, H.V.; Draper, M.; Kelly, R.T.; Woolley, A.T. Electrically actuated, pressure-driven microfluidic pumps. *Lab Chip* **2003**, *3*.

[57] Ateya, D.A.; Shah, A.A.; Hua, S.Z. An electrolytically actuated micropump. *Rev. Sci. Instrum.* **2004**, *75*, 915-920.

[58] Fuentes, H.V.; Woolley, A.T. Electrically actuated, pressure-driven liquid chromatography separations in microfabricated devices. *Lab Chip* **2007**, *7*, 1524-1531.

[59] Sotoh, W.; Shimizu, Y.; Kaneto, T.; Suzuki, H. On-chip microfluidic transport and bio/chemical sensing based on electrochemical bubble formation. *Sens. Actuators. B Chem.* **2007**, *123*, 1153-1160.

[60] Ramadan, Q.; Samper, V.; Poenar, D.; Yu, C. On-chip micro-electromagnets for magnetic-based bio-molecules separation. *J. Magnetism Magnetic Mat.* **2004**, *281*, 150-172.

[61] Gijs, M.A.M. Magnetic bead handling on-chip: new opportunities for analytical applications. *Microfluid. Nanofluidics* **2004**, *1*, 22-40.

[62] Pankhurst, Q.A.; Connolly, J.; Jones, S.K.; Dobson, J. Applications of magnetic nanoparticles in biomedicine. *J. Phys. D: Appl. Phys.* **2003**, *36*, R167-R181.

[63] Pamme, N. Magnetism and microfluidics. *Lab Chip* **2006**, *6*, 24-38.

[64] Lee, H.; Purdon, A.M.; Westervelt, R.M. Manipulation of biological cells using a microelectromagnet matrix. *Appl. Phys. Lett.* **2004**, *85*, 1063.

[65] Liu, Y.-J.; Guo, S.-S. Integration of minisolenoids in microfluidic device for magnetic bead-based immunoassays. *J. Appl. Phys.* **2007**, *102*, 084911.

[66] Ahn, C.H.; Allen, M.G.; Trimmer, W.; Jun, Y.-N.; Erramilli, S. A fully integrated micromachined magnetic particle separator. *J. Microelectromech. Syst.* **1996**, *5*, 151-158.

[67] Pekas, N.; Granger, M.; Tondra, M.; Popple, A.; Porter, M.D. Magnetic particle diverter in an integrated microfluidic format. *J. Magnetism Magnetic Mat.* **2005**, *293*.

[68] Pamme, N.; Wilhelm, C. Continuous sorting of magnetic cells via on-chip free-flow magnetophoresis. *Lab Chip* **2006**, *6*, 974-980.

[69] Smistrup, K.; Kjeldsen, B.G.; Reimers, J.L.; Dufva, M.; Petersen, J.; Hansen, M.F. On-chip magnetic bead microarray using hydrodynamic focusing in a passive magnetic separator. *Lab Chip* **2005**, *5*, 1315-1319.

[70] Deng, T.; Prentiss, M.; Whitesides, G.M. Fabrication of magnetic microfiltration systsems using soft lithography. *Appl. Phys. Lett.* **2002**, *80*, 461-463.

[71] Lacharme, F.; Vandevyver, C.; Gijs, M.A.M. Full On-Chip Nanoliter Immunoassay by Geometrical Magnetic Trapping of Nanoparticle Chains. *Anal. Chem.* **2008**, *80*, 2905-2910.

[72] Choi, J.-W.; Ahn, C.H.; Bhansali, S.; Henderson, H.T. A new magnetic bead-based filterless bio-separator with planar electromagnet surfaces for integrated bio-detection systems. *Sens. Actuators. B Chem.* **2000**, *68*, 34-39.

[73] Inglis, D.W.; Riehn, R.; Austin, R.H.; Sturm, J.C. Continuous microfluidic immunomagnetic cell separation. *Appl. Phys. Lett.* **2004**, *85*, 5093.

[74] Furdui, V.I.; Harrison, D.J. Immunomagnetic T cell capture from blood for PCR analysis using microfluidic systems. *Lab Chip* **2004**, *4*, 614-618.

[75] Lee, H.; Purdon, A.M.; Westervelt, R.M. Manipulation of biological cells using a microelectromagnet matrix. *Appl. Phys. Lett.* **2004**, *85*, 1063-1065.

[76] Melville, D.; Paul, F.; Roath, S. Direct magnetic separation of red cells from whole blood. *Nature* **1975**, *255*, 706.

[77] Molday, R.S.; Yen, S.P.S.; Rembaum, A. Application of magnetic microspheres in labelling and separation of cells. *Nature* **1977**, *268*, 437-438.

[78] Sieben, S.; Bergemann, C.; Lubbe, A.; Brockmann, B.; Rescheleit, D. Comparison of different particles and methods for magnetic isolation of circulating tumor cells. *J. Magnetism Magnetic Mat.* **2001**, *255*, 175-179.

[79] Sun, L.; Zborowski, M.; Moore, L.R.; Chalmers, J.J. Continuous, Flow-Through Immunomagnetic Cell Sorting in a Quadrupole Field. *Cytometry* **1998**, *33*, 469-475.

[80] Tibbe, A.G.J.; Grooth, B.G.d.; Greve, J.; Dolan, G.J.; Rao, C.; Terstappen, L.W.M.M. Magnetic field design for selecting and aligning immunomagnetic labeled cells. *Cytometry* **2002**, *47*, 163-172.

[81] McCloskey, K.; Chalmers, J.J.; Zborowski, M. Magnetic Cell Separation: Characterization of Magnetophoretic Mobility. *Anal. Chem.* **2003**, *75*, 6868-6874.

[82] Chemicell. www.chemicell.com.

[83] Bioclone. www.bioclon.com.

[84] Millipore. www.millipore.com.

[85] BangsLaboratories. www.bangslabs.com.

[86] Spherotech. www.spherotech.com.

[87] Invitrogen. www.invitrogen.com.

[88] Grumann, M.; Geipel, A.; Riegger, L.; Zengerle, R.; Ducree, J. Batch-mode mixing on centrifugal microfluidic platforms. *Lab Chip* **2005**, *5*, 560-565.

[89] Rida, A.; Gijs, M.A.M. Manupulation of self-assembled structures of magnetic beads for microfluidic mixing and assaying. *Anal. Chem.* **2004**, *76*, 6239-6246.

[90] Frommelt, T.; Kostur, M.; Wenzel-Shafer, M.; Talkner, P.; Hanggi, P.; Wixforth, A. Microfluidic Mixing via Acoustically Driven Chaotic Advection. *Phys. Rev. Lett.* **2008**, *100*, 034502.

[91] Suzuki, H.; Ho, C.-M.; Kasagi, N. A Chaotic Mixer for Magnetic Bead-Based Micro Cell Sorter. *J. Microelectromech. Syst.* **2004**, *13*, 779-790.

[92] Rong, R.; Choi, J.W.; Ahn, C.H. A Novel Magnetic Chaotic Mixer for In-Flow Mixing of Magnetic Beads. In, Squaw Valley, CA, Year, pp. 335-338.

[93] Lind-Olesen, T.; Dufva, M.; Hansen, M.F. Capture of DNA in microfluidic channel using magnetic beads: Increasing capture efficiency with integrated microfluidic mixer. *J. Magnetism Magnetic Mat.* **2006**, *311*, 396-400.

[94] Liu, R.H.; Yang, J.; Pindera, M.Z.; Athavale, M.; Grodzinski, P. Bubble-induced acoustic micromixing. *Lab Chip* **2002**, *2*, 151-157.

[95] Liu, R.H.; Lenigk, R.; Grodzinski, P. Acoustic micromimxer for enhancement of DNA biochip systems. *J. Monolithr. Microfabrication, Microsyst.* **2003**, *2*, 178.

[96] Stroock, A.D.; Dertinger, S.K.W.; Ajdari, A.; Mezic, I.; Stone, H.A.; Whitesides, G.M. Chaotic Mixer for Microchannels. *Science* **2002**, *295*, 647-651.

CHAPTER 4

INTEGRATED MICROFLUIDIC PATHOGEN DETECTION PLATFORMS

4.0 Introduction

Recently, there has been an increase in demand for rapid and accurate methods of detecting pathogenic bacteria, viruses, and other disease-causing agents, particularly in the agriculture and food industry. In the past couple years, we have seen several recurrences of food-borne disease outbreaks associated with fresh produce and processed foods. With the most prevailing scenario being contamination in the field due to suboptimal hygiene or contamination by animals, the need for field deployable detection systems to survey food and water supplies using fast and sensitive methods is very clear. Food supply surveillance is one of the main motivators for the development of new detection technologies. The current methodology falls into two broad classes: (a) field-deployable methods that are rapid but fail in clearly detecting a specific pathogen, and (b) laboratory-based methods that are highly-sensitive and specific but present limited utility due to the time necessary for sample transport from the field to the laboratory. The first class of detection methods lack sensitivity, and therefore present researchers with an opportunity to look for indicators and improve upon the technology. While some field deployable instruments have been developed most require considerable sample preparation which is an impediment to field usage [2]. As we discussed earlier in Chapter 3, one of the major bottlenecks in the development of field-deployable instruments is the considerable sample preparation necessary to separate the target from contaminants in a raw sample.

4.1 Salmonella Detection in Raw Chicken Samples using the Microfluidics Desktop

As one of the most common causes of food-borne disease, *Salmonella* remains one of the major targets for rapid test methods such as PCR and real-time PCR[3, 4]. A

variety of different assays with varying specificities, accuracies, and detection limits have been developed for this pathogen, with recent assays dramatically shortening the speed of detection. PCR still represents one of the best opportunities to develop a field deployable instrument that will be sufficiently robust to detect small numbers of a target pathogen in real samples [5-11]. Other methods are extremely sensitive but they often rely upon signal amplification which is prone to false-positives [12]. In addition some of the methods target signals that are potentially unique to a pathogen but are masked in systems that are not pristine [2, 4, 6-9, 11]. We propose to further reduce complexity and size of the instrument by integrating the fluid handling on the chip and making a single disposable cartridge that will carry reagents requiring only the addition of the sample.

Previous studies have demonstrated real-time PCR-based detection of S. typhi using stationary laboratory equipment with high accuracy and sensitivity, providing detection limits as low as 10-100 cell copies/ml [13]. While portable real time PCR instruments have been developed, most do not include that capability to collect and process samples [14-16]. Therefore the utility in the field is limited because of the necessity for sophisticated manual fluid handling. Our instrument has already been demonstrated to be capable of sample processing and detection without manual fluid handling and has been applied to the detection of a number of pathogens with sensitivity levels in the sub-50 CFU range [17]. For the past several years, our laboratory has been involved in a variety of fluorescence-based DNA amplification assays. These assays include the development of 5' nuclease (or TaqMan) assays for a variety of pathogens including *Listeria monocytogenes, Escherichia coli, Yersinia enterocolitica, Bacillus cereus,* and *Salmonella* [17-20].

We report here on a miniaturized lab-on-a-chip sample preparation system used in conjunction with our previously developed integrated microfluidic detection platform, named the microFLUIDICS DESKTOP. The previous system demonstrated successful DNA purification and real-time PCR of the food pathogen *Listeria monocytogenes*, a gram-positive bacterium responsible for several food-related outbreaks in the past decade. The small footprint of the system components, as well as low power requirements, promotes the microFLUIDICS DESKTOP as an ideal candidate for further miniaturization into a hand-held, point-of-case device.

4.1.1 Bacterial Growth and Preparation

Salmonella typhi was obtained from frozen cell stock and grown in a trypsin soy broth (TSB, BD, Franklin Lakes, NJ) agar plate culture for 24 hours. A single bacterial colony was removed from the plate culture and grown aerobically in 5 mL of liquid TSB media at 37°C and gentle shaking for 12 hours. The final culture concentration was estimated to be approximately 5 x 10^9 cells/ml thorugh determination by serial dilution and standard plate counting on TSB agar plates. Chicken samples were purchased from a local grocery store and parsed into 1 g samples. 10 mL cell culture samples of different concentrations diluted in phosphate buffered saline (PBS) were vortexed and incubated with the chicken samples to form a chicken wash, which was subsequently filtered through a 100-micron filter to remove larger chicken particles. 2 mg/ml of bovine serum albumin (BSA) was flown through the microfluidic chips for surface passivation prior to experimentation. The cell lysis buffer used was composed of 5M guanidinium isothiocyanate (GuSCN), 1% Triton X100, and 0.1M acetate buffer, at a pH of 6.4 (Sigma).

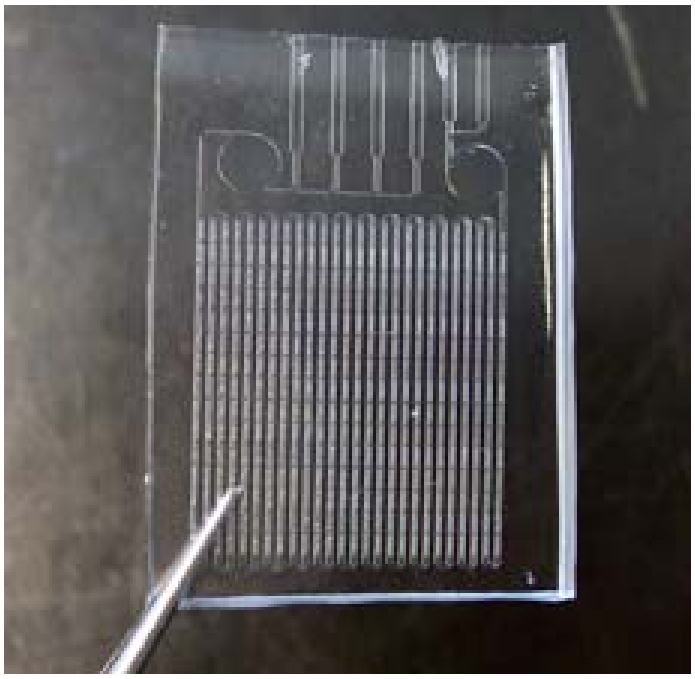

Figure 4-1. Photograph of the cell lysis chip. The concept of this chip is based upon the herringbone-grooved passive mixer, where the shape and height of the grooves causes a kneading motion in the liquids, enhancing the mixing of liquids. The chip is constructed of a single patterned slab of PDMS bonded to a PDMS membrane. The primary purpose of this chip is to achieve passive magnetic bead-based capture and mixing with lysis buffer for efficient cell lysis.

4.1.2 Device fabrication

Microfabrication of this device was conducted at the Cornell Nanoscale Facility (Ithaca, NY). The cell lysis chip was constructed of a single patterned slab of PDMS bonded to a PDMS membrane, using the protocol described earlier in Chapter 3. A photograph of the cell lysis chip is shown in Figure 4-1. The DNA purification and amplification chip was fabricated using the same protocol as described previously. Briefly, an array of 10 μm square pillars was etched 50 μm deep into silicon to form a purification channel. The PCR amplification chamber was constructed using soft lithography with PDMS cured in an SU-8 mold of the PCR chamber, and then aligned and bonded to the patterned silicon wafer containing the purification region. Fluidic connections were made using 30 gauge stainless steel tubing inserted into pre-defined inlets and outlets in the PDMS and fixed in place using Miller-Stephenson 907 epoxy (Danbury, CT). Connections between the stainless steel tubing and the custom syringe pumps in the instrument were made using 0.010" microbore tubing (Small Parts, Miami Lakes, FL). In addition, the connections between the different chips on the instrument were made using the same tubing. An assembled DNA purification and amplification microchip can be seen in Figure 1-9(b).

4.1.3 Apparatus

A microcontroller-based instrument was designed to automate the fluid handling and thermal cycling events, while keeping low power requirements (20W) and system footprint size in mind. As reported previously, the instrument contains a variety of different components, including a controller board, power amplifiers for driving automated custom-designed syringe pumps, a thermoelectric heater/cooler, a fluorescence excitation/emission module, and a pressure valve [17]. A photograph of the instrument layout is depicted in Figure 4-2. During operation, the entire system is

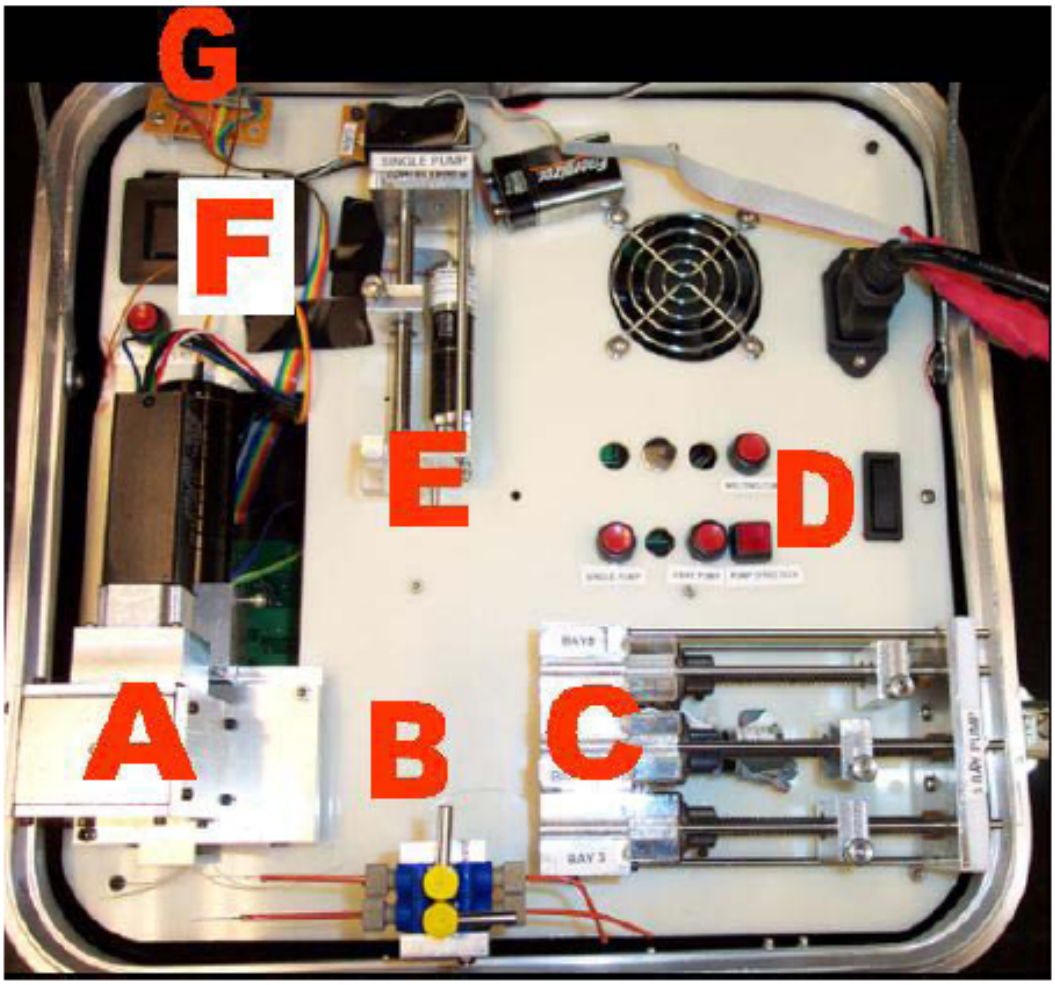

Figure 4-2. The microFLUIDICS DESKTOP. The system consists of multiple components: **A**, fluorescence detection system (chip and thermocycler are located below this); **B**, fluidic valves; **C**, 3-bay syringe pump; **D**, electronic switches; **E**, single-bay syringe pump; **F**, fluorescence gain display; G, temperature control resistors.

controlled by a Z-world microcontroller board (Rabbit, Davis, CA). The entire system is mounted in a portable box enclosure, measuring 36 cm x 28 cm x 15 cm and weighing a total of 4 kg. During a typical detection protocol, the automated program executes fluid pumping, chip pressurization, thermal cycling, and fluorescence detection sequentially. The application of the external magnetic field required during the sample preparation step involves sliding a permanent rare-earth magnet into place manually when signaled by the program. During the real-time PCR reaction, fluorescence data is collected during the 60°C step and directly output to a laptop computer.

4.1.4 Magnetic bead-based cell separation

A major challenge with any micro or nanoscale detection component is the interface with the macroscale world. Samples are typically collected in milliliter or gram amounts and these large samples need to be processed and the target concentrated into a much smaller volume. We have constructed a unique manual processing component to take samples and perform the initial concentration them before further processing on the microfluidic chip. Taking advantage of existing expertise in the area of magnetic bead capture, The Magnetic Cell Separator is shown in Figure 4-3 and allows a bulk sample up to 10 mL to be quickly concentrated into a 100 μL volume for further processing. The basic Separator design consists of a PDMS base containing a serpentine channel with a total volume of approximately 20 μl attached to a second PDMS sleeve designed to support a 50cc modified luer-lock syringe. The plunger of the syringe is modified by attaching a round, flat-faced piece of PDMS elastomer and trimmed to allow waste fluid to escape. Inlets and outlets are threaded with 0.010" diameter Tygon tubing inserted into the PDMS base and secured with epoxy. This step

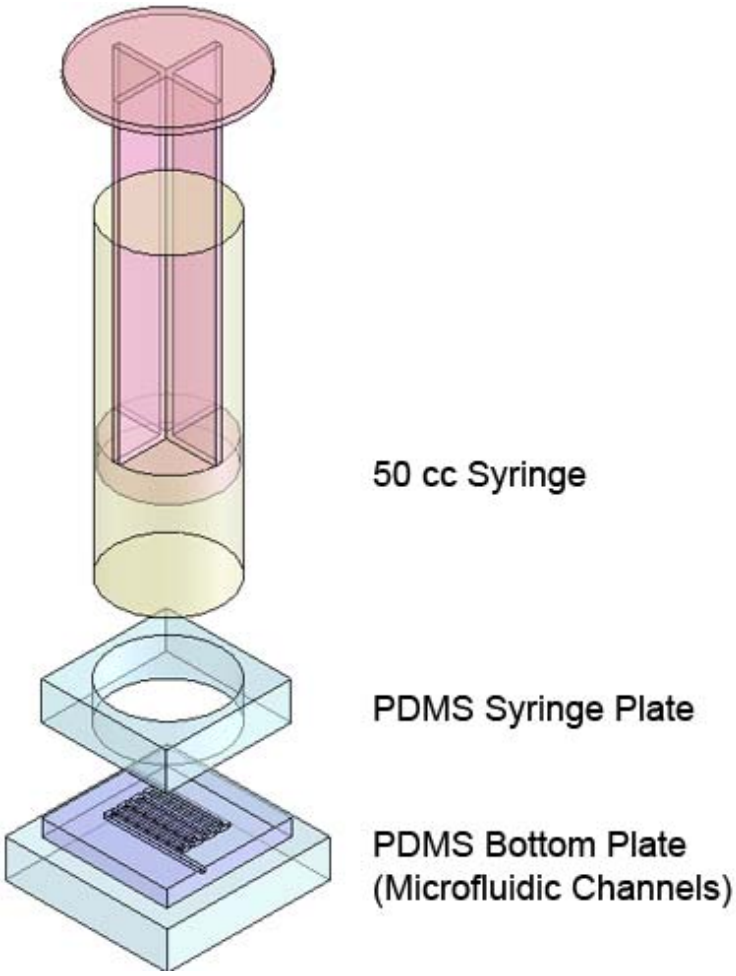

Figure 4-3. The Magnetic Cell Separator. The design consists of a PDMS base containing a serpentine channel with a total volume of approximately 20 μl attached to a second PDMS sleeve designed to support a 50cc modified luer-lock syringe. The plunger of the syringe is modified by attaching a round, flat-faced piece of PDMS elastomer and trimmed to allow waste fluid to escape. The basic operation of the device involves a user-friendly push-down activation that allows a bulk sample up to 10 mL to be quickly concentrated into a 100 μL volume for further processing.

is the entry interface for the user to the device and represents the only point where the user handles the sample.

10 ml of the liquid sample and 100 µL of anti-*Salmonella* magnetic beads are poured into the Cell Separator, incubated for 5 minutes for bead capture, and the plunger is pressed, forcing out the remaining fluid. All the sample handling is directly designed into the rest of the system eliminating any need for manual fluid handling once the sample is introduced into the Magnetic Cell Separator. The output from the Magnetic Cell Separator is pumped into the herringbone-grooved passive mixer chip (shown in Figure 4-1) along with lysis buffer, and the mixing of the two fluids occurs passively via the kneading action caused by the grooves and incubated for 10 minutes. The magnetic beads are immobilized with an external permanent magnet (20k Gauss) and the cell lysate is pumped through to the next chamber. As a control experiment, 100 µl of the resulting lysate from the mixer chip was collected. DNA purification with Qiagen kits and real-time PCR with an ABI 7000 thermocycler was performed to evaluate the performance of the cell separator and mixer combination.

4.1.5 Microfluidic DNA purification and amplification

The output cell lysate obtained from the previous microfluidic magnetic bead-based cell separation step was pumped into the purification region of the DNA chip, followed by 200 µl of 70% ethanol to wash away proteins and/or other contaminants. Finally, the DNA was eluted with the introduction of nuclease-free water, and 30 µl of the DNA elution was pumped into the amplification along with the mastermix solution. For DNA quantification and benchmarking, lysed cells of known concentrations were purified using a standard Qiagen DNeasy kit and eluted in 50 µl

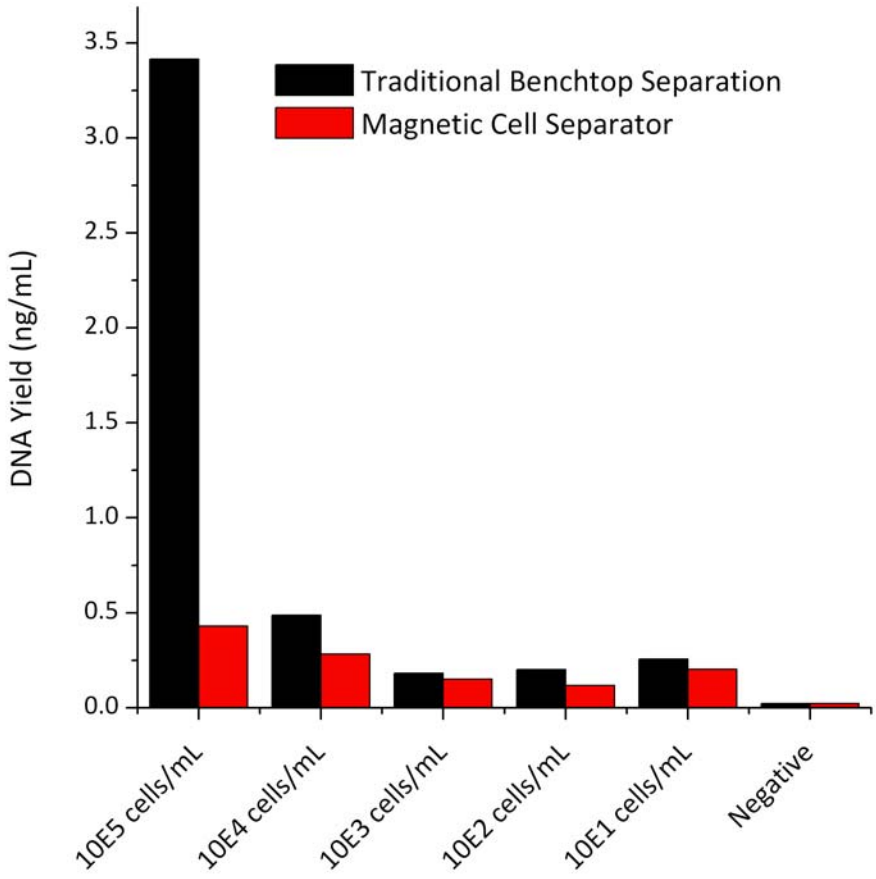

Figure 4-4. DNA yields calculated from the real-time PCR results obtained using the magnetic cell separator. 100 µl anti-Salmonella magnetic beads were incubated with pure cell cultures of varying concentrations, concentrated with the magnetic cell separator, and lysed in an Eppendorf tube. To benchmark, the same capture experiments are performed on the benchtop with a falcon tube and rare-earth magnet setup. DNA purification with Qiagen kits and real-time PCR with an ABI 7000 thermocycler was performed to evaluate the performance of the cell separator. The data shown suggests the ability to detect at low concentration levels of 10 cells/ml.

of elution buffer to create standard curves. The concentration of the DNA was determined by measuring the optical density at 260 nm with a NanoDrop spectrophotometer instrument (Thermo Fisher Scientific Inc., Wilmington, DE). PCR amplification of nucleic acid targets was carried out using standard protocols. A 363-bp fragment from the *Salmonella typhi ttrRSBCA* locus was amplified using forward and reverse primers *ttr-6* and *ttr-4*, employing the protocol previously reported by Malorny et al [21]. PCR reactions consisted of 400 nM forward and reverse primers, 250 nM *Salmonella* probe (*ttr-5*), 50% volume of TaqMan® Fast Universal PCR Master Mix (Applied Biosystems, Foster City, CA), and nuclease-free water in a total volume of 40 µl. As a benchmark, real-time PCR reactions were cycled in an ABI7000 real-time thermocycler (Applied Biosystems, Foster City, CA) under the following conditions: 95°C denaturation for 2 min, 50 cycles of 95°C for 15 seconds and 65°C for 30 seconds. For the microchip based amplification, 1 µl SureStart mix was included in the reaction to jumpstart the reaction. The syringe loaded with mastermix solution consisted of 75 µl of ABI mix, 33 µl of nuclease-free water, 1 µl of SureStart Taq, and 3 µl each of the forward primer, reverse primer, and probe. The thermocycler in the microFLUIDICS DESKTOP was run under the following conditions: 50 cycles of 95°C for 15 seconds and 63°C for 30 seconds. Fluorescence was monitored during the during the 63°C step of each cycle.

4.1.6 Results & Discussion

DNA yields calculated from the real-time PCR results obtained using the magnetic cell separator are shown in Figures 4-4 and 4-5. In Figure 4-4, we see the results from cell separations of varying concentrations of pure cell cultures in order to determine the effectiveness of the cell capture as compared to conventional benchtop methods. The data shown suggests that the capture efficiency is low for higher cell

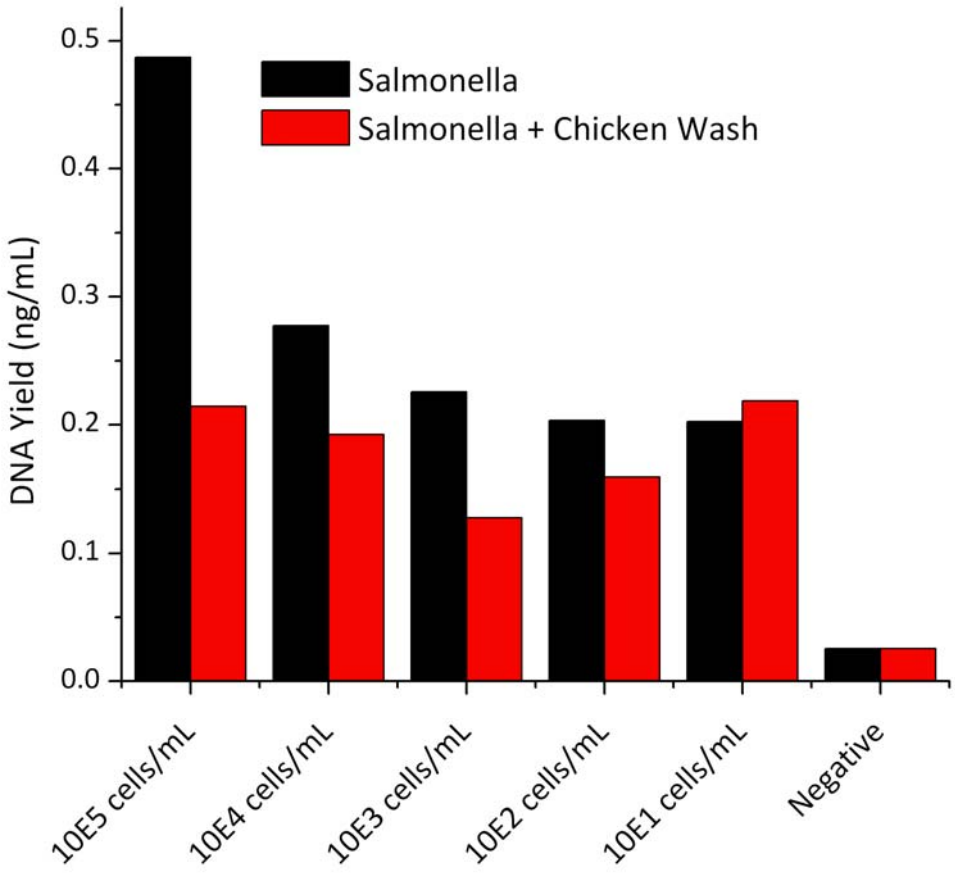

Figure 4-5. DNA yields calculated from the real-time PCR results obtained using the magnetic cell separator and samples spiked with chicken wash obtained from vortexing and incubating with 1g of chicken. 100 µl anti-Salmonella magnetic beads were incubated with samples of varying initial cell concentrations, concentrated with the magnetic cell separator, and lysed in an Eppendorf tube. To benchmark, these results are compared with the capture experiments performed in the absence of chicken wash. DNA purification with Qiagen kits and real-time PCR with an ABI 7000 thermocycler was performed to evaluate the performance of the cell separator in the presence of chicken wash as a contaminant. Though the data shown still suggests the ability to detect at low concentration levels of 10 cells/ml, with the addition of the chicken wash contaminant, there is a decreased ability to differentiate between the starting concentrations based on the final DNA yield reported by real-time PCR.

concentrations, but with decreasing cell concentrations, we see an improvement in capture efficiency. The data collected suggests the ability to detect at low concentration levels (10 cells/ml), which shows promise for further development of this technology to target scenarios where low cell copy detection is critical. In the next step forward, we tested the Magnetic Cell Separator and cell lysis chip in conjunction with samples tainted with chicken wash. The cell separator results of this experiment using tainted chicken wash are shown in Figure 4-5. Though the data shown from the cell separator experiments still suggests the ability to detect at low concentration levels (10 cells/ml) in the presence of chicken wash, the addition of the contaminant causes a decreased ability to differentiate between the starting concentrations based on the final DNA yield reported by real-time PCR. One explanation for this phenomenon is the possibility that the chicken was already pre-contaminated before the incubation with the cell culture samples, resulting a skew of the results. Also, the inability to differentiate between different initial starting cell concentrations suggests the possibility of false positives at lower concentrations. The final set of experiments involved interfacing the cell separator and cell lysis modules with the existing DNA purification and amplification chip on the microFLUIDICS DESKTOP. Results from these experiments are graphed in Figure 4-6. In Figure 4-6(a), real-time PCR results using the microFLUIDICS DESKTOP are shown of unspiked *Salmonella* samples of different concentrations that were put through the cell separator, cell lysis module, and DNA purification and amplification chip. The microFLUIDICS DESKTOP in conjunction with the sample preparation modules demonstrated the ability to detect *Salmonella* down at concentrations of 100 cells/ml. Figure 4-6(b) shows the real-time PCR data of microFLUIDICS DESKTOP experiments using *Salmonella* samples spiked with chicken wash. Though amplification still occurs at concentrations of 100

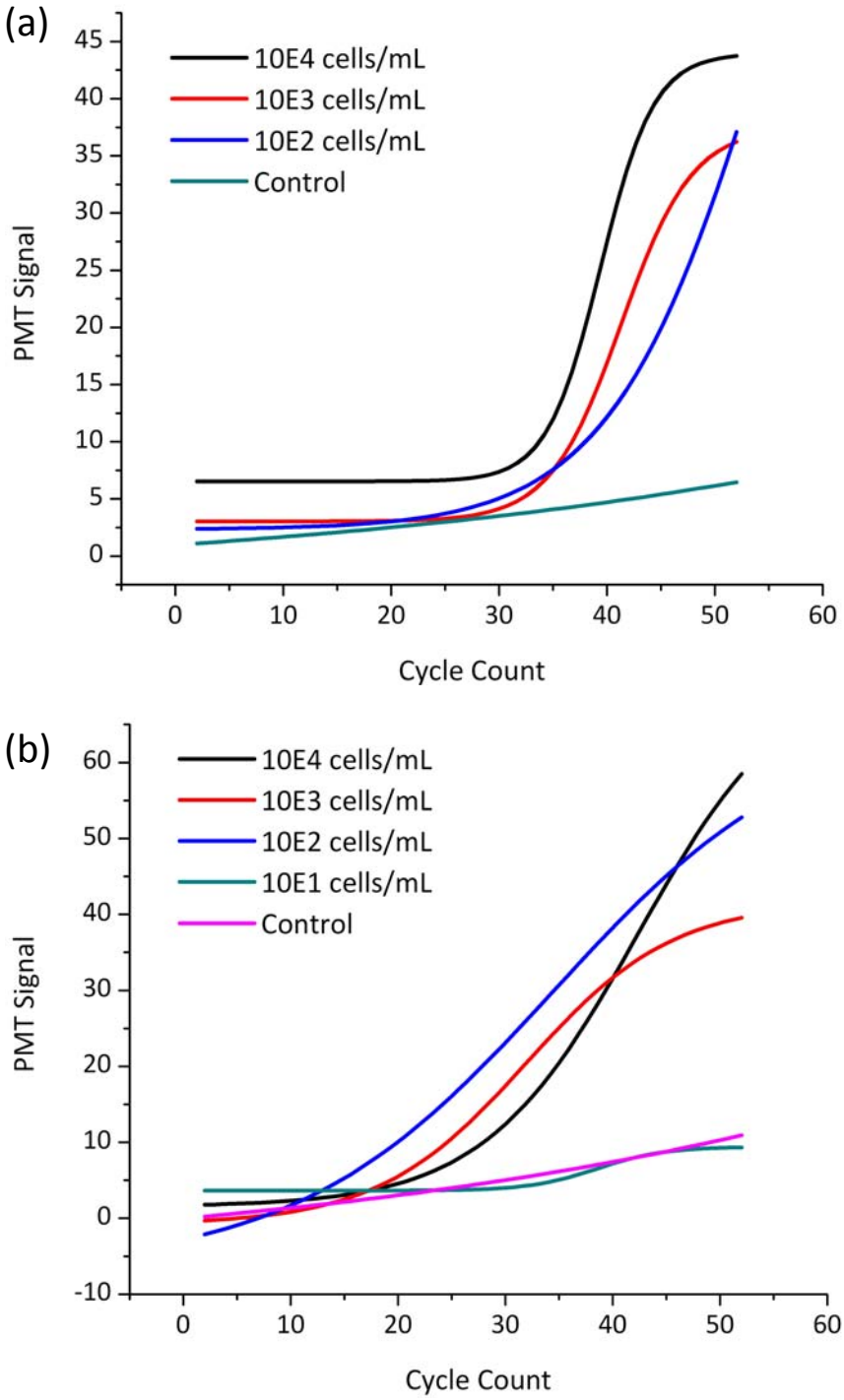

Figure 4-6. Real-time PCR detection recorded using the microFLUIDICS DESKTOP in conjunction with the sample preparation module using (a) *S. typhi* cultures and (b) *S. typhi* cultures spiked with chicken wash.

cells/mL, the presence of chicken wash again makes it difficult to differentiate between different initial starting cell concentrations. One of the major challenges in of optimizing detection protocols in this instrument was the difficulty in achieving perfect seals in the microfluidic devices. Most of the device failures occurred in the form of leaks, ranging from weak seals in the PDMS-to-PDMS or PDMS-to-silicon junctions to poor epoxy seals unable to sustain the high pressures. The large number of input and output tubing need to interface with the various reagent syringes also raised the probability of device leakage. Another challenge was the issue with unwanted bubbles arising within the microfluidic channels. Attempts at de-gassing solutions prior to the experiments did not eliminate bubbles since the vast majority of the bubbles were formed at the interface between the syringe and the tubing. In order to circumvent these problems and decrease the amount of interfacing needed with external parts, we have attempted to integrate on-chip pumps and reagent storage, as well as the sample preparation, DNA purification, and real-time PCR amplification regions, all onto a single chip. The following section will discuss the details of our endeavors in miniaturizing and automating an integrated pathogen detection platform.

4.2 Miniaturized Integrated Pathogen Detection Platform

In this section, we present an integrated pathogen detection platform with on-chip pumps, reagent storage, sample preparation modules, and DNA purification and amplification regions. LabView software was designed to automate the pumping, fluid handling, piezoelectric mixing, electromagnetic capture, thermal cycling events, and laser shutter operation and PMT readout, allowing the user to easily interface with the instrument and modify parameters. By eliminating the fluid handling system that consisted of several syringe pumps on the microFLUIDICS DESKTOP, we can

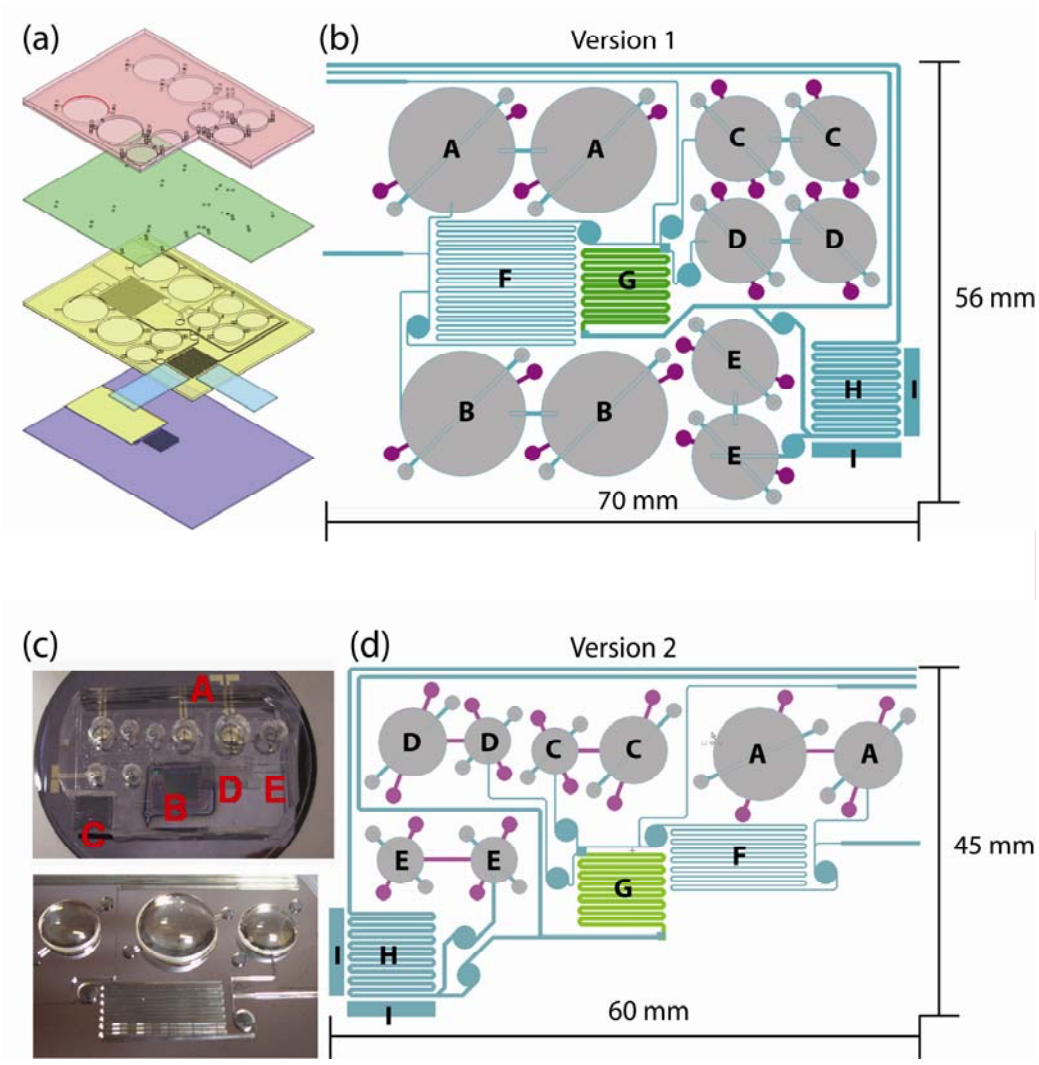

Figure 4-7. Previous design iterations for the integrated pathogen detection platform. (a) Schematic of first design of the integrated microfluidic platform showing individual layers for pumps, membrane, microfluidic channels and pump reservoirs, optical waveguides and DNA purification; (b) Top-down view of the first design; (c) Photographs of the version 2 design as a fully-assembled device (top) and the lens-modified SU-8 mold for the bottom PDMS layer; (d) Top-down view of the second design. In both the top-down view schematics, the labels are as follows: A, lysis buffer reagent pump; B, wash buffer reagent pump; C, ethanol reagent pump; D, elution buffer pump; E, mastermix solution pump; F, cell lysis chamber; G, DNA purification chamber; H, DNA amplification chamber; and I, optical waveguide insertion points.

potentially reduce the size, weight, and power consumption for a more efficient portable device. In the field, the instrument is envisioned to undergo repeated runs, hence leaky connections or accidental fluid mishandling can result in contamination of new samples with PCR amplicons from previous runs and result in false positives. The integrated pathogen detection platform should exist in a cartridge format that can be "plugged" into a miniaturized control system that performs the raw-sample-to-PCR-result analysis. This cartridge should be self-contained and disposable, with the ability to be quickly loaded and replaced without requiring any fluid handling by the user. By eliminating the unreliable user handling of tubing lines, syringes, and fluids, foreseeable contamination issues should be avoided through careful inspection of the device cartridge and the on-board pumping system prior to shipment to the user.

4.2.1Bacterial Growth and Preparation

Salmonella typhi was obtained from a single bacterial colony on a TSB agar plate culture and grown in 5 mL of liquid TSB media at 37°C and gentle agitation for 12 hours. The final culture concentration was estimated to be 5 x 10^9 cells/ml determined through serial dilution and standard plate counting on TSB agar plates.

4.2.2 Microfluidic Modules and Design Layout

The current layout of the integrated microfluidic platform has undergone several design iterations, as illustrated in Figure 4-7. The design incorporates four different modules: electrohydraulic pumps, piezoelectric mixing chamber, DNA pillar-based purification, and laser-excited real-time PCR. The first three modules were described in previous chapters and sections. The laser-excited real-time PCR emerged as an attempt to further miniaturize the optical detection scheme of the microFLUIDICS

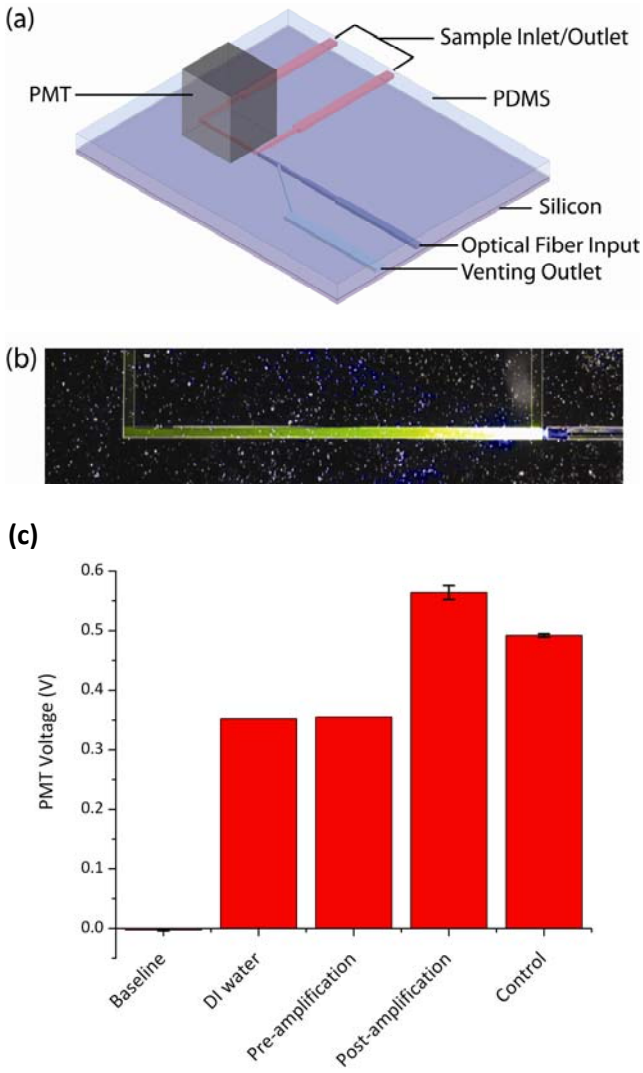

Figure 4-8. Schematic and preliminary results from the laser-excited PCR system: (a) A 3D schematic showing the PMT mounted atop amplification region of the the laser-excited microfluidic PCR chip; (b) The amplification region was filled with rhodamine solution and excited with an optical fiber input coupled to a blue laser; (c) The PMT voltage was monitored various different scenarios: baseline (laser off), DI water, pre-amplified DNA, and post-amplified DNA and a control without DNA that were both amplified using a benchtop thermocycler. Preliminary results show that the system is capable of differentiating between an amplified DNA product and a control in the amplification region using the setup shown. Further studies to optimize the PMT detection and laser coupling are needed to improve the system.

DESKTOP. Essentially, the glass waveguide from the previous design was replaced with an optical fiber that coupled light from a blue laser to the amplification region. he amplification region was reduced in size to achieve a smaller footprint and reagent volumes. A diagrammatic representation of the design, some preliminary results, and a microscope image of the excited amplification region are shown in Figure 4-8. Preliminary results show that the system is capable of differentiating between an amplified DNA product and a control in the amplification region using the setup shown. Further studies to optimize the PMT detection and laser coupling are needed to improve the system. Bubble traps are designed in throughout the module to prevent disturbances to the fluorescence signal during PCR by the presence or formation of unwanted bubbles, and the complications associated with reagent filling were kept in mind during the design.

4.2.3 Integrated Microfluidic Platform Fabrication

Microfabrication of the device was primarily carried out in the Cornell NanoScale Facility (CNF, Ithaca,, NY). The basic fabrication process is illustrated in Figure 4-9. Briefly, 4" silicon wafers were cleaned and 500nm of LPCVD low-stress nitride is deposited with the GSI plasma enhanced chemical vapor deposition (PECVD) system to passivate the surface. The wafers were then primed, spin-coated with Shipley 1827 photoresist (Marlborough, MA) and patterned with hard contact using aEV620 contact aligner (EV Group, Austria). The exposed resist was developed in MIF300 developer and a quick descum was performed using the Aura 1000 GaSonics downstream asher. Using the CHA Mark 50 e-beam evaporator in conjunction with a lift-off dome, 250 nm gold electrodes were deposited with a 50 nm chrome adhesion layer and metal lift-off was achieved by soaking in acetone overnight.

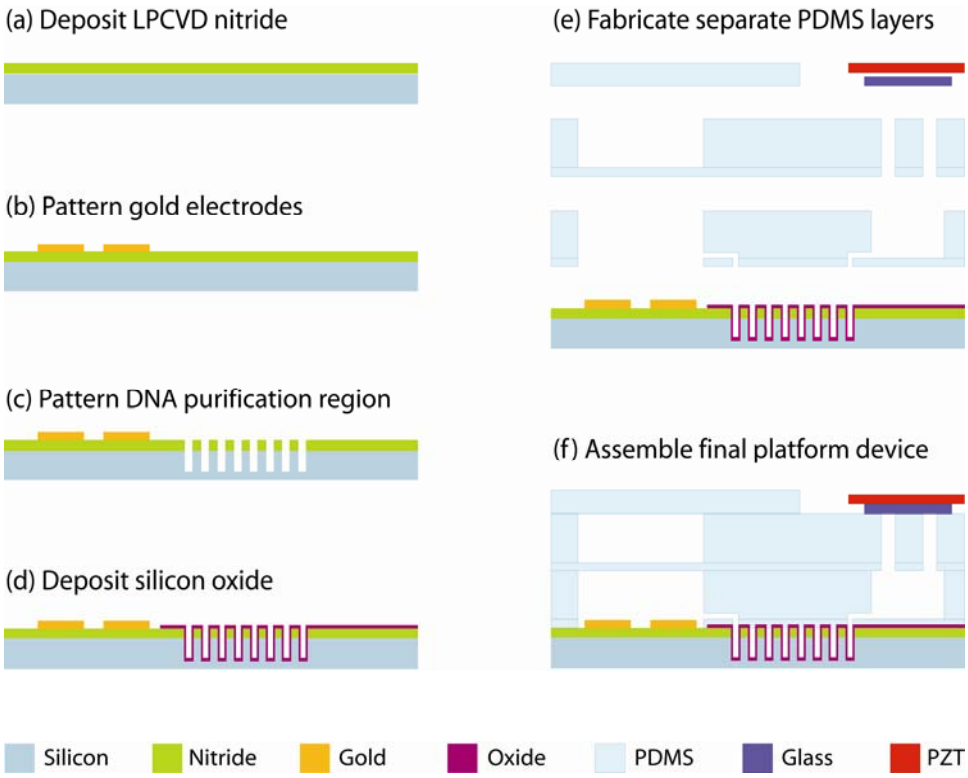

Figure 4-9. The fabrication process for the integrated pathogen detection platform. (a) First, the LPCVD nitride is deposited onto a bare silicon substrate; (b) Gold electrodes are patterned using standard e-beam evaporation and lift-off procedures; (c) The DNA purification region array of 10 μm square pillars are defined by etching through the LPCVD nitride and 50 μm into the silicon; (d) Silicon oxide is deposited in the purification region; (e) In a separate process, SU-8 molds are fabricated and standard PDMS casting is used to form patterned layers, which are adhered to PDMS membranes. Important fluidic connection areas are defined in the membranes; (f) Finally, the different PDMS, silicon, and glass layers are plasma-treated, aligned, assembled into a final platform device and baked for 1 hour. The piezoelectric diaphragm is fixed on top of the glass layer using fast-drying epoxy. After assembly, fluidic and optical fiber connections are inserted and secured.

Next, the DNA purification region containing an array of 10 μm square pillars is defined using the same Shipley 1827 photolithography protocol with the added step of removing the edge bead, and the wafers were plasma etched using the Oxford PlasmaLab 80+ RIE System, following the standard nitride etch recipe of 50 sccm CHF_3 and 2 sccm O_2 recipe at 50 mTorr at 200W in order to punch through the LPCVD nitride thin film. The wafers are then plasma etched in a Unaxis SLR 770 reactive ion etcher (St. Petersburg, FL) using the standard 0Trench recipe to 50μm deep. After etching, a glass microscope slide is affixed to the wafer to protect the electrodes before depositing 100 nm of silicon dioxide (silica) onto the wafers through plasma enhanced chemical vapor deposition (PECVD) using a IPE 1000 System. Wafers were subsequently cleaned of remaining photoresist using the Aura 1000 GaSonics downstream asher.

The bottom EHP-pump layer, capture and lysis chamber, amplification region, and bubble traps are constructed using standard soft lithography techniques for poly(dimethylsiloxane) (PDMS) and SU-8 photoresist, as described previously in Chapter 3. Briefly, a thin layer of PDMS was cured in a bottom-layer SU-8 mold, removed from the mold, placed in between clean transparencies in order to use a stainless steel bore to punch out the chambers and necessary connections. The layer was then bonded to a 60μm thick PDMS membrane. The top EHP-pump layer along with the piezoelectric bubble-based actuation traps are defined separately in another PDMS layer that is bonded to another 60μm thick PDMS membrane. The separate assemblies are baked at 60°C for 1 hour to achieve maximum bonding strength. The two PDMS pieces are exposed to oxygen plasma for 30 seconds in a Harrick Model PDC-001 (Ossinning, NY) Plasma Cleaner/Sterilizer at 200-600 mTorr with 30W DC power applied to the RF coil, carefully aligned using sterile tweezers, and pressed

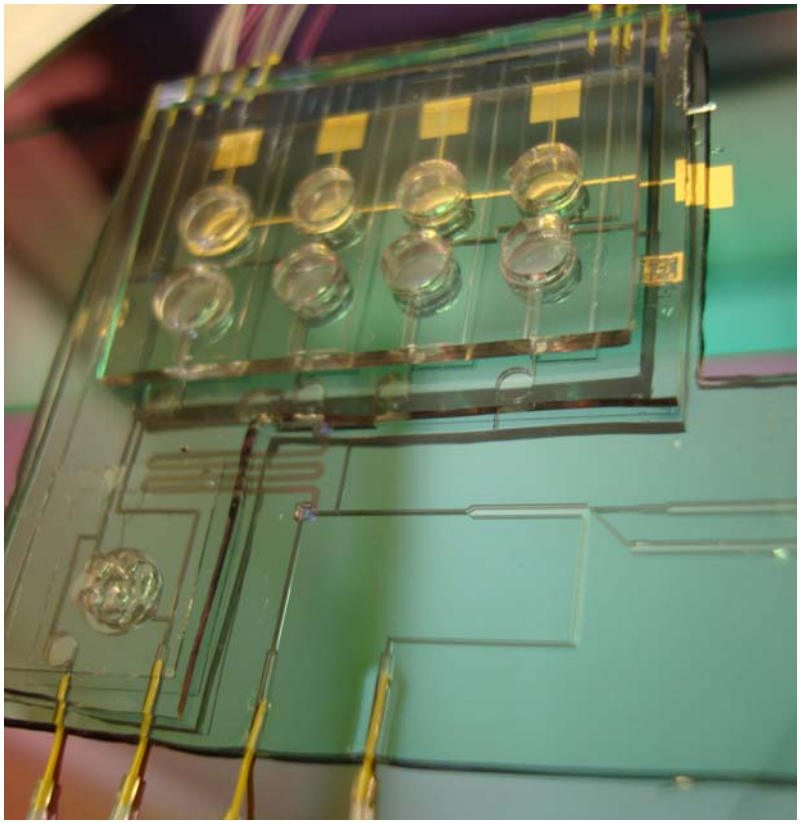

Figure 4-10. Photograph of a partially assembled integrated platform device prior to electrohydraulic pump and reagent chamber fluid filling.

together. The underside of the PDMS assembly and the processed silicon wafer is then exposed to plasma, aligned, pressed together, and baked at 60°C for 1 hour to achieve the fully-assembled device. For fluidic connections, yellow PEEK polymer 0.006" tubing (Upchurch Scientific, Oak Harbor, WA) was threaded into thicker 0.010" microbore tubing (Small Parts, Miami Lakes, FL), and inserted into pre-defined inlets and outlets in the PDMS and fixed in place using silicone adhesive. A small microscope slide was diced into a 1 cm square using a diamond-tip pen and affixed to the topside of the piezoelectric bubble-based mixing chamber using the standard plasma protocol. Scotch-Weld CA40 instant adhesive (St. Paul, MN) was used to glue the brass-side of the piezoelectric diaphragm to the glass cover slip. To introduce the laser light, a 0.22-NA 50μm core multimode Vis-IR optical fiber (ThorLabs AFS50/125Y, Newton, NJ) was stripped, cleaned and inserted into the designated optical fiber channel and fixed using optical adhesive (Norland 63, Cranbury, NJ) and 5-minute ultraviolet light curing. A partially assembled integrated platform is shown in Figure 4-10.

4.2.4 Apparatus

A LabView®-based instrument was designed to automate the pumping, fluid handling, piezoelectric mixing, electromagnetic capture, thermal cycling events, and laser shutter operation and PMT readout, allowing the user to easily interface with the instrument and modify parameters via laptop-controlled software. The instrument contains a variety of different components, including a low-cost NI Multifunction DAQ (NI USB-6008). USB-to-GPIB connections are used to control the DC power supply (Agilent E3631A) and waveform generator (Agilent 33220A). A simple control circuit was constructed using CMOS quad analog switches (MAX4602) to interface

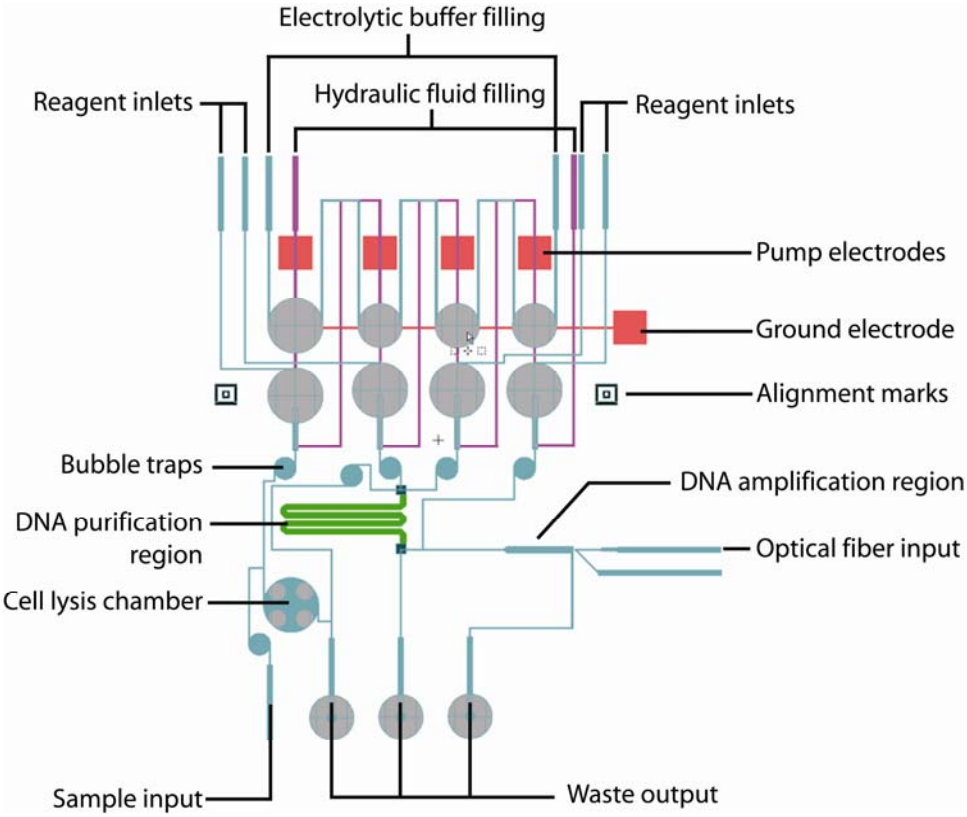

Figure 4-11. The current integrated platform design. Several different layers are shown, along with the input and output specifications. The green serpentine channel is the DNA purification region of 10 μm pillar arrays etched into silicon and coated with oxide. The red electrodes are for the EHP pumps, the base layer of PDMS is shown in blue, and the top layer of PDMS is shown in purple. A PDMS membrane lies in between each of the layers. The entire assembly averages about 5 cm x 5 cm x 0.5 cm.

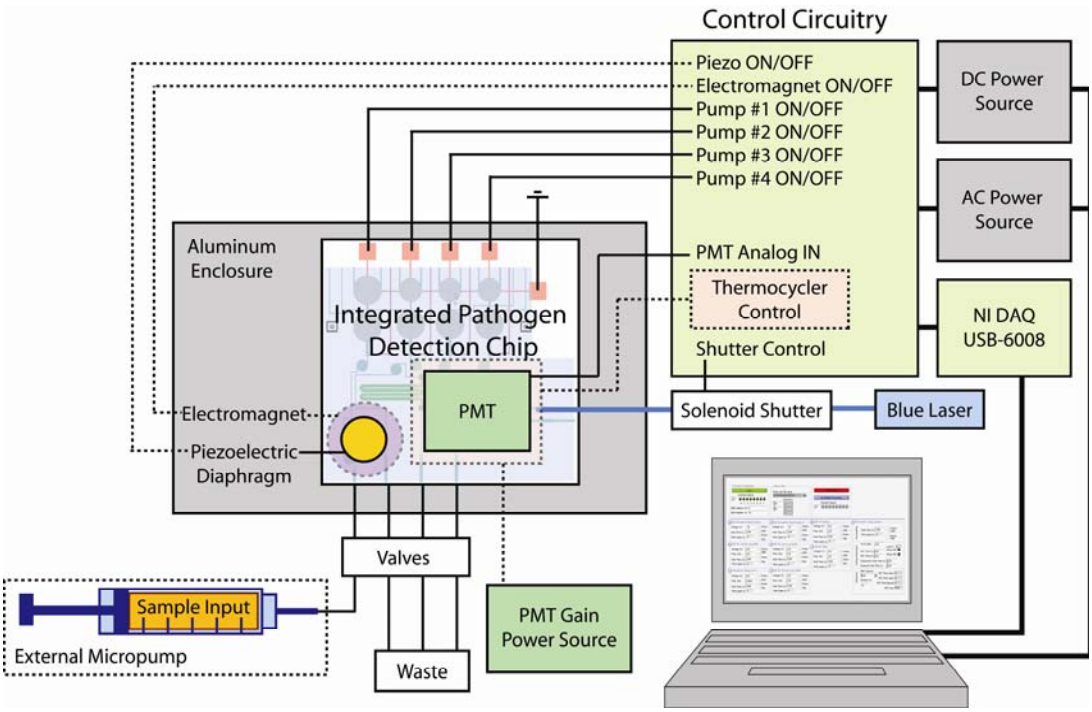

Figure 4-12. Diagrammatic representation of the instrument setup. The integrated pathogen detection chip, along with the electromagnet, piezoelectric diaphragm, PMT, and thermocycler heater, are housed within an aluminum enclosure with connections to the control circuitry, sample input, fluidic valves, and power sources. The LabView® software interfaces with the power sources and the control circuitry to automate the experimental process.

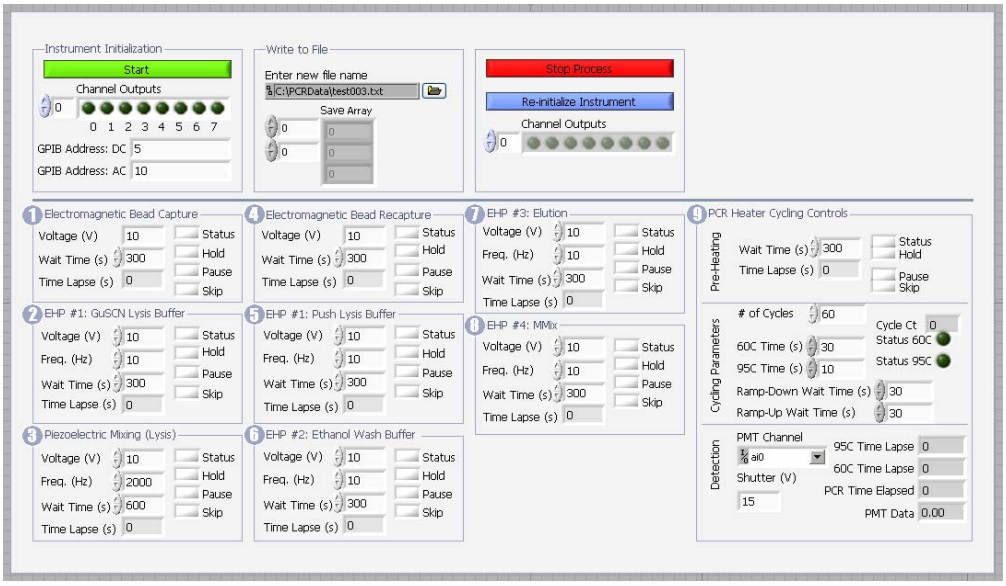

Figure 4-13. Front-panel of the LabView® user interface.

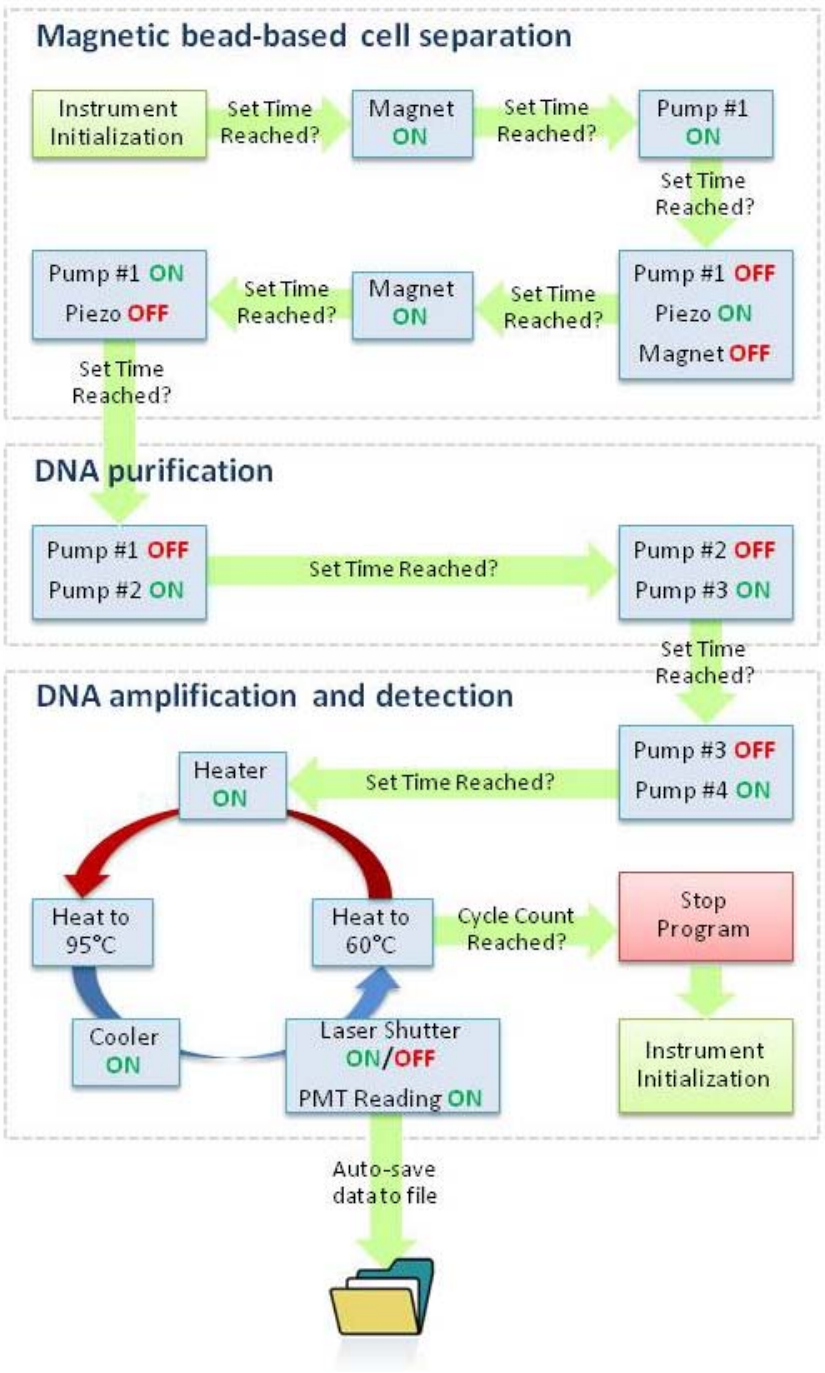

Figure 4-14. Diagrammatic representation of the LabView® software process flow as it moves through the cell separation, DNA purification, and DNA amplification & detection modules. The reagents contained in pumps #1, #2, #3, and #4 are lysis buffer, ethanol, nuclease-free water, and mastermix solution, respectively.

with the DAQ and sequentially activate the electromagnet (Magnetool EM-R75, Troy, MI), piezoelectric diaphragm (CUI CEB-20D64, Tualatin, OR), gold electrode EHP pumps, thermoelectric heater/cooler module (HY5640, Hytek TEC Controller, Carson City, NV) linked to a Peltier module (CUI CP60133, Tualatin, OR) and 10 kΩ epoxy-coated chip thermistor (GE Sensing C100, Edison, NJ), and solenoid-controlled (SMT-1350S, Sun Magnet, Taiwan) custom-designed laser shutter. A diagrammatic representation of the integrated chip, the instrument setup and the LabView® interface is presented in Figure 4-11, 4-12 and 4-13, respectively.

During a typical detection protocol, the automated LabView® program executes magnetic bead and target pathogen capture, piezoelectric mixing with lysis buffer, activation of the individual EHP pumps to deliver the lysis buffer, ethanol wash, elution buffer, and PCR master mix, initial thermal activation of the polymerase, and thermal cycling of the Peltier module between the temperatures of 60°C and 95°C. The detailed process flow for the program is shown in Figure 4-14. During the real-time PCR reaction, the shutter is signaled open and fluorescent data is collected as a direct analog voltage signal during the 60°C step and the time, cycle number, and voltage signal is automatically saved to a data file upon completion of the cycling. It is critical that the PMT signal be sampled at the same temperature during the cycle since the fluorescence of the dye is temperature-sensitive.

For testing purposes, the integrated microfluidic platform device is mounted inside a custom-machined aluminum enclosure and sealed with electrical tape to reduce the noise levels detected by the photomultiplier tube (PMT). The entire system is can be easily miniaturized into a smaller footprint via designing a custom PCB board for the control and thermal cycling circuitry. The DC power supply and waveform generator

can also be further miniaturized through the purchase of smaller off-the-shelf parts that can be integrated into the system for greater portability. In terms of lowering the power requirements of the system, the main power draw arises from the current thermoelectric heater/cooler configuration. Smaller, low-power Peltier modules are available for purchase from various vendors with lower power requirements, and can be further investigated in future work.

4.2.5 Experiment: Reagent Filling and Testing Methodology

The reagent filling of the integrated platform is performed just prior to the experiment. The deionized water for the hydraulic layer of the EHP pumps are introduced first, followed by the TAE electrolyte solution and each of the individual reagents (lysis buffer, ethanol, nuclease-free water, and mastermix solution, in that particular order). The tubing lines are then clamped off securely, and a careful incision is made in the PDMS to expose the electrode connections without severing. The inlets and outlets are then re-sealed with silicone sealant and baked at 60°C for 5 minutes. Wiring is connected to the exposed electrode connections using conductive silver epoxy and baked for an additional 5 minutes. The assembly is allowed to cool at room temperature in a high-humidity environment for 10 minutes.

For our preliminary experiments 1 mL of *Salmonella typhi* at a concentration of 1 x 10^8 cells/ml was incubated with 40 µl of anti-*Salmonella* magnetic beads for 10 minutes in a standard Eppendorf tube. The entire sample was introduced into the integrated pathogen detection platform at 20 µl/min while the magnetic capture module was active. As per the LabView® process flow shown in Figure 4-13, the lysis buffer pump is run for 3 minutes at 10VAC (10 Hz), the piezoelectric diaphragm is activated for enhanced mixing of the captured cell with lysis buffer for 5 minutes at

20VAC (2 kHz), the magnetic beads are re-captured, and the lysis buffer pump is activated for another 2 minutes to push the cell lysate into the DNA purification region. Next, the ethanol wash pump run for 5 minutes at 10VAC (10 Hz), followed by elution with nuclease-free water pump for 2 minutes at 10VAC (10 Hz) and activation of the mastermix solution pump for 2 minutes at 10VAC (10 Hz). The elution pump moves the bound DNA from the purification region into the amplification region along with the mastermix, and the chip is pressurized before thermal cycling. The heater is activated, and thermal cycling of the Peltier module between the temperatures of 60°C and 95°C is carried out for 60 cycles. The voltage signal from the PMT is monitored during the 2-second laser shutter opening just prior to the 60°C step, and the data is automatically saved to a designated file upon completion of the cycling.

4.2.6 Results & Discussion

The PMT voltage signals monitored using LabView® software during 60°C steps for 60 cycles are shown in Figure 4-15. The integrated pathogen detection platform on using 10E+8 cells/ml *S. typhi* starting samples (red) pre-mixed with anti-*Salmonella* magnetic beads, and introduced into the mixing chamber. The automated program cycled through the lysis, DNA purification, and real-time PCR steps. The control experiment was run with the exact same protocol with a solution of anti-*Salmonella* magnetic beads suspended in PBS (black), and shows little change in fluorescent signal over the 60 cycle count. Another control experiment was performed using 1µl of DNA extracted from 10E+8 cell/ml run (blue) with only the real-time PCR portion of the instrument which shows a significant improvement in signal, signifying that the

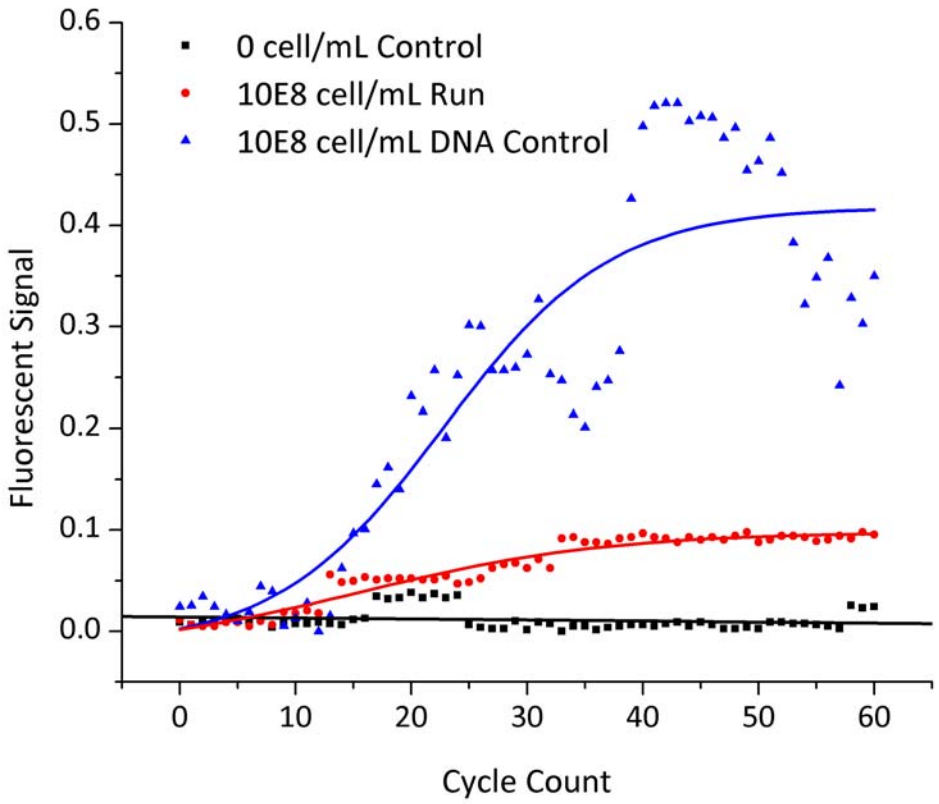

Figure 4-15. PMT readings recorded using LabView® software in conjunction with the integrated pathogen detection platform on using 10E+8 cells/ml *S. typhi* starting samples (red). The control experiment with no cells (black) shows little change in fluorescent signal over the 60 cycle count. Another control experiment using 1µl of DNA extracted from 10E+8 cell/ml shows a significant improvement in signal, signifying that the sample preparation and DNA purification modules prior to the real-time PCR introduces an element of signal degradation.

sample preparation and DNA purification modules prior to the real-time PCR introduces an element of signal degradation. The automation of the instrument was highly successful and flexible, sequentially carrying out all the steps from sample preparation to detection with minimal user input.

Currently, the only non-automated aspect of the system lies in the valving of fluids, which is currently manually controlled using clips and hemostats. Many research groups have investigated the incorporation of on-chip microfluidic valves, though few are actually capable of withstanding the high pressures necessary for our protocol. Though mechanical valves at the tubing inlets and outlets can be easily incorporated and automated using our system, more investigations are necessary for determining the best valving mechanism for our integrated chip. In order the expedite and simplify the reagent filling procedures, which can be a slow and difficult process due to the interference of air bubbles and pressure leaks, on-chip valving mechanisms designed to isolate the reagent chambers from the rest of the chip should be further investigated. The successful integration of microfluidic valves would allow automation of the filling process in addition to enhanced controllability of the fluid flow.

The key microfluidic components in the integrated platform, including the electrohydraulic pumps, piezoelectric bubble-based mixing, and purification and amplification chambers are simple in design, inexpensive and simple to fabricate, and easy to scale up to a manufacturing process. Although technical challenges still remain in increasing cell capture efficiencies, detection sensitivities, and assay optimization, the current platform presented here provides a solution for the portable field-deployable detection of foodborne pathogens with raw-sample-to-result capabilities. As this system develops further, applications could be foreseen in other areas that

require rapid and sensitive nucleic acid-based detection systems, such as point-of-care genetic analysis or disease diagnosis.

REFERENCES

[1] Stroock, A.D.; Dertinger, S.K.W.; Ajdari, A.; Mezic, I.; Stone, H.A.; Whitesides, G.M. Chaotic Mixer for Microchannels. *Science* 2002, *295*, 647-651.

[2] Eijkelkamp, J.M.; Aarts, H.J.M.; Fels-Klerx, H.J.v.d. Suitability of Rapid Detection Methods for Salmonella in Poultry Slaughterhouses. *Food Analytical Methods* 2008, *2*, 1-13.

[3] Lazcka, O.; Del Campo, F.J.; Muñoz, F.X. Pathogen detection: A perspective of traditional methods and biosensors. *Biosens. Bioelectron.* 2006, *22*, 1205-1217.

[4] Whyte, P.; McGill, K.; Collins, J.D.; Gormley, E. The prevalence and PCR detection of Salmonella contamination in raw poultry. *Veterinary Microbiology* 2002, *89*, 53-60.

[5] Nandakumar, V.; La Belle, J.T.; Reed, J.; Shah, M.; Cochran, D.; Joshi, L.; Aslford, T.L. A methodology for rapid detection of Salmonella typhimurium using label-free electrochemical impedance spectroscopy. *Biosens. Bioelectron.* 2008, *24*, 1039-1042.

[6] Mercanoglu, B.; Griffiths, M.W. Combination of Immunomagnetic Separation with Real-time PCR for Rapid Detection of Salmonella in Milk, Ground Beef, and Alfafa Sprouts. *Journal of Food Protection* 2005, *68*, 557-561.

[7] Cheng, C.-M.; Lin, W.; Thien Van, K.; Phan, L.; Tran, N.N.; Farmer, D. Rapid Detection of Salmonella in Foods using Real-Time PCR. *J. Food Protection* 2008, *71*, 2436-2441.

[8] Bhagwat, A.A. Rapid detection of Salmonella from vegetable rinse-water using real-time PCR. *Food Microbiology* 2004, *21*, 73-78.

[9] Nam, H.-M.; Srinivasan, V.; Gillespie, B.E.; Murinda, S.E.; Oliver, S.P. Application of SYBR green real-time PCR assay for specific detection of Salmonella spp. in dairy farm environmental samples. *Int. J. Food Microbiol.* 2005, *102*, 161-171.

[10] Klerks, M.M.; Zijlstra, C.; von Bruggen, A.H.C. Comparison of real-time PCR methods for detection of Salmonella enterica and Escherichia coli O157:H7 and introduction of a general internal amplification control. *J. Microb. Methods* 2004, *59*, 337-349.

[11] Patel, J.R.; Bhagwat, A.A.; Sanglay, G.C.; Solomon, M.B. Rapid detection of Salmonella from hydrodynamic pressure-treated poultry using molecular beacon real-time PCR. *Food Microbiology* 2005, *23*, 39-46.

[12] Ko, S.; Grant, S.A. A novel FRET-baswed optical fiber biosensor for rapid detection of Salmonella typhimurium. *Biosens. Bioelectron.* 2005, *21*, 1283-1290.

[13] Reynisson, E.; Josefsen, M.H.; Krause, M.; Hoorfar, J. Evaluation of probe chemistries and platforms to improve the detection of real-time PCR. *J. Microb. Methods* 2005, *66*, 206-216.

[14] Wang, Z.; Sekulovic, A.; Kutter, J.P.; Bang, D.D.; Wolff, A. Towards a portable microchip system with integrated thermal control and polymer waveguides for real-time PCR. *Electrophoresis* 2006, *27*, 5051-5058.

[15] Lai, R.Y.; Lagally, E.T.; Lee, S.-H.; Soh, H.T.; Plaxco, K.W.; Heeger, A.J. Rapid, sequence-specific detection of unpurified PCR amplicons via a reusable electrochemical sensor. *Proc. Natl. Acad. Sci. U.S.A.* 2006, *103*, 4017-4021.

[16] Neuzil, P.; Pipper, J.; Hsieh, T.M. Disposable real-time microPCR device: lab-on-a-chip at low cost. *Mol. BioSyst.* 2006, *2*, 292-298.

[17] Cady, N.C.; Stelick, S.; Kunnavakkam, M.V.; Batt, C.A. Real-time PCR detection of *Listeria monocytogenes* using an integrated microfluidics platform. *Sens. Actuators. B Chem.* 2005, *107*, 332-341.

[18] Cady, N.C.; Stelick, S.J.; Batt, C.A. Rapid Detection of Bacillus Anthracis in a Microchip-Based Real-Time PCR Biosensor. In Mater. Res. Soc. Symp. Proc., 2007.

[19] Cady, N.C.; Stelick, S.J.; Kunnavakkam, M.V.; Liu, Y.; Batt, C.A. A microchip-based DNA purification and real-time PCR biosensor for bacterial detection. In Sensors, Proc. of IEEE, 2004, pp. 1191-1194.

[20] Cady, N.C.; Stelick, S.; Batt, C.A. Nucleic acid purification using microfabricated silicon structures. *Biosens. Bioelectron.* 2003, *19*, 59-66.

[21] Malorny, B.; Paccassoni, E.; Fach, P.; Bunge, C.; Martin, A.; Helmuth, R. Diagnostic Real-time PCR for Detection of Salmonella in Food. *Appl. Environ. Microbiol.* 2004, *70*, 7046-7052.

CHAPTER 5

MICROFABRICATED CANTILEVER SENSORS

5.0 Introduction

Recent advances in micro- and nanofabrication techniques have allowed for promising developments of new technologies in biosensing, including pathogen detection [1-7], antibody-antigen recognition [8-10], DNA hybridization [11-15], and cellular dynamics [16-19], particularly for single-cell and single-molecule studies [20-23]. Atomic force microscopy (AFM) has been demonstrated to be useful for imaging single biomolecules and to confirm inferences on shape and interactions. The AFM is considered a mass-sensing technique, where the resonance frequency shift or bending of the cantilever is associated with changes in mass, viscosity, or biomaterial adsorption [24]. The ability of microcantilevers to detect biomolecular interactions due to change in surface stress on the cantilevers leading to a change in resonance frequency has also been studied [25]. The traditional measurement of resonance shift involves direct acoustic excitation of the cantilever, which requires complicated signal processing. Examination of thermal noise is preferred because of its simplicity, however, in liquid, the high viscous damping of fluid may result in low quality factors [26]. Also, with the thermal-noise method, cantilevers with a lower reflectivity may exhibit inadequate signal-to-noise ratio in liquids [27].

5.1 Microfabrication of Gold-coated Nitride Cantilevers with Exposed Nitride Pad

In this section, we will discuss in-depth the methods and protocols that were used in our development of the gold-coated nitride cantilevers with exposed nitride pad. The final fabrication process is briefly illustrated in Figure 5-1.

5.1.1 Substrate Preparation

Double-side polished silicon wafers of 4 inch diameter and 400 μm thickness were used as our starting substrate, and were modified through the growth of thin films in

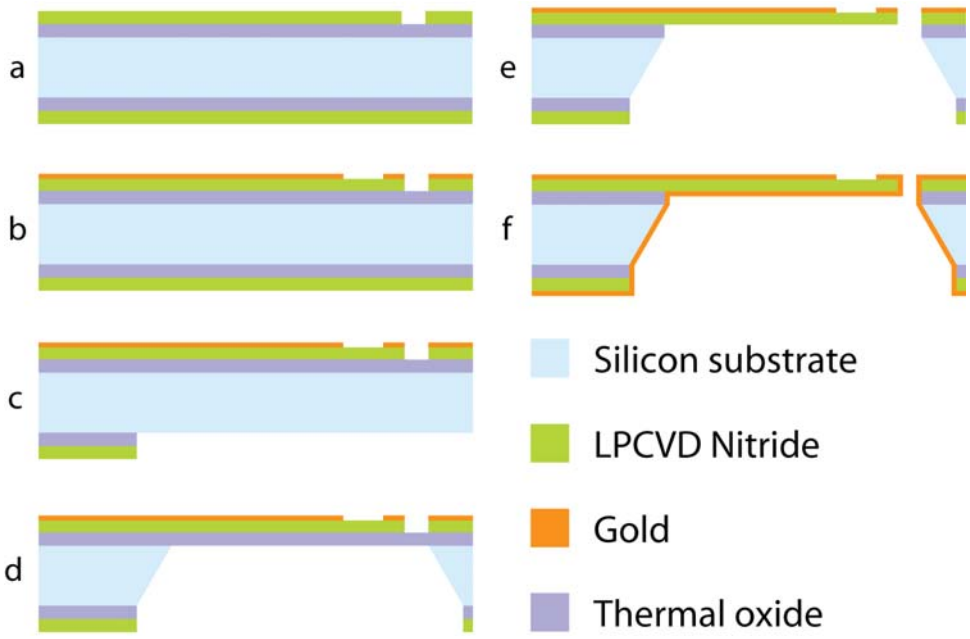

Figure 5-1. Cross sectional diagram depicting the fabrication process for creating the tipless gold-coated silicon nitride cantilever array with 10 μm square nitride openings at the tip.

the Cornell NanoScale Facility. For our initial investigations and fabrication process development, silicon-on-insulator (SOI) wafers with 340 nm of thermal oxide and 2000 nm of silicon were used.

MOS Clean. Substrate wafers need to be properly cleaned of contaminants, such as dust particles or chemical contaminants, to avoid problems such as surface unevenness, blocked patterns, or unexpected changes in the chemical properties of the photoresist. Though it is common practice that new wafers do not require additional cleaning, the standard protocol for CMOS processes at the Cornell Nanoscale Facility (CNF) requires a standard MOS clean prior to any furnace deposition of thin films. Though the preparation of ultraclean silicon surfaces by cleaning and surface conditioning for the manufacture of integrated circuits (IC) has evolved immensely over the years, wet chemical processes are still the simplest and most widely used method. The MOS clean, otherwise known as the "RCA Standard Clean", consists of two consecutively applied heated solutions. The first solution consists of a mixture of NH_4OH (ammonium hydroxide), H_2O_2 (hydrogen peroxide) and deionized water. The second solution comprises of a mixture of HCl (hydrochloric acid), H_2O_2 (hydrogen peroxide) and deionized water. The solutions are both heated to approximately 75°C, and the standard cleaning time of 10 minutes is each followed by a quench and overflow rinse in running deionized water. The wafers are then spun dry and immediately transferred to a pre-cleaned enclosure for storage before further processing [28].

Oxidation of Silicon. The growth of thermal oxide on a silicon wafer involves heating the wafer in a stream of steam at 1 atm or in wet or dry oxygen/nitrogen mixtures at elevated temperatures. At room temperature, silicon readily oxidizes to form a native

oxide of approximately 20 angstroms. Higher temperatures help diffuse the oxidant through the surface oxide to the silicon interface in order to rapidly form thick oxides [28]. Silicon oxide is a common insulating layer, can act as a mask, and is often used as a sacrificial release layer, as in our case. For our wafers, we grew a layer of thermal oxide using a wet procedure with HCl gas for 6.7 hours at 1100°C to form a 2 μm layer, which was verified using a FilMetrics F20optimal measurement system for transparent thin film measurements.

LPCVD Nitride Deposition. Chemical vapor deposition (CVD) involves introducing the constituents of a vapor phase diluted with an inert carrier gas in order to bring about a deposition reaction the hot surface of a substrate to form a solid thin film. The mass transport of reactant and diluents gases in the bulk gas flow region and subsequent by-products away from the deposition zone are precisely flow-controlled in horizontal tube hot-wall furnaces in order to achieve uniform deposition [28]. Low-pressure CVD (LPCVD) silicon nitride films are often used for structural layers in micromechanical systems due to low film stress and purity. The LPCVD reaction coats not only the wafers but also the reaction chamber walls, and therefore the reaction tubes require frequent cleaning to avoid serious particulate contaminations. While in between cleans, however, particulate contamination and issues with furnace particle-spitting can be largely avoid by flanking the wafers boats with dummy wafers. 1.0 μm of low-stress nitride is deposited on top of the thermal oxide layer at 800°C for 6.7 hours.

5.1.2 Wafer Cleaning and Priming

Before photoresist spinning, the wafer is centered on the spinner chuck and spun at 3000 rpm. Upon reaching the target spin speed, a spray bottle is used to target a stream

of acetone at the wafer center for 10 seconds to remove any existing contaminants or dust particles that may have settled on the substrates during storage or handling. Without removing the acetone stream, a second spray bottle full of isopropyl alcohol (IPA) is targeted at the same spot for an additional 5 seconds. Finally, the acetone stream is removed, and the IPA is continued for additional 5 seconds before allowing the wafer to spin dry.

In order to prepare the substrate wafer for photolithography, wafer priming is commonly performed to improve the adhesion of photoresist to the silicon wafer. Additives such as plasticizers, adhesion promoters, speed enhancers, and nonionic surfactants have been shown to promote resist performance. Positive photoresists in particular have difficulty in adhering to a substrate, especially if the humidity is high or if the wafer has been previously immersed in water. Increasing the hydrophobicity of the wafer surface will improve the resist adhesion [28]. In order to achieve this increased hydrophobic surface, a number of different techniques were employed:

(1) Hexamethyldisilazane (HDMS) vapor priming is widely used in the semiconductor industry to improve photoresist adhesion to oxide surfaces. A dehydration bake is performed at 200 to 250°C for 30 minutes to remove adsorbed water from the silanol groups at the silicon surface, and then the wafer is exposed to HDMS vapor in a stream of dry nitrogen. The reactive Si-NH-Si functional groups in HDMS react with the oxide surface via silylation, forming a strong bond to enhance photoresist adhesion [28].
(2) P20 Adhesion spin-on promoter is a quick and easy solution to promote photoresist adhesion in the event of time limitations and for larger design features.

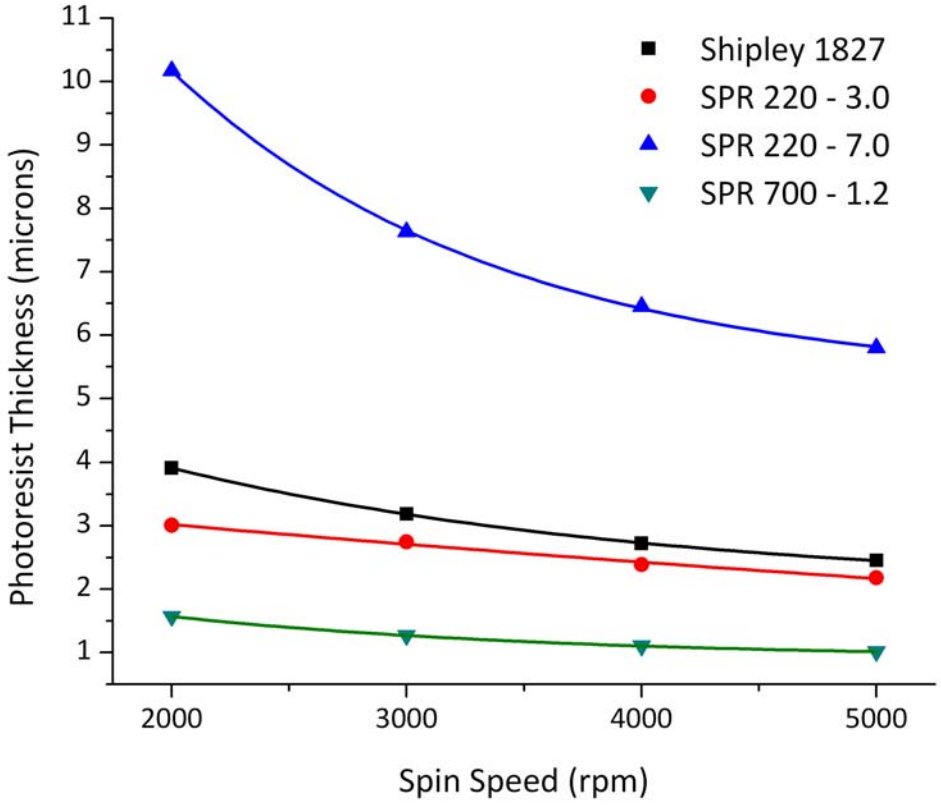

Figure 5-2. Spin speed curves for the photoresists Shipley 1827, SPR 220-3.0, SPR 220-7.0, and SPR 700-1.2 using a standard 1000 rpm/s ramp.

5.1.3 Pattern Transfer

The process of pattern transfer from masks onto thin films is accomplished almost exclusively via photolithography. Extensively developed for the integrated circuit industry, photolithography has matured rapidly and is now able to resolve ever smaller features. For our masks, the computer-aided design (CAD) software L-Edit (v.12.1) was used to create the patterns, which were transferred onto 5-inch chrome-coated quartz masks using either a laser-interferometer metered pattern generater (GCA/MANN 3600F) or a laser pattern direct writer (Heidelberg DWL66). The photoresists used for our cantilever process include: Shipley 1827, SPR220-3.0, SPR 220-7.0, and SPR 700-1.2. Spin speed curves for different resists were characterized and shown in Figure 5-2.

In our initial cantilever designs, we utilized electron-beam lithography to pattern 250 nm x 250 nm gold squares at the tips of cantilevers fabricated from an SOI wafer (340/2000 nm Si/SiO_2). E-beam lithography is a high-resolution patterning technique that uses high-energy electrons to expose electron-sensitive resists. We used a two-layer resist technique for gold-lift off using PMMA (polymethyl methacrylate): (1) 4% PMMA 495 in anisole was spun at 4000 rpm (500 rpm/s ramping) and baked at 170°C for 15 min. and cooled (2) 1% PMMA 950 in methyl isobutyl ketone (MIBK) was spun at 2000 rpm (500 rpm/s ramping) and baked at 170°C for 15 min. and cooled. The JEOL JBX-9300FS electron beam lithography system was used to transfer the pattern onto the photoresist.

Electron Beam Evaporation of Metals. E-beam evaporation is a type of physical vapor deposition process that uses the thermal energy from an electron beam to evaporate a material from a source crucible and transfer it to a substrate. The CHA

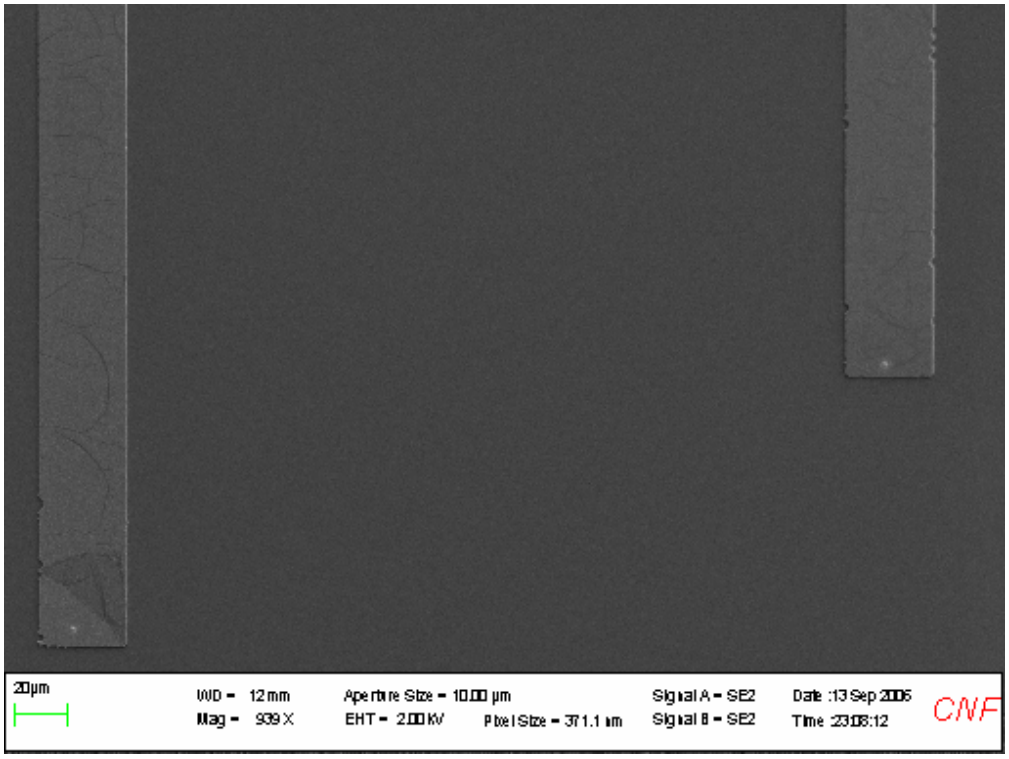

Figure 5-3. Scanning electron micrograph of an unreleased cantilever patterned with 5 µm platinum squares using the focused-ion bean system.

Mark 50 Evaporator, a double stack cryo-pumped, six pocket electron beam deposition system, was employed to deposit uniform thin films to form our patterned gold cantilever surfaces. A lift-off dome, capable of mounting 19 wafers, is mounted and rotated at a rate of 40 rpm during the deposition. 50 nm of gold is deposited on top of 10 nm of chrome, which acts as an adhesion layer between the gold and the silicon nitride surface.

Focused-Ion Beam Patterning. As part of an exploratory process in our cantilever development, we attempted to pattern platinum 5μm squares using a focused ion beam system (FEI 611 FIB system) at the tips of unreleased cantilevers. The tool employs a high-brightness gallium liquid metal ion source coupled with a double lens focusing system capable of producing an intense beam of ions that can mill a variety of materials. A Kleindiek micromanipulator system is enclosed within the specimen chamber, and can be coupled to a platinum deposition tool to allow direct patterning of metallic structures onto a wafer. An unreleased cantilever patterned with platinum squares using the FIB system is shown in Figure 5-3.

Our design was eventually modified for enhanced cell capture capabilities, and the 250 nm square boxes were replaced by larger 10μm squares. Single-cell capture studies were performed at the wafer scale using gold-coated silicon oxide and silicon nitride wafers. Images shown in Figure 5-4 depict the successful capture of single bacterial cell using μm squares. The probability of single bacteria capture with squares of smaller dimensions decreased dramatically, and larger 20 μm squares were shown to capture an average of 4-5 cells/square. This shift rendered the e-beam patterning and FIB patterning procedures unnecessary as the patterning could be achieved with simple contact photolithography.

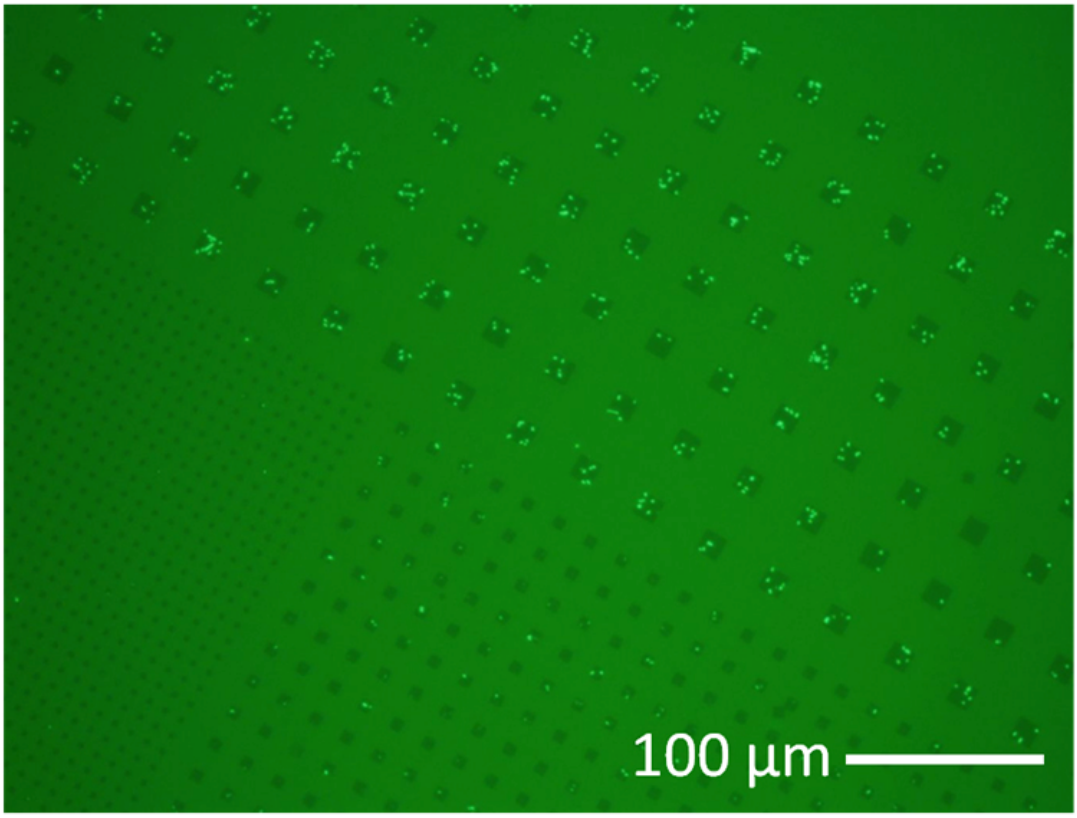

Figure 5-4. Fluorescent micrograph shows the minimum square size needed to capture single *E. coli* cells. Arrays of 5, 10, and 20 µm square boxes are shown. The gold is passivated using PEG-dithiol and the square nitride openings are modified with poly-L-lysine. The chip is dipped in a concentrated bacterial culture with of 10E8 cells/ml for 15 minutes and washed extensively using phosphate buffered saline.

5.1.4 Thin Film Etch

Patterning of the LPCVD nitride thin film in order to define the cantilevers was achieved through dry etching techniques, primarily using the Oxford PlasmaLab 80+ system. Prior to each etch, an oxygen clean at 60 mTorr, 50sccm O_2 and 150W was performed for 15 min. to cleanse the chamber, and the chamber was seasoned for 5 min. to stabilize the etch rates. The nitride etch employed a fluorine-based reactive ion etch protocol as follows: 50 mTorr, 50 sccm CHF_3, 2 sccm O_2, 200W. The etch rates were characterized for each run, although the average varied from 30-50 nm/min. The backside oxide etch was performed using the Oxford PlasmaLab 100 reactive ion etching system for fluorine-based deep SiO_2/glass etching in order to punch through the 2 μm film more quickly at rates of around 100 nm/min.

5.1 5 Deep Silicon Bosch Etch

For deep etching of silicon, particularly for through-wafer processes requiring straight side walls with high aspect ratios of approximately 20 to 30:1, the Bosch advanced silicon etch is often used. The process cycles between sequential polymeric passivation and RIE etching for a user-defined number of loops with standard etch rates of approximately 2 μm/min. One issue that was encountered during deep RIE of our wafers was the common problem of silicon grass that developed on the surface of wafer. Silicon grass, also known as black silicon, consists of silicon pillars that accumulate on the wafer, likely due to contamination from the photoresist mask and/or reactor walls. The development of silicon grass, along with inherent non-uniform rates of etching across the wafer, made it difficult to accurately gauge the etch stop location during the through-wafer etch. As a result, single-sided KOH wet etch was chosen as a more controllable and repeatable process.

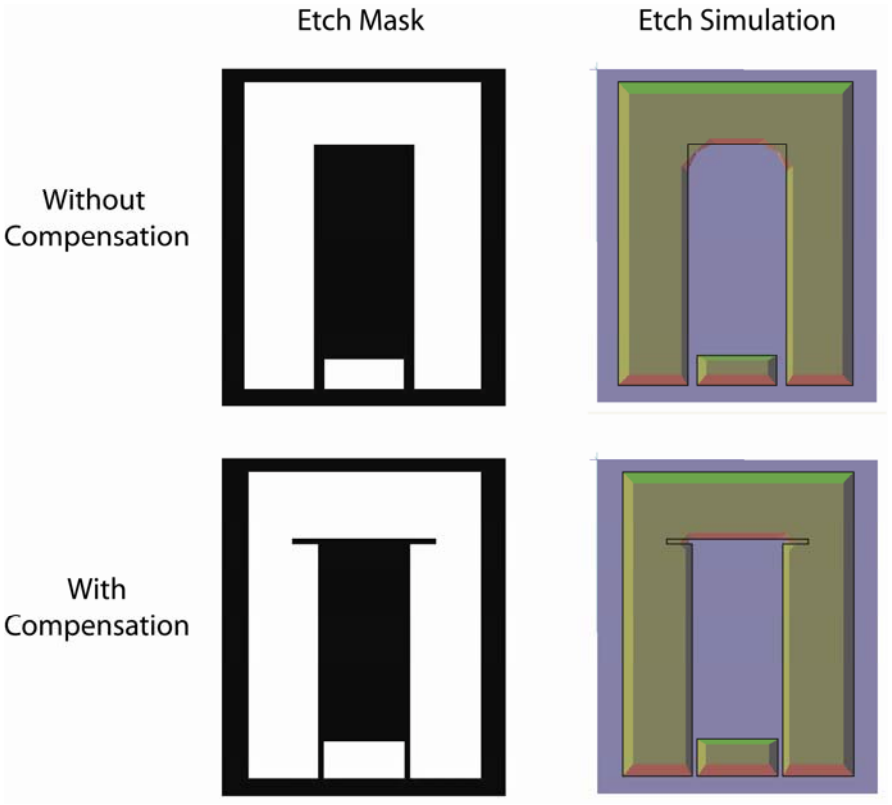

Figure 5-5. The anisotropic etch of potassium hydroxide on <100> silicon wafers. Using the Anisotropic Crystalline Etch Simulation (ACES) software, the etch profile can be simulated as a function or our etchant concentration, etch rates, and temperature, allowing us to optimize our etch mask design. The etch masks above were simulated using a 9-hour standard 30% KOH etch without design compensation for the edges and corners (top) and with design compensation (bottom). The corner compensation allows the cantilever due to maintain the structural integrity of the device to allow for ease of removal and handling.

5.1.6 Wet Etch Cantilever Release

The simple potassium hydroxide (KOH) etch is one of the most popular silicon anisotropic etchants. A single-sided Teflon etch holder was used to secure the wafer to allow exposure to the stirred 80°C-heated 30% w/v KOH solution on only one face of the wafer. Etching at approximately 1 μm/min, the single-sided through-wafer etch requires 9 hours for completion. Since KOH etch rates for different crystal planes are vastly different, the nitride KOH etch mask needs to be predesigned to accommodate for corner compensation. Our standard <100> 4-inch silicon wafers etch anisotropically with a 54.75° angle from the plane. Using the Anisotropic Crystalline Etch Simulation (ACES), a PC-based 3-D etch simulator, the etch profile of our 2-D mask pattern can be simulated as a function of etchant concentration, etch rates, and temperature. A depiction of the etch by ACES is shown in Figure 5-5. Immediate after the termination of the KOH etch, the wafer is carefully rinsed twice in DI water and placed in 1:6 buffered oxide etch. Also known as buffered HF, this etchant is comprised of a mixture of buffering agent and hydrofluoric acid (HF).

5.1.7 Critical Point Drying

Subsequent to a wet HF release of the cantilever structure, critical point drying is performed to prevent water stiction from affecting or destroying the structure of the cantilevers. This method involves placing the wafer in methanol soaks of increasing concentration, to gradually replace the water. The sample is placed within a chamber, and the methanol is slowly replaced by liquid carbon dioxide. Carbon dioxide has a critical point of 1072 psi and 31°C, and is a suitable liquid for this process. Liquid carbon dioxide is heated beyond its critical point, and the chamber pressure is slowly released, allowing the CO_2 gas to escape and leave a dried sample.

5.1.8 Cantilever Calibration

Before the wet etch release of the cantilevers, an optical micrograph was taken of the wafer frontside, as shown in Figure 5-6 (a). Prior to chemical functionalization of the gold surface of the cantilever, scanning electron micrographs were taken of the completed cantilevers, as shown in Figure 5-6(b).

In air, the resonance frequency has a high quality factor and can be easily identified. In liquid, however, viscous damping and inertial effects of the fluid results in lower quality factors and higher noise. The spring stiffness (k) of the cantilevers both in air and liquid can be calculated from the Thermal K measurement using equation (1):

$$k = 0.1906\, \rho_f\, b^2\, L\, Q_f\, \Gamma_i(\omega_f)\, \omega_f^2 \qquad (1)$$

where ρ_f is the density of fluid, b and L are the width and length of the cantilever, Q_f is the quality factor, $\Gamma_i(\omega_f)$ is the imaginary part of the hydrodynamic function, and ω_f is the resonance frequency of the cantilever [29]. The resonance frequency (ω_f) and spring constant (k) for each cantilever were characterized in air and in phosphate buffered saline (PBS). The resonance frequency, quality factors, and calculated spring constants for the different length cantilevers are listed.

An atomic force microscope (AFM) with a liquid cell setup (Molecular Imaging PicoPlus® Scanning Probe Microscope), was used to measure the thermal noise vibration of individual cantilevers and extract the resonance frequency from the thermal noise spectrum, both in air and in liquid. The PicoPlus® auxiliary software ThermalK allows us to obtain the thermal noise vibration and carry out a fast Fourier

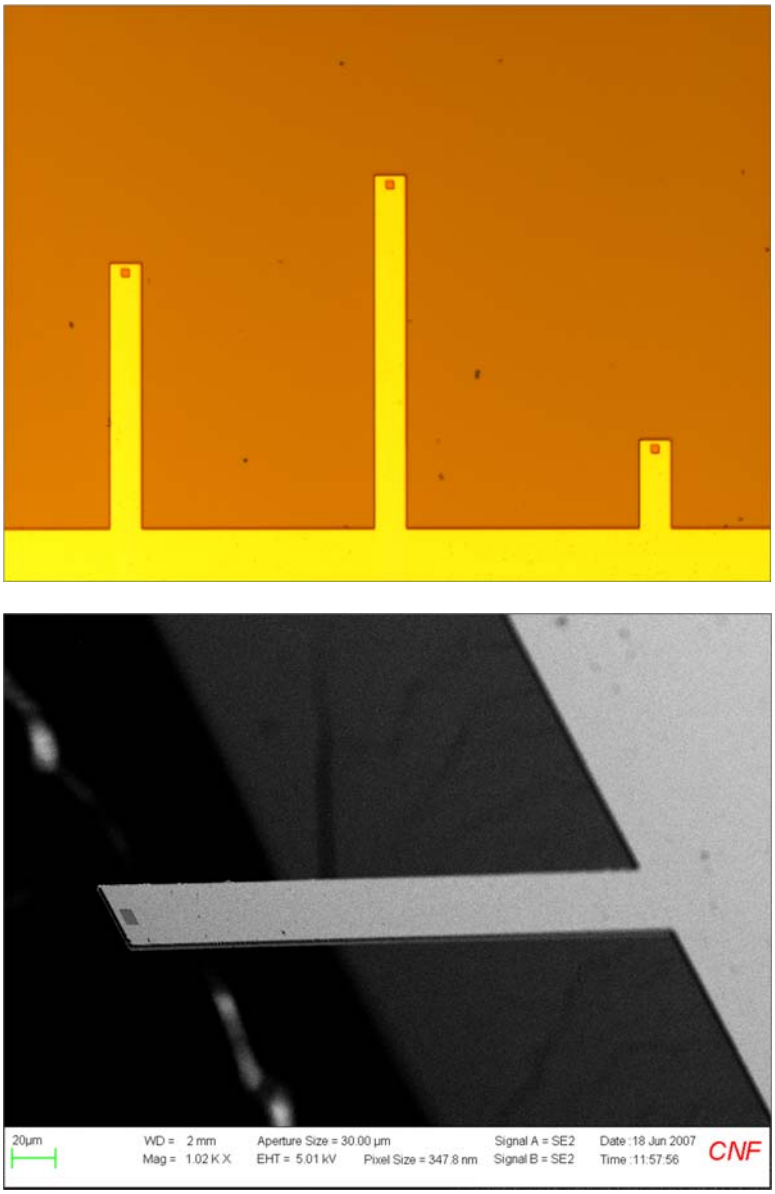

Figure 5-6. (a) Optical micrograph of the cantilevers prior to release, with lengths of 300 µm, 400 µm, and 100 µm, shown from left to right (b) Angled scanning electron microscope image showing a single released cantilever with an exposed nitride pad at the tip.

transform (FFT) of the signal to generate the power spectrum of the cantilever. Measurements of the thermal noise response of the different lengths of cantilevers were collected, and the resonance frequency and spring constant for each cantilever was characterized in air and in phosphate buffered saline (PBS). An adjacent-averaging smoothing was performed to remove the fluctuation and extract the fundamental mode resonance frequency using a Lorentz function. The results of this analysis are shown in Figure 5-7.

5.2 Detection of Increased Bacterial Activity

This section presents a method for measuring the mechanical response of flagella on a single *Escherichia coli* cell to chemotactic agents using a microfabricated gold-coated silicon nitride cantilever. Changes in flagella motion on the cell immobilized near the free end of the cantilever due to changes in the chemical environment are sensed by shift in resonance frequency (1st flexural-mode) of the cantilever. The thermally excited resonance frequency of the cantilever is measured using PicoPlus® AFM liquid cell setup, by focusing the laser on the back of the cantilever. The cantilever with the cell immobilized on it when immersed in leucine solution, an *E. coli* chemo-attractant, is observed to increase the frequency by 0.69%. This is due to increase in tensile stress on the cantilever leading to spring stiffening, as a result of stimulated flagellar motion of the cell attached to the top. Thus the flagellar response of single-cell *E. coli* to chemotactic agents can be quantified.

5.2.1 Introduction to Activity of Bacterial Flagella

Bacterial flagella are involved in bacterial motility and chemotaxis. The flagellar motion of bacteria has been shown to be dependent on the chemical environment, and

(a)

Length	Resonant Frequency	Quality Factor	Spring Constant
100	53.63 kHz	77.8	0.49 N/m
200	40.63 kHz	101.5	0.73 N/m
300	19.09 kHz	63.6	0.23 N/m
400	10.51 kHz	43.9	0.08 N/m

(b)

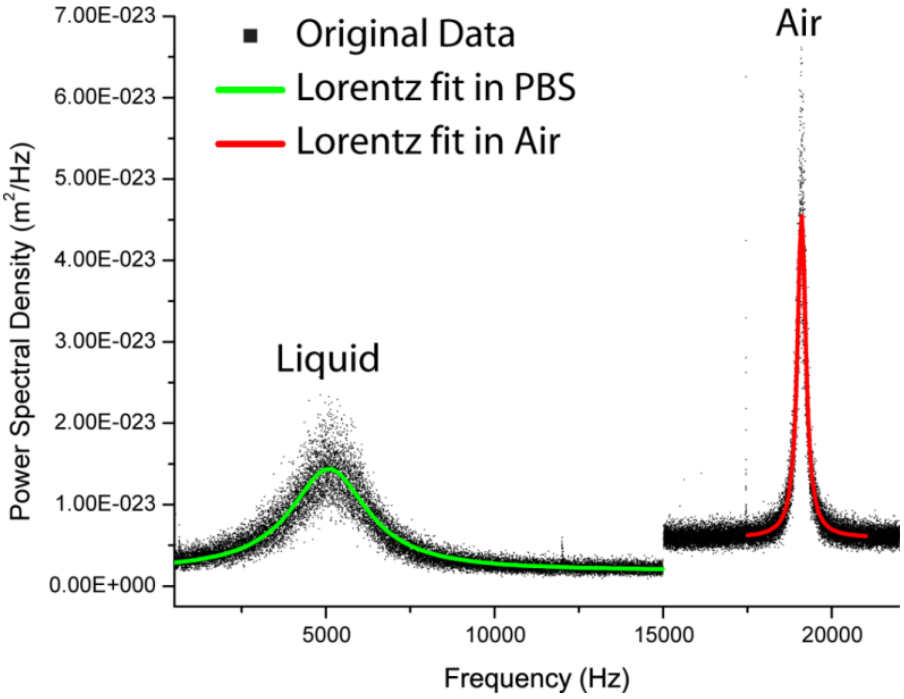

Figure 5-7. (a) Experimental values for the resonance frequency, quality factor, and spring constant of the cantilevers in air and (b) Dampening effects due to complete immersion in liquid (phosphate buffered saline) of a 300 µm-long cantilever.

can produce approximately 0.5 pN of force as observed in optical trapping bead experiments [30]. Bacterial adhesion to modified surfaces has been extensively studied for sensor development, cell assays, and biomaterials. Optical monitoring studies have shown that bacteria can bind to modified surfaces via the flagella and cellular wall, with observed viability for up to 4 hours[31]. Chemotaxis assays with *E. coli* show a strong attraction response of bacteria at low concentrations of leucine [32]. By taking advantage of the high sensitivity of cantilevers to changes in surface stress, we can measure the response of single-cell bacteria due to flagellar activity when immersed in different stimulants. In this study, we have designed tipless gold-coated silicon nitride cantilevers with an exposed nitride pad at the end of the tip to study the activity of a single bacteria cell. The gold film allowed for patterning of chemistry as well as enhanced signals from the thermal noise spectra due to the higher reflectivity. An active single *E. coli* cell is captured onto the end of the cantilever for thermal-noise based vibration analysis of single-cell bacterial activity in liquid. Increase in resonance frequency was observed in the presence of low concentration leucine, which suggests an increase of cellular activity that induces stress on the cantilever thus leading to spring-stiffening (k) of the cantilever.

5.2.2 Fabrication of the silicon nitride cantilever array

The fabrication process is described earlier in greater detail. Briefly, double-side polished silicon wafers of 4 inch diameter and 400 μm thickness underwent growth of 2 μm thermal oxide and 1 μm of LPCVD low-stress nitride. The silicon nitride cantilevers were defined down to the silicon substrate by a reactive ion etching (RIE) with CHF3/O2 gases. The front-side gold and exposed nitride pads are patterned using an image reversal mask, followed by a lift-off E-beam evaporation process to deposit a chrome/gold layer of total 0.05 μm thickness onto the nitride cantilevers. The

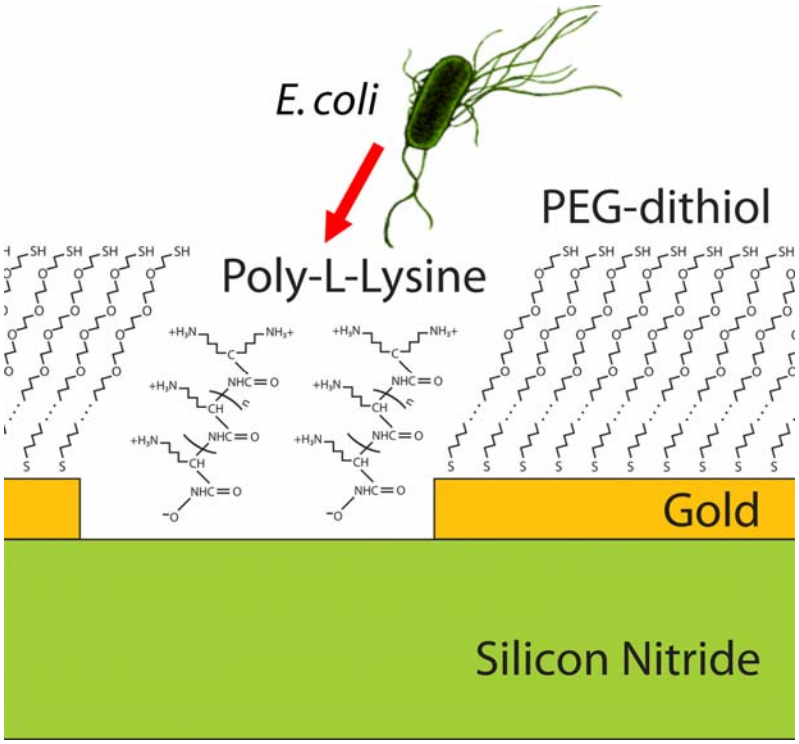

Figure 5-8. Schematic of the chemical functionalization on the surface of the cantilever

cantilevers are released via backside patterning of the nitride and oxide, followed by a 9-hour heated potassium hydroxide (30% w/v KOH, 80°C) one-sided through-wafer etch, followed by a 6:1 buffered oxide etch and critical point drying. E-beam evaporation of 0.05 μm Cr/Au is performed on the backside of the cantilever. Finally, individual cantilever dies each containing four cantilevers of varying lengths (100 μm, 200 μm, 300 μm and 400 μm) are manually removed using tweezers.

5.2.3 Chemical functionalization of the cantilever

A single cantilever die was cleaned in heated (70°C) Nanostrip® solution to remove residual organics. After thoroughly rinsing with deionized water, the cantilever was transferred into a 1.0 mM solution of PEG-dithiol in DI water for passivation of the gold. The cantilevers were incubated overnight at room temperature. Subsequently, the cantilevers were thoroughly rinsed and incubated in 1.0 mM poly-L-lysine (PLL) hydrobromide solution for 15 minutes. PLL is highly positively charged and allows for cell capture onto the exposed silicon nitride pad via electrostatic interactions [31]. An illustration of the chemical functionalization process is shown in Figure 5-8.

5.2.4 Bacterial culture and attachment

The bacteria strain used was E. coli Top10 with pCR 2.1 GFP insert. A single bacterial colony was taken from a plate culture and grown in 25 mL of liquid LB media with kanamycin at 37°C and gentle agitation for 12 hours. Prior to the experiment, 1.0 mM of IPTG solution was added to the culture and incubated for 30 minutes in order to enhance GFP protein expression. The final culture concentration was estimated to be 5×10^9 cells/ml. The cells are centrifuged into a pellet, the supernatant is removed, and the cells are resuspended in 1x phosphate buffered saline (PBS) solution. Chemically-functionalized cantilevers were incubated in the cell solution at 37°C to promote

bacterial adhesion onto the PLL-silicon nitride surface, and then rinsed in PBS to remove unspecific adhesion. After the incubation and wash of the cantilever die in the cell culture, successful attachment of a single bacterial cell at the nitride pad was verified using an upright fluorescent microscope (Olympus BX51) fitted with a CCD camera, which is shown in Figure 5-9. The adhesion of E. coli to patterned PLL surfaces is believed to be mediated by an electrostatic interaction between the positively charged PLL layer and the negatively charged lipopolysaccharide groups of the surface of bacterial cells [6]. The removal of unspecific cell attachment on the backside of the cantilever is verified using an inverted fluorescent microscope (Olympus® IX71). In addition, AFM mounting setup allowed for the cell attachment to be monitored at intervals during the data collection.

5.2.5 Experimental Setup

The gold-coated silicon nitride cantilevers were measured to be 35 μm wide and 1.3 μm thick, with varying lengths between 100 μm and 400 μm. An atomic force microscope (AFM) with a liquid cell setup (Molecular Imaging PicoPlus® Scanning Probe Microscope), was used to measure the thermal noise vibration of individual cantilevers and extract the resonance frequency from the thermal noise spectrum, both in air and in liquid. Briefly, the PicoPlus® was mounted on top of an inverted fluorescent microscope (Olympus® IX71) to allow for simultaneous fluorescent imaging and thermal noise spectrum acquisition. A schematic of the experimental setup is shown in Figure 5-10. The Thermal K software from PicoPlus® interfaces with the AFM imaging software to obtain the thermal noise vibration and carry out a fast Fourier transform (FFT) of the signal to generate the power spectrum of the cantilever. Measurements of the thermal noise response of the different cantilevers

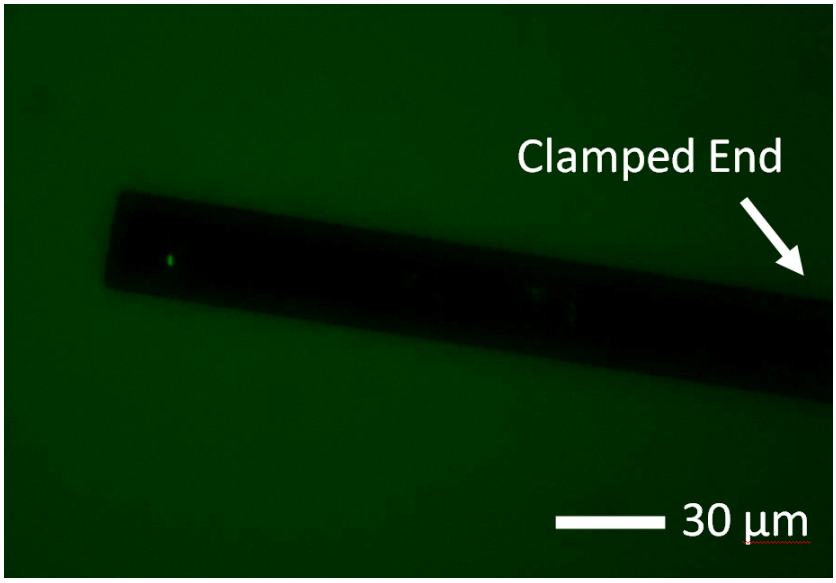

Figure 5-9. Fluorescent micrograph showing the attachment of a single GFP-labeled *E. coli* cell at the top of the cantilever.

were collected, and the resonance frequency and spring constant for each cantilever was characterized in air and in phosphate buffered saline (PBS) prior to cell capture and cell activity measurement. An adjacent-averaging smoothing was performed to remove the fluctuation and extract the fundamental mode resonance frequency using a Lorentz function. The response for the 300 μm long cantilever, with and without an attached bacteria cell, was also measured in the presence of low concentration leucine (0.05 mM).

5.2.6 Results and Discussion

The measured frequency response of the cantilever is shown with and without a bacterial cell at the free end of the cantilever in leucine-free solution (PBS) in Figure 5-11. In leucine-free solution bacteria cells attached to the cantilever exhibit low flagellar activity, therefore applying less stress on the cantilever. With the addition of a single cell on the nitride pad at the free end of the cantilever, we see a consistent decrease in resonant frequency for all lengths of cantilevers in our liquid AFM experiments, which is probably due to a combination of damping and mass loading effects. Addition of low concentrations of leucine, a known *E. coli* chemo-attractant, resulted in a repeatable increase in the resonant frequency as well as an increase in the quality factor. Results obtained from experiments using a 300 μm long cantilever are shown in Figure 5-12. Low concentrations of leucine do not change the viscosity of the solution, and therefore is not seen to affect the resonant frequency of the cantilever without an attached cell. The increased activity of the single bacteria cell in the presence of a stimulant (leucine) induces stress on the cantilever. This increased stress results in spring stiffening of the cantilever, causing an increase in the resonance frequency. For a given cantilever length, we can estimate the following relationship for the stiffness k of the cantilever from equation (1):

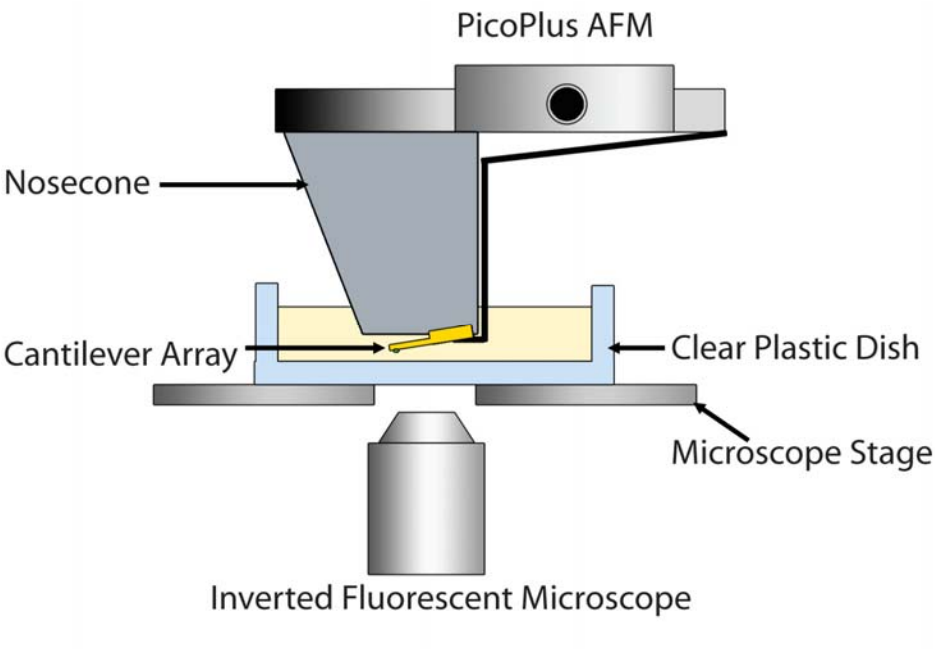

Figure 5-10. Schematic diagram of a cantilever array with captured cells used in conjunction with an atomic force microscope liquid cell setup mounted atop an inverted fluorescent microscope.

$$k \propto Q_f (\omega_f)^2 \qquad (2)$$

The effective increase in the spring constant *k* of the cantilever with a bound single bacteria cell in leucine was calculated to be 5.28%. Thus by varying the concentration of the chemo-attractant and monitoring the spring constant, the strength of the flagellar response can be quantified. This shows that by monitoring the spring constant of the cantilever, forces of the order of fractions of a picoNewton can be sensed. Since the effect of increased cell activity (i.e. increase in ω_f) due to the induced stress is orthogonal to that of mass loading (i.e. decrease in ω_f) of the cantilever, the mass of the cell and its activity can be characterized adding a new dimension to single-cell cantilever measurements.

5.2.7 Section summary

In summary, we fabricated an array of tipless gold-coated silicon nitride cantilevers with an exposed nitride pad at the tip for characterization of single bacterial cell activity in liquid. The chemically-functionalized cantilevers with captured cells were mounted onto an AFM-fluorescent microscope setup to measure the activity of a live bacteria cell in physiological conditions. Increased activity of the attached cell in the presence of a stimulant was found to induce a stress on the cantilever that caused a spring stiffening effect on the cantilever, resulting in an increase of resonance frequency. In future work, we are interested in studying the activity of single cells in different concentrations of stimulants and perform simultaneous mass and activity measurements.

Cantilever Length (μm)	Peak Frequency (kHz)		*Freq. Shift (%)*
	No Cell	*With Cell*	
100	54.12± 0.05	54.02± 0.05	-0.18
200	13.20± 0.01	13.19±0.01	-0.11
300	5.35± 0.01	5.20± 0.01	-2.82
400	2.65± 0.01	2.62± 0.01	-1.12

Figure 5-11. Resonant frequency response to the attachment of a single bacterial cell at the tip of the cantilever.

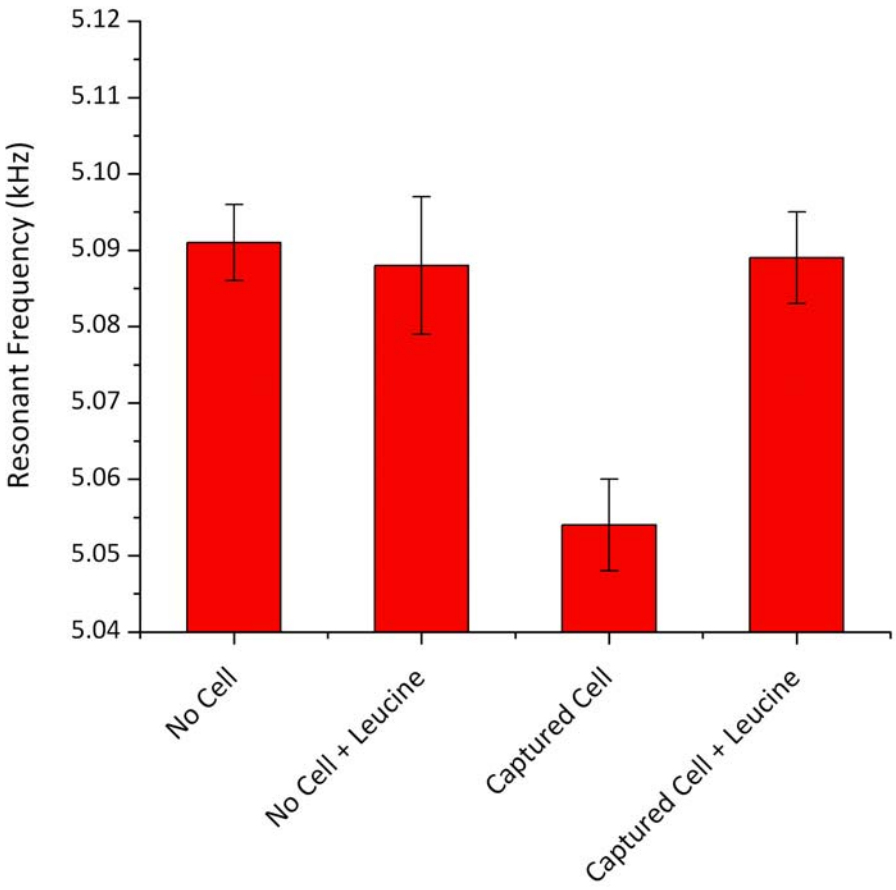

	Control [Leucine] = 0 mM	**Experiment [Leucine] = 0.05 mM**
no cell attached	5.091±0.005 kHz	5.088±0.009 kHz
cell attached	5.054±0.006 kHz	5.089±0.006 kHz

Figure 5-12. Resonant frequency response of a 300 μm-long cantilever with a single bacterial cell attached at the free tip upon exposure to low concentrations of leucine, a known chemoattractant.

5.3 Detection of Immunogenic Activity

One goal of modern biology is to understand the molecular mechanisms underlying cellular function. The ability to manipulate and analyze single cells is vital for this undertaking, since it is known that individual cells that are identical in appearance can manifest vastly different characteristics due to cellular heterogeneity. The majority of cell-based biological assays generate data that are averaged across larger groups of cells, and often overlook the wealth of information that can be provided by single-cell studies. In addition, single-cell measurements are able to provide us with valuable information on mixed cell populations of normal and diseased cells. Single-cell studies of tumor biopsies have shown that the majority of cells within a tumor may actually be normal, and that there exists significant heterogeneity among the abnormal cells [20-23].

Much of the physiological processes of cells are outwardly manifested in quantifiable changes in mass and size, and recent efforts have been increasingly focused on the measurements of the physical properties of single cells. These physical changes can be attributed to a variety of cell activity, including the synthesis and accumulation of proteins, replication of DNA, and other large molecules during cell growth and differentiation. Though many methods, such as optical microscopy, confocal microscopy, and suspended microchannel resonators, are currently used to estimate or directly measure the mass of single cells in suspension, there are very few techniques to directly measure the mass of an adherent cell in a time-varying fashion. The traditional determination of cell mass involves an indirect estimation by multiplying the cell volume and cell mass density. However, this method assumes a constant

density, which has been shown to be inaccurate – fluctuations in cell density has been seen throughout the cell cycle [21].

5.3.1 Background on Mast cells

First discovered by Paul Ehrlich, mast cells are multifunctional tissue-dwelling cells that are traditionally associated with the allergic response [33]. Mast cells develop from progenitor cells that are derived from uncommitted hematopoietic stem cells in the bone marrow, and are known to express the receptor (FcεRI) for immunoglobulin E (IgE). FcεRI is a multimeric complex consisting of four chains, with the IgE-binding domain α, β, and the two disulfide-linked γ chains. The β and γ chains of FcεRI have the immune receptor tyrosine-based activation motifs, which are considered to be crucial for signal transduction, and the bridging of two IgE molecules by an antigen in the presence of a carrier molecule results in Lyn kinase activation, which phosphorylates the β and γ chains and leads to a chain of events that result in degranulation. In a typically allergic reaction, the antigen or allergen crosslinks to IgE molecules occupying the FcεRI, which results in a cascade of rapid sequence signaling events that lead to degranulation and elaboration of mediators [34]. In the past 20 years, however, there has been an increase in the study of mast cells in connection with IgE-independent clinical disease processes, such as cancer, ulcerative colitis, and neuronal diseases [35-40].

Besides antigens and allergens, mast cells can also be activated to degranulate by a number of other stimuli, including opiates, neuropeptides, superoxide anion, radiocontrast media, histamine releasing factors, chemokines, pathogenic bacteria, parasites, enterotoxin B, cholera toxin, among others. Mast cells have been incriminated in a diverse range of diseases, such as allergy, asthma, rheumatoid

arthritis, atherosclerosis, interstitial cystitis, inflammatory bowel disease, progressive systemic sclerosis, fibrotic diseases, ischemic heart disease, and malignancy [33, 37, 41, 42]. Recent studies with these cells suggest involvement with broader functions, such as inflammation regulation, host defense, and development of innate immunity.

5.3.2 RBL Mast Cell Culture

Rat basophilic leukemia (RBL) mast cells offer an excellent model system for testing the sensitivity of our cantilever biosensor because they are robust and can undergo a dramatic exocytotic response within minutes of antigen addition [43]. RBL-2H3 cells were maintained in monolayer culture in minimum essential medium supplemented with 20% fetal bovine serum (Invitrogen, Carlsbad, CA) and 10μg/ml gentamicin sulfate. Cells were harvested using trypsin/EDTA and resuspended in buffered saline solution (BSS; 135 mM NaCl, 5 mM KCl, 1.8 mM $CaCl_2$, 1 mM $MgCl_2$, 5.6 mM glucose, 1 mg/mL BSA, and 20 mM Hepes, pH 7.4).

5.3.3 Fluorescent Monitoring

Fluo-4 AM was purchased from Molecular Proves Inc. (Eugene, OR). Acridine Orange was purchased from Sigma-Aldrich (St. Louis, MO). Mouse monoclonal anti-2,4-dinitrophenyl (DNP) IgE and BSA conjugated with an average of 15 DNP groups (DNP-BSA) was obtained from Agave Biosciences [43]. For our fluorescent imaging experiments, 1.0 mL of this cell suspension was seeded at 1.0 x 10^6 cells/ml and cultured on glass cover slips in a Petri dish. The cells were sensitized by the addition of anti-DNP-IgE (1 μg/ml) for overnight incubation at 37°C. Adherent cells were loaded with either acridine orange (4.5 μm) for 5 min. or Fluo-4-AM (2.5 μM) for 20 min. at 37°C. Fluo-4 loaded cells were washed with BSS supplemented with 0.25 mM sulfinpyrazone to inhibit the due from leaking out of the cell Adherent cells in 3 ml of

BSS in a Petri dish were imaged with an upright Olympus BX-50 microscope equipped with a MetaMorph system for image acquisition. Images were collected every 5 seconds for 5 min. before and after the addition of multivalent antigen, DNP-BSA. Images obtained from fluorescent monitoring of RBL mast cells for verification of degranulation events are shown in Figure 5-13.

5.3.4 Mast cell Experimental Setup

Briefly, the PicoPlus® was mounted on top of an inverted fluorescent microscope (Olympus® IX71) to allow for simultaneous fluorescent imaging and thermal noise spectrum acquisition. A schematic of the experimental setup is shown in Figure 5-10. The cantilevers used in this experiment were removed from the same wafer as discussed in the previous section. Since the capture of the masts cells are performed by manually bringing the tip of the cantilever into close contact with a resting cell, the passivation of the gold was less critical. Instead, the cantilever is incubated in 1.0 mM poly-L-lysine (PLL) hydrobromide solution for 15 minutes. PLL is highly positively charged and allows for cell capture onto the cantilever via electrostatic interactions. 1.0 mL of cell suspension was seeded at 1.0 x 10^6 cells/ml on glass cover slips in a Petri dish, and grown to 60% confluency. The cells were sensitized by the addition of anti-DNP-IgE (1 μg/ml) for overnight incubation at 37°C. The cells on the glass cover slips were stained with either acridine orange or Fluo-4 AM, using the protocols described earlier. The cover slips were placed in a modified liquid cell holder for the PicoPlus AFM instrument along with 4 mL of BSS. The liquid cell holder was previously modified with inlet and outlet tubing and sealed with silicone sealant to allow for easy introduction of antigen with minimal disturbance to the setup. The entire AFM/fluorescent microscope setup is placed atop a vibration isolation table and surrounded with a cardboard housing unit lined with flexible egg-carton polyeurethane

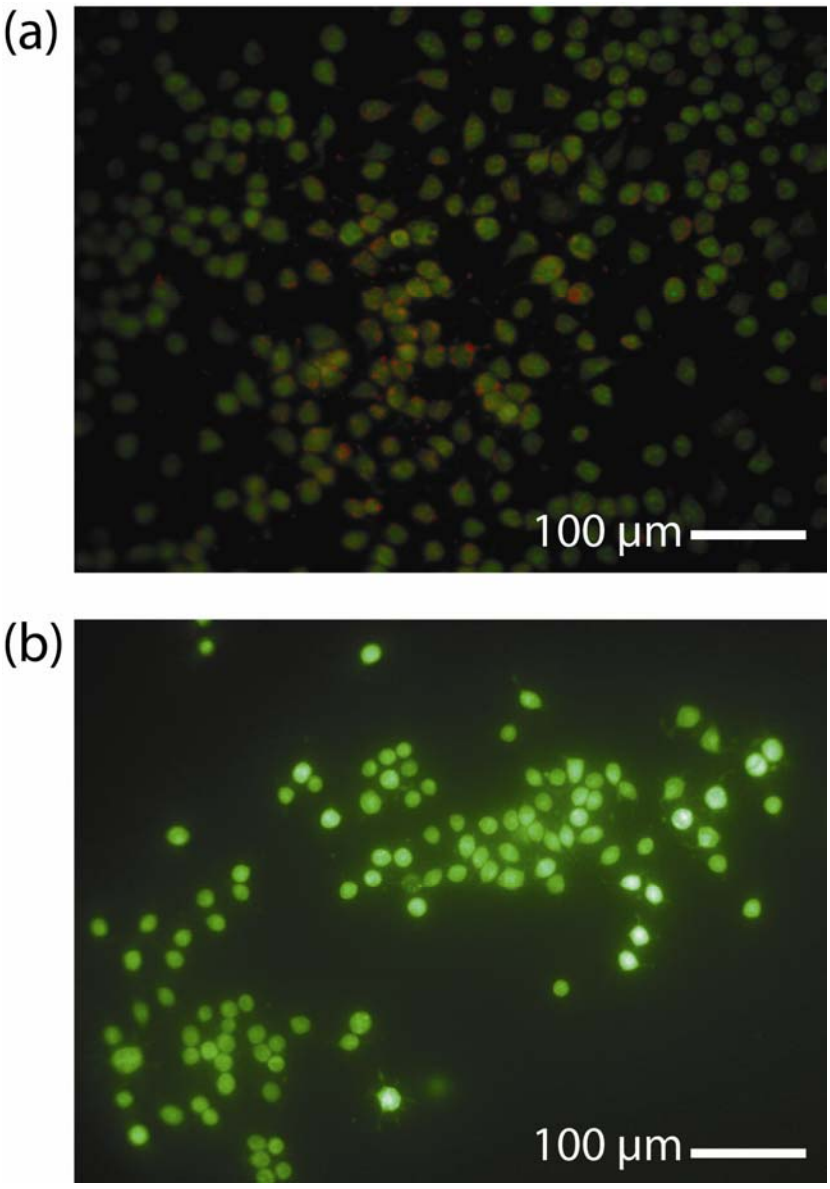

Figure 5-13. Fluorescent images of RBL mast cells stained with (a) acridine orange and (b) Fluor-4-AM upon exposure to 50 ng/ml of DNP-BSA

(McMaster-Carr, Robbinsville, NJ) for acoustic foam. Figure 5-14 shows the shadow of a PLL-modified cantilever poised approximately 50 μm above the layer of sensitized cells stained with acridine orange.

The 300 μm-long cantilever is brought into close contact with the sparsely-grown layer of RBL mast cells on the cover slip and baseline measurements are taken. A single cell can be chosen through careful alignment of the cantilever tip with the cell. The cantilever is lowered onto the single cell and cell adhesion is encouraged with a 10 min. incubation time. The cantilever with the single captured cell is withdrawn 200 microns from the surface. The thermal noise response of the cantilever was collected prior to and after single-cell capture, and the resonance frequency extrapolated using an adjacent-averaging smoothing and fitting to a Lorentz function. The antigen DNP-BSA (50 ng/ml) is introduced into the tubing-modified liquid cell holder. BSA was used as a control. The cantilever response is monitored every 30 seconds for 10 min using the Thermal K software. An overview of the experiment is illustrated in Figure 5-15.

5.3.5 Results & Discssion

Resonant frequency shifts attributable to changes in mass due to adhesion of single RBL mast cells can be seen in Figure 5-16. The extracted frequency peak is shown to decrease with the addition of each single mast cell. Monitoring of the thermal response of the cantilevers upon addition of DNP-BSA is shown in Figure 5-17. For single cell capture, the addition of DNP-BSA showed a marked increase in the resonant frequency, indicating a decrease in the mass of the single mast cell at the tip of the cantilever, which we attribute to the degranulation event, in which cell signaling molecules are released into solution. Subsequent exposure to the BSA control was

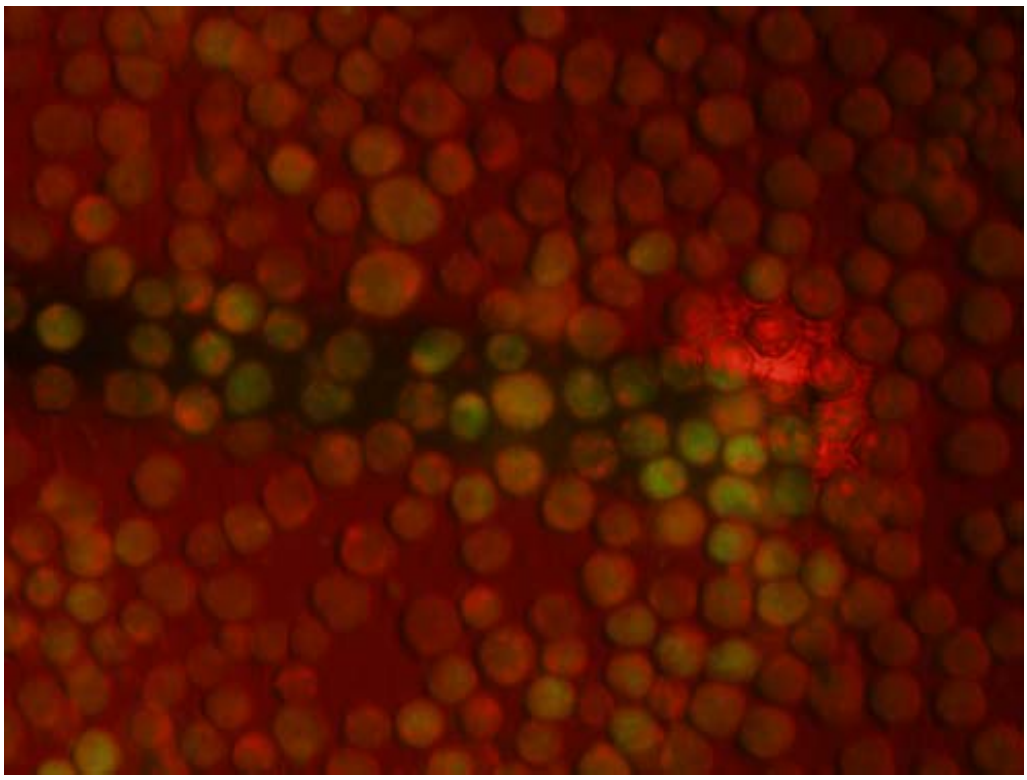

Figure 5-14. Fluorescent micrograph of the PLL-modified cantilever poised 50 μm above a layer of sensitized RBL mast cells stained with acridine orange on a glass cover slip.

shown to decrease the resonant frequency. Increasing the number of cells (12 cells shown) captured on the cantilever amplified the effects of the DNP-BSA and BSA on the resonant frequency. The controls using cantilevers without cells showed very little frequency shifts. This confirms that the larger resonant frequency shifts experienced are due to changes in the attached cells upon exposure to the antigen instead of interactions of the antigens with the cantilever itself.

Due to the cantilever's small surface area and the relatively short incubation time given for cell attachment, it is possible that the cell on the cantilever may exhibit different behavior than that of a mast cell that has attached to the substrate and grown in a confluent layer. Depending on how the cantilever lowers onto the cell, the process of detaching the cell from the surface can sometimes cause rupturing of the cell. The stress exerted on the cell for attachment may interfere with the response to the antigen. The AFM laser spot size reflecting off the back of the cantilever was approximately 10 μm in diameter, and the bright illumination in the area surrounding the laser spot could interfere with the behavior of the cell.

The limited camera capabilities and shuttering options on the inverted fluorescence microscope setup was a impediment in our experiment for acquiring simultaneous fluorescent image data along with AFM data. The thermal noise measurements were also taken manually. Therefore, some of the parameters such as the frequency sweep range and the rate of data acquisition were inflexible. By moving away from the commercial AFM setup towards a more customized home-built system, many of these parameters may become more adjustable. Another perhaps simpler solution would be to use a breakout box to intercept the laser signal and route it to a spectrum analyzer

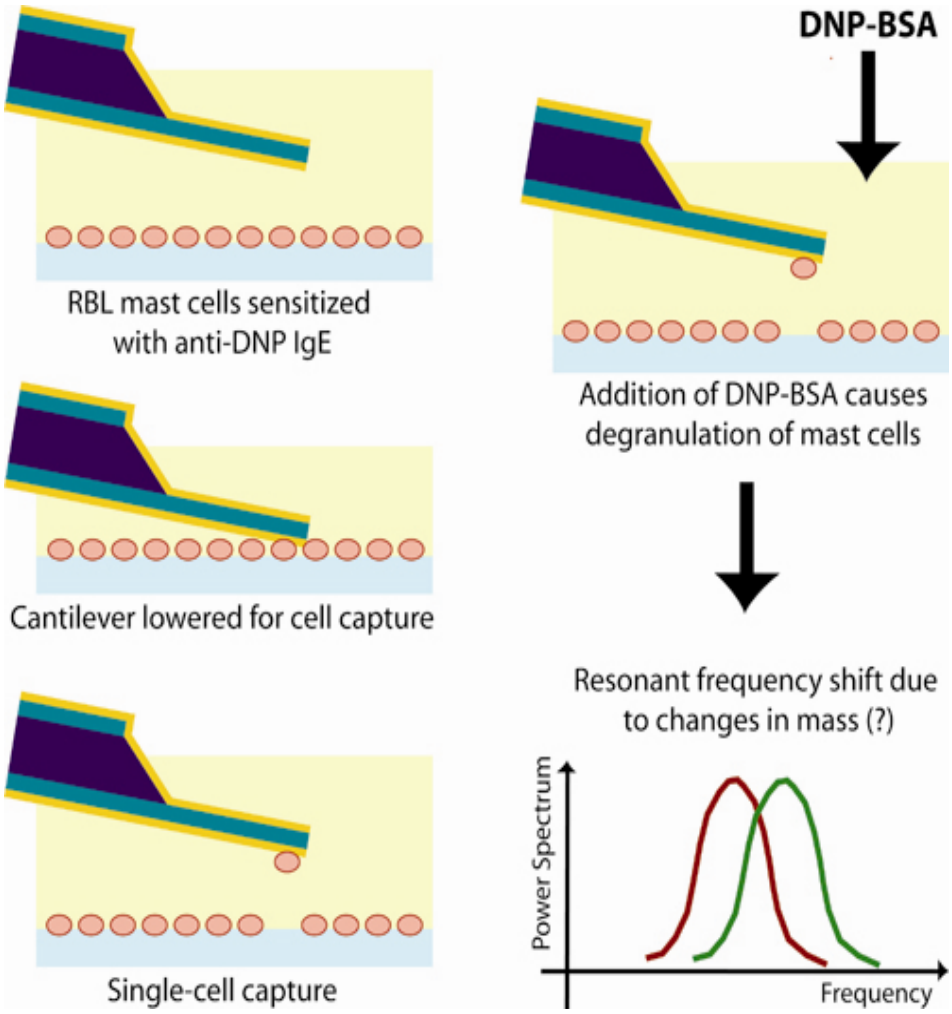

Figure 5-15. Overview diagram of the mast cell experiment protocol. First, the cantilever approaches the RBL mast cell layer and stops at a distance of 200 μm away from the surface for baseline measurements. The cantilever is lowered onto a single cell for 10 minutes for capture, and then raised back to a distance of 200 μm with the single cell attached at the tip. Resonant frequency measurements are recorded to monitor the mass change due to the addition of a single cell. Finally, DNP-BSA is added to the liquid cell holder to induce degranulation in the single cell. The subsequent resonant frequency shift recorded is indicative of a decrease in mass due to the degranulation event.

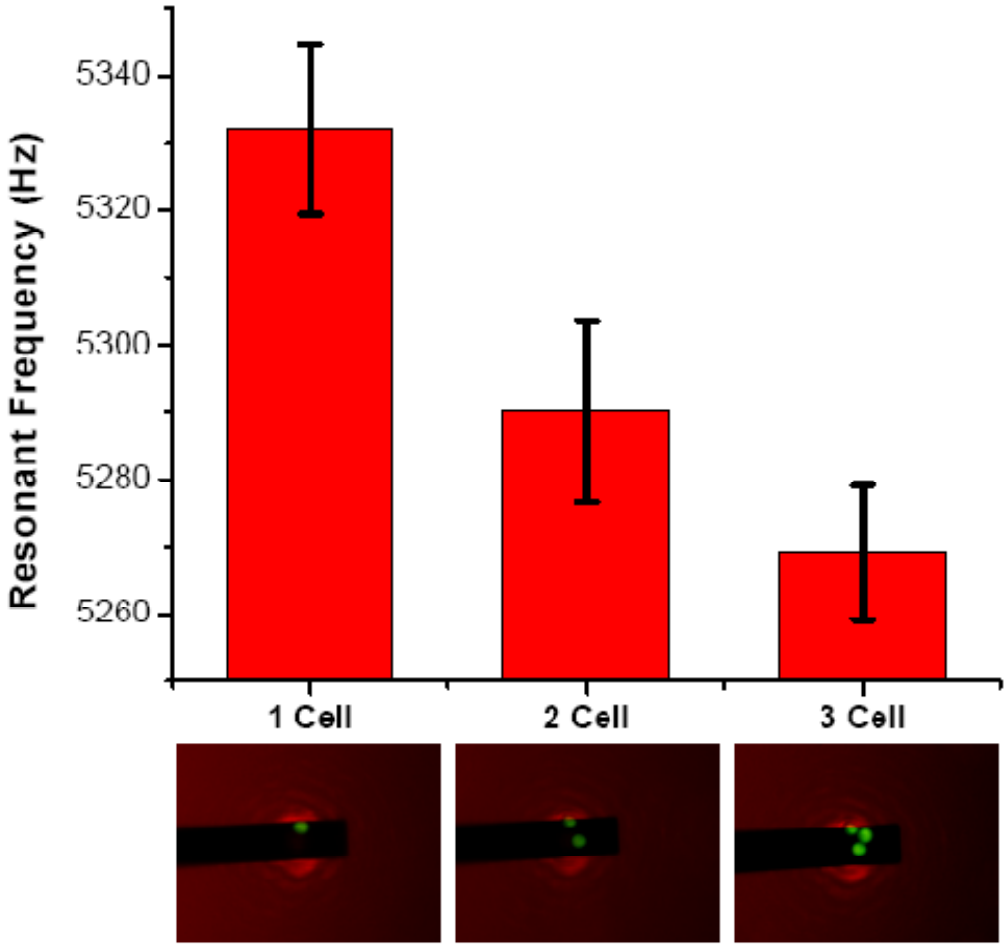

Figure 5-16. Changes in resonant frequency due to the added mass of a single RBL mast cell adhered at the tip of a cantilever. Single RBL mast cells stained with acridine orange are picked up sequentially using a PLL-modified 300 μm long cantilever and thermal noise measurements are recorded at each interval.

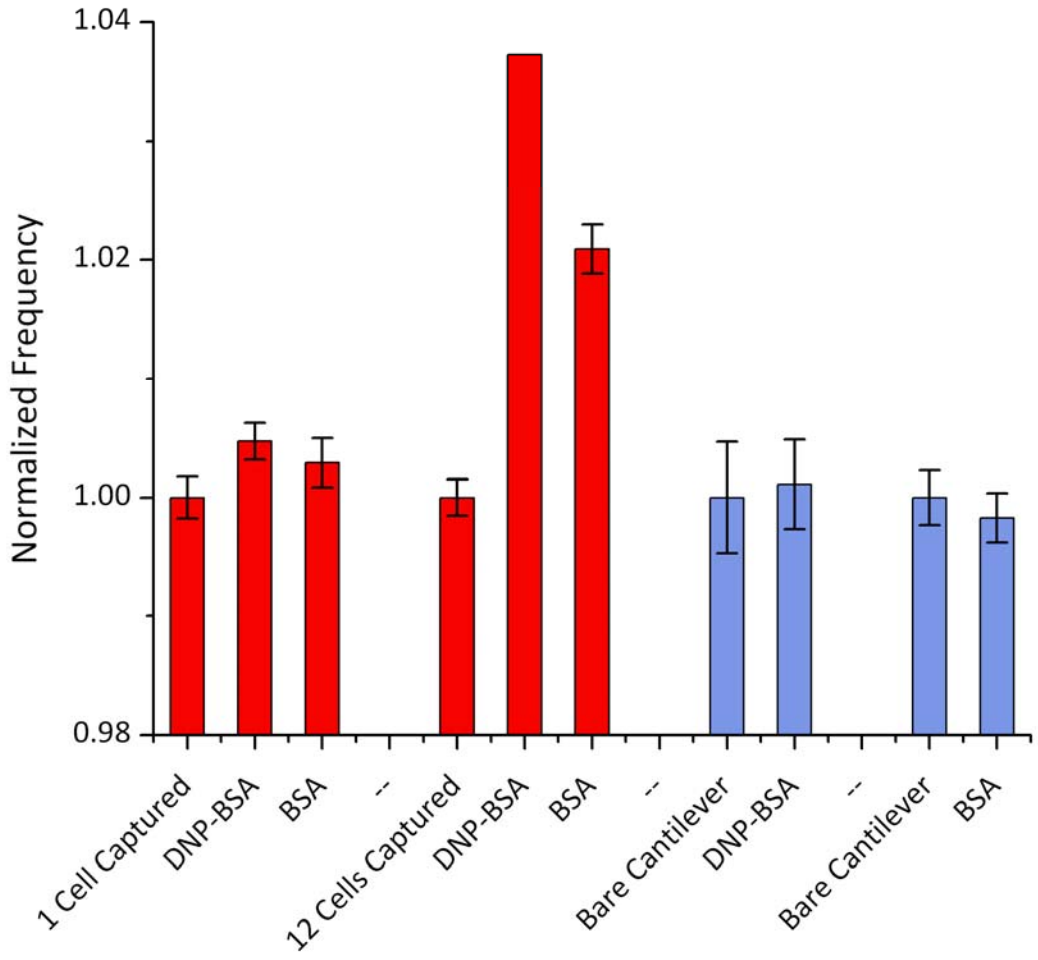

Figure 5-17. Monitoring of the thermal noise response of the cantilevers upon addition of DNP-BSA was performed. For single cell capture, the addition of DNP-BSA showed a marked increase in the resonant frequency, indicating a decrease in the mass exerted on the cantilever due to mast cell degranulation and subsequent exposure to the BSA control was shown to decrease the resonant frequency. When 12 cells are loaded onto the cantilever, the effects are significantly more pronounced. The controls (shown in blue) are performed on individual PLL-modified cantilevers in the absence of cells.

for data acquisition. Long-term monitoring of the mast cell in liquid often leads to a degradation of the AFM laser signal due to leakages in the nosecone which led to condensation forming on the inside of the nosecone window. Issues with isolating the signal from the noise in the environment were largely avoided by mounting the setup on a vibration isolation table inside acoustic housing.

5.3.6 Section Summary

In summary, the tipless gold-coated silicon nitride cantilevers with an exposed nitride pad we had previously fabricated were used for the characterization of single RBL mast cell degranulation events. The chemically-functionalized cantilevers were used in conjunction with a commercial AFM instrument mounted atop an inverted fluorescent microscope setup to select a single cell and monitor its response upon exposure to a stimulant. Degranulation activity of the attached sensitized RBL mast cell in the presence of a stimulant was found to induce a mass change on the cantilever, resulting in an increase of resonance frequency.

REFERENCES

[1] Leonard, P.; Hearty, S.; Brennan, J.; Dunne, L.; Quinn, J.; Chakraborty, T.; O'Kennedy, R. Advances in biosensors for detection of pathogens in food and water. *Enzyme Microb. Technol.* **2003**, *32*, 3-13.

[2] Campbell, G.A.; Mutharasan, R. Detection of pathogen Escherichia coli O157:H7 using self-excited PZT-glass microcantilevers. *Biosens. Bioelectron.* **2005**, *21*, 462-473.

[3] Zaytseva, N.V.; Goral, V.N.; Montagna, R.A.; Baeumner, A.J. Development of a microfluidic biosensor module for pathogen detection. *Lab Chip* **2005**, *5*, 805-811.

[4] Arora, K.; Chand, S.; Malhotra, B.D. Recent developments in bio-molecular electronics techniques for food pathogens. *Anal. Chim. Acta* **2006**, *568*, 259-274.

[5] Lazcka, O.; Del Campo, F.J.; Muñoz, F.X. Pathogen detection: A perspective of traditional methods and biosensors. *Biosens. Bioelectron.* **2006**, *22*, 1205-1217.

[6] Mothershed, E.A.; Whitney, A.M. Nucleic acid-based methods for the detection of bacterial pathogens: Present and future considerations for the clinical laboratory. *Clin. Chim. Acta* **2006**, *363*, 206-220.

[7] Weeks, B.L.; Camarero, J.; Noy, A.; Miller, A.E.; Yoreo, J.J.D.; Stanker, L. A microcantilever-based pathogen detector. *Scanning* **2006**, *25*, 297-299.

[8] Dutta, P.; Tipple, C.A.; Lavrik, N.V.; Datskos, P.G.; Hofstetter, H.; Hofstetter, O.; Sepaniak, M.J. Enantioselective Sensors Based on Antibody-Mediated Nanomechanics. *Anal. Chem.* **2003**, *75*, 2342-2348.

[9] Zhang, J.; Ji, H.-F. An Anti E. Coli O157:H7 Antibody-immobilized Microcantilever for the Detection of Escherichia coli (E. coli). *Analytical Sci.* **2004**, *20*, 585.

[10] Usui-Aoki, K.; Shimada, K.; Nagano, M.; Kawai, M.; Koga, H. A novel approach to protein expression profiling using antibody microarrays combined with surface plasmon resonance technology. *Proteomics* **2005**, *5*, 2396-2401.

[11] Hansen, K.M.; Ji, H.-F.; Wu, G.; Datar, R.; Cote, R.; Majumdar, A.; Thundat, T. Cantilever-Based Optical Deflection Assay for Discrimination of DNA Single-Nucleotide Mismatches. *Anal. Chem.* **2001**, *73*, 1567-1571.

[12] Gheorghe, M.; Guiseppi-Elie, A. Electrical frequency dependent characterization of DNA hybridization. *Biosens. Bioelectron.* **2003**, *19*, 95-102.

[13] Hang, T.C.; Guiseppi-Elie, A. Frequency dependent and surface characterization of DNA immobilization and hybridization. *Biosens. Bioelectron.* **2004**, *19*, 1537-1548.

[14] Wang, J.; Rivas, G.; Cai, X. Screen-printed electrochemcial hybridization biosensor for the detection of DNA sequences from the *Escherichia coli* pathogen. *Electroanalysis* **2005**, *9*, 395-398.

[15] Hagan, M.F.; Majumdar, A.; Chakraborty, A.K. Hybridization dynamics of surface immobilized DNA. *J. Chem. Phys.* **2004**, *120*, 4958.

[16] Chan, G.; Mooney, D.J. New materials for tissue engineering: towards greater control over the biological response. *Trends in Biotechnology* **2008**, *26*, 382-392.

[17] Duncan, A.C.; Weisbuch, F.; Rouais, F.; Lazare, S.; Baquey, C. Laser microfabricated model surfaces for controlled cell growth. *Biosens. Bioelectron.* **2002**, *17*, 413-426.

[18] Falconnet, D.; Csucs, G.; Grandin, H.M.; Textor, M. Surface engineering approaches to micropattern surfaces for cell-based assays. *Biomaterials* **2006**, *27*, 3044-3063.

[19] Vogel, V.; Sheetz, M. Local force and geometry sensing regulate cell functions. *Nature Reviews Molecular Cell Biology* **2006**, *7*, 265-275.

[20] Borland, L.M.; Kottegoda, S.; Phillips, K.S.; Allbritton, N.L. Chemical Analysis of Single Cells. *Ann. Rev. Anal. Chem.* **2008**, *1*, 165-190.

[21] Burg, T.P.; Godin, M.; Knudsen, S.M.; Shen, W.; Carlson, G.; Foster, J.S.; Babcock, K.; Manalis, S.R. Weighing of biomolecules, single cells and single nanoparticles in fluid. *Nature* **2007**, *446*, 1066-1069.

[22] Gao, J.; Yin, X.F.; Fang, Z.L. Integration of single cell injection, cell lysis, separation and detection of intracellular constituents on a microfluidic chip. *Lab Chip* **2004**, *4*, 47-52.

[23] Ilic, B.; Czaplewski, D.; Zalalutdinov, M.; Craighead, H.G.; Neuzil, P.; Campagnolo, C.; Batt, C. Single cell detection with micromechanical oscillators. *J. Vac. Sci. Technol. B* **2001**, *19*, 2825-2828.

[24] Park, K.; Jang, J.; Irimia, D.; Sturgis, J.; Lee, J.; Robinson, J.P.; Toner, M.; Bashir, R. 'Living cantilever arrays' for characterization of mass of single live cells in fluids. *Lab Chip* **2008**, *8*, 1034-1041.

[25] Hwang, K.S.; Eom, K.; Lee, J.H.; Chun, D.W.; Cha, B.H.; Yoon, D.S.; Kim, T.S. Dominant surface stress driven by biomolecular interactions in the dynamical response of nanomechanical microcantilevers. *Appl. Phys. Lett.* **2006**, *89*, 173905.

[26] Ramos, D.; Tamayo, J.; Mertens, J.; Calleja, M. Origin of the response of nanomechanical resonators to bacteria adsorption. *J. Appl. Phys.* **2006**, *100*.

[27] Tanaka, S.; Sugasawa, H.; Morii, T.; Okada, T.; Abe, M.; Kato, N.; Kuroda, R.; Nasu, T.; Nagai, M.; Umemura, K. A new method of biosensing with 1 μl of Escherichia coli suspension using atomic force microscopy. *Anal. Biochem.* **2005**, *345*, 116-121.

[28] Madou, M.J. *Fundamentals of microfabrication: the science of miniaturization*, 2nd Ed. Ed.; CRC Press LLC, 2002.

[29] Sader, J.E.; Chon, J.W.M.; Mulvaney, P. Calibration of rectangular atomic force microscope cantilevers. *Rev. Sci. Instrum.* **1999**, *70*, 3967.

[30] Behkam, B.; Sitti, M. Bacterial flagella-based propulsion and on/off motion control of microscale objects. *Appl. Phys. Lett.* **2007**, *90*, 023902.

[31] Rozhok, S.; Shen, C.K.-F.; Littler, P.-L.H.; Fan, Z.; Liu, C.; Mirkin, C.A.; Holz, R.C. Methods for Fabricating Microarrays of Motile Bacteria. *Small* **2005**, *1*, 445-451.

[32] Khan, S.; Trentham, D.R. Biphasic Excitation by Leucine in Escherichia coli Chemotaxis. *J. Bacteriology* **2004**, *186*, 588-592.

[33] Krishnaswamy, G.; Ajitawi, O.; Chi, D.S. The Human Mast Cell: An Overview. In *Mast Cells: Methods and Protocols*, Ed., Ed.^Eds.; Humana Press, Totowa, NJ, 2006; 315 315, pp. 13-34,

[34] Mappes, T.; Achenbach, S.; Mohr, J. X-ray lithography for devices with high aspect ratio polymer submicron structures. *Microelec. Eng.* **2007**, *84*, 1235-1239.

[35] Teo, P.; Utz, P.; Mollick, J. OR.69. Using the Allergic Immune System to Target Cancer: Cell Activation by Tumor Specific IgE Monoclonal Antibodies. *Clin. Immunology* **2008**, *127*, S28.

[36] Jr., D.M. IgE receptor and signal transduction in mast cells and basophils. *Curr. Opin. Biotech.* **2008**, *20*, 717-723.

[37] Galli, S.J.; Kalesnikoff, J.; Grimbaldeston, M.A.; Piliponsky, A.M.; Williams, C.M.M.; Tsai, M. Mast cells as "tunable" effector and immunoregulatory cells: recent advances. *Ann. Rev. Immunology* **2005**, *23*, 749-786.

[38] Galli, S.J.; Nakae, S.; Tsai, M. Mast cells in the development of adaptive immune responses. *Nature Immunology* **2005**, *6*, 135-142.

[39] Okayama, Y.; Kawakami, T. Development, migration and survival of mast cells. *Immunologic Res.* **2006**, *34*, 97-115.

[40] Theoharides, T.C.; Rozniecki, J.J.; Sahagian, G.; Jocobson, S.; Kempuraj, D.; Conti, P.; Kalogeromitros, D. Impact of stress and mast cells on brain metastases. *J. Neuroimmunology* **2008**, *205*, 1-7.

[41] Gilfillan, A.M.; Tkaczyk, C. Integrated signalling pathways for mast-cell activation. *Nature Reviews Immunology* **2006**, *6*, 218-230.

[42] Metcalfe, D.D.; Baram, D.; Mekori, Y.A. Mast Cells. *Phys. Rev.* **1997**, *77*, 1033-1079.

[43] Curtis, T.; Naal, R.M.Z.G.; Batt, C.; Tabb, J.; Holowka, D. Development of a mast cell-based biosensor. *Biosens. Bioelectron.* **2008**, *23*, 1024-1031.

CHAPTER 6

CONCLUSIONS AND FUTURE DIRECTIONS

6.0 Concluding Remarks

Integrated biosensing systems utilizing microfluidic and cantilever technologies are promising for the next generation of rapid and reliable detectors for the monitoring of specific organisms or biochemical molecules. Today with the massive growth of our global population, we face immediate challenges in the arena of healthcare, food safety and environmental monitoring. This dissertation has aimed to tackle some of the challenges associated with developing innovative and portable biosensor platforms.

One of the primary goals of the research presented in this dissertation was the development of an integrated pathogen detection platform. As a contribution to the field of microfluidic-based sensors, this thesis work has shown the development of microfluidic electrohydraulic pumps and sample preparation modules, as well as successful integration of the various modules onto a single platform. Another major objective of the research conducted in this dissertation was to develop a cantilever-based biosensing system for the monitoring of changes biological activity. As part of these investigations, experiments were performed which successfully demonstrated the possibility of monitoring changes in the activity of bacterial flagella and detection of immunogenic events in RBL mast cells.

Overall, the results of the studies presented in this dissertation reaffirm the high potential of incorporation into a portable point-of-care and field-testable system, which will undoubtedly encourage further exploratory efforts in this area of research. While this dissertation has addressed many of the technically challenging issues associated with this topic, many fundamental and practical issues remain. In the

sections presented next, some final thoughts and suggestions for future work are presented.

6.1 Automated Microfluidic Pathogen Detection Platforms

The rapid and reliable detection of pathogens is important for a variety of industries, spanning food, healthcare, and bio-defense. The miniaturization and automation of integrated detection systems utilizing microfluidic technologies presents an opportunity for rapid and portable field-based testing. In recent years, our laboratory has been intimately involved with the development of automated pathogen detection platform based on microfluidic technology for the detection of various food pathogens [1-5]. In this dissertation, we have extended the functionality of our existing platform with the addition of on-board microfluidic pumps and sample preparation modules. In addition, we have further miniaturized and integrated the different modules onto a single microfluidic chip. Further optimization of this system for increased sensitivity, selectivity, and rapidity would require the resolution of many different challenges associated with this technology. We have attempted to address these challenges in this section.

6.1.1 Exploration of Alternative Materials, Designs, and Fabrication Processes

Over the years, microfluidic technology has progressed from silicon and glass-based devices to polymer-based structures. The search for new substrate materials is still a burgeoning area, and many recent microfluidic devices for biosensing applications have been fabricated using SU-8, PEEK, PTFE, Cyclic-Olefin-Copolymer (COC), and other polymers. Though PDMS is still the standard research material, issues relating to quality control remain for the manufacturing of microfluidic devices. The sealing of

PDMS devices to the substrate using plasma treatment, as well as the introduction of tubing to the inlets and outlets, is often prone to leakages. Other methods of manufacturing, such as injection molding, could be explored, for better manufacturing consistency and lower rates of device failure.

6.1.2 Improvements in Microfluidic Fluid Handling

A significant technical challenge is the ability to efficiently manipulate fluids within an integrated device at the microscale. In our current integrated platform, the fluid control within the channels is operated via the operation of microfluidic electrohydraulic pumps and piezoelectric bubble-actuated mixers. The valving of the inlets and outlets, however, are still regulated using standard hemostats, and need to be further integrated into the platform. Many approaches for microfluidic valving have been investigated [6-12], and future explorations in this technology are necessary for the optimization of our instrument. Additionally, having microfluidic valves present within the platform itself could be highly effective in simplifying the reagent filling and pumping protocols.

6.1.3 Further Miniaturization of the Detection Platform

The current setup of the latest version of our detection platform can be further miniaturized in order to move towards our goal of a hand-held system with disposable plug-and-play microfluidic cartridges. The current breadboard circuitry can be easily optimized and integrated into a printed circuit board (PCB) and custom manufactured. Additionally, the ideal AC and DC voltage sources could be integrated onto the PCB to further reduce the footprint of the instrument. Further investigations into the laser-excited polymerase chain reaction module would be necessary to determine the feasibility of replacing the laser with a light emitting diode for excitation. In order to

have a plug-and-play functionality, the development of fitted, watertight connections between the microfluidic cartridge and the instrument would be a critical but interesting area of exploration.

6.1.4 Multiplexing for Multiple Target Detection

The ability to simultaneously detect for multiple target pathogens within a single sample is an attractive and useful feature in an integrated pathogen detection system. Multiplexing is a highly sought after objective within the field of microfluidic-based analytical systems, and has demonstrated by various groups with varying degrees of selectivity and sensitivity [13-16]. One of the major challenges in designing a multi-color detection system for multiplex real-time PCR assays is the spectral overlap for the excitation and emission wavelengths of many fluorescent dyes. The TaqMan probe system is based upon a series of fluorescent dyes that are significantly separated in the visible spectrum, and is capable of emission and detection without significant overlap. The addition of multiplexing functionality in our instrument as the next step in improving our integrated platform would be a highly desirable and motivating pursuit.

6.2 Microcantilever-Based Monitoring of Biological Activity

Cantilever-based sensing is a growing field of interest with many research groups around the world, offering a method for rapid, label-free, and in-situ detection of specific biological or chemical analytes by monitoring of the mechanical response of a cantilever sensor. In general, the sensitivity of microcantilever sensors can be optimized and customized to the application through tweaking the geometric design and specific coatings. Cantilevers can be easily integrated into a multiplexed portable system, which shows great promise for many field testing and point-of-care

applications. In this project, we have developed arrays of gold-coated silicon nitride cantilevers with exposed nitride tips to capture single cells for monitoring of biological activity. Increased activity of a single attached E. coli cell in the presence of a stimulant was shown to cause a spring stiffening effect on the cantilever, resulting in an increase of resonance frequency. The cantilevers were also used to monitor the degranulation activity of a single sensitized RBL mast cell in the presence of an antigen by measuring the changes in mass. There are several fronts that are promising for further explorations, which are discussed below.

6.2.1 Incorporation of Piezoelectric Materials

A piezoresistive material, such as doped silicon, changes its electrical conductivity when strained, and are suitable for monitoring the changes in stress and bending of a cantilever. Piezoresistive stress sensors have been easily integrated inside a cantilevered structure and monitored with a simple Wheatstone bridge by multiple groups [17-20]. The adoption of the piezoelectric readout method over the optical method has multiple advantages. Primarily, the cost of incorporating piezoresistors will decrease the monitoring cost significantly. Without the expensive and macroscopic optical components, the size of the monitoring setup can be miniaturized. Additionally, the time-consumer laser alignment would not be necessary. Optical techniques are also subject to artifacts due to artifacts caused by changes in the optical properties in the surrounding medium, whereas piezoresistive detection can work in non-transparent solutions [21]. Elimination of the bulky and expensive optical setup in favor of the piezoelectric readout method would allow us to further miniaturize the system in our pursuit of an integrated and portable biosensing system.

6.2.2 Increased Control of Microenvironment of the Cantilever

One major avenue for further exploration is to study different methods to increase control of the microenvironment in which the cantilever is placed in. One intriguing approach, pioneered by Manalis *et al.*, is the incorporation of microfluidic channels within the cantilever device [22]. This method successfully circumvents the dampening effects on the cantilever readout signal due to complete immersion in a liquid for increased sensitivity and signal-to-noise ratios. In order to effectively control the parameters that can influence the cantilever readout signal, the incorporation of microfluidics could be highly beneficial in controlling stimulant concentration gradients and flow rates, as well as decreasing the volume of reagents consumed during each experiment and simplifying the single cell capture and wash protocols. As with the previous recommendation for the adoption of the piezoelectric readout method, microfluidic manipulation of the fluids surrounding the cantilever would also allow for the further miniaturization and integration of the biosensing system. Additionally, the ability to control the liquid environment experienced by the single attached cell through diffusion or more active mixing elements is an exciting opportunity.

6.2.3 Improving the Selectivity of the Cantilever Surface Chemistry

Our current method for attachment of a single cell at the tip of the cantilever involves passivation of the gold surface with PEG-dithiol to prevent nonspecific adhesion and functionalizing the exposed nitride pad with poly-L-lysine. Though an effective protocol for capturing single cells, the method lacks selectivity and needs to be further developed in order to explore opportunities for multiplexing our cantilever arrays for parallel processing of different cell types. One possibility is to use antibodies that

target specific cells, a method that several groups have used for specific cantilever-detection of cells and other targets [23, 24].

6.2.4 Exploration of Cantilever Materials

Silicon and silicon nitride cantilevers have been studied and characterized extensively, however, recent interest in polymeric materials have spawned a handful of polymer-based cantilevers that tout increased surface stress sensitivities, reduced fabrication times, as well as lower costs of fabrication [25]. Therefore, it will be interesting to explore the use of alternative materials in the fabrication of our cantilever arrays. In particular, we believe that SU-8 is an interesting polymer that could be investigated as an alternative material for cantilevers.

6.2.1 Development of Automated Monitoring System

Finally, the commercial monitoring setup that we are currently using is not customized for our application, and therefore the collection of data remains slow and labor-intensive. The development of a monitoring system that will automatically acquire signals at designated intervals from the cantilever sensors and perform the necessary analysis to determine the changes in the surface stress or bending of the cantilever over a specified length of time would be extremely beneficial. Furthermore, automation of the data acquisition and analysis through interfacing with control software as LabView®, as we have successfully demonstrated in our microfluidic pathogen detection platform, would continue our pursuit for platform portability.

In closing, the proposed studies outlined above are expected not only to lead to improvements in microfluidic devices and cantilever-based sensing technologies, but also provide exciting new avenues toward the development of innovative integrated

biosensor systems. Additional, we hope to expand our explorations of the potential technological applications of such systems for the improvement of global human health.

REFERENCES

[1] Cady, N.C.; Stelick, S.; Batt, C.A. Nucleic acid purification using microfabricated silicon structures. *Biosens. Bioelectron.* **2003**, *19*, 59-66.

[2] Cady, N.C.; Stelick, S.; Kunnavakkam, M.V.; Batt, C.A. Real-time PCR detection of *Listeria monocytogenes* using an integrated microfluidics platform. *Sens. Actuators. B Chem.* **2005**, *107*, 332-341.

[3] Cady, N.C.; Stelick, S.; Kunnavakkam, M.V.; Batt, C.A. Real-time PCR detection of Listeria monocytogenes using an integrated microfluidics platform *Sens. Actuators. B Chem.* **2005**, *107*.

[4] Cady, N.C.; Stelick, S.J.; Batt, C.A. Rapid Detection of Bacillus Anthracis in a Microchip-Based Real-Time PCR Biosensor. In Mater. Res. Soc. Symp. Proc., 2007.

[5] Cady, N.C.; Stelick, S.J.; Kunnavakkam, M.V.; Liu, Y.; Batt, C.A. A microchip-based DNA purification and real-time PCR biosensor for bacterial detection. In Sensors, Proc. of IEEE, 2004, pp. 1191-1194.

[6] Feng, Y.; Zhou, Z.; Ye, X.; Xiong, J. Passive valves based on hydrophobic microfluidics. *Sens. Actuators. A Phys.* **2003**, *108*, 138-143.

[7] Grover, W.H.; Skelley, A.M.; Liu, C.N.; Lagally, E.T.; Mathies, R.A. Monolithic membrane valves and diaphram pumps for practical large-scale integration into glass microfluidic devices. *Sens. Actuators. B Chem.* **2003**, *89*, 315-323.

[8] Liu, R.H.; Bonanno, J.; Yang, J.; Lenigk, R.; Grodzinski, P. Single-use, thermally actuated paraffin valves for microfluidic applications. *Sens. Actuators. B Chem.* **2004**, *98*, 328-336.

[9] Rinderknecht, D.; Hickerson, A.I. A valveless micro impedance pump driven by electromagnetic actuation. *J. Micromech. Microeng.* **2005**, *15*, 861-866.

[10] Selvaganapathy, P.; Carlen, E.T.; Mastangelo, C.H. Electrothermally actuated inline microfluidic valve. *Sens. Actuators. A Phys.* **2003**, *104*, 275-282.

[11] Studer, V.; Hang, G.; Pandolfi, A.; Ortiz, M.; Anderson, W.F.; Quake, S.R. Scaling properties of a low-actuation pressure microfluidic valve. *J. Appl. Phys.* **2004**, *95*, 393-398.

[12] Yu, Q.; Bauer, J.M.; Moore, J.S.; Beebe, D.J. Responsive biomimetic hydrogel valve for microfluidics. *Appl. Phys. Lett.* **2001**, *78*, 2589-2591.

[13] Belgrader, P.; Young, S.; Yuan, B.; Primeau, M.; Christel, L.A.; Pourahmadi, F.; Northrup, M.A. A Battery-Powered Notebook Thermal Cycler for Rapid Multiplex Real-Time PCR Analysis. *Anal. Chem.* **2001**, *73*, 286-289.

[14] Docherty, F.T.; Monaghan, P.B.; Keir, R.; Graham, D. The first SERRS multiplexing from labelled oligonucleotides in a microfluidics lab-on-a-chip. *Chem. Commun.* **2004**, 118-119.

[15] Lesuffleur, A.; Im, H.; Lindquist, N.C.; Lim, K.S.; Oh, S.-H. Laser-illuminated nanohole arrays for multiplex plasmonic microarray sensing. *Opt. Express* **2008**, *16*, 219-224.

[16] Yeung, S.-W.; Lee, T.M.-H.; Cai, H.; Hsing, I.-M. A DNA biochip for on-the-spot multiplexed pathogen identification. *Nucleic Acids Res.* **2006**, *34*, e118.

[17] Thaysen, J.; Boisen, A.; Hansen, O.; Bouwstra, S. Atomic force microscopy probe with piezoresistive read-out and highly symmetrical Wheatstone bridge arrangement. *Sens. Actuators. A Phys.* **2000**, *83*.

[18] Chui, B.W.; Stone, T.D.; Kenny, T.W.; Mamin, H.J.; Terris, B.D.; Rugar, D. Low-stiffness silicon cantilevers for thermal writing and piezoresistive readback with the atomic force microscope. *Appl. Phys. Lett.* **1996**, *69*, 2767-2769.

[19] Minne, S.C.; Manalis, S.R.; Quate, C.F. Parallel atomic force microscopy using cantilevers with integrated piezoresistive sensors and integrated piezoelectric actuators. *Appl. Phys. Lett.* **1995**, *67*, 3918-3920.

[20] Wee, K.W.; Kang, G.Y.; Park, J.; Kang, J.Y.; Yoon, D.S.; Park, J.H.; Kim, T.S. Novel electrical detection of label-free disease marker proteins using piezoresistive self-sensing micro-cantilevers. *Biosens. Bioelectron.* **2004**, *20*, 1932-1938.

[21] Raiteri, R.; Grattarola, M.; Butt, H.-J.; Skládal, P. Micromechanical cantilever-based biosensors. *Sens. Actuators. B Chem.* **2001**, *79*, 115-126.

[22] Burg, T.P.; Godin, M.; Knudsen, S.M.; Shen, W.; Carlson, G.; Foster, J.S.; Babcock, K.; Manalis, S.R. Weighing of biomolecules, single cells and single nanoparticles in fluid. *Nature* **2007**, *446*, 1066-1069.

[23] Dutta, P.; Tipple, C.A.; Lavrik, N.V.; Datskos, P.G.; Hofstetter, H.; Hofstetter, O.; Sepaniak, M.J. Enantioselective Sensors Based on Antibody-Mediated Nanomechanics. *Anal. Chem.* **2003**, *75*, 2342-2348.

[24] Zhang, J.; Ji, H.-F. An Anti E. Coli O157:H7 Antibody-immobilized Microcantilever for the Detection of Escherichia coli (E. coli). *Analytical Sci.* **2004**, *20*, 585.

[25] Nordstrom, M.; Keller, S.; Lillemose, M.; Johansson, A.; Dohn, S.; Haefliger, D.; Blagoi, G.; Havsteen-Jakobsen, M.; Boisen, A. SU-8 Cantilevers for Bio/chemical Sensing; Fabrication, Characterisation and Development of Novel Read-out Methods. *Sensors* **2008**, *8*, 1595-1612.